CHAPTER 6. RIVER HYDRODYNAMICS RESULTS

by

Peter Sucsy, Ph.D.
Kijin Park, Ph.D.
Getachew Belaineh, Ph.D., P.H.
Ed Carter
David Christian
Michael Cullum
Joseph Stewart, P.E.
Yanfeng Zhang

St. Johns River Water Management District
Palatka, Florida

2011

This page intentionally left blank.

TABLE OF CONTENTS

RIVER HYDRODYNAMICS WORKING GROUP

Name (Organization)	Roles
Peter Sucsy, Ph.D. (SJRWMD)	Working Group Leader, Editor, Author
Kijin Park, Ph.D. (SJRWMD)	Author
Getachew Belaineh, Ph.D., P.H. (SJRWMD)	Author
Ed Carter (SJRWMD)	Author
David Christian (SJRWMD)	Author
Michael Cullum (SJRWMD)	Technical Director
Joseph Stewart, P.E. (SJRWMD)	Author
Yanfeng Zhang (SJRWMD)	Author

LIST OF FIGURES

LIST OF TABLES

ACRONYMS, ABBREVIATIONS, AND CONVERSION FACTORS

AVAD	Average absolute difference
AVRD	Average relative difference
b	Intercept of the linear regression line
C_v	Coefficient of variation
DSC	Dimensionless sensitivity coefficient
EFDC	Environmental Fluid Dynamics Computer Code
Ev	Evaporation
FAC	Florida Administrative Code
FOEA	First order error analysis
H	Depth
h_{NT}	Ocean non-tide
HSPF	Hydrologic Simulation Program–FORTRAN
h_T	Ocean tide
m	Slope of the linear regression line
M_2	Principle lunar semidiurnal tidal constituent
MCA	Marsh Conservation Area
MCS	Monte Carlo simulation
MFLs	Minimum flows and levels
MSL	Mean sea level
mgd	million gallons per day
NAVD88	North American Vertical Datum of 1988
NGVD29	National Geodetic Vertical Datum of 1929
PSS78	Practical Salinity Scale 1987
Q	Tributary discharge
r^2	Coefficient of determination
r_i	Percent contribution to total uncertainty
RMSD	Root-mean-square difference
Rn	Rain
Sal_{GW}	Groundwater salinity
Sal_O	Ocean salinity
Sal_Q	Tributary salinity
S^h	water level
SR	State Road
S^{Sal}	Salinity
S^V	Current speed
USACE	U.S. Army Corps of Engineers
W	Wind speed
WMA	Water Management Area
WWTP	Wastewater Treatment Plant
Z_0	Bottom roughness

1 INTRODUCTION

This chapter summarizes the hydrodynamic modeling results for the Water Supply Impact Study (WSIS). The hydrodynamic model results examine the effects of proposed surface water withdrawals and other expected hydrologic changes on water level, salinity, and water age throughout the model domain. The model domain extends from the river mouth through Lake Harney and includes Lakes George, Monroe, and Jesup. In addition to a summary of hydrodynamic results for WSIS scenarios, this chapter also includes an uncertainty analysis, an analysis of the possible effects of reject water from reverse osmosis processes in the middle St. Johns River, and an analysis of the combined effects of several possible, but uncertain, future conditions that could have importance for long-range resource management planning.

The primary goal of WSIS is to evaluate ecological effects on the St. Johns River caused by withdrawal of water from the middle and upper St. Johns River for public water supply. Both hydrodynamic and hydrologic models are used to quantify the effects of hydrologic alterations on key physical variables throughout the river system for a range of defined scenarios. The hydrologic alterations to the upper St. Johns River are assessed using the Hydrologic Simulation Program–FORTRAN (HSPF) hydrologic model and are described in Chapter 3, Watershed Hydrology . The hydrodynamic alterations described in this chapter are assessed using the Environmental Fluid Dynamics Computer Code (EFDC) hydrodynamic model over the lower 310 km of the river, from Lake Harney to the river mouth. Results from the HSPF hydrologic model and EFDC hydrodynamic model are used for analyses of biological, chemical, and ecological impacts as described in Chapters 7 through 13.

At the beginning of WSIS, several questions were raised concerning the nature and extent of hydrodynamic alterations to the St. Johns River that would be caused by a proposed surface water withdrawal of 155 mgd upstream of DeLand (river km 232). These questions focused on three primary areas, reduction of water levels, increase of salinity, and increase of flushing. The question of water level reduction was previously addressed by Robison (2004) for the upper and middle St. Johns River who found mean reductions of water levels of about 3 cm. Salinity impacts for the estuarine reach of the lower St. Johns River were previously addressed by Environmental Consulting & Technology, Inc. (2008); the study examined changes to mean salinity and minimum and maximum salinity over a 5-yr period due to withdrawal rates of 80 to 230 mgd. Environmental Consulting & Technology, Inc. found mean salinity increases of less than 0.5 PSS78 and upstream shifts of isohalines of 0.5 to 3 km. They concluded that withdrawals up to 155 mgd adequately protected estuarine resources.

Although considerable information concerning hydrodynamic impacts of water withdrawals was available prior to WSIS, previous studies did not address water level reductions in the lower St. Johns River, salinity alteration in the middle St. Johns River, or questions regarding alterations to flushing. In addition, WSIS expanded questions of hydrodynamic alteration to include not only the effects of water withdrawals, but also the effects of other anticipated hydrologic changes to the system. The additional alterations considered are projects resulting in structural changes within the Upper St. Johns River Basin, urbanization of watersheds, and sea level rise. These additional alterations are considered together with water withdrawals because they are all factors that are reasonably expected to occur over the time frame (1995 to 2030) for implementing water withdrawal projects.

The hydrodynamic results presented in this chapter have importance for assessing whether the St. Johns River is a viable alternative water supply for future population growth. At present, public water supply is primarily supplied through groundwater pumping. This practice is unsustainable for protection of water resources and natural systems dependent on the maintenance of adequate groundwater levels (St. Johns River Water Management District 2006) given projected water demand. Surface water withdrawals from the St. Johns River must also be at a level that will prevent unacceptable harm to surface water resources (Florida Statutes 373.0421). The St. Johns River Water Management District (SJRWMD), in cooperation with federal, state, and local governments, has invested considerable resources toward the restoration and protection of the river's natural resources. The goal of WSIS is to identify water supply alternatives that are protective of both groundwater and surface water resources.

Similar to Robison (2004), we found that water level reductions due to a 155-mgd withdrawal are small (~4 cm) in the middle St. Johns River and essentially undetectable in the lower St. Johns River and Lake George. The most dominant effect on water level over the 1995 to 2030 time frame is increased water level caused by sea level rise. Over that time frame, sea level will rise at least 14 cm, thus dwarfing any reduction in water level by water withdrawals over the lower 310 km of the St. Johns River.

Our estimated salinity differences in the estuarine reach of the river due to a 155-mgd withdrawal are consistent with previous results (Environmental Consulting & Technology, Inc. 2008). Salinity differences in the upstream areas of Lake George and the middle St. Johns River were quite small (<0.05 PSS78). Over the 1995 to 2030 time frame, urbanization of watersheds will occur simultaneously with water demand. In Chapter 3, Watershed Hydrology, urbanization is shown to increase stormwater runoff to the St. Johns River through decreased evapotranspiration in the watersheds. Increased runoff due to increased urbanization decreases salinity in the estuarine river and offsets the effects of increasing salinity caused by water withdrawals over the 1995 to 2030 time frame.

Flushing is examined using the EFDC hydrodynamic model through a surrogate state variable called water age. Water age is a numerically derived variable closely related to residence time and is useful for understanding ecological changes dependent on residence time. Water age is the average time elapsed since a volume of water first entered the model, either as rainfall, as discharge from several sources (e.g., tributaries, springs, groundwater, wastewater treatment plants [WWTPs]), or as ocean water. A lower flushing rate caused by reduction of discharge results in a higher water age.

The greatest change to water age occurs in Lake George, although water age differences (~5 days) are small relative to the large natural variation (20 to 200 days) of water age in the lake. Water age differences are greatest when absolute water age is high, and water age differences caused by a 155-mgd withdrawal only rarely exceed 10% of ambient water age. Water age changes due to water withdrawals are unlikely to contribute appreciably to water quality alterations in the St. Johns River or Lake George over the 1995 to 2030 time frame, particularly relative to the expected increased stormwater flows that will increase delivery of nutrients, toxics, and pathogens to the river. The deleterious effects of pollution resulting from increased stormwater runoff due to urbanization of the St. Johns River watersheds is a greater threat to water quality than are the small predicted changes to water age.

The EFDC hydrodynamic model output is defined qualitatively as having very low or low uncertainty. These uncertainty levels are established because the EFDC hydrodynamic model is highly mechanistic and the calibrated model statistics show a good match between simulated and observed time series. Model results, then, can be used for environmental assessments with a high degree of certainty that the model's predicted responses realistically simulate real world system responses.

Water withdrawal from the middle St. Johns River for public water supply could require treatment using reverse osmosis to remove excessive chloride and other salts. The chloride and salts removed in this process would likely be returned to the St. Johns River as reject water. A far field analysis of the effects of reject water on the middle St. Johns River indicates increases of salinity during drought periods. The largest salinity changes due to reject water occur in the narrow river channel between Lake Monroe and Lake Jesup due to a 50-mgd withdrawal near Lake Jesup. Under the most extreme conditions tested, salinity is elevated from 1.5 to more than 3 PSS78 (Practical Salinity Scale 1978) (Lewis and Perkin 1978), although these effects are localized and infrequent. The combined effects of two withdrawal locations, one near State Road (SR) 46 at Lake Jesup and the other at Yankee Lake downstream of Lake Monroe, do not appreciably alter salinity either in Lake Monroe or in areas downstream of the lake. The far field effects of reject water on salinity should be considered for design of reverse osmosis plants in the middle St. Johns River.

Finally, the EFDC hydrodynamic model is used to test combinations of future conditions that are important to long-range resource management planning. These future conditions include channel deepening in Jacksonville Harbor near the river mouth, removal of discharge from WWTPs for reuse, enhanced rates of sea level rise, and additional withdrawal of surface water from the lower Ocklawaha River.

With the exception of sea level rise, none of the future conditions affect water levels. An additional water withdrawal of 107 mgd from the lower Ocklawaha River had no effect on water levels in the St. Johns River, because the lower Ocklawaha River enters downstream of Lake George. Future water levels throughout the lower and middle St. Johns River will increase largely due to sea level rise. Mean rates of sea level rise will not be as rapid in the middle St. Johns River, because river water level at high flows are not as affected by ocean level in that reach, but water levels at low flow will increase 14 to 28 cm between 1995 and 2030. Water level at high flow in the middle St. Johns River will also rise due to increased runoff from urbanization. Overall, water levels throughout the lower 310 km of the St. Johns River will gradually increase at a rate of about 4 to 8 mm yr^{-1} throughout this century.

The only variable notably altered by the future conditions is salinity in the estuarine reach of the river. All four future conditions tested have the effect of raising estuarine salinity. Salinity in the estuarine reach exhibits a nonlinear interaction between channel deepening and other future conditions. Salinity changes are greater when future conditions are combined within the model than when salinity changes are calculated separately for each condition and linearly superimposed. For this reason, the estimation of changes to estuarine salinity for scenarios that include channel deepening are best made by direct numerical experimentation using the EFDC hydrodynamic model.

The combined effect of all future conditions increases mean salinity 3 PSS78 at Acosta Bridge. Mean salinity increases between 0.1 and 1.0 PSS78 between Shands Bridge and Buckman Bridge. Salinity change predicted for this combination of future conditions is an extreme upper bound for marine salinity intrusion into the oligohaline–fresh zone of the river. Even for this extreme set of conditions, however, the salinity regime is not appreciably altered. These results indicate that the present salinity regime of the river will remain stable for a long time into the future, although sea level rise will continue to gradually elevate salinity levels. The future rate of sea level rise will largely determine the rate at which the broad expanse of the lower St. Johns River upstream of Acosta Bridge transitions from an oligohaline to mesohaline estuarine system.

The removal of WWTP discharge for reuse has an extremely small effect on water levels and salinity. Reuse should be encouraged as a means of water conservation and for the benefit of nutrient reduction to the river. These benefits far outweigh any possible deleterious impacts to salinity.

2 Analysis of the Hydrodynamic Effects of Water Supply Impact Study Scenarios

2.1 Introduction

The hydrodynamic effects of water withdrawals were determined by comparison of a base scenario with various withdrawal scenarios. The hydrodynamic modeling considered two distinct sets of change scenarios. One set is based on forecasting conditions for the year 2030, and a second set is based on factors that are possible, but uncertain, to occur in that year. The base scenario is different for the two different sets of change scenarios. The base scenario used for evaluating forecast conditions is a hindcast scenario. The hindcast scenario simulated river hydrodynamics for the model simulation period of 1996 through 2005 using 1995 land use, existing structures and surface water withdrawals in the upper St. Johns River, and observed ocean water level. The observed ocean water level includes actual sea level rise that occurred over the 10-yr hindcast period. The base scenario used for evaluating future conditions is the expected 2030 condition without additional water withdrawals. This 2030 scenario assumes increased urbanization of watersheds, projects resulting in structural changes within the Upper St. Johns River Basin, and expected sea level rise for the period 1995 through 2030.

The year 2030 was selected for forecasting hydrologic alterations to the river for WSIS based on an estimate of when population would reach a level requiring an additional 155 mgd of water supply. The need to define a time frame was a practical consideration for estimating changes to different factors affecting river hydrology and hydrodynamics based on a common reference in time. Two of the largest factors affecting hydrologic change, water withdrawals and urbanization of watersheds, are both linked to population growth and are generally expected to change in tandem. The exact year that the 155-mgd withdrawal is required, then, is less important to the results than the underlying assumption of population growth and its direct association to both water consumption and land use alterations.

The forecast scenarios consider proposed water withdrawals of up to 155 mgd from the St. Johns River above DeLand in conjunction with other changes expected to occur over the time frame (1995 to 2030) due to population growth that would require that additional rate of water supply. The additional changes expected over that time frame are structural changes within the Upper St. Johns River Basin, urbanization of watersheds, and sea level rise. The primary goal of these scenarios is to forecast, as realistically as possible, the hydrologic conditions of the river that will exist when sources of alternative water supply will be needed.

For the purpose of WSIS analyses, many scenarios were constructed from various permutations of the individual factors identified for the forecast scenarios (e.g., water withdrawal, structural changes, urbanization, and sea level rise). The permutations of factors can be used to isolate the effects of each factor in WSIS analyses. This leads to having forecast scenarios that are not realistic. For example, some forecast scenarios exclude the effect of sea level rise in order to examine other effects in isolation from sea level rise. These forecast scenarios are unrealistic, because sea level rise is virtually certain to occur, but these scenarios allow the determination of how other factors separately affect water level and, therefore, provide insight for resource managers.

The future scenarios include additional changes that could occur over the 1995 to 2030 time frame, but are less certain. These future scenarios include channel deepening, reuse of wastewater now discharged to the river, increased rates of sea level rise caused by global climate change, and additional water withdrawal from the Ocklawaha River. Future scenarios also include permutations of factors to isolate the effects of individual factors. One future scenario considers all these possible future factors occurring simultaneously. This scenario provides an extreme test of future hydrologic change, but because it is a combination of uncertain factors, it is extremely unlikely to occur.

Certain scenarios were drawn from among the forecast and future scenarios for environmental analyses (see Chapters 7 through 13). These scenarios were selected by the individual working groups to meet the goals of the biological, chemical, and ecological analyses and form the core of scenarios analyzed for WSIS.

This section summarizes hydrodynamic effects for both forecast and future conditions using only a subset of all scenarios. In this case, scenarios were selected that demonstrate the magnitude and patterns of hydrodynamic changes. Results for scenarios that do not add relevant information to the understanding of hydrodynamic effects are not shown. This summary details how water level, salinity, and water age is altered for both forecast and future conditions.

2.2 Description of Scenarios

2.2.1 Hindcast Scenario

The hindcast scenario (Base1995NN, Table 2–1) is a simulation of river hydrodynamics for the period 1996 through 2005. The hindcast scenario attempts to simulate, as accurately as possible, past hydrodynamic conditions. The hindcast scenario uses 1995 land use, operation of structures and surface water withdrawal in the upper St. Johns River for the hindcast period, observed ocean water level, average 1995 WWTP discharges to the river, and (primarily) 1995 bathymetry (see Chapter 5. River Hydrodynamics Calibration).

2.2.2 FORECAST SCENARIOS

The forecast scenarios consider hydrodynamic changes caused by additional surface water withdrawal and, also, changes that are expected to occur over the 1995 to 2030 time frame. The forecast scenarios include the following factors:

- Additional surface water withdrawal from the St. Johns River upstream of DeLand
- Projected land use expected to coincide with population growth
- Projects within the USJRB
- Sea level rise over a 35-yr period (1995 to 2030)

Water Withdrawal from the St. Johns River Upstream of DeLand

WSIS examined surface withdrawal rates of 0, 77.5, and 155 mgd, corresponding to no withdrawal, half withdrawal, and full withdrawal scenarios. The full withdrawal is the maximum continuous withdrawal rate that meets the established minimum flows and levels (MFLs) for DeLand (Robison 2004).

Withdrawals upstream of DeLand were sited at three locations presently considered most suitable for water supply development (Figure 2–1). These locations, along with the maximum annual average withdrawal rate, are as follows:

- Lake Poinsett (55 mgd) in the upper St. Johns River
- St. Johns River near SR 46 at Lake Jesup (50 mgd) in the middle St. Johns River
- Yankee Lake (50 mgd) downstream of Lake Monroe in the middle St. Johns River

Withdrawals near SR 46 at Lake Jesup and Yankee Lake are simulated with the EFDC hydrodynamic model as constant withdrawal rates. Withdrawals from Lake Poinsett occur outside of the EFDC hydrodynamic model domain and are simulated using the HSPF hydrologic model (see Chapter 3. Watershed Hydrology). The effects of withdrawals from Lake Poinsett are input to the EFDC hydrodynamic model through the specification of discharge entering the EFDC hydrodynamic model above Lake Harney. Withdrawals from Lake Poinsett vary with local river discharge and level of Taylor Creek Reservoir used for storage (see Chapter 3. Watershed Hydrology). Half withdrawal scenarios reduce all three withdrawal locations by half the maximum withdrawal rate.

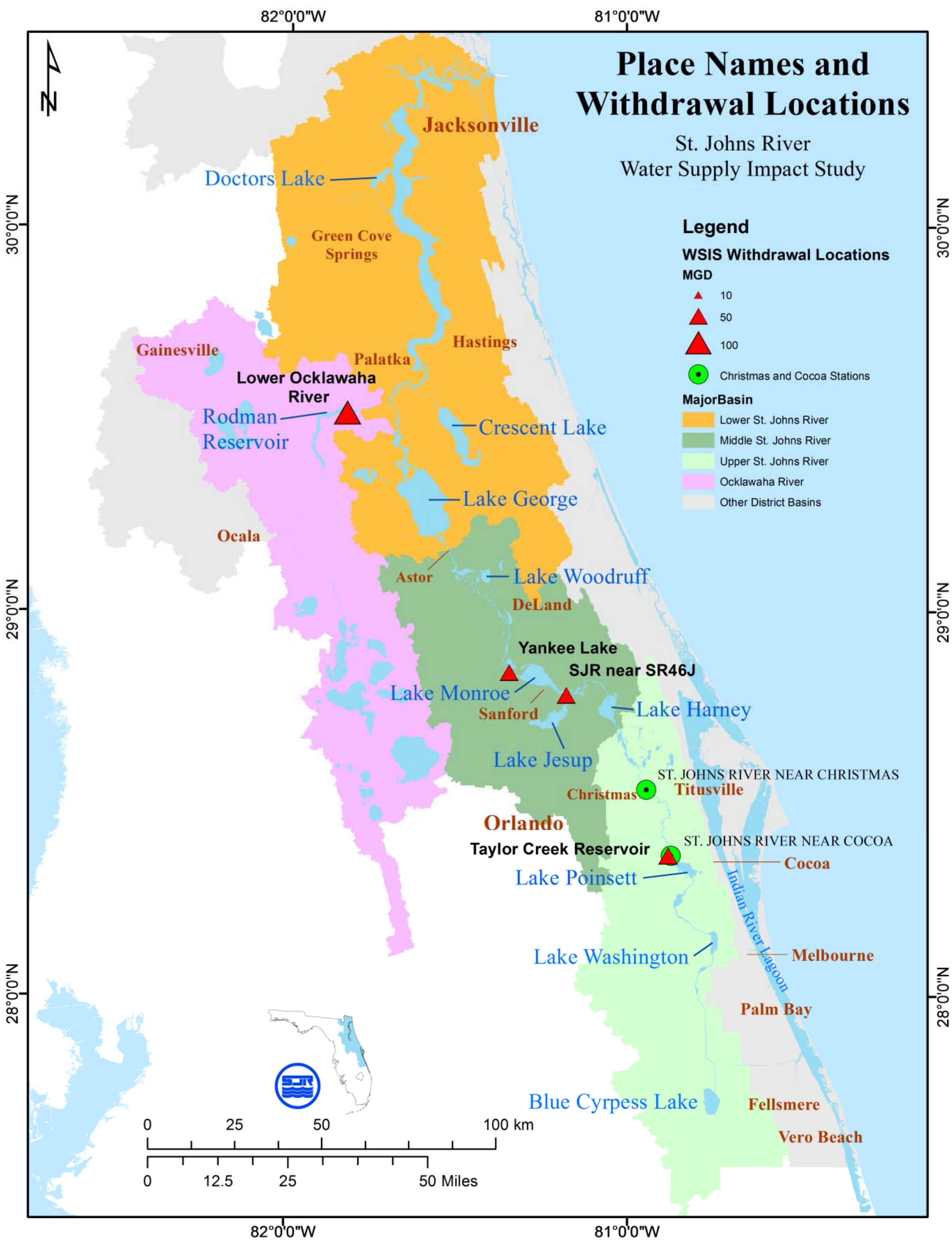

Figure 2–1. Map of withdrawal locations used for model scenarios.

Land Use Changes Expected to Coincide with Population Growth

Population growth will increase demand for public water supply and will also cause alterations to land use throughout the St. Johns River Basin. The predominant alteration to land use due to population growth is increased urbanization with an increase in the fraction of impervious surface within watersheds. Hydrologic modeling indicates that urbanization of the St. Johns River Basin will increase surface water runoff to the river, mainly by reduction of evapotranspiration (see Chapter 3. Watershed Hydrology).

The effects of urbanization are assessed by comparison of the hydrologic effects of 1995 land use with projected 2030 land use. Average discharge to the middle and lower St. Johns River increases about 8% for 2030 compared with 1995 land use. The greatest absolute increases in discharge occur during wet periods.

Projects Within the Upper St. Johns River Basin

The Upper St. Johns River Basin (USJRB) provides discharge to the EFDC hydrodynamic model through the upstream model boundary at SR 46 above Lake Harney. Large portions of USJRB are hydraulically controlled through a system of compartmentalized areas—cordoned off by levees, and interconnected by spillways, gates, control culverts, and weirs. Environmental restoration projects associated with construction of this managed system are ongoing, and the projects expected to be completed by the year 2030 are part of the forecast scenarios. Significant USJRB projects include diversion of waters now discharging to the Indian River Lagoon (C-1 Canal Project), creation of a large storage reservoir (Fellsmere Water Management Area project), and completion of a marsh restoration area (Three Forks Marsh Conservation Area project).

USJRB projects increase average discharge to Lake Harney by 20 mgd (0.86 m^3s^{-1}). By design, the projects have a proportionately greater effect at the lowest discharges. When discharge entering Lake Harney is less than 685 mgd (30 m^3s^{-1}) mean discharge increases 32 mgd (1.4 m^3s^{-1}), a greater than 5% increase. For discharge between 685 mgd (30 m^3s^{-1}) and 2050 mgd (90 m^3s^{-1}) mean discharge declines slightly by 16 mgd (0.68 m^3s^{-1}), approximately 1% to 2%.

Sea Level Rise

Sea level rise has been occurring at the river mouth at least since the beginning of observations at Mayport in the 1920s. The average rate of sea level rise over the observed record at Mayport is 2.4 mm yr^{-1}, although eustatic sea level rise (the rise of global ocean levels alone) is likely about 1.2 mm yr^{-1} (Dornstauder 2009) with the difference between local and eustatic sea level rise explained by land subsidence. The rate of sea level rise has varied over the last century, and the present rate of rise is likely at the maximum rate for the period (Rahmstorf 2007). The minimum projected sea level rise at Mayport over the period 1995 through 2030, based on both the results of Rahmstorf and Dornstauder, is 14 cm.

Forecast Scenario Permutations

Fourteen scenarios were used as forecast scenarios for WSIS (Table 2–1). The hindcast scenario (Base1995NN) is included in the table because it is a useful base condition for comparison of hydrodynamic changes caused by the forecast scenarios. Base2030PS is the likely condition of the river in the year 2030 without additional surface water withdrawals. Full2030PS is the likely condition of the river in the year 2030 with a 155-mgd surface water withdrawal.

Table 2–1. Forecast scenarios used for WSIS.

Scenario Name	Withdrawal Rate*	Land Use†	USJRB Projects‡	Sea Level Rise§
Base1995NN**	0	1995	No	0
Half1995NN	77.5 mgd	1995	No	0
Full1995NN	155 mgd	1995	No	0
Base1995PN	0	1995	Yes	0
Half1995PN	77.5 mgd	1995	Yes	0
Full1995PN	155 mgd	1995	Yes	0
Base1995PS	0	1995	Yes	+14 cm
Full1995PS	155 mgd	1995	Yes	+14 cm
Base2030PN	0	2030	Yes	0
Half2030PN	77.5 mgd	2030	Yes	0
Full2030PN	155 mgd	2030	Yes	0
Base2030PS	0	2030	Yes	+14 cm
Half2030PS	77.5 mgd	2030	Yes	+14 cm
Full2030PS	155 mgd	2030	Yes	+14 cm

*Water withdrawal rate from three locations upstream of DeLand
†Year of land use used to simulate runoff from contributing watersheds
‡Whether expected 2030 structural and operational changes to upper St. Johns River are used in scenario
§Rise in mean sea level relative to 1995
**The hindcast scenario is included here for comparison with forecast scenarios.

2.2.3 FUTURE SCENARIOS

Future scenarios include factors that affect river hydrodynamics, but are uncertain to occur over the 1995 to 2030 time frame. The following factors are considered in future scenarios:

- Additional surface water withdrawal from the lower Ocklawaha River
- Channel deepening of the navigational channel downstream of Jacksonville
- Accelerated rate of sea level rise due to global climate change
- Removal of wastewater discharge from the river for reuse

Additional Surface Water Withdrawal from the Lower Ocklawaha River

Future scenarios consider an additional 107-mgd water withdrawal from the lower Ocklawaha River. This level of withdrawal is based on a SJRWMD feasibility study performed for broad-scale water supply planning (Hall 2005). Unlike the middle St. Johns River, there is presently low interest in using the Ocklawaha River as a water supply of this magnitude. The 2005 District Water Supply Plan identifies only a 20-mgd project in this area as a viable water supply development project (St. Johns River Water Management District 2006). Because of the uncertainty about whether the Ocklawaha River is a viable alternative water supply for 2030 demand, this factor is considered as a future scenario.

Channel Deepening of the Navigational Channel Downstream of Jacksonville

The lower 30 km of the St. Johns River has a dredged navigational channel for safe passage of commercial vessels to cargo terminals located along Jacksonville Harbor. The channel depth may be increased in the future to allow passage of larger container ships. At present, the U.S. Army Corps of Engineers (USACE) Jacksonville is examining channel deepening scenarios that would allow for post-Panamax ships to reach cargo terminals. (Post-Panamax ships denote a size class of ship greater than those ships that can presently navigate through the Panama Canal). At present, the size, scope, and economic viability of a channel deepening project are under study, and the scope of the final project is uncertain. The channel deepening scenario used for this study is conservatively large and assumes creation of a 50 ft (NGVD29) navigational channel from the jetties at the mouth of the St. Johns River to Jacksonville (Talleyrand Marine Terminal) and including the north Blount Island channel.

Accelerated Rate of Sea Level Rise

The forecast scenarios include sea level rise of 14 cm over the 1995 to 2030 time frame based on projecting the present rate of sea level rise. Global climate change studies allow for the possibility of greater rates of sea level rise over this period. A high rate of sea level rise, with a high uncertainty, for the St. Johns River is estimated as 28 cm for the 1995 to 2030 time frame (U.S. Army Corps of Engineers 2009).

Removal of Wastewater Discharge for Reuse

The St. Johns River receives treated wastewater from numerous wastewater treatment plants (WWTPs) as direct point source discharges. Most of these WWTPs are located in the estuarine reach of the lower St. Johns River (see Chapter 5. River Hydrodynamics Calibration). Reuse of wastewater, largely for irrigation, conserves the water supply and reduces nutrient input to the river, which can degrade water quality. Population growth could lead to increased percentage of reuse in the future as an alternative water supply, reducing wastewater discharge to the river. At the same time population growth increases flow to the WWTPs. These competing factors add uncertainty to how much net change in discharge is expected over the 1995 to 2030 time frame. For WSIS, we estimated that 1995 level wastewater discharges of 165 mgd would be reduced to 100 mgd, a net decrease in river flow of 65 mgd.

Future Scenario Permutations

Nine scenarios are used as future scenarios for WSIS (Table 2–2). Because WSIS necessarily emphasizes the effects of surface water withdrawals, six future scenarios include an additional 107-mgd withdrawal from the lower Ocklawaha River in addition to a 155-mgd withdrawal from the St. Johns River.

Table 2–2. Future scenarios used for WSIS.

Scenario Name	Withdrawal Rate* (mgd)	Land Use†	USJRB Projects‡	Sea Level Rise§ (cm)	Wastewater Treatment Plant Reuse** (mgd)	Channel Deepening††
FwOR1995NN	262 mgd	1995	No	0	0	No
FwOR1995PN	262 mgd	1995	Yes	0	0	No
FwOR1995PS	262 mgd	1995	Yes	+14 cm	0	No
FwOR2030PS	262 mgd	2030	Yes	+14 cm	0	No
FwOR2030PN	262 mgd	2030	Yes	0	0	No
Base2030PH	none	2030	Yes	+28 cm	0	No
CHND2030PS	none	2030	Yes	+14 cm	0	Yes
WWTP2030PS	none	2030	Yes	+14 cm	65 mgd	No
FALL2030PH	262 mgd	2030	Yes	+28 cm	65 mgd	Yes

*Combined water withdrawal rate from St. Johns River upstream of DeLand (155 mgd) and the lower Ocklawaha River (107 mgd)
†Year of land use used to simulate runoff from contributing watersheds
‡Whether expected 2030 structural and operational changes to upper St. Johns River are used in scenario
§Rise in mean sea level relative to 1995
**Reduction of wastewater treatment plant discharge
††Navigational channel of 50 ft NGVD29 in Jacksonville Harbor

2.2.4 Water Withdrawals Outside the EFDC Hydrodynamic Model Domain

Water withdrawals from the St. Johns River at Lake Poinsett and the lower Ocklawaha River fall outside the EFDC hydrodynamic model domain. The effects of water withdrawals at these locations are simulated using the HSPF hydrologic model and provided as inputs to the EFDC hydrodynamic model. The simulated discharge that accounts for water withdrawal at Lake Poinsett enters the EFDC hydrodynamic model at SR 46 above Lake Harney. The simulated discharge that accounts for water withdrawal from the lower Ocklawaha River enters the EFDC hydrodynamic model at the confluence of the Ocklawaha and St. Johns rivers.

The maximum annual withdrawal rates used for scenario tests are 55 mgd from Lake Poinsett and 107 mgd from the lower Ocklawaha River. (An additional 100-mgd maximum withdrawal rate occurs inside the EFDC hydrodynamic model in many scenarios.) Operational rules applied to withdrawals from Lake Poinsett and the lower Ocklawaha River causes variability of daily and monthly averaged discharge reductions. The distribution of 1- and 30-day averaged discharge differences between the hindcast scenario (Base1995NN) and maximum rate withdrawal scenario (FwOR1995NN) are shown in Table 2–3 for SR 46 above Lake Harney and the confluence of the Ocklawaha and St. Johns rivers. Negative values indicate a reduction in discharge.

Discharge increases at SR 46 above Lake Harney for a small fraction of time. This increase is due to the designed operation of the Taylor Creek Reservoir to augment base flow for environmental benefit during drought periods. A small fraction of large negative discharge differences also occur at this location and are caused by filling of Taylor Creek Reservoir during periods of high river discharge. The fairly wide range of discharge differences at SR 46 above Lake Harney is possible because of the storage capacity of Taylor Creek Reservoir.

In contrast to Taylor Creek Reservoir, the storage capacity provided by Rodman Reservoir on the lower Ocklawaha River is more restricted because its management emphasizes fisheries. Discharge differences entering the EFDC hydrodynamic model at the confluence of the Ocklawaha and St. Johns rivers show only slight deviations from the mean reduction of -107 mgd.

Table 2–3. Distribution of discharge differences between hindcast scenario (Base1995NN) and a maximum rate withdrawal scenario (FwOR1995NN) at SR 46 above Lake Harney (SR46H) and the confluence of the Ocklawaha and St. Johns rivers, from 1995 to 2005, for 1- and 30-day averaging periods. Negative values indicate a reduction in discharge from the hindcast scenario.

	Discharge Difference (mgd) at SR46H for a 55-mgd Annual Withdrawal*		**Discharge Difference (mgd) at Ocklawaha and St. Johns Rivers Confluence for a 107-mgd Annual Withdrawal**	
Percent of values less than or equal to given level	**1-day averaging period**	**30-day averaging period**	**1-day averaging period**	**30-day averaging period**
Maximum	+89.0	+10.6	-0.9	-9.4
95%	+7.9	+5.6	-11.1	-75.4
75%	-16.8	-19.7	-79.4	-103.2
50%	-45.8	-46.6	-105.9	-107.3
25%	-68.1	-66.9	-125.0	-111.0
5%	-157.6	-153.0	-221.6	-130.9
Minimum	-1,107.6	-338.3	-939.7	-355.8

*Contribution to 155-mgd withdrawal at this location.

2.2.5 SCENARIOS SELECTED FOR ENVIRONMENTAL ANALYSES

WSIS working groups selected a subset of scenarios for assessing biological, chemical, and ecological impacts (see Chapters 7 through 13). Practical constraints prevented the working groups from examining the entire suite of forecast and future scenarios. The scenarios selected for environmental analyses are shown in Table 2–4.

Table 2–4. Scenarios selected for environmental analyses.

Scenario Name	Withdrawal Rate* (mgd)	Land Use†	USJRB Projects‡	Sea Level Rise§ (cm)
Base1995NN	0	1995	No	0
Half1995NN	77.5 mgd	1995	No	0
Full1995NN	155 mgd	1995	No	0
Base1995PN	0	1995	Yes	0
Half1995PN	77.5 mgd	1995	Yes	0
Full1995PN	155 mgd	1995	Yes	0
Full1995PS	155 mgd	1995	Yes	+14 cm
Base2030PN	0	2030	Yes	0
Half2030PN	77.5 mgd	2030	Yes	0
Full2030PN	155 mgd	2030	Yes	0
Base2030PS	0	2030	Yes	+14 cm
Half2030PS	77.5 mgd	2030	Yes	+14 cm
Full2030PS	155 mgd	2030	Yes	+14 cm
FwOR1995NN	262 mgd	1995	No	0
FwOR1995PN	262 mgd	1995	Yes	0
FwOR1995PS	262 mgd	1995	Yes	+14 cm
FwOR2030PN	262 mgd	2030	Yes	0
FwOR2030PS	262 mgd	2030	Yes	+14 cm

*Water withdrawal rate from lower Ocklawaha River and/or St. Johns River upstream of DeLand
† Year of land use used to simulate runoff from contributing watersheds
‡Whether expected 2030 structural and operational changes to upper St. Johns River are used in scenario
§Rise in mean sea level relative to 1995

2.3 Methods and Model Scenarios

2.3.1 Forecast Scenarios

Hydrodynamic changes expected to occur over the 1995 to 2030 time frame are analyzed using the hindcast scenario (Base1995NN) and the following four forecast scenarios: Base1995PN, Base2030PN, Base2030PS, and Full2030PS (Table 2–1). The hindcast scenario serves as a baseline condition against which changes resulting from the forecast scenarios are compared.

Successive differencing of these five scenarios determines the contribution of individual factor to the total change of hydrodynamic conditions over 1995 to 2030 as follows:

- Base1995PN minus Base1995NN = Contribution of USJRB projects
- Base2030PN minus Base1995PN = Contribution of projected 2030 land use
- Base2030PS minus Base2030PN = Contribution of sea level rise
- Full2030PS minus Base2030PS = Contribution of 155-mgd withdrawal

The final difference above (Full2030PS minus Base2030PS) simulates the effects of a 155-mgd water withdrawal in conjunction with other changes expected to occur when this alternative water source is needed. Differencing of the final scenario with the hindcast scenario (Full2030PS minus Base1995NN) represents the total change between the1995 hindcast scenario and the 2030 forecast scenario including the effects of water withdrawal.

2.3.2 FUTURE SCENARIOS

Hydrodynamic changes to future conditions were analyzed using the Base2030PS scenario (Table 2–1) as a reference condition and five future scenarios: Base2030PH, CHND2030PS, WWTP2030PS, FwOR2030PS, and FALL2030PH (Table 2–2). The Base2030PS is used as a baseline instead of the hindcast scenario (Base1995NN) because future conditions are considered factors of hydrodynamic change that are additional to the projected changes for the year 2030.

Differencing of the first four future scenarios with the reference condition (Base2030PS) determines the effect of each individual future condition as follows:

- Base2030PH minus Base2030PS = Effect of additional sea level rise
- CHND2030PS minus Base2030PS = Effect of channel deepening
- WWTP2030PS minus Base2030PS = Effect of wastewater reuse
- FwOR2030PS minus Base2030PS = Effect of 262-mgd withdrawal

Differencing of the combined scenario (FALL2030PH) with the base scenario (Base2030PS) simulates the effects of all future conditions occurring simultaneously. Because each future condition is itself highly unlikely, the combined scenario (FALL2030PH) is an implausible and extreme condition.

2.3.3 METHODS FOR ANALYZING DIFFERENCES BETWEEN SCENARIOS

Linearity of Response

The separation of individual factors for analyzing forecast and future conditions is most useful when the effects of individual factors are linear. Linearity of factors implies that the effects of individual factors can be added to approximate the effects of factors occurring simultaneously. If effects are linear, the effects of different permutations of factors can be estimated by simple addition without needing to run additional model scenarios.

The linearity of factors was tested for the forecast conditions against the hindcast scenario (Base1995NN) and for the future conditions against the Base2030PS scenario by comparing the ratios of the simulated total effects, derived directly from the EFDC hydrodynamic model, against the linear sum of the individual effects. These ratios are calculated from simulated time series of water level, salinity, and water age at points along the main stem of the lower and middle St. Johns River.

The linearity results are presented as bar plots showing the percent deviation of the total effect against the sum of the individual effects in Section 2.4. A value of 100% at a location indicates that the total effect is identical to the linear sum of the individual effects. A value greater than 100% indicates that the linear sum of the individual effects exceeds the total effect. This means that estimating the total effect by summing individual factors overpredicts the true effect. Similarly, a value less than 100% indicates that estimating the total effect by summing individual factors underpredicts the true effect.

The results from testing the linearity of factors indicate whether individual factors influencing a variable can be summed to yield a total effect. In addition, the percent contribution of each individual factor is shown for each location and indicates the relative importance of each individual factor to the total effect at selected points along the river.

Time Series Comparisons

Differences between scenarios are shown by direct graphical comparison of simulated time series at selected locations and by graphical comparison of the differences between simulated time series in Section 2.4. The plotted time series show the variation of similarities and differences among scenarios over a 10-yr period.

Comparative Statistics

Comparative statistics for water level, salinity, and water age at selected locations are presented in tables (see Section 2.4) with the following information:

- Number of paired values (*NRECS*)
- Slope (*m*) and intercept (*b*) of the linear regression line
- Coefficient of determination (r^2) of the paired data
- Root mean square difference (*RMSD*)
- Average relative difference (*AVRD*)
- Average absolute difference (*AVAD*)

The three statistics used for representing central tendencies of differences between two scenarios, *RMSD*, *AVRD*, and *AVAD*, are defined as follows, where B_i = the i-th value of a base scenario and W_i = the i-th value of a change scenario:

$$RMSD = \sqrt{\frac{\sum_{i=1}^{NRECS}(W_i - B_i)^2}{NRECS}} \tag{2.1}$$

$$AVRD = \frac{\sum_{i=1}^{NRECS}(W_i - B_i)}{NRECS} \tag{2.2}$$

$$AVAD = \frac{\sum_{i=1}^{NRECS}|W_i - B_i|}{NRECS} \tag{2.3}$$

RMSD and *AVAD* are both measures of the aggregate deviations between the two data sets and are always positive. Because *RMSD* values are squared differences, *RMSD* is always greater than or equal to *AVAD*. These statistics are equal only when the values of the paired differences do not vary. *RMSD* greater than the average absolute error (*AVAD*) indicates variability among the paired differences. *RMSD* much greater than *AVAD* indicates at least some very large paired differences.

AVRD is the mean of the paired differences, and the sign indicates the direction of the change. Because we subtract the base scenario from the change scenario, a negative *AVRD* indicates that the variable being examined is decreased in magnitude in the change scenario compared to the base scenario.

The comparative statistics are useful for quickly assessing the global difference between two scenarios. r^2 and m near 1 indicate the two scenarios have near identical variation. *AVRD* shows the change and direction of change of the mean difference between scenarios.

Longitudinal Plots

Longitudinal plots show mean values of a variable along the river thalweg. Longitudinal difference plots show the mean difference between scenarios. The longitudinal plots graphically show the spatial variation, along the river thalweg, of mean differences between two scenarios.

Contour Plots

Color contour plots are used to show spatial differences between scenarios. Contour plots quickly show the areal extent of relative differences of change over the model domain.

Discharge Difference Plots

Discharge difference plots are constructed by pairing daily differences between scenarios with river discharge. Discharges are then binned by 570-mgd (25 m^3s^{-1}) intervals. All differences falling within a bin are sorted, and the results plotted as box-and-whisker diagrams of differences. These plots show the full range of differences between two scenarios for all conditions occurring over the 10-yr simulation period. The plots show how differences between scenarios vary with river discharge.

Intensity-Frequency-Duration Plots

Intensity-frequency-duration plots are developed for both simulated variables and the simulated differences between scenarios. These plots are developed by ranking annual maximum and minimum values for 1-, 2-, 5-, 7.5-, 10-, 20-, 30-, 50-, 100-, 125-, 150-, 175-, 200-, and 365-day averaging periods. Return periods of 10, 5, and 2 years are determined by a Weibull plotting position (Viessman, et al. 1977). These plots show the hydrodynamic responses between scenarios for extreme events within the model simulation period.

2.4 RESULTS

2.4.1 FORECAST SCENARIOS

Linearity of Response

Linearity of factors for the forecast conditions are tested by comparison of selected forecast scenarios against the hindcast scenario (Section 2.3.1). Results show essentially complete linearity for water level (Figure 2–2), salinity (Figure 2–3), and water age (Figure 2–4) at all locations.

It is important to note that the fractional contributions for each individual factor shown in the figures do not indicate the direction of the change. For water level, only the 155-mgd withdrawal causes a decline, while the other three factors (sea level rise, land use change, and USJRB projects) cause water level to increase. Figure 2–2 shows that factors that increase water level predominate and clearly shows the dominance of sea level rise relative to other factors.

For salinity, the important changes occur in the estuarine reach, represented in Figure 2–3 by Acosta, Orange Park, and Shands Bridge. At these locations two factors, 155-mgd withdrawal and sea level rise, increase salinity, while two factors, land use change and USJRB projects, decrease salinity. The net change in salinity between the Full2030PS and Base1995NN scenarios is expected, then, to be small because of the competing effects of the individual factors.

For water age, identically to salinity, both a 155-mgd withdrawal and sea level rise increase water age, while land use change and USJRB projects decrease water age. As for salinity, the net change in water age is expected to be small.

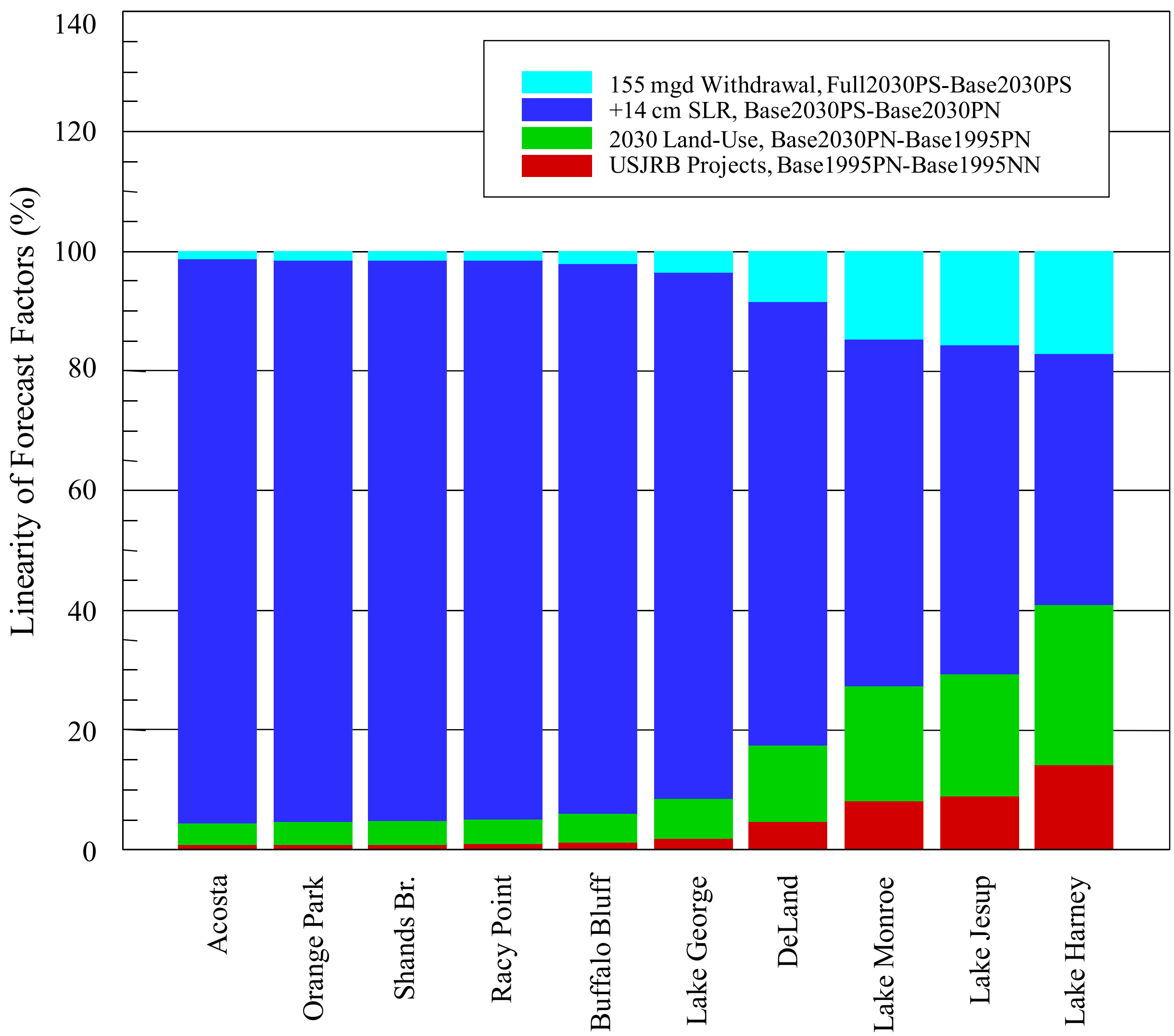

Figure 2–2. Linearity of factors affecting water level for forecast conditions relative to the hindcast condition (Base1995NN). SLR = sea level rise, USJR = upper St. Johns River.

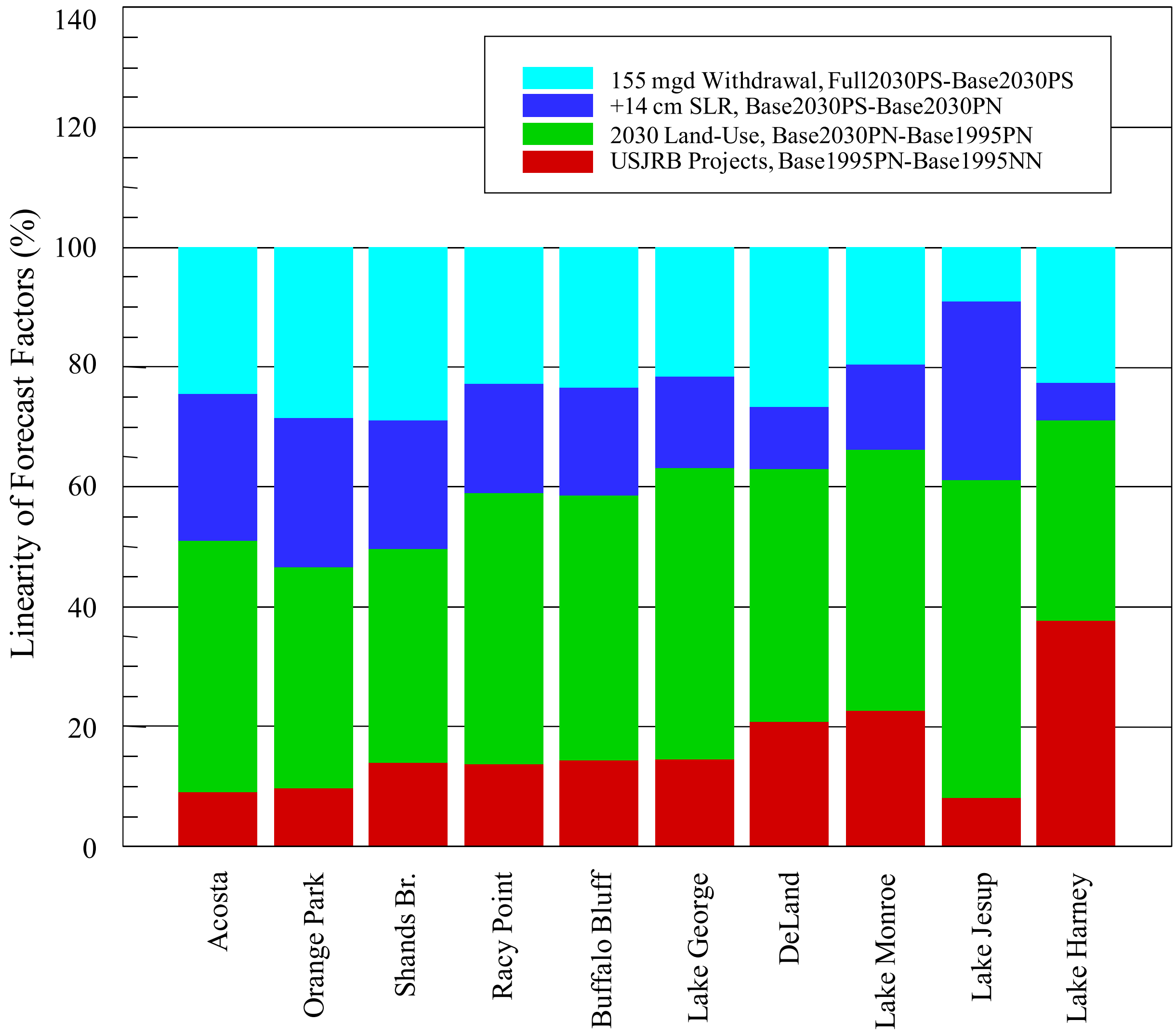

Figure 2–3. Linearity of factors affecting salinity for forecast conditions relative to the hindcast scenario (Base1995NN). SLR = sea level rise, USJR = upper St. Johns River.

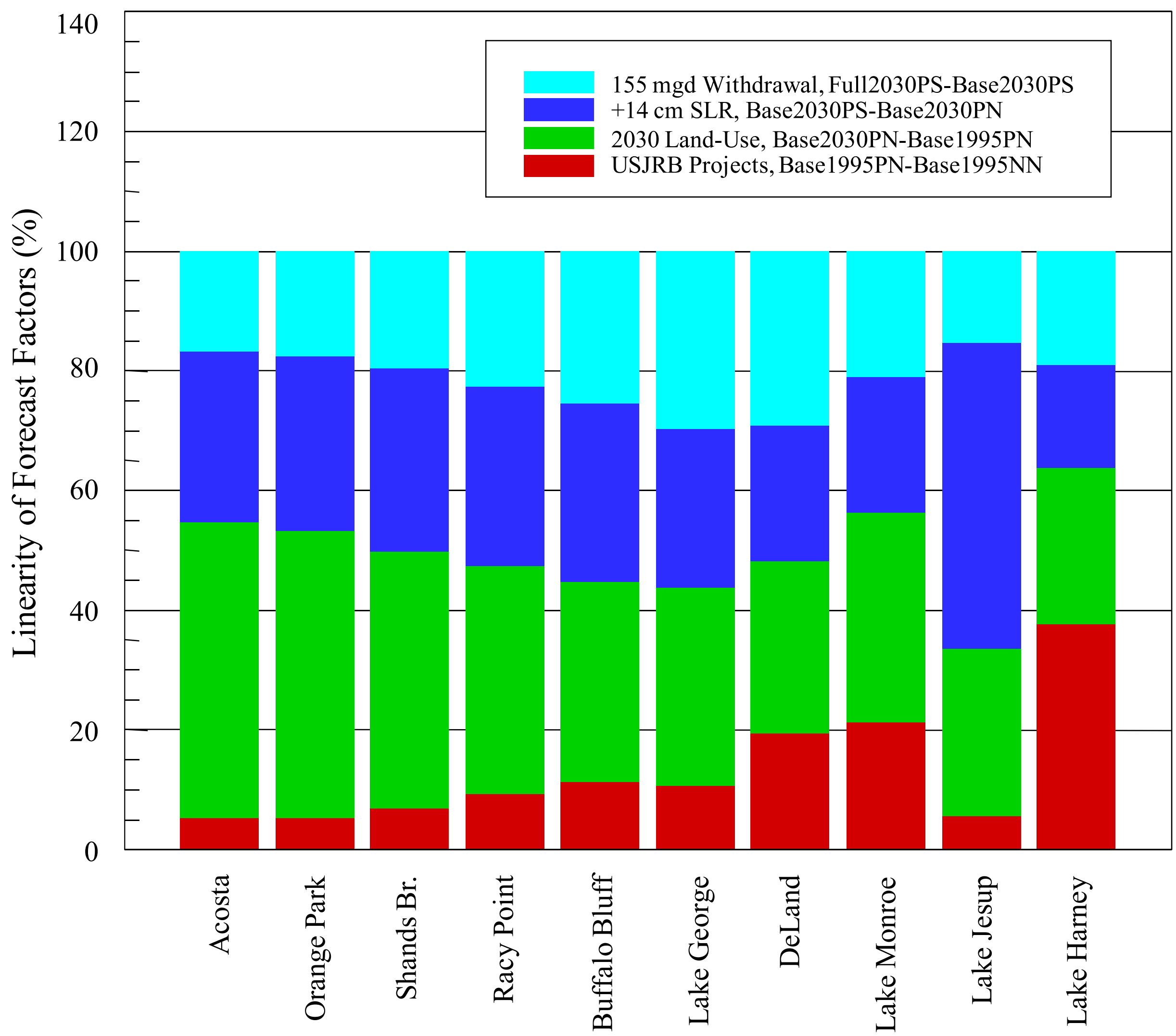

Figure 2–4. Linearity of factors affecting water age for forecast conditions relative to the hindcast scenario (Base1995NN). SLR = sea level rise, USJR = upper St. Johns River.

Water Level

This section summarizes the differences in water level between the Full2030PS (projected 2030 conditions with a 155 mgd withdrawal) and Base1995NN scenarios (hindcast condition). Water withdrawal has the greatest effect at the most upstream locations (Lake Harney). Water withdrawals have essentially no effect on water levels in the lower St. Johns River and Lake George. Sea level rise dominates water level change throughout the model domain, and water levels are expected to increase over the 1995 to 2030 time frame even when including a 155-mgd withdrawal.

Time Series Comparisons

Time series plots of monthly averaged water level compare the hindcast scenario (Base1995NN) with four forecast scenarios for Lake George (Figure 2–5) and Lake Monroe (Figure 2–6).

Monthly averaged values are used for visual clarity, although daily averaged values show similar results. In both locations, time series plots show the dominance of sea level rise (Base2030PS and Full2030PS) over the 10-yr period. In Lake George (Figure 2–5) sea level rise caused a nearly uniform uplift of the entire time series, while in Lake Monroe (Figure 2–6) the highest water levels are not as affected by sea level rise.

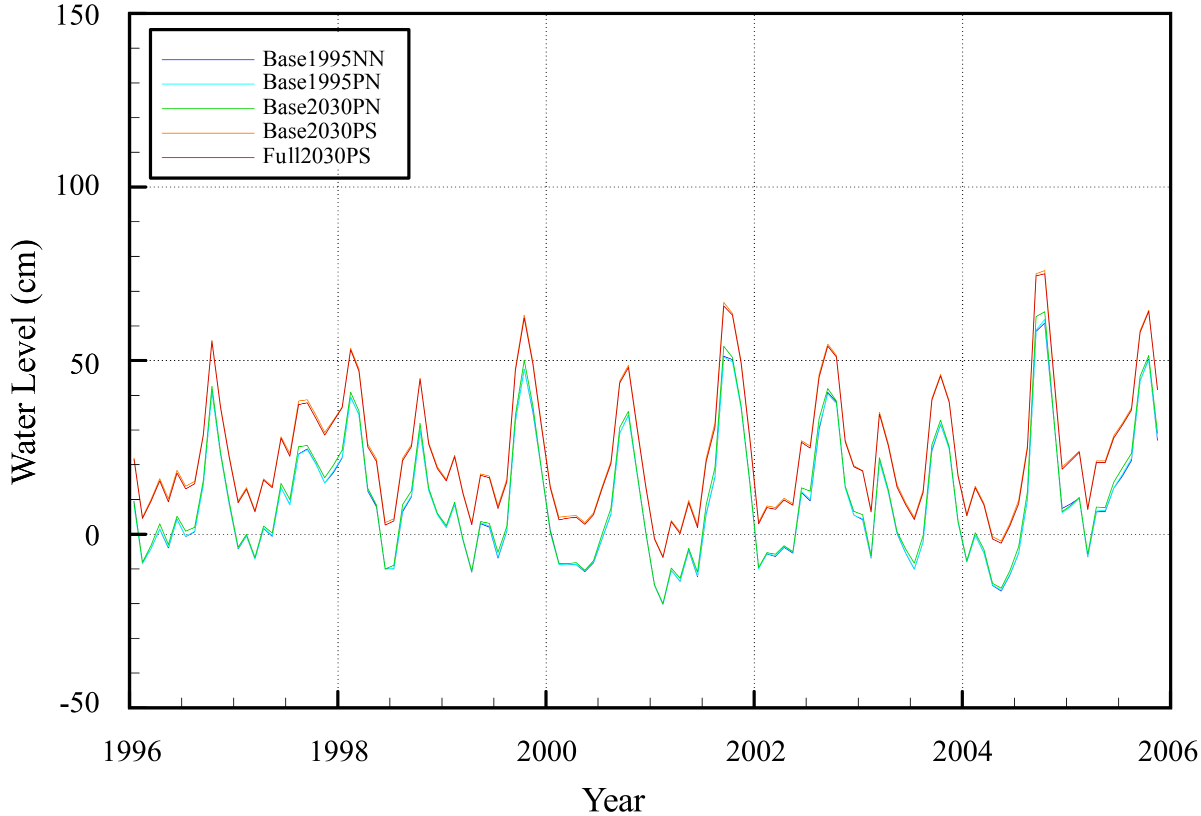

Figure 2–5. Monthly averaged water level in Lake George for the hindcast scenario (Base1995NN) and selected forecast scenarios. (Water level relative to NAVD88). Full2030PS is the projected 2030 conditions with a 155-mgd withdrawal.

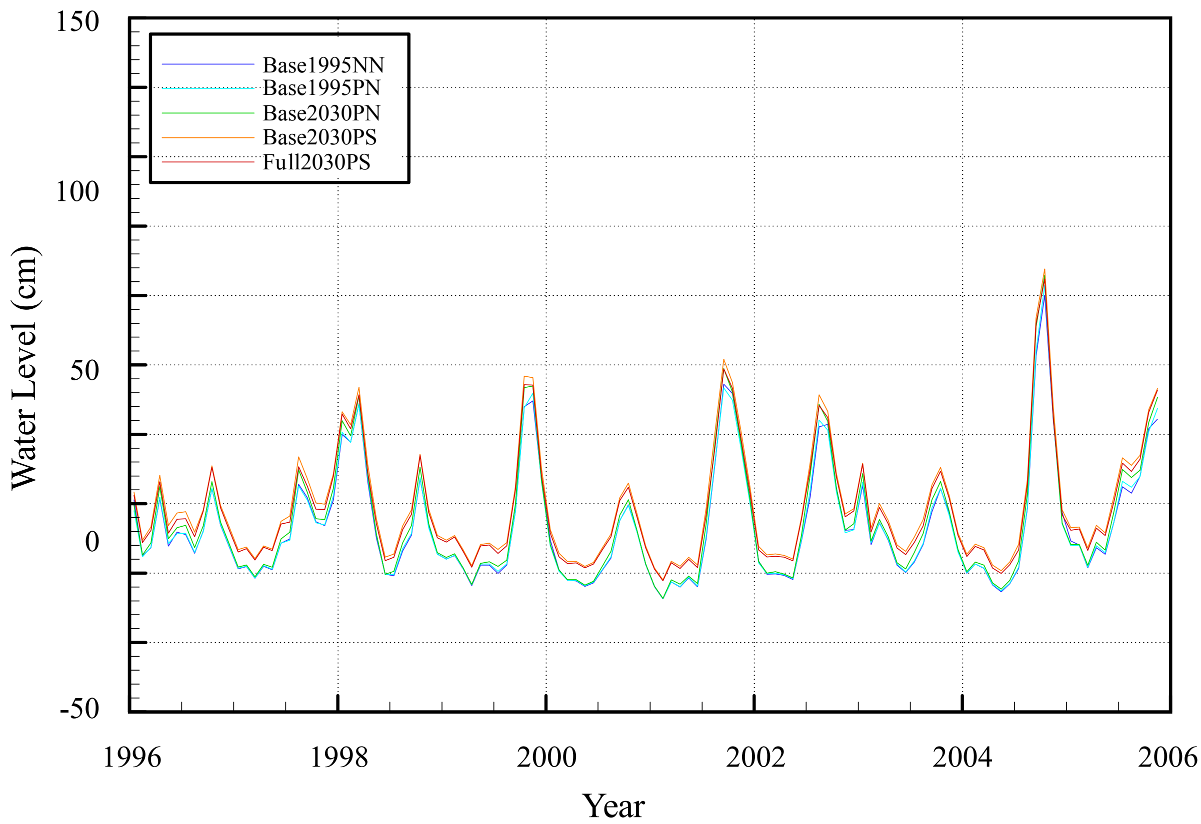

Figure 2–6. Monthly averaged water level in Lake Monroe for the hindcast scenario (Base1995NN) and selected forecast scenarios. (Water level relative to NAVD88). Full2030PS simulates projected 2030 conditions with a 155-mgd withdrawal.

Difference plots for water level scenarios in Lake George (Figure 2–7) and Lake Monroe (Figure 2–8) are shown below. The total effect (red line) shows differences between the Full2030PS and Base1995NN scenarios. Other lines show the contribution of each individual factor to the total effect. Because the effects of the individual factors are linear (see Figure 2–2), superposition of the individual effects closely approximates the total effect.

In Lake George, sea level rise is clearly the dominant factor affecting water level change, resulting in a nearly uniform increase of 14 cm. Projected 2030 land use changes cause small increases (generally less than 2 cm) in Lake George water level, while USJRB projects and a 155-mgd water withdrawal have negligible effect on water level.

Water level differences in Lake Monroe exhibit greater variability than differences in Lake George. Sea level rise still dominates the total effect in Lake Monroe, so that over the 10-yr simulation period only one event caused a brief lowering of water level compared with the hindcast scenario. A 155-mgd withdrawal (orange line) decreases water level 1 to 10 cm. This decline is often compensated by changes to land use and the USJRB projects. The USJRB projects increase water levels on average, but can contribute to a decline during periods of high flow. This effect is by design, because these projects restore storage capacity to the USJRB that reduces storm peaks. Reduction of water level by withdrawal is smaller than the various factors causing water level to increase, so that overall water levels throughout the middle St. Johns River are expected to increase 10 to 15 cm between 1995 and 2030.

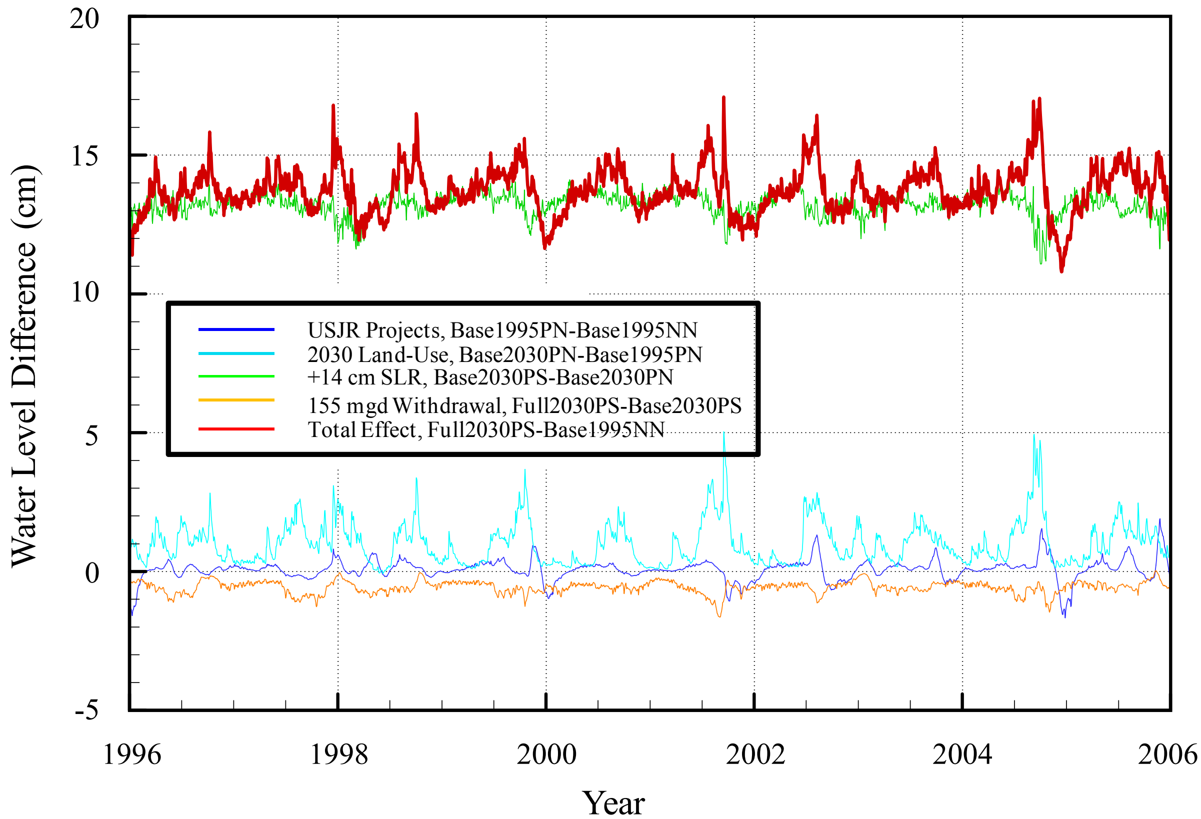

Figure 2–7. Daily averaged differences in water level in Lake George for the total effect (Full2030PS minus Base1995NN) and individual contributions to the total effect. (Water level relative to NAVD88.) USJR = upper St. Johns River, SLR = sea level rise.

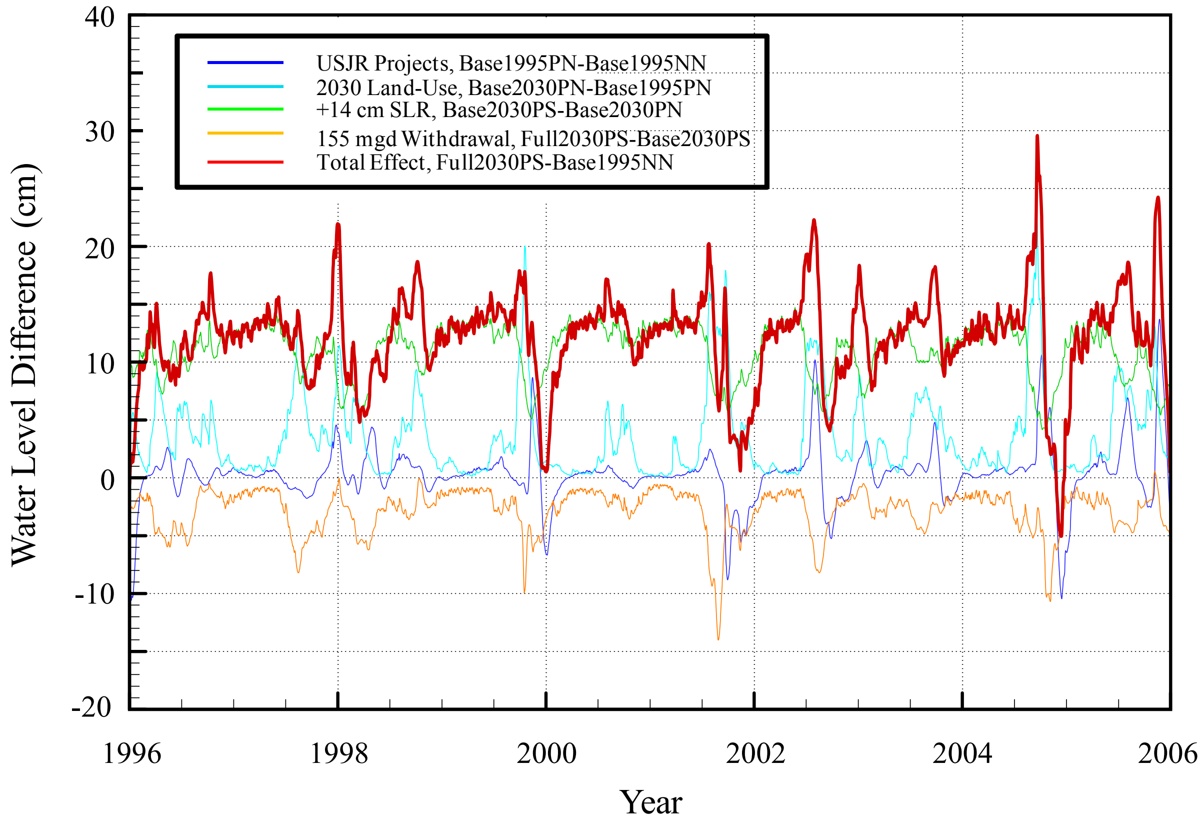

Figure 2–8. Daily averaged differences in water level in Lake Monroe for the total effect (Full2030PS minus Base1995NN) and individual contributions to the total effect. (Water level relative to NAVD88.) USJR = upper St. Johns River, SLR = sea level rise.

Comparative Statistics

Comparative statistics for the differences of daily averaged water level between the hindcast scenario (Base1995NN) and projected 2030 condition with a 155-mgd withdrawal (Full2030PS) are shown in Table 2–5. r^2 and m values indicate that changes to water level variability are small. *AVRD* shows mean water level increases 12 to 14 cm throughout the model domain.

Table 2–5. Comparative statistics for differences in daily averaged water level between the Full2030PS and Base1995NN scenarios.

Station	*NRECS*	r^2	*m*	*b*	*RMSD* (cm)	*AVRD* (cm)	*AVAD* (cm)
Acosta	3,652	1.000	0.990	-13.846	13.958	13.952	13.952
Orange Park	3,652	0.999	0.990	-13.830	13.990	13.983	13.983
Shands Bridge	3,652	0.999	0.990	-13.813	13.979	13.972	13.972
Racy Point	3,652	0.999	0.990	-13.777	13.948	13.939	13.939
Buffalo Bluff	3,652	0.999	0.990	-13.686	13.876	13.865	13.865
Lake George	3,652	0.998	0.989	-13.456	13.746	13.721	13.721
DeLand	3,652	0.994	1.000	-12.911	13.072	12.906	12.906
Lake Monroe	3,652	0.991	0.998	-12.056	12.792	12.126	12.173
Lake Jesup	3,652	0.990	1.000	-11.850	12.699	11.865	11.966
Lake Harney	3,652	0.988	0.995	-11.402	13.864	11.778	12.466

Note:
NRECS = Number of paired values
r^2 = Coefficient of determination
m = Slope of the linear regression line
b = Intercept of the linear regression line
RMSD = Root-mean-square difference
AVRD = Average relative difference
AVAD = Average absolute difference

Longitudinal Plots

A longitudinal plot comparing mean water level for the hindcast scenario (Base1995NN) and selected forecast scenarios again shows the dominance of sea level rise on water level change (Figure 2–9).

A longitudinal plot of mean differences in water level (Figure 2–10) shows how the contribution of each individual factor to the total effect (red line) changes over the river's length. A 155-mgd withdrawal (orange line) decreases mean water level less than 1 cm downstream of Astor. The withdrawal effect increases upstream and reduces mean water level between Lake Monroe and Lake Harney from 3 to 4 cm.

Increases in water level caused by sea level rise are slightly less in the upstream lakes because sea level rise effects are diminished in this region during high flow. The increased runoff caused by land use changes, however, has the greatest effect in the upstream lakes and compensates for the reduction of water level caused by withdrawals.

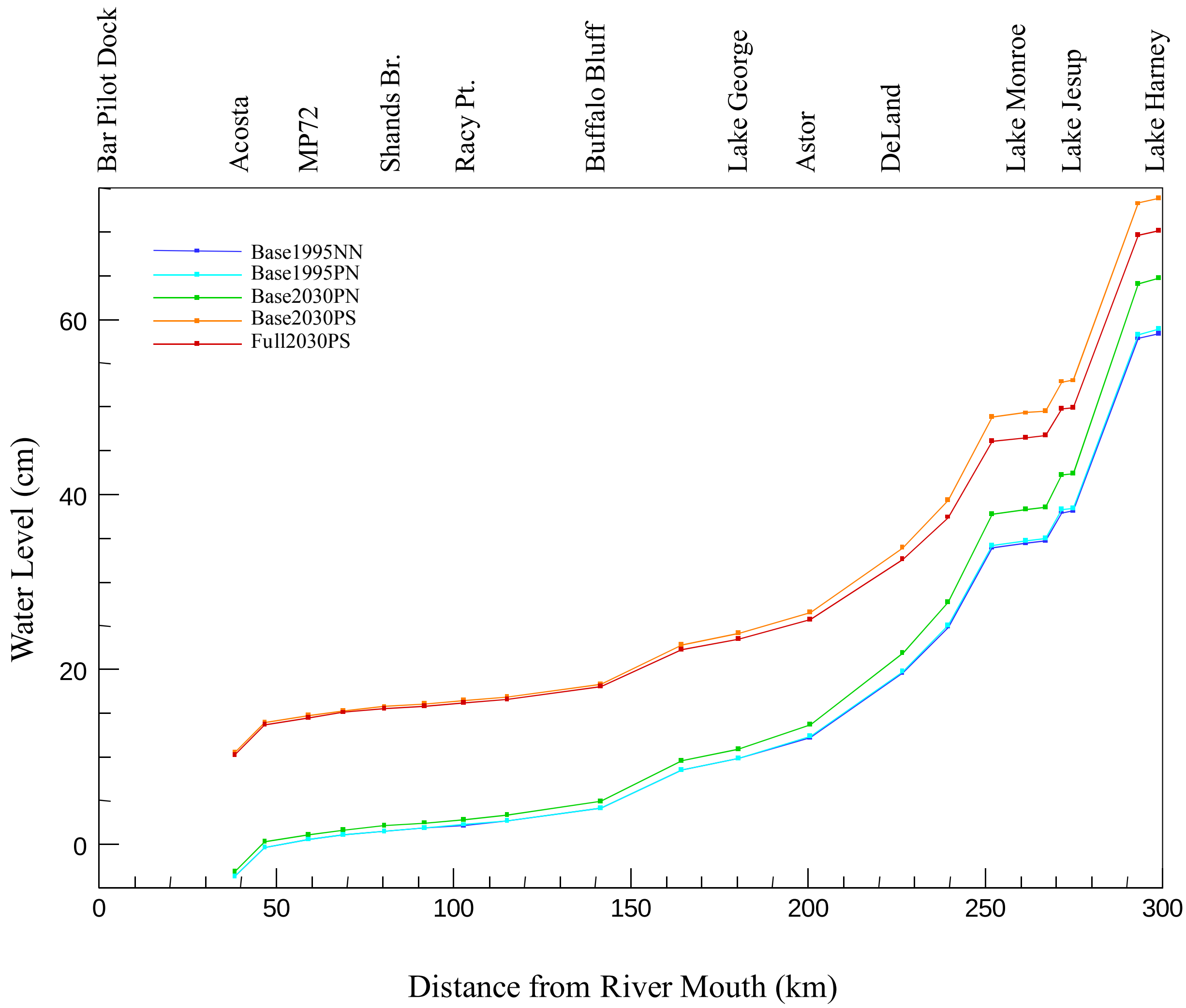

Figure 2–9. Longitudinal plot comparing mean water level for the hindcast scenario (Base1995NN) and selected forecast scenarios. (Water level relative to NAVD88).

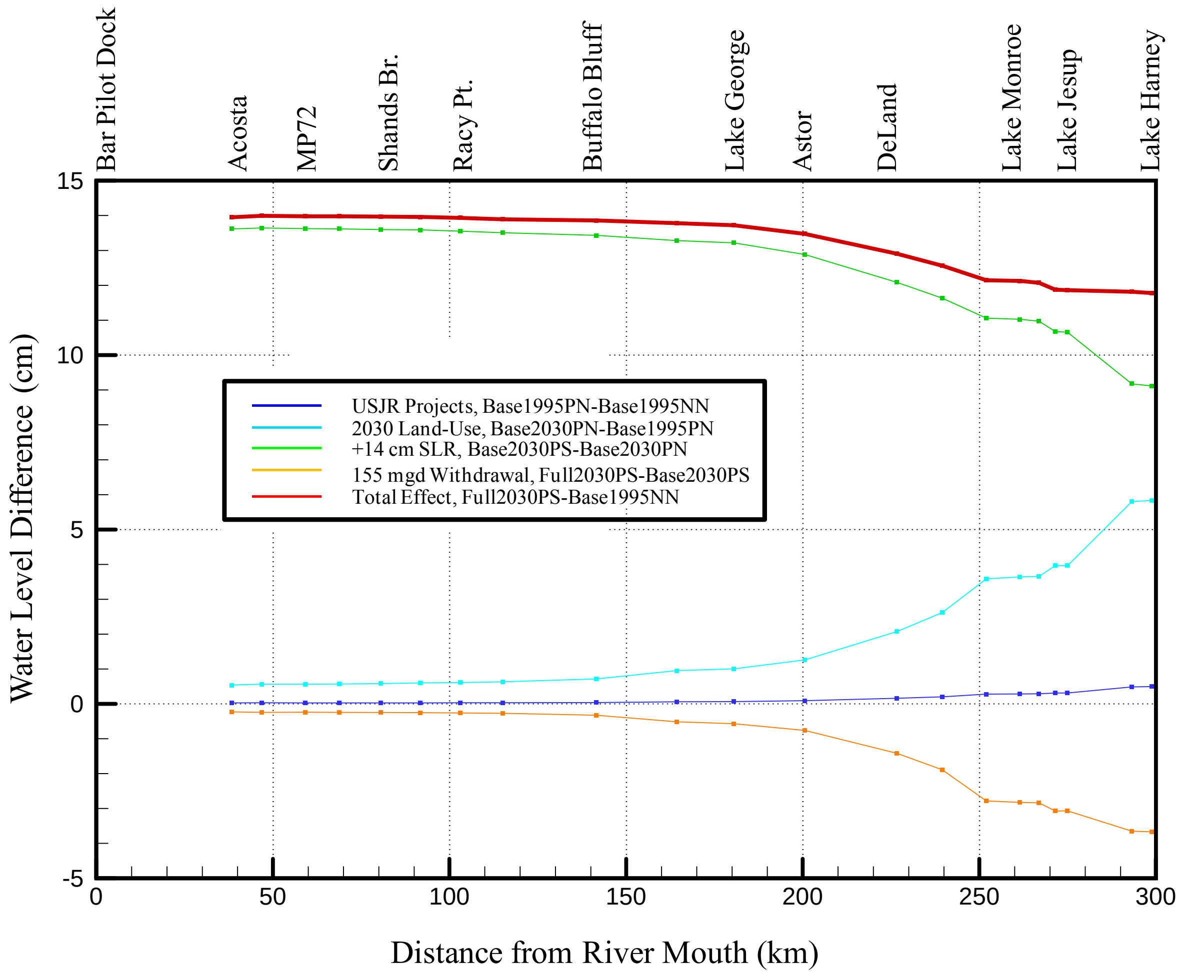

Figure 2–10. Longitudinal plot comparing mean differences in water for the total effect (Full2030PS minus Base1995NN) and individual contributions to the total effect. USJR = upper St. Johns River, SLR = sea level rise.

Discharge Difference Plots

Discharge difference plots for water level differences are shown for Lake Harney. Lake Harney was selected because it is the location in the middle St. Johns River where water level is most affected by water withdrawal. The series of plots show the individual effects of USJRB projects (Figure 2–11), projected 2030 land use (Figure 2–12), sea level rise (Figure 2–13), and a 155-mgd withdrawal (Figure 2–14) relative to the hindcast scenario (Base1995NN). The final plot shows the total effect of all four factors (Figure 2–15).

Water level differences are plotted over a range of monthly discharge at DeLand. Discharge at DeLand serves here as an index for middle St. Johns River discharge.

The USJRB projects cause only slight changes to median water levels (Figure 2–11). Variability of differences about the median is caused by alteration in timing of flows from the USJRB entering Lake Harney. Projected 2030 land use changes (Figure 2–12) increase water levels in Lake Harney with the greatest increases occurring for higher discharges. Sea level rise also increases water level across all discharge levels, but has the greatest effect at low flows (Figure 2–13). Water level reductions caused by a 155-mgd withdrawal (Figure 2–14) are greatest at high discharge and minimal at low discharge because water withdrawals from the USJRB are small or completely shut-off during periods of low flow. The total effect of 2030 conditions is a general increase of water level for all flow conditions compared with the hindcast scenario (Figure 2–15).

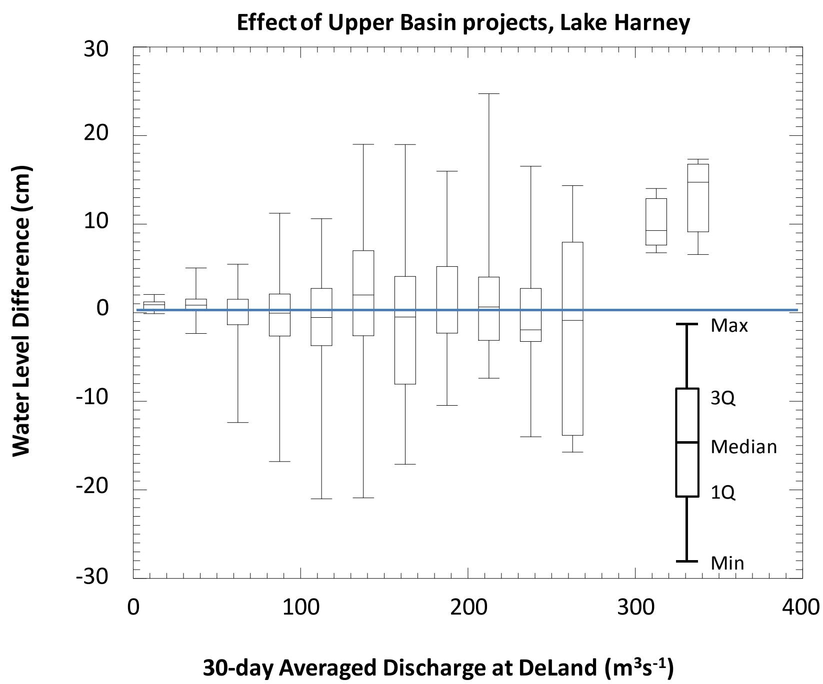

Figure 2–11. Water level differences in Lake Harney caused by USJRB projects for a range of discharge conditions at DeLand.

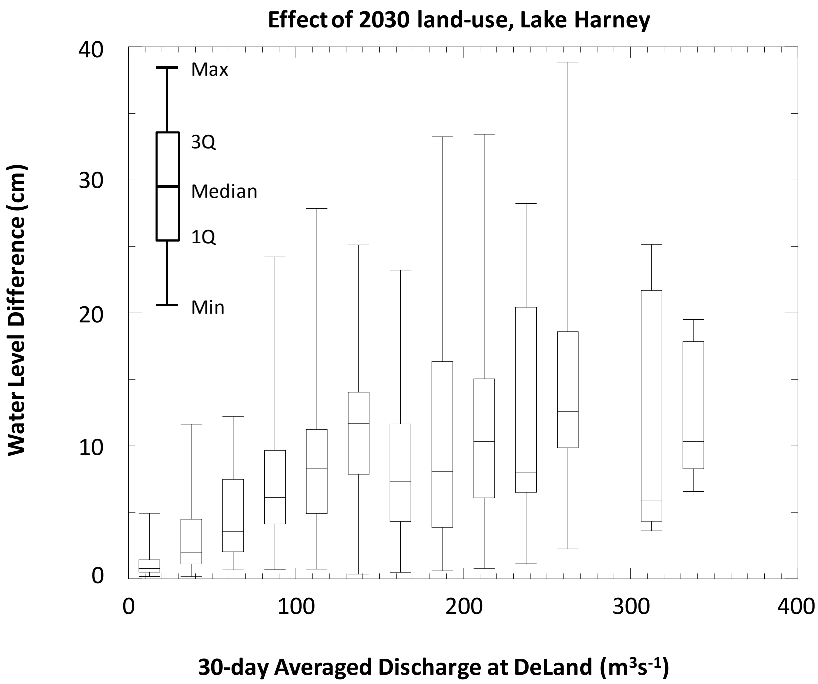

Figure 2–12. Water level differences in Lake Harney caused by projected 2030 land use for a range of discharge conditions at DeLand.

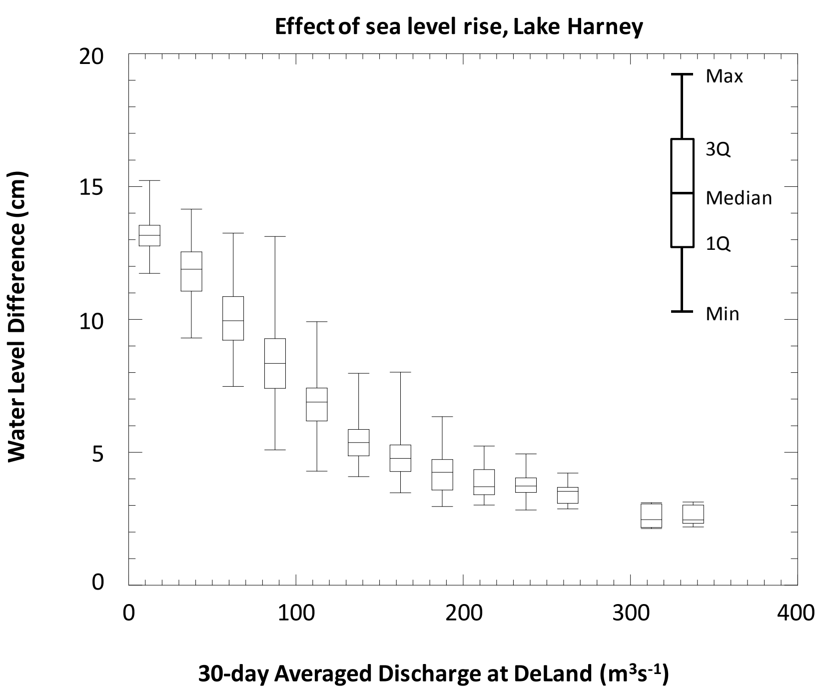

Figure 2–13. Water level differences in Lake Harney caused by sea level rise for a range of discharge conditions at DeLand.

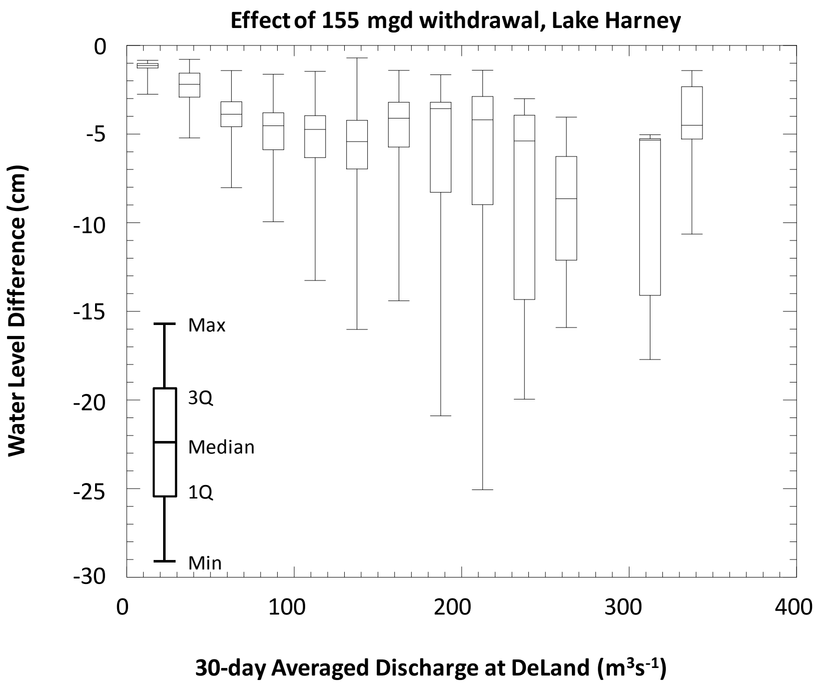

Figure 2–14. Water level differences in Lake Harney caused by a 155-mgd withdrawal for a range of discharge conditions at DeLand.

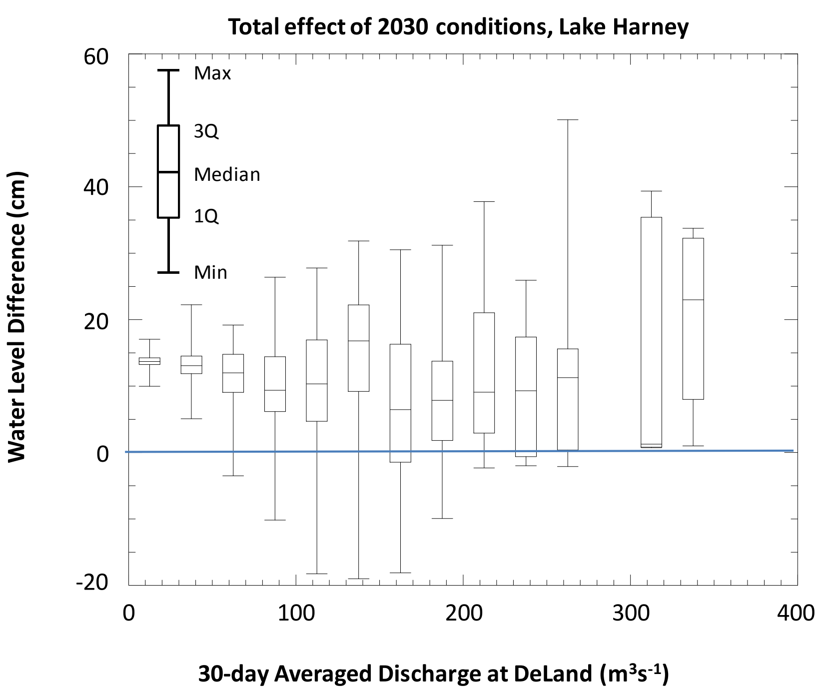

Figure 2–15. Water level differences in Lake Harney for 2030 forecast conditions with a 155-mgd withdrawal (total effect) for a range of discharge conditions at DeLand.

Intensity-Frequency-Duration Plots

Intensity-frequency-duration plots are shown for both high (Figure 2–16) and low (Figure 2–17) water level events in Lake Harney. Within each figure, the top plot shows absolute water level for three model scenarios, and the bottom plot shows water level differences between scenario pairs. The scenarios shown are the hindcast scenario (Base1995NN), and the 2030 forecast condition both with (Full2030PS) and without (Base2030PS) a 155-mgd withdrawal.

For high water level events, the Base2030PS scenario increases the 10-yr flood stage 34 cm for durations less than 5 days compared with the hindcast scenario. The addition of a 155-mgd withdrawal reduces flood stage only 5 cm. The increase in flood stage is caused by an increase in peak storm flows due to urbanization of watersheds. Increased urbanization, then, will likely increase flood stages in the middle St. Johns River. The level of low water level events increases primarily because of sea level rise. Water withdrawals have negligible effect on low water level events.

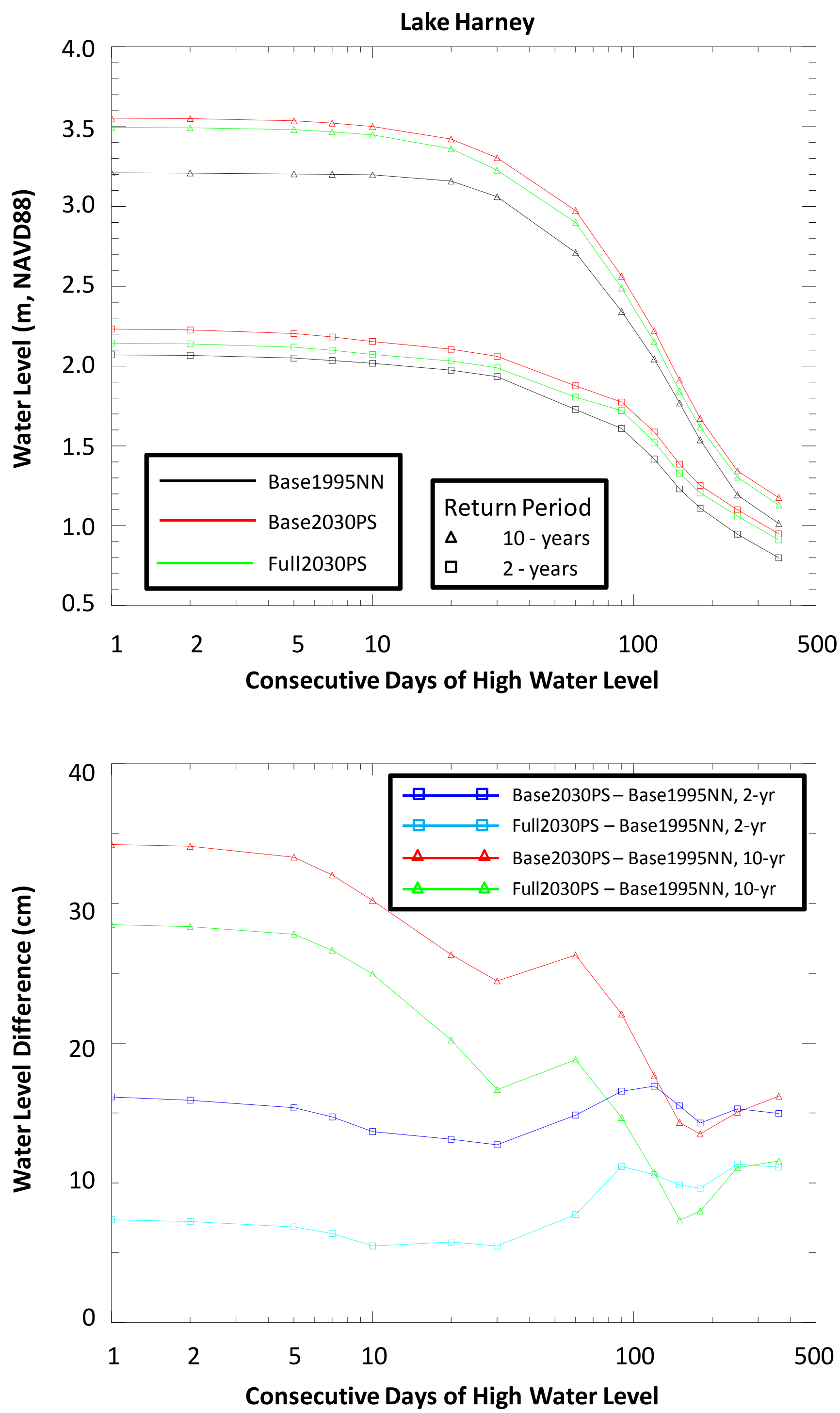

Figure 2–16. High water level duration frequency curves for Lake Harney. Top: water level for base scenario (Base1995NN) using 1995 land use, and projected 2030 land use both with (Full2030PS) and without (Base2030PS) a 155-mgd withdrawal. Bottom: water level differences among scenarios.

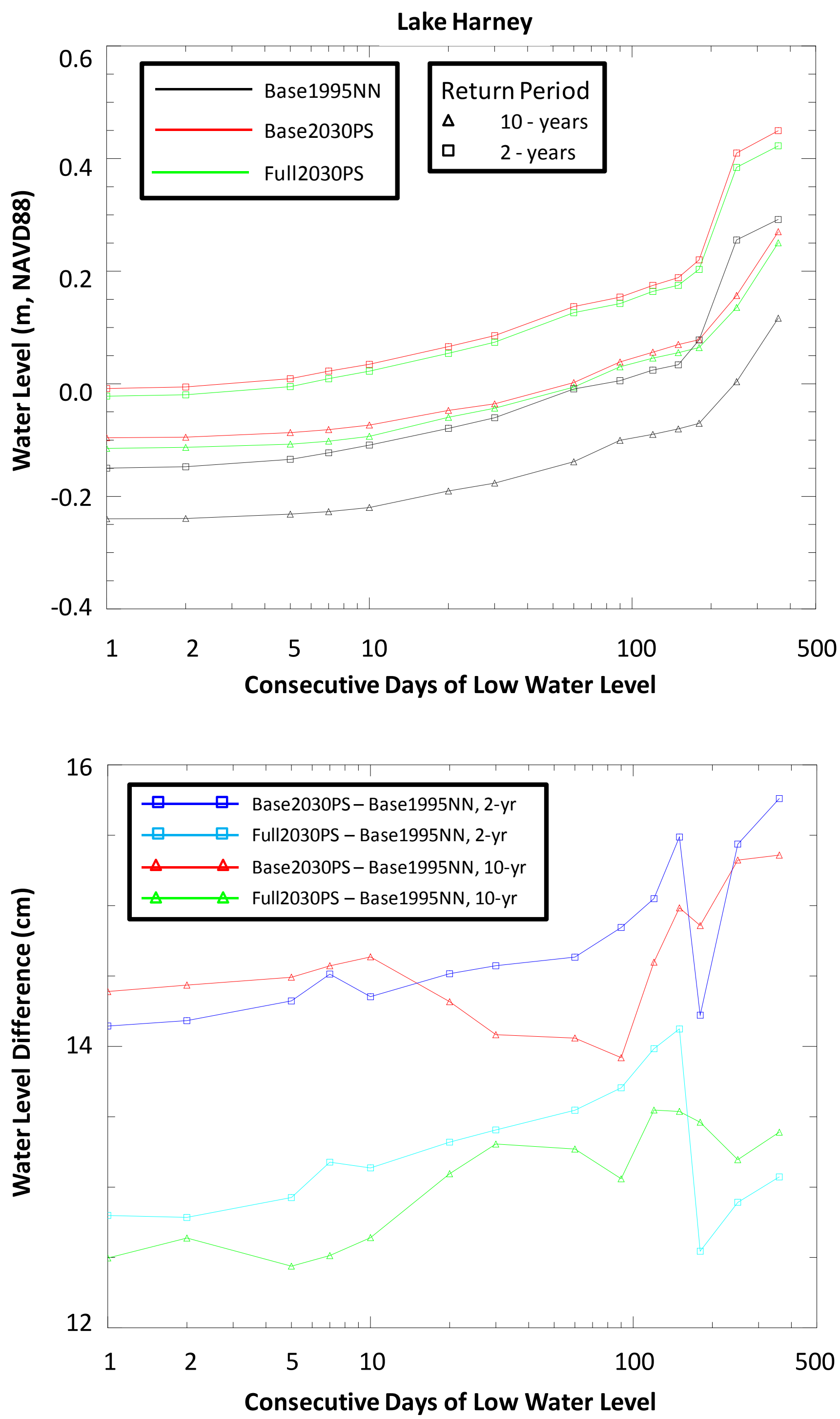

Figure 2–17. Low water level duration frequency curves for Lake Harney. Top: water level for base scenario (Base1995NN) using 1995 land use, and projected 2030 land use both with (Full2030PS) and without (Base2030PS) a 155-mgd withdrawal. Bottom: water level differences among scenarios.

Salinity

Time Series Comparison

Time series of salinity are shown for three representative locations. Shands Bridge (Figure 2–18) is a lower St. Johns River location affected by ocean salinity, Lake George (Figure 2–19) is a lower St. Johns River location upstream of the influence of ocean salinity, and Lake Monroe (Figure 2–20) is a middle St. Johns River location. All three locations show seasonal variability of salinity due to variability of discharge.

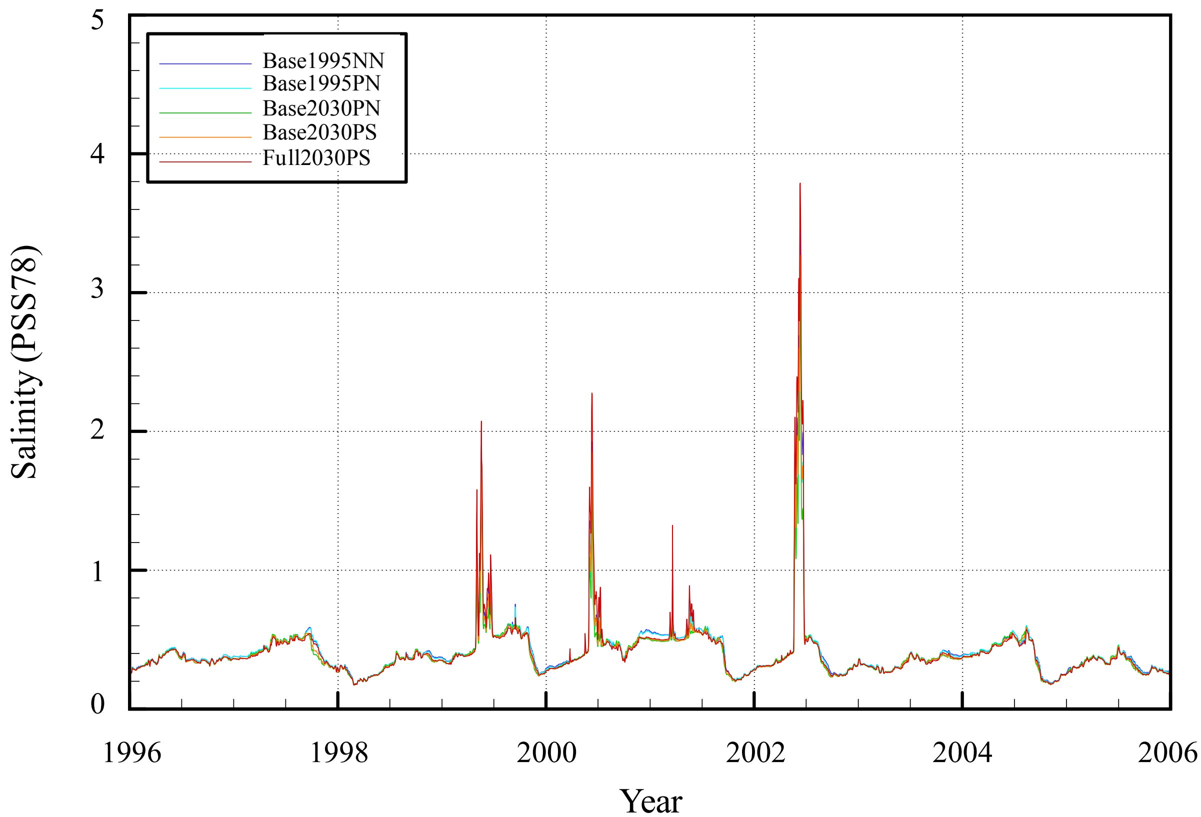

Figure 2–18. Daily averaged salinity at Shands Bridge for the 1995 hindcast scenario (Base1995NN), 1995 conditions with USJRB projects (Base1995PN), and a range of 2030 forecast scenarios.

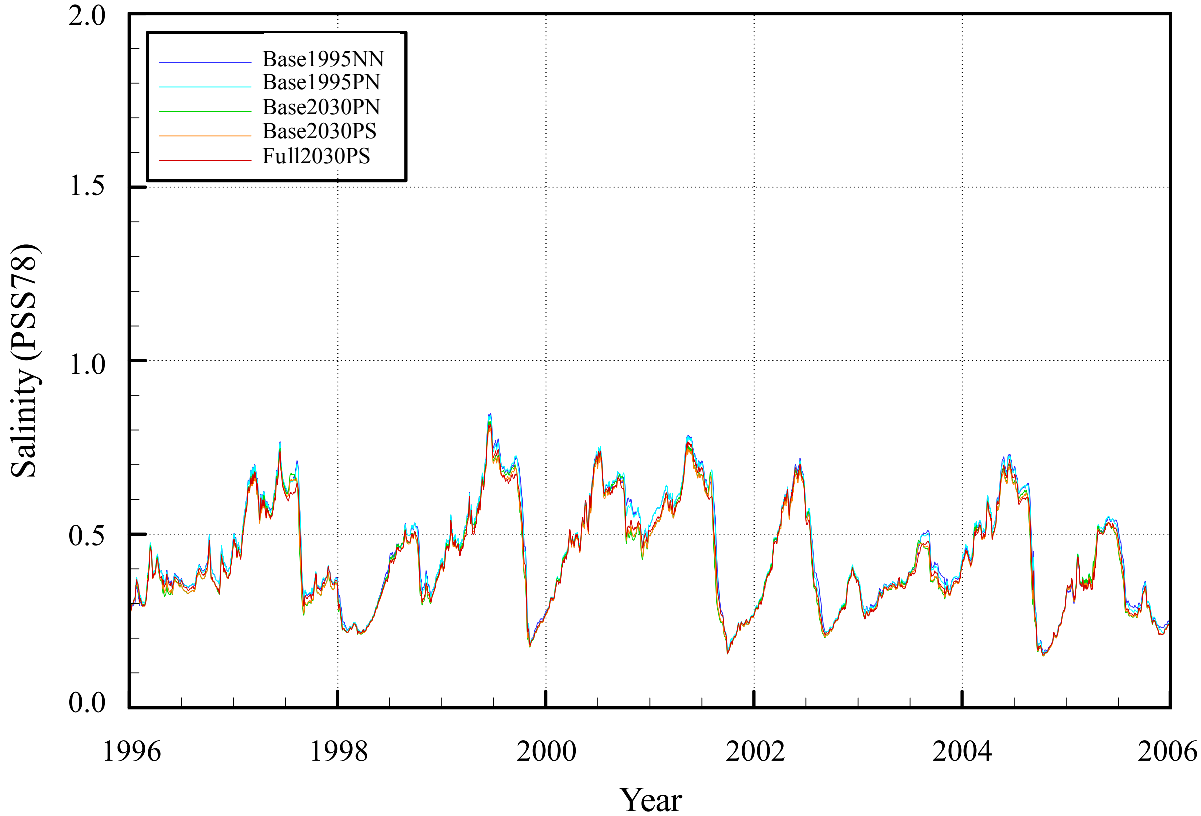

Figure 2–19. Daily averaged salinity in Lake George for the 1995 hindcast scenario (Base1995NN), 1995 conditions with USJRB projects (Base1995PN), and a range of 2030 forecast scenarios.

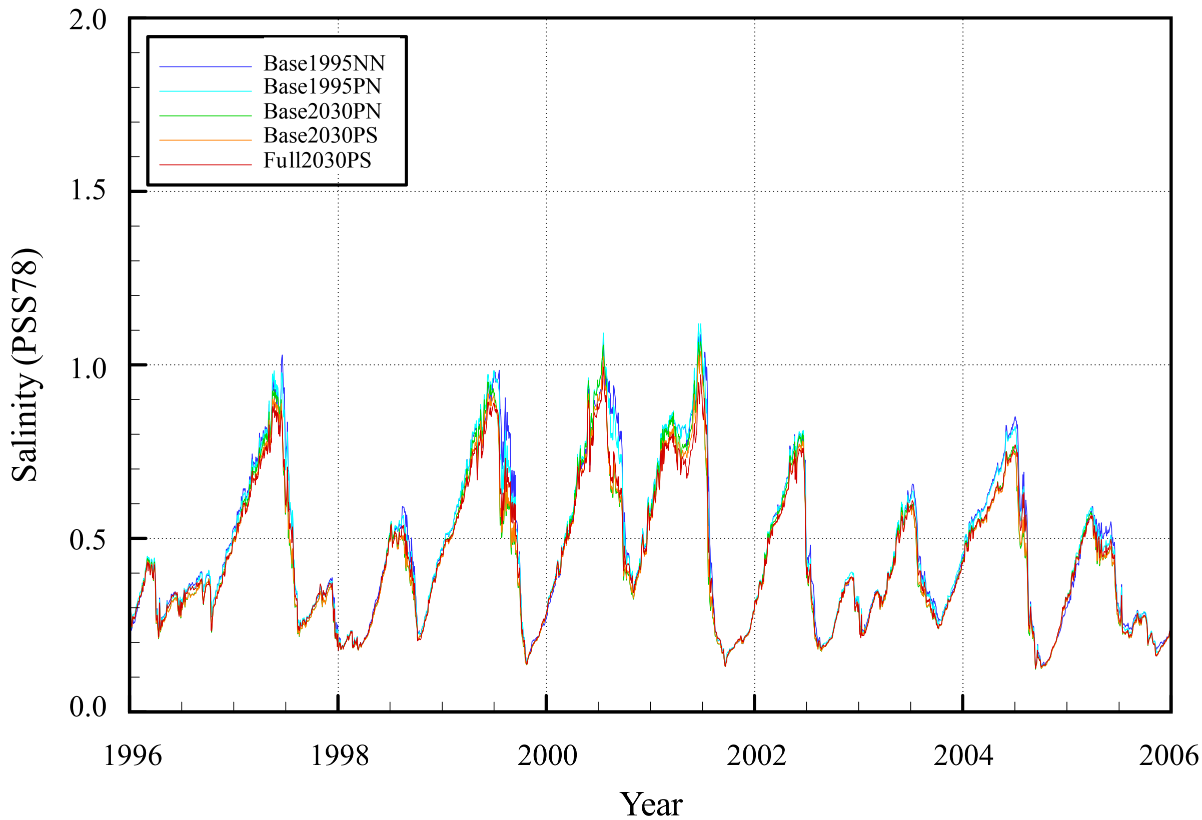

Figure 2–20. Daily averaged salinity in Lake Monroe for the 1995 hindcast scenario (Base1995NN), 1995 conditions with USJRB projects (Base1995PN), and a range of 2030 forecast scenarios.

Salinity differences among scenarios at Shands Bridge (Figure 2–21) show that both sea level rise and water withdrawals increase salinity at Shands Bridge during salinity intrusion events. Increased discharge from USJRB projects and projected 2030 land use decrease salinity at this location. The total effect is an increase in salinity during salinity intrusion events of approximately 0.2 to 0.4 PSS78. Salinity is essentially unchanged during other time periods.

Salinity differences in Lake George (Figure 2–22) and Lake Monroe (Figure 2–23) are minimal for all scenarios. Salinity differences in Lake George are within ±0.1 PSS78. Salinity in Lake Monroe decreases slightly due to water withdrawals during low flow conditions. This decrease occurs because the lowering of discharge by water withdrawals allows for occasional upstream movement of fresher waters from the Wekiva River to influence the northern end of Lake Monroe. The maximum decrease of salinity, however, is small (0.2 PSS78). These plots show that a 155-mgd water withdrawal would only have an appreciable effect on salinity in the estuarine portion of the river.

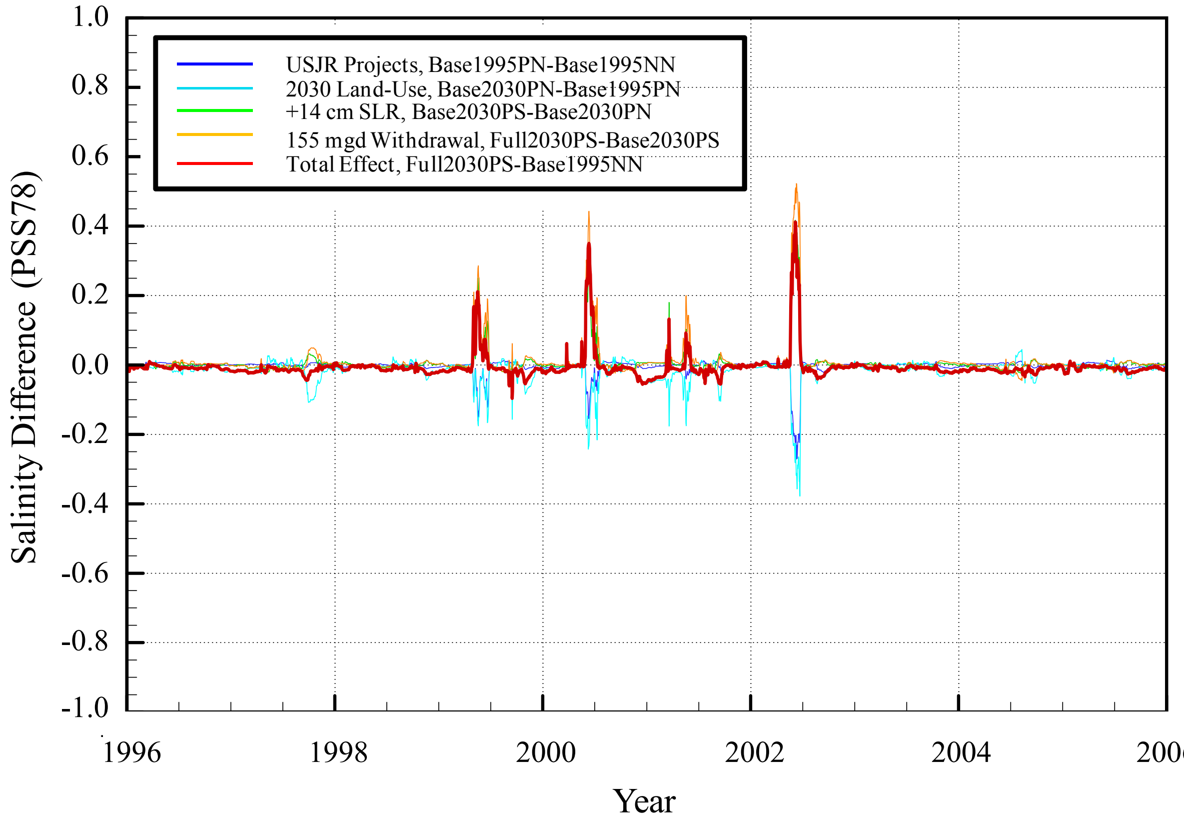

Figure 2–21. Daily averaged differences in salinity at Shands Bridge for the total effect (Full2030PS minus Base1995NN) and individual factors contributing to the total effect. USJR = upper St. Johns River, SLR = sea level rise.

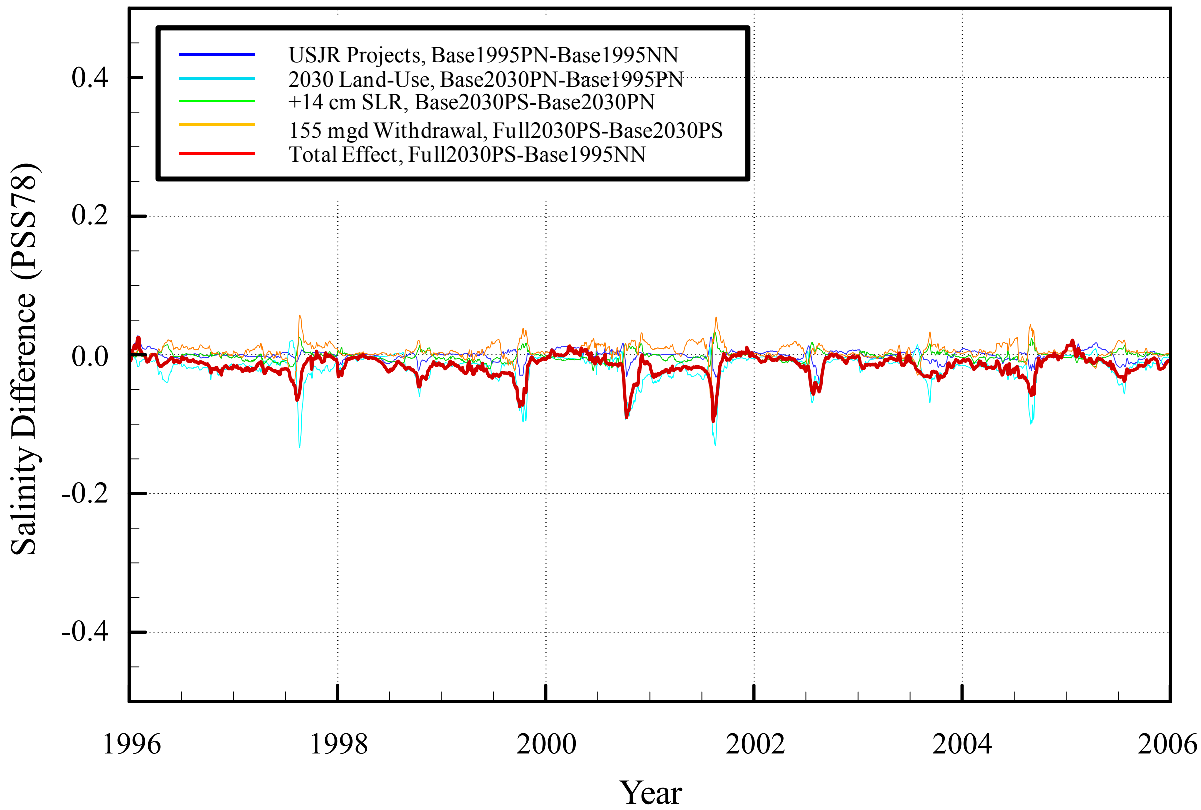

Figure 2–22. Daily averaged differences in salinity in Lake George for the total effect (Full2030PS minus Base1995NN) and individual factors contributing to the total effect. USJR = upper St. Johns River, SLR = sea level rise.

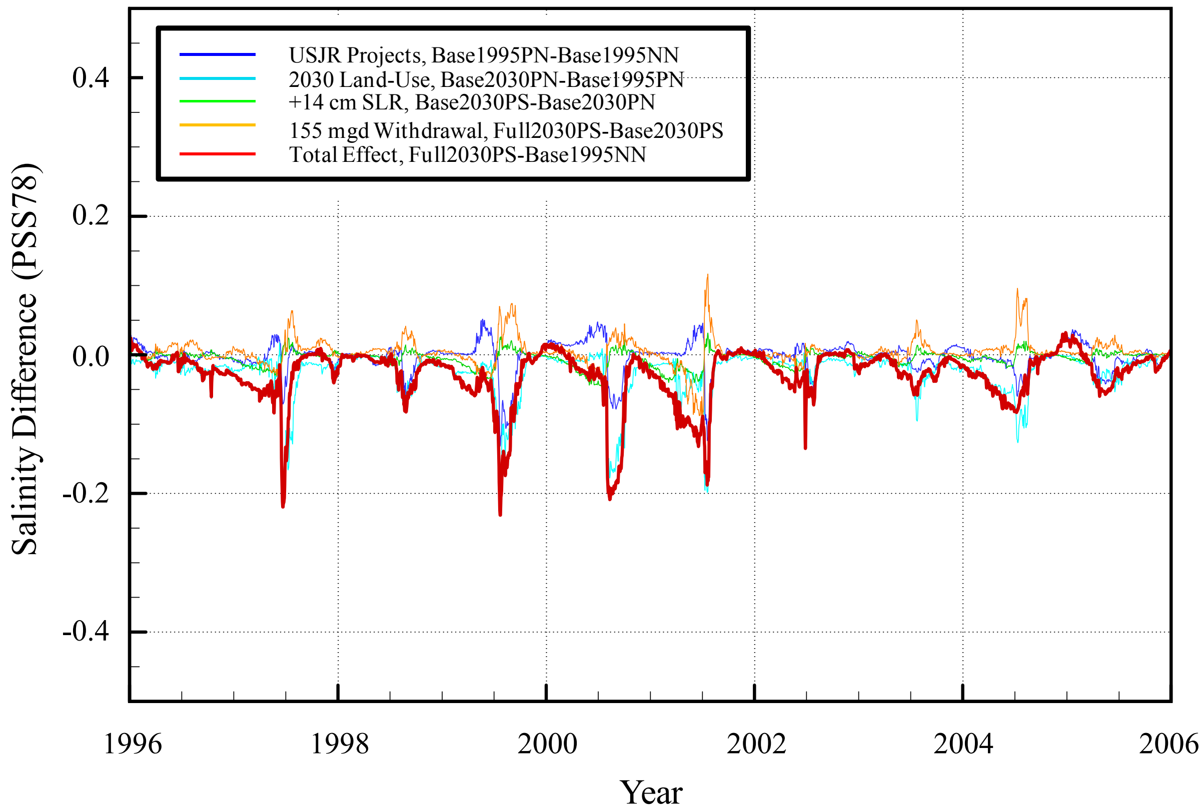

Figure 2–23. Daily averaged differences in salinity in Lake Monroe for the total effect (Full2030PS minus Base1995NN) and individual effects contributing to the total effect. USJR = upper St. Johns River, SLR = sea level rise.

Comparative Statistics

Comparative statistics for differences between the Full2030PS and Base2030PS scenarios isolate the effect of a 155-mgd withdrawal on salinity (Table 2–6). *AVRD* values indicate an increase in mean salinity of 0.01 to 0.3 PSS78 for the stations in the estuarine reach (Shands Bridge, Orange Park, and Acosta). Mean salinity for all areas upstream of Shands Bridge are unaffected by the withdrawal. Salinity differences between Full2030PS and the hindcast scenario (Base1995NN) are quite small (Table 2–7) even in the estuarine reach, with the greatest increase in mean salinity only 0.04 PSS78 at Acosta Bridge.

Table 2–6. Comparative statistics for differences in daily salinity between Full2030PS and Base2030PS.

Station	*NRECS*	r^2	*m*	*b*	*RMSD*	*AVRD*	*AVAD*
Acosta	3,652	0.999	0.970	-0.119	0.372	0.294	0.294
Orange Park	3,652	0.997	0.920	-0.016	0.234	0.118	0.120
Shands Bridge	3,652	0.986	0.814	0.066	0.055	0.010	0.016
Racy Point	3,652	0.990	1.020	-0.008	0.010	0.000	0.007
Buffalo Bluff	3,652	0.990	1.013	-0.006	0.012	0.001	0.008
Lake George	3,652	0.995	0.991	-0.002	0.012	0.005	0.008
DeLand	3,652	0.980	1.018	-0.011	0.023	0.004	0.014
Lake Monroe	3,652	0.992	1.021	-0.013	0.019	0.004	0.011
Lake Jesup	3,652	1.000	0.992	0.003	0.004	0.001	0.003
Lake Harney	3,652	0.989	0.973	-0.002	0.030	0.014	0.018

Note:
NRECS = Number of paired values
r^2 = Coefficient of determination
m = Slope of the linear regression line
b = Intercept of the linear regression line
RMSD = Root-mean-square difference
AVRD = Average relative difference
AVAD = Average absolute difference

Table 2–7. Comparative statistics for differences in daily salinity between Full2030PS and Base1995NN (total effect).

Station	*NRECS*	r^2	*m*	*b*	*RMSD*	*AVRD*	*AVAD*
Acosta	3,652	0.995	1.001	-0.044	0.415	0.036	0.298
Orange Park	3,652	0.993	0.975	-0.001	0.184	0.033	0.097
Shands Bridge	3,652	0.989	0.871	0.058	0.041	-0.005	0.019
Racy Point	3,652	0.990	1.045	-0.004	0.017	-0.013	0.013
Buffalo Bluff	3,652	0.990	1.048	-0.006	0.019	-0.014	0.015
Lake George	3,652	0.992	1.036	0.000	0.021	-0.015	0.016
DeLand	3,652	0.972	1.075	-0.013	0.036	-0.019	0.024
Lake Monroe	3,652	0.982	1.121	-0.025	0.048	-0.029	0.031
Lake Jesup	3,652	0.998	1.098	-0.023	0.032	-0.024	0.024
Lake Harney	3,652	0.979	1.203	-0.057	0.077	-0.038	0.044

NRECS = Number of paired values
r^2 = Coefficient of determination
m = Slope of the linear regression line
b = Intercept of the linear regression line
RMSD = Root-mean-square difference
AVRD = Average relative difference
AVAD = Average absolute difference

Longitudinal Plots

A longitudinal plot for mean salinity is shown in Figure 2–24. The plot is split into two sections to show salinity above and below Racy Point at different vertical scales. Salinity below Racy Point increases slightly between the Full2030PS and Base 1995NN scenarios, while salinity above Racy Point decreases slightly.

The individual factors contributing to the total salinity difference between these two scenarios are clearly shown in the accompanying longitudinal difference plot (Figure 2–25). The longitudinal difference plot shows that increased runoff due to projected 2030 land use (cyan line) is the principle factor reducing salinity in the middle St. Johns River. Projected 2030 land use has an even greater effect in the lower St. Johns River with reductions in mean salinity of up to 0.5 PSS78 at Acosta Bridge. Both sea level rise and water withdrawal increase salinity in the lower St. Johns River, however, resulting in an opposing effect on salinity between 2030 land use and the combination of sea level rise and water withdrawal. The total effect of all factors combined is a net increase in salinity for the Full2030PS scenario of only 0.05 PSS78 compared with the Base1995NN scenario.

Because water withdrawal effects on salinity are only appreciable in the estuarine zone, a longitudinal difference plot is shown for areas below Racy Point (Figure 2–26). The greatest increase in salinity due to a 155-mgd withdrawal (green line) occurs near river km 20. Sea level rise has a nearly equivalent effect on mean salinity as the withdrawal. These two factors are offset by projected 2030 land use; therefore, the total effect on mean salinity for 2030 conditions is negligible.

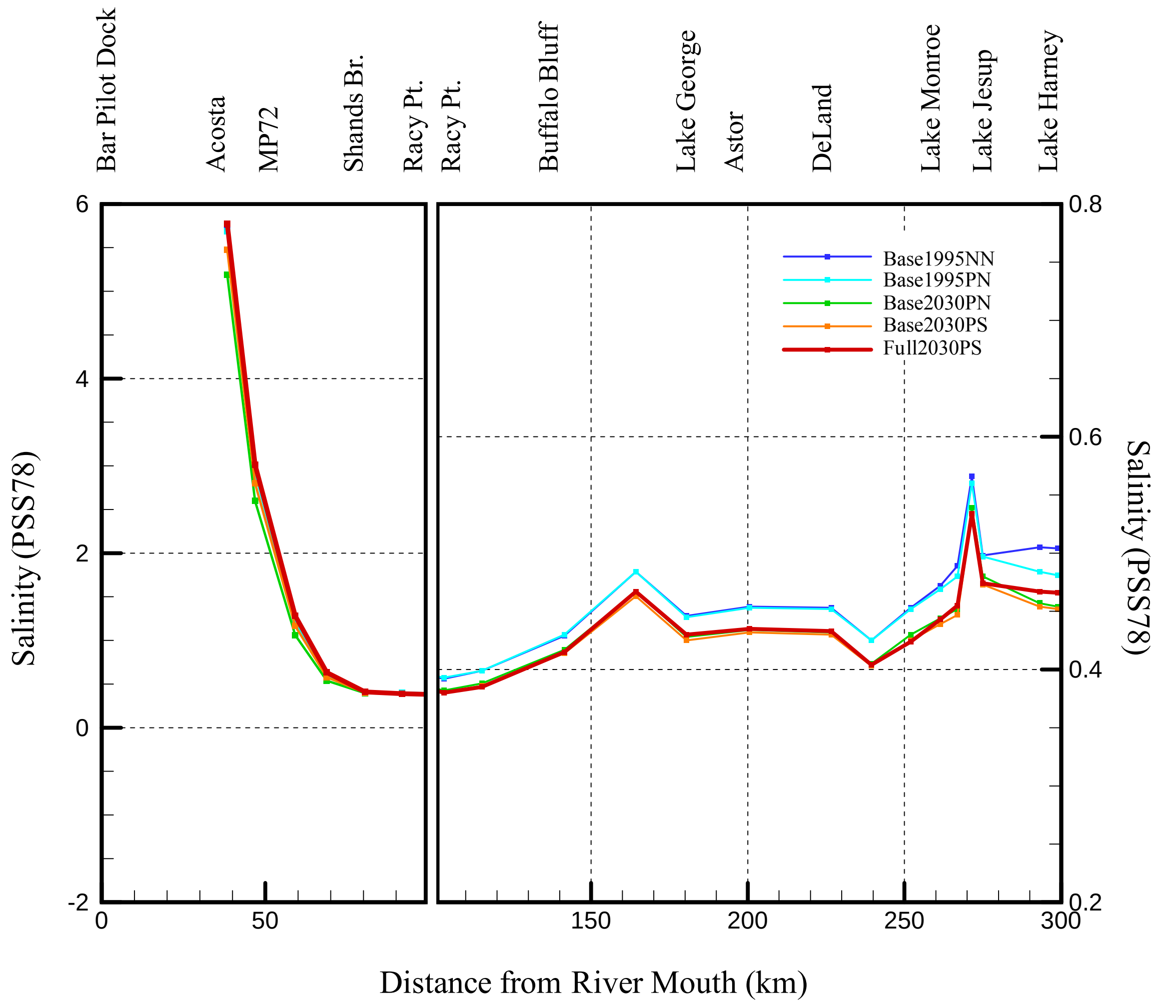

Figure 2–24. Longitudinal plot comparing mean salinity for the hindcast scenario (Base1995NN) and selected forecast scenarios.

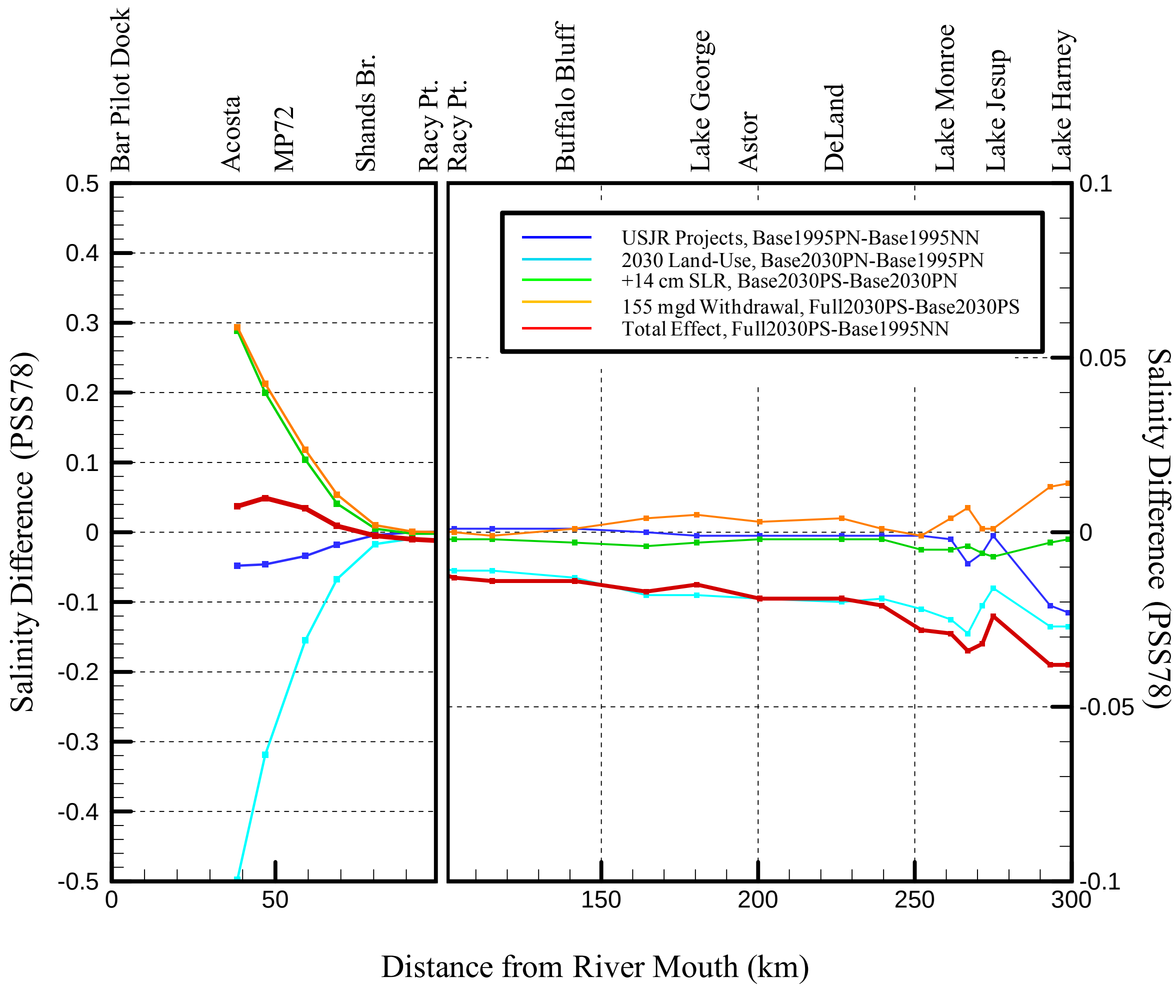

Figure 2–25. Longitudinal plot comparing mean differences in salinity for the total effect (Full2030PS minus Base1995NN) and individual effects contributing to the total effect. USJR = upper St. Johns River, SLR = sea level rise.

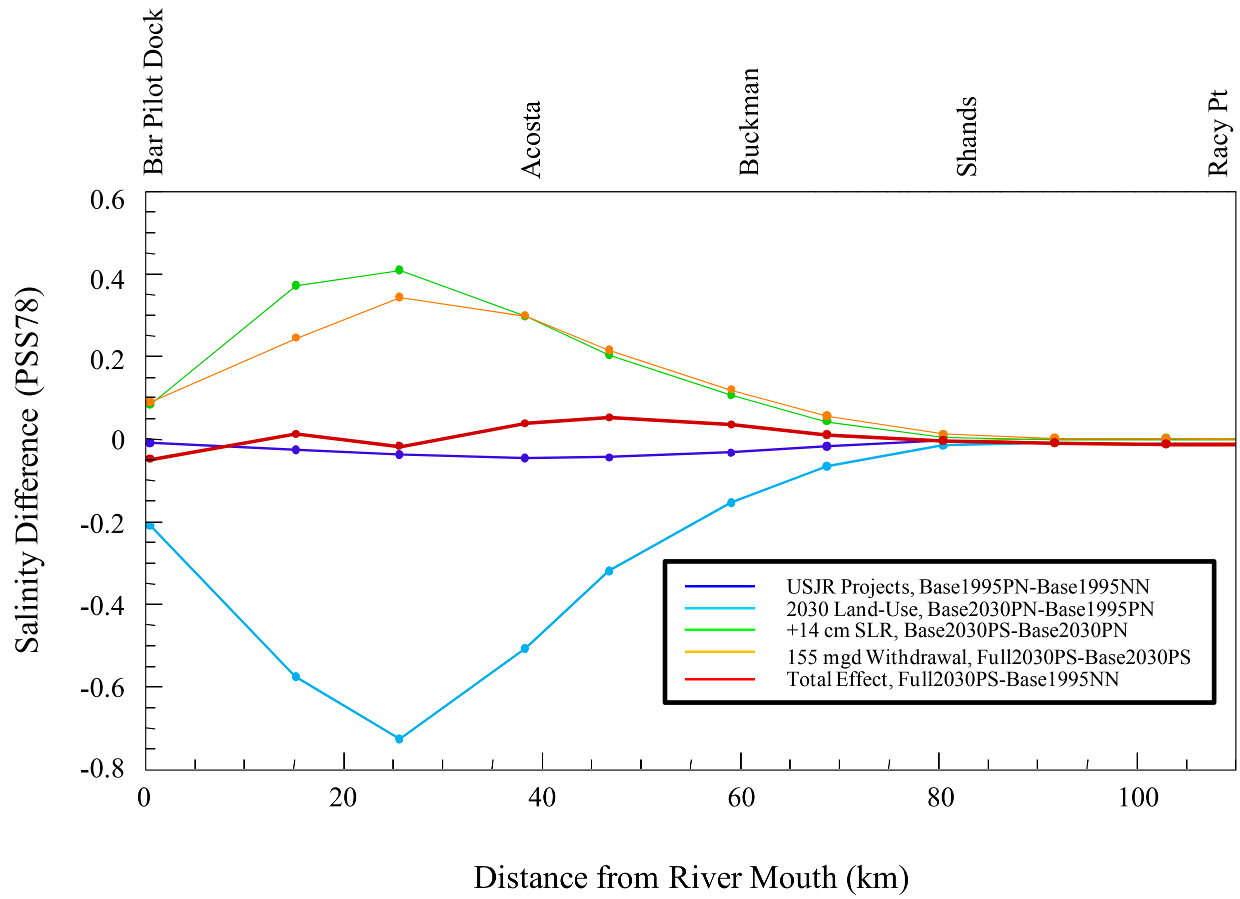

Figure 2–26. Longitudinal plot comparing mean differences in salinity for the total effect (Full2030PS minus Base1995NN) and individual effects contributing to the total effect for the estuarine reach below Racy Point. USJR = upper St. Johns River, SLR = sea level rise.

Contour Plots

Color contours of mean salinity differences for the forecast scenarios visually show the spatial distribution of salinity differences throughout the model area (Figure 2–27). The plot shows that the greatest changes to individual factors consistently occur in the estuarine zone downstream of Doctors Lake. The total effect on salinity for 2030 conditions is negligible.

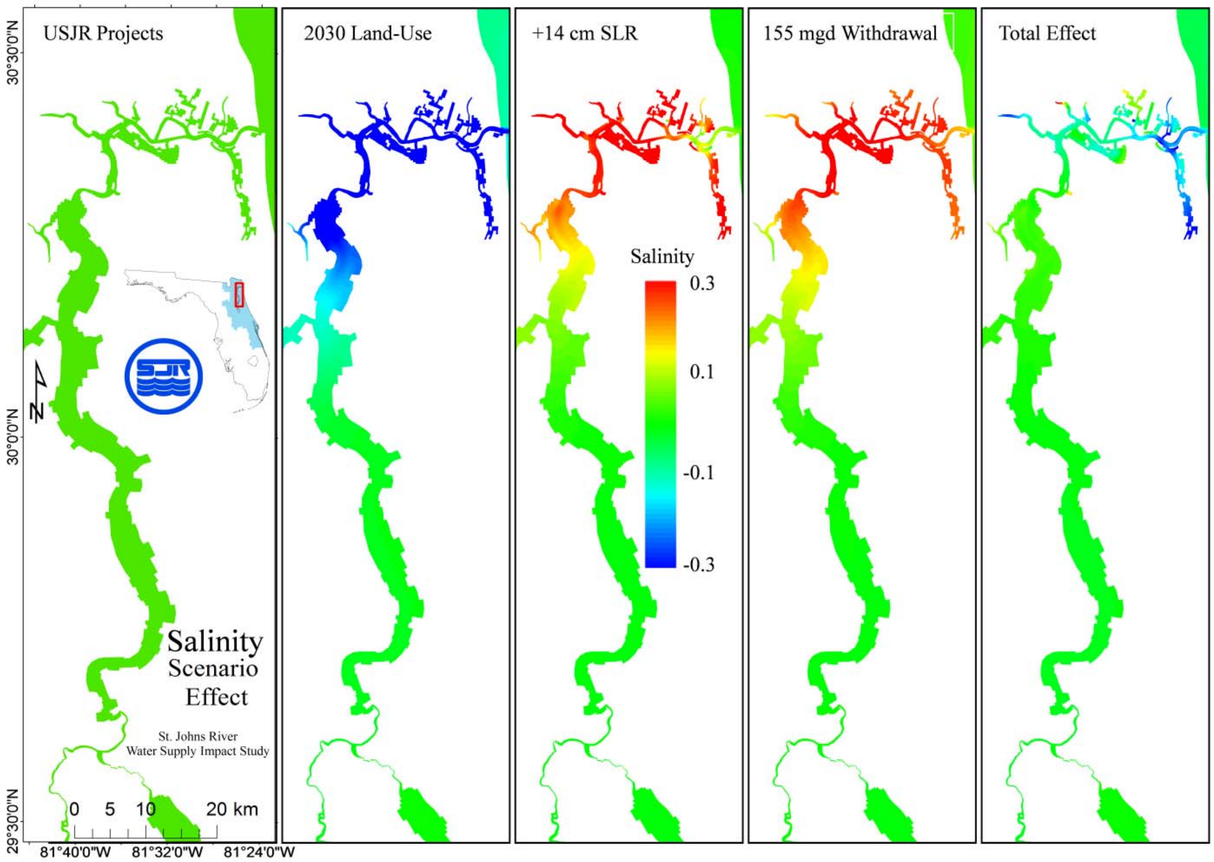

Figure 2–27. Contour plots of mean difference in salinity for the total effect (Full2030PS minus Base1995NN) and individual effects contributing to the total effect. USJR = upper St. Johns River, SLR = sea level rise.

The river reach between Acosta Bridge and Shands Bridge is an area of transition between ocean-influenced salinity and fresher river waters. Environmental analyses of salinity effects on biota tended to focus on salinity alterations in this reach. The following plot (Figure 2–28) shows the position of the 1, 3, 5, and 7 PSS78 salinity contour for the hindcast scenario (Base1995NN) and selected forecast scenarios. Contours for the hindcast scenario (dark blue) and Full2030PS scenario (red line, total effect) are nearly coincident.

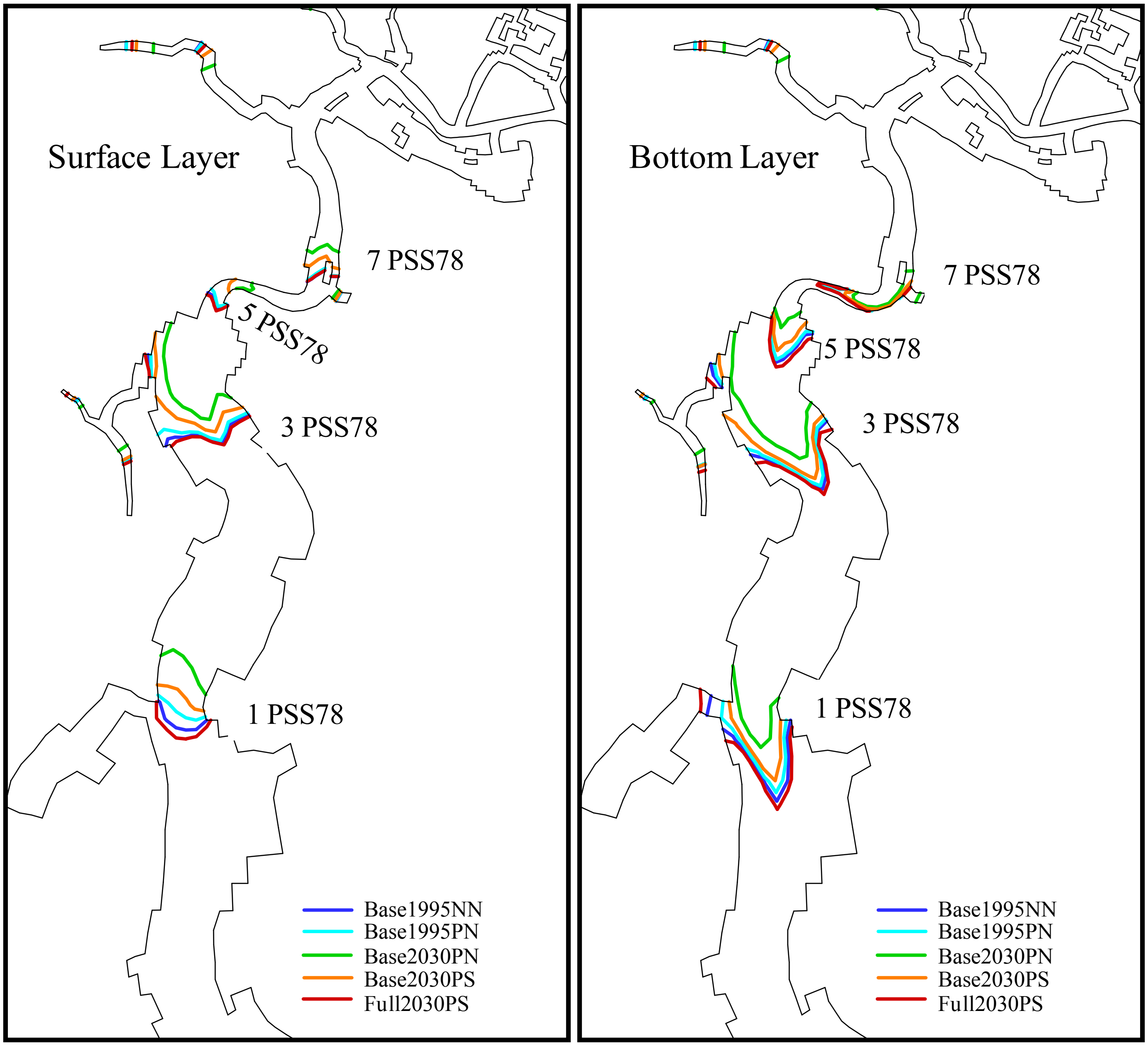

Figure 2–28. Contour plot showing the shift of the 1, 3, 5, and 7 PSS78 salinity contours in the lower St. Johns River between Acosta and Shands bridges for the hindcast scenario (Base1995NN) and selected forecast scenarios. Full2030PS represents the total effect.

Discharge Difference Plots

Discharge difference plots for salinity are shown below at Station MP72 for two scenario pairs. Station MP72 is located at river km 58 near Buckman Bridge. Salinity differences between the Full2030PS and Base2030PS scenarios isolate the effect of a 155-mgd withdrawal (Figure 2–29). Salinity differences between Full2030PS and Base1995NN show the total effect for salinity between the hindcast scenario and 2030 conditions with a 155-mgd withdrawal (Figure 2–30).

Monthly averaged discharge at Buffalo Bluff is used as an index for lower St. Johns River discharge.

Salinity increases caused by water withdrawals are most likely when Buffalo Bluff discharge is less than about 2,300 mgd (100 m^3s^{-1}). An increase in median salinity of 0.55 PSS78 occurs during low flow conditions. Salinity differences are not large, however. Single day salinity differences never exceeded 1 PSS78 over the 10-yr simulation period.

Salinity differences under projected 2030 conditions show the compensating effects of increased discharge from 2030 land use relative to a 155-mgd withdrawal (Figure 2–30). Salinity differences for the lowest flow conditions are similar to those shown for the 155-mgd withdrawal alone. This result shows that although mean salinity differences for the Full2030PS scenario are nearly unchanged from the Base1995NN scenario, salinity levels increase about 0.5 PSS78 under low flow conditions.

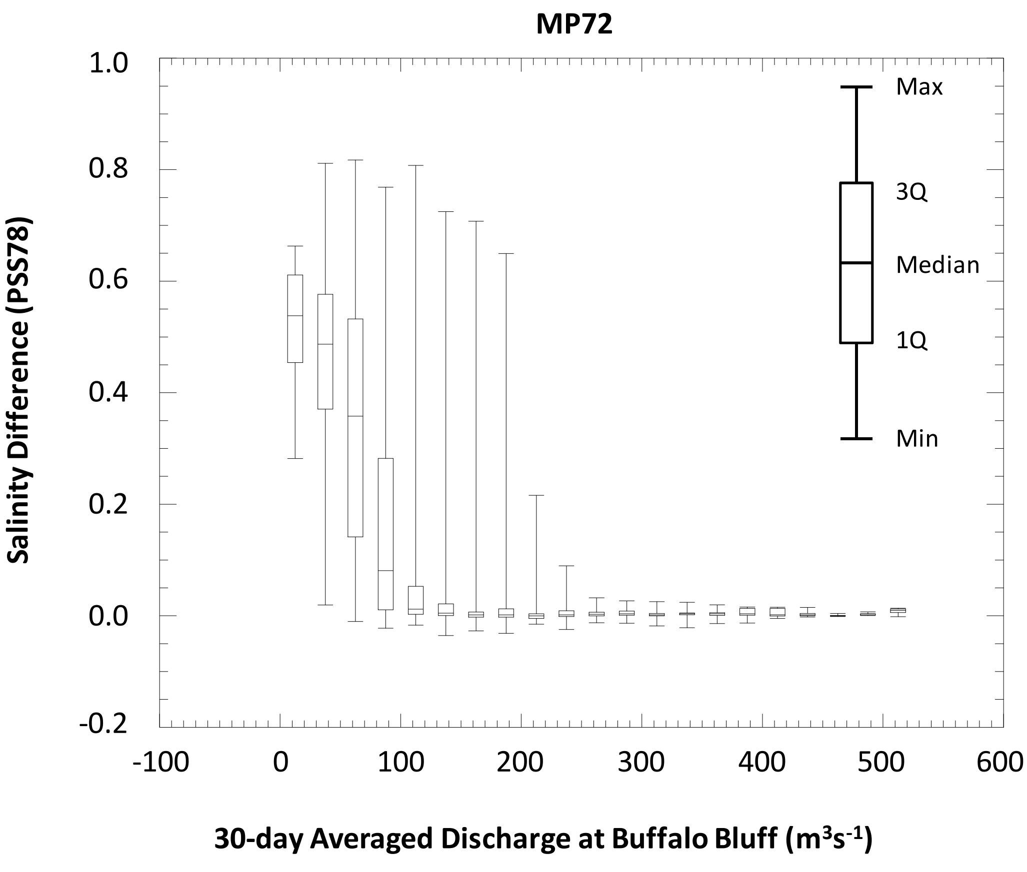

Figure 2–29. Salinity differences at station MP72 caused by 155-mgd withdrawal scenario compared with 30-day averaged discharge at Buffalo Bluff.

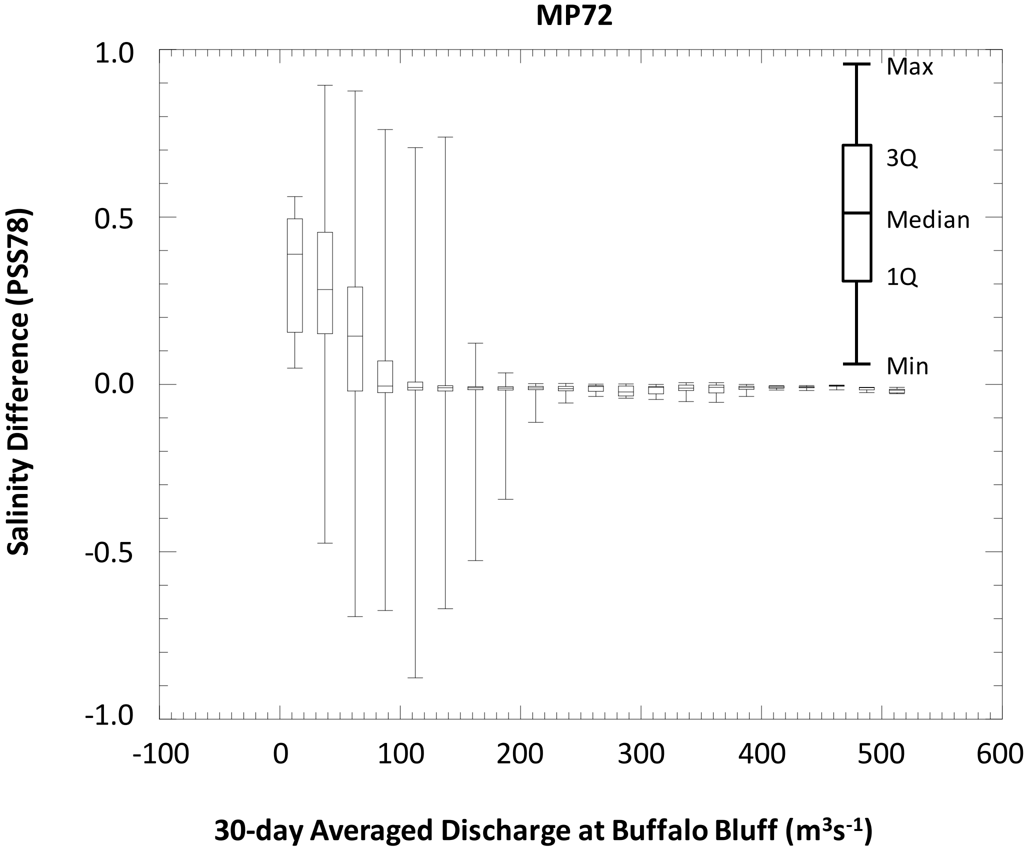

Figure 2–30. Salinity differences at station MP72 between the Full2030PS and Base1995NN scenarios (total effect) compared with 30-day averaged discharge at Buffalo Bluff.

Intensity-Frequency-Duration Plots

Intensity-frequency-duration plots are shown below for high salinity events at Shands Bridge in the lower St. Johns River (Figure 2–31). The 2-yr maximum salinity event remains fresh at this location, showing that ocean intrusion of salinity reaches this location infrequently. The 10-yr maximum 1-day salinity event for the hindcast scenario is 3.5 PSS78. This event increases about 0.3 PSS78 for the Full2030PS scenario (green line, bottom plot, total effect). This level of salinity increase is nearly identical for durations of 1 to 30 days. The uniformity of salinity change over a wide range of durations indicates that there were no conditions over the 10-yr simulation period that produced any unusual or anomalous salinity events.

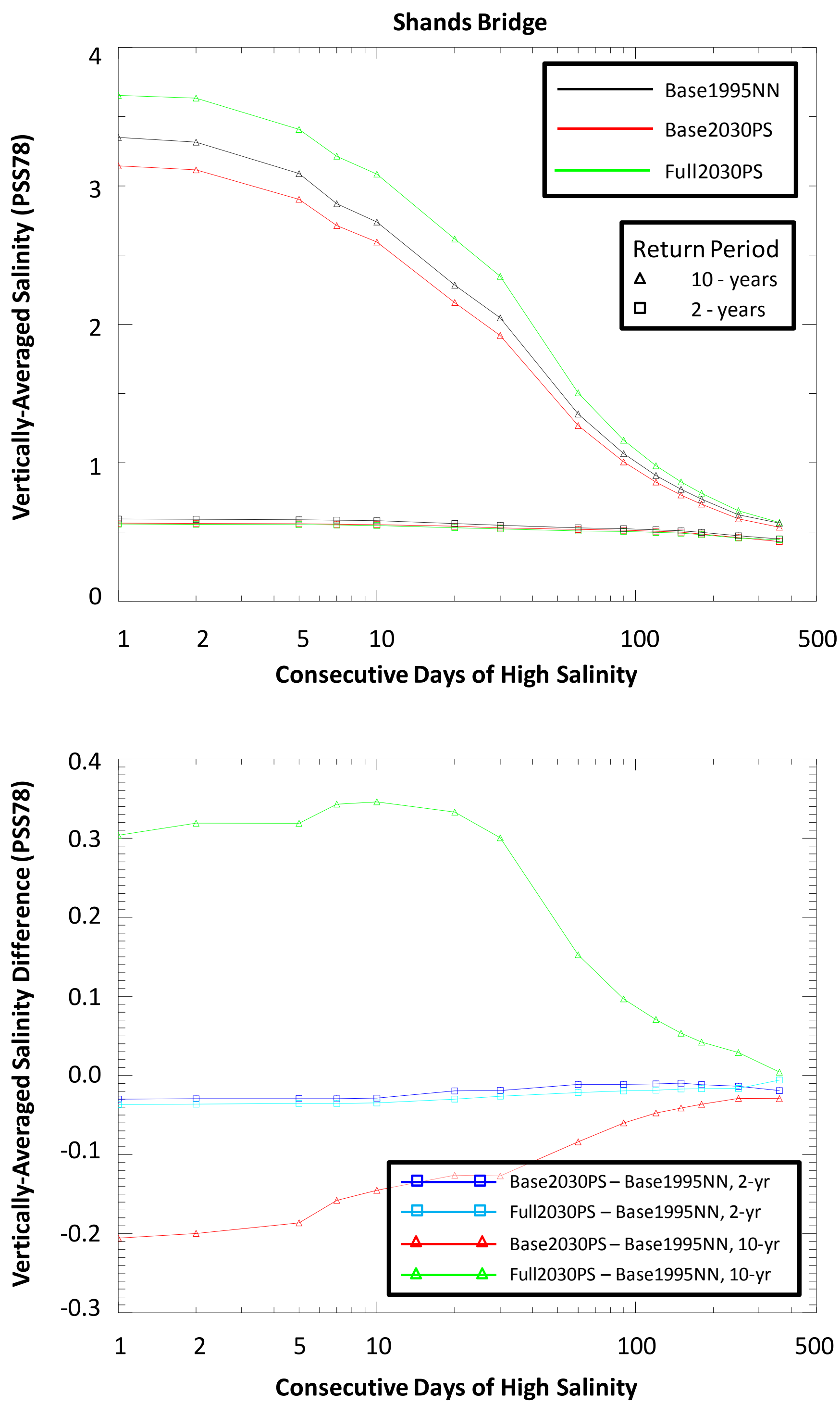

Figure 2–31. High salinity duration frequency curves for Shands Bridge. Top: salinity for base scenario (Base1995NN), and projected 2030 land use both with (Full2030PS) and without (Base2030PS) a 155-mgd withdrawal. Bottom: salinity differences between scenarios.

<u>Water Age</u>

Time Series Comparisons

Daily time series of water age for Lake George (Figure 2–32) and Lake Monroe for the hindcast scenario (Base1995NN) and selected future scenarios (Figure 2–33) are shown below. Water age is inversely related to discharge and maximum water ages occur during periods of low flow. Differences in water ages among scenarios are generally greatest when water ages are high, discharge is low, and local conditions can exert the greatest effect on water age.

Water ages generally increase from upstream to downstream as waters age during transit. Water age can also be diluted during transit, however, and dilution is particularly evident at the confluences of the St. Johns River with the Wekiva and Ocklawaha rivers.

The variability of water age is large at all locations, ranging from 20 to 200 days in Lake George and 10 to 150 days in Lake Monroe.

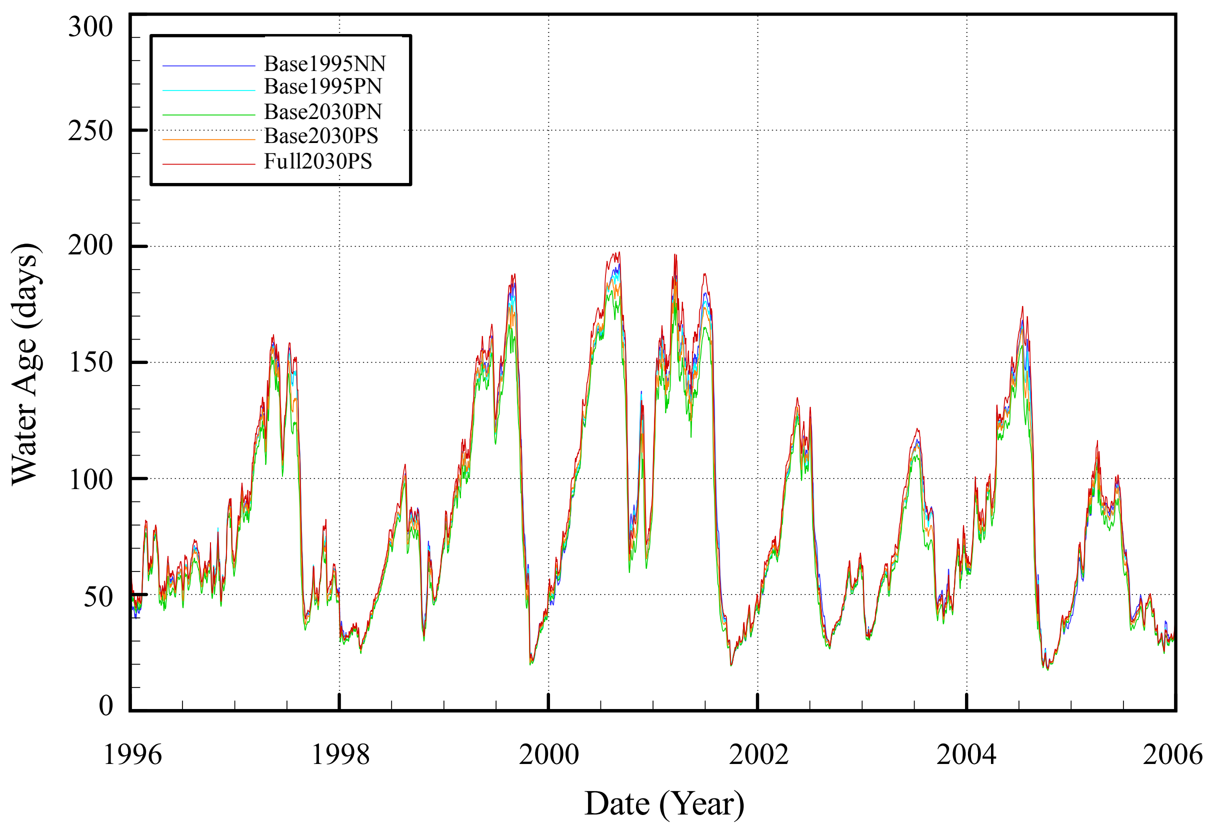

Figure 2–32. Daily averaged water age in Lake George for the hindcast scenario (Base1995NN) and selected forecast scenarios.

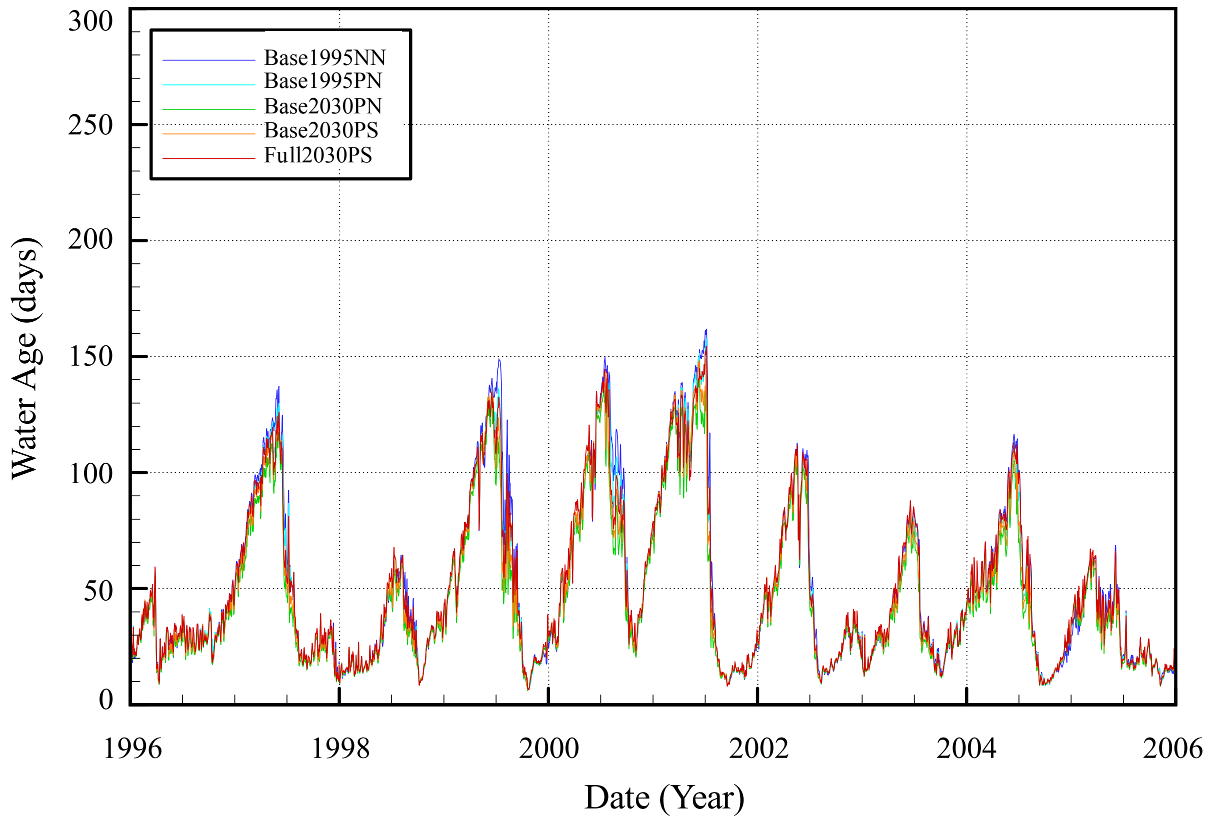

Figure 2–33. Daily averaged water age in Lake Monroe for the hindcast scenario (Base1995NN) and selected forecast scenarios.

Water age differences between forecast scenarios and the hindcast scenario (Base1995NN) show that projected 2030 land use changes (cyan line) notably decrease water age in Lake George (Figure 2–34), and Lake Monroe (Figure 2–35). Sea level rise increases water age at both locations (green line), and the magnitude of the increase in water age is similar. Water withdrawal (orange line) increases water age similarly at both locations. Change in water age due to water withdrawals is most pronounced during periods of low flow.

The total effect (Full2030PS minus Base1995NN) generally results in increased water age in Lake George, with maximum increases of about 10 days. In contrast, water age in Lake Monroe occasionally increases, also up to 10 days, but exhibits frequent periods when water age is reduced by 20 to 40 days.

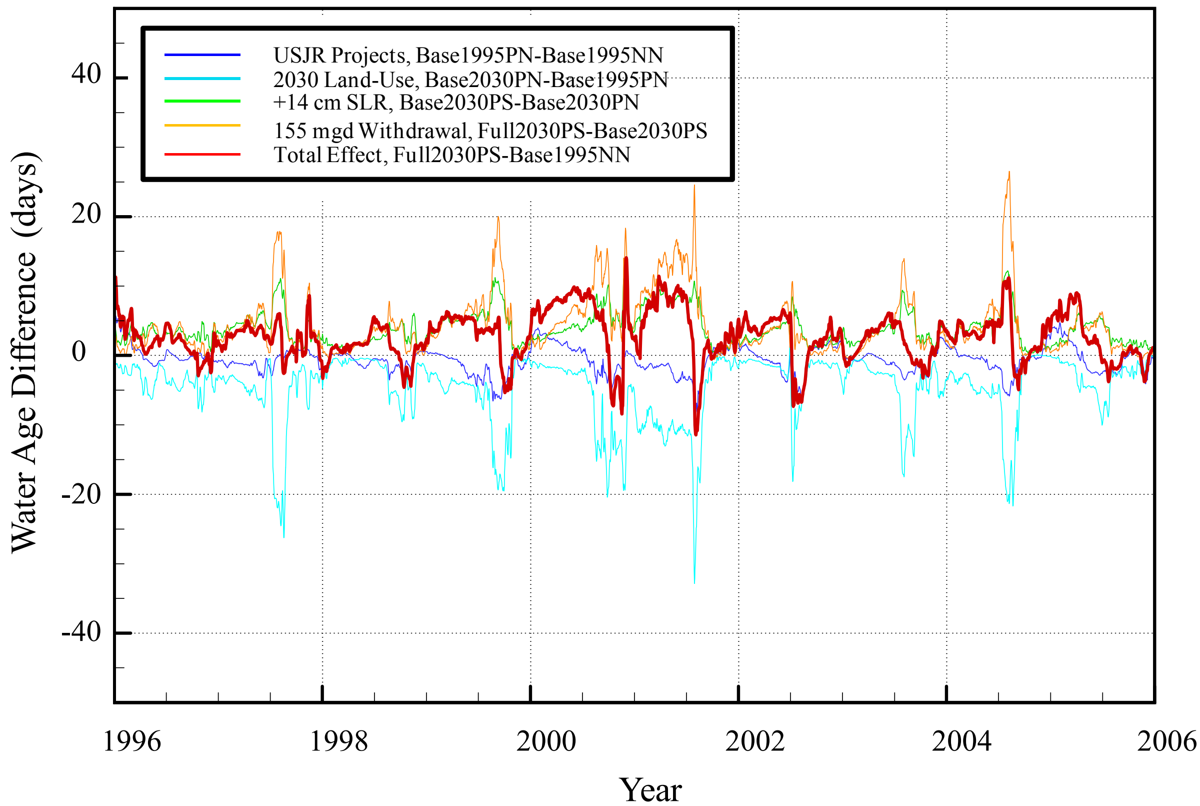

Figure 2–34. Daily averaged differences in water age in Lake George for the total effect (Full2030PS minus Base1995NN) and individual factors contributing to the total effect. USJR = upper St. Johns River, SLR = sea level rise.

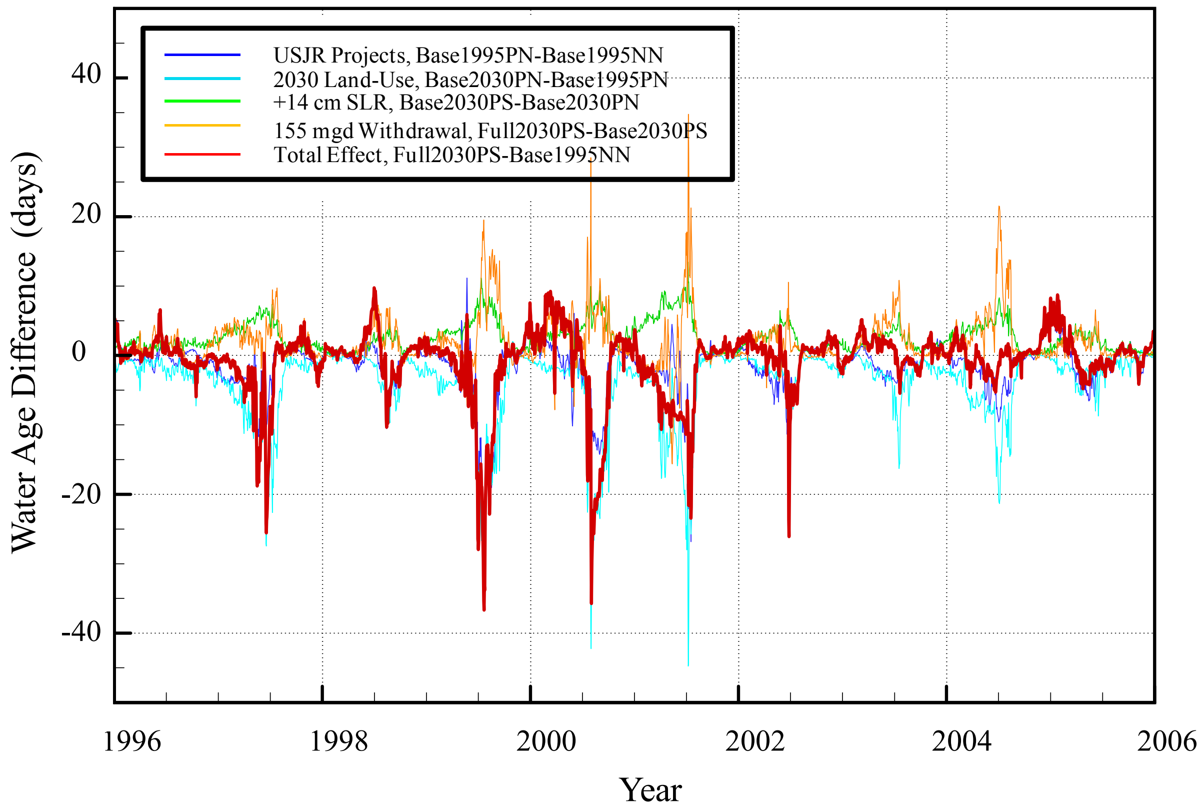

Figure 2–35. Daily averaged differences in water age in Lake Monroe for the total effect (Full2030PS minus Base1995NN) and individual factors contributing to the total effect. USJR = upper St. Johns River, SLR = sea level rise.

Comparative Statistics

Comparative statistics for daily averaged water age are provided here for two sets of scenario differences. Differences between Full2030PS and Base 2030PS isolate the effects of a 155-mgd withdrawal (Table 2–8). Differences between Full2030PS and Base1995NN provide the total effect between the hindcast scenario and projected 2030 conditions with a 155-mgd withdrawal (Table 2–9). The greatest *AVRD* occurs in Lake George. Average water age increases 4.3 days due to a 155-mgd withdrawal, and 2.7 days for the total effect. r^2 and m values are near 1 at all locations indicating that the variability of water age scenarios are nearly identical.

Table 2–8. Comparative statistics for differences in daily water age between Full2030PS and Base2030PS that isolate the effect of a 155-mgd withdrawal.

Station	***NRECS***	***r*²**	***m***	***b***	***RMSD* (days)**	***AVRD* (days)**	***AVAD* (days)**
Acosta	3,652	0.998	0.984	-0.603	3.535	2.844	2.869
Orange Park	3,652	0.998	0.968	0.977	4.120	3.015	3.067
Shands Bridge	3,652	0.996	0.972	0.371	4.021	2.720	2.887
Racy Point	3,652	0.992	0.967	0.982	4.308	2.140	2.906
Buffalo Bluff	3,652	0.989	0.955	1.653	4.543	1.922	2.989
Lake George	3,652	0.996	0.926	2.043	6.100	4.297	4.315
DeLand	3,652	0.912	0.987	0.994	5.178	-0.562	2.610
Lake Monroe	3,652	0.990	0.966	-0.260	4.007	1.938	2.390
Lake Jesup	3,652	1.000	1.012	0.836	2.358	-2.118	2.126
Lake Harney	3,652	0.979	0.973	-0.264	2.515	0.768	1.300

NRECS = Number of paired values
r^2 = Coefficient of determination
m = Slope of the linear regression line
b = Intercept of the linear regression line
RMSD = Root-mean-square difference
AVRD = Average relative difference
AVAD = Average absolute difference

Table 2–9. Comparative statistics for differences in daily water age between Full2030PS and Base1995NN (total effect).

Station	***NRECS***	***r*²**	***m***	***b***	***RMSD* (days)**	***AVRD* (days)**	***AVAD* (days)**
Acosta	3,652	0.996	1.017	-1.387	3.382	-0.987	2.491
Orange Park	3,652	0.996	1.016	-1.374	3.348	-0.651	2.435
Shands Bridge	3,652	0.996	0.997	-0.391	3.015	0.761	2.322
Racy Point	3,652	0.993	0.977	0.781	3.633	1.383	2.741
Buffalo Bluff	3,652	0.992	0.962	1.305	3.943	1.698	2.888
Lake George	3,652	0.996	0.957	1.012	4.433	2.710	3.610
DeLand	3,652	0.950	1.057	-1.177	4.236	-0.782	2.393
Lake Monroe	3,652	0.984	1.063	-2.187	5.172	-0.965	2.915
Lake Jesup	3,652	0.998	0.994	-0.065	1.872	0.718	1.468
Lake Harney	3,652	0.967	1.233	-2.308	5.716	-2.068	2.789

NRECS = Number of paired values
r^2 = Coefficient of determination
m = Slope of the linear regression line
b = Intercept of the linear regression line
RMSD = Root-mean-square difference
AVRD = Average relative difference
AVAD = Average absolute difference

Longitudinal Plots

Longitudinal plots for mean water age (Figure 2–36), and mean water age difference among scenarios (Figure 2–37) are presented below. Mean water age generally increases from upstream to downstream locations, although Lake George exhibits a relative maximum. Because Lake Jesup is off-line from the main river flow, it has a lower flushing rate, which causes the large mean water age.

Water withdrawals (orange line, Figure 2–37) cause the greatest increase in water age in Lake George, although the mean increase of 5 days equates to less than a 6% change in mean value.

The decrease in water age due to projected 2030 land use (green line, Figure 2–37) offsets factors increasing water age. Sea level rise (green line, Figure 2–37) increases water age and is comparable in contribution to water withdrawal. Projected 2030 land use (cyan line, Figure 2–37) decreases mean water age throughout the river and has the greatest effect between Lake George and Acosta. Under 2030 conditions (total effect), the greatest increase of water age is in Lake George, where mean water age increases approximately 4%

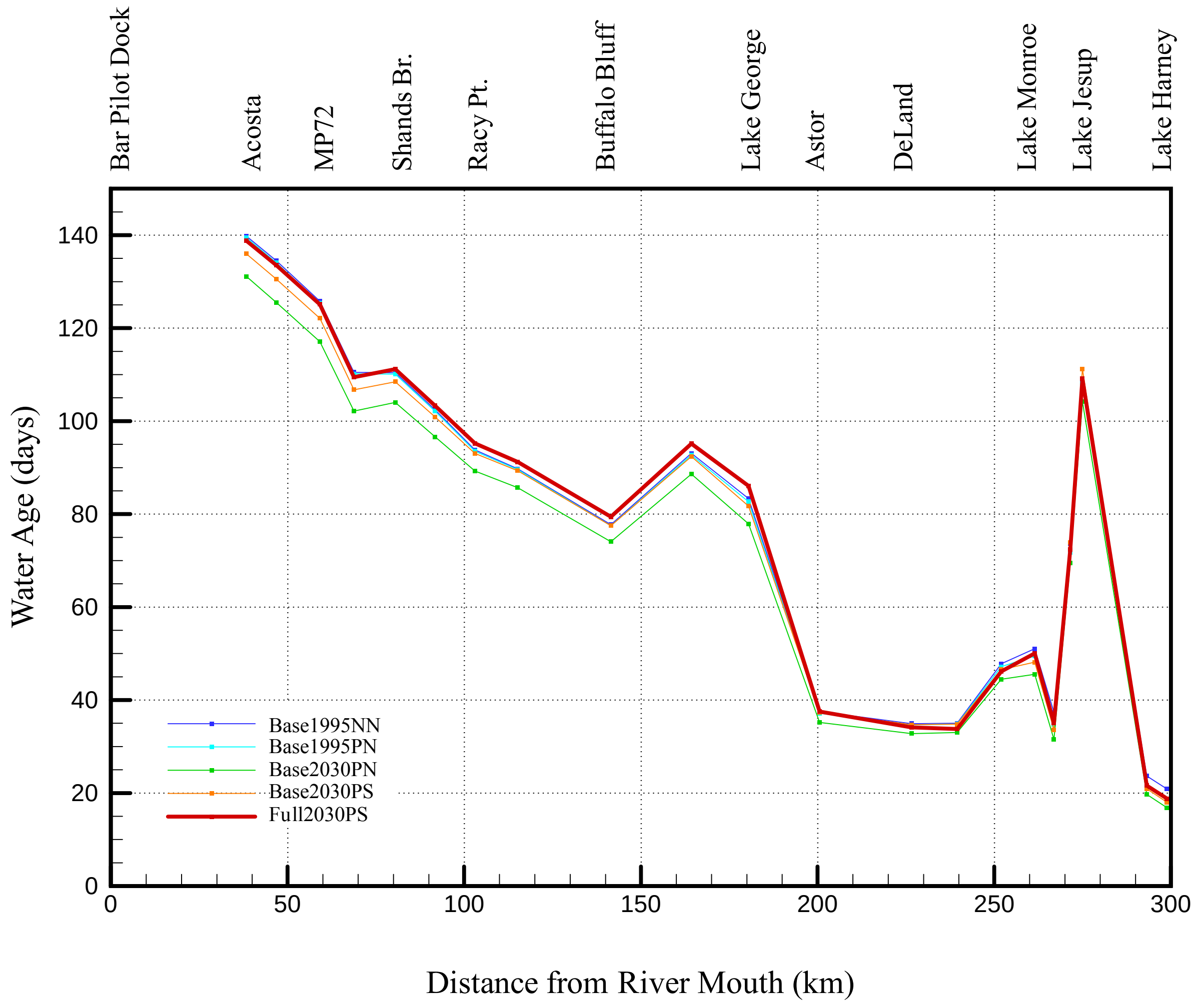

Figure 2–36. Longitudinal plot comparing mean water age for the hindcast scenario (Base1995NN) and selected forecast scenarios.

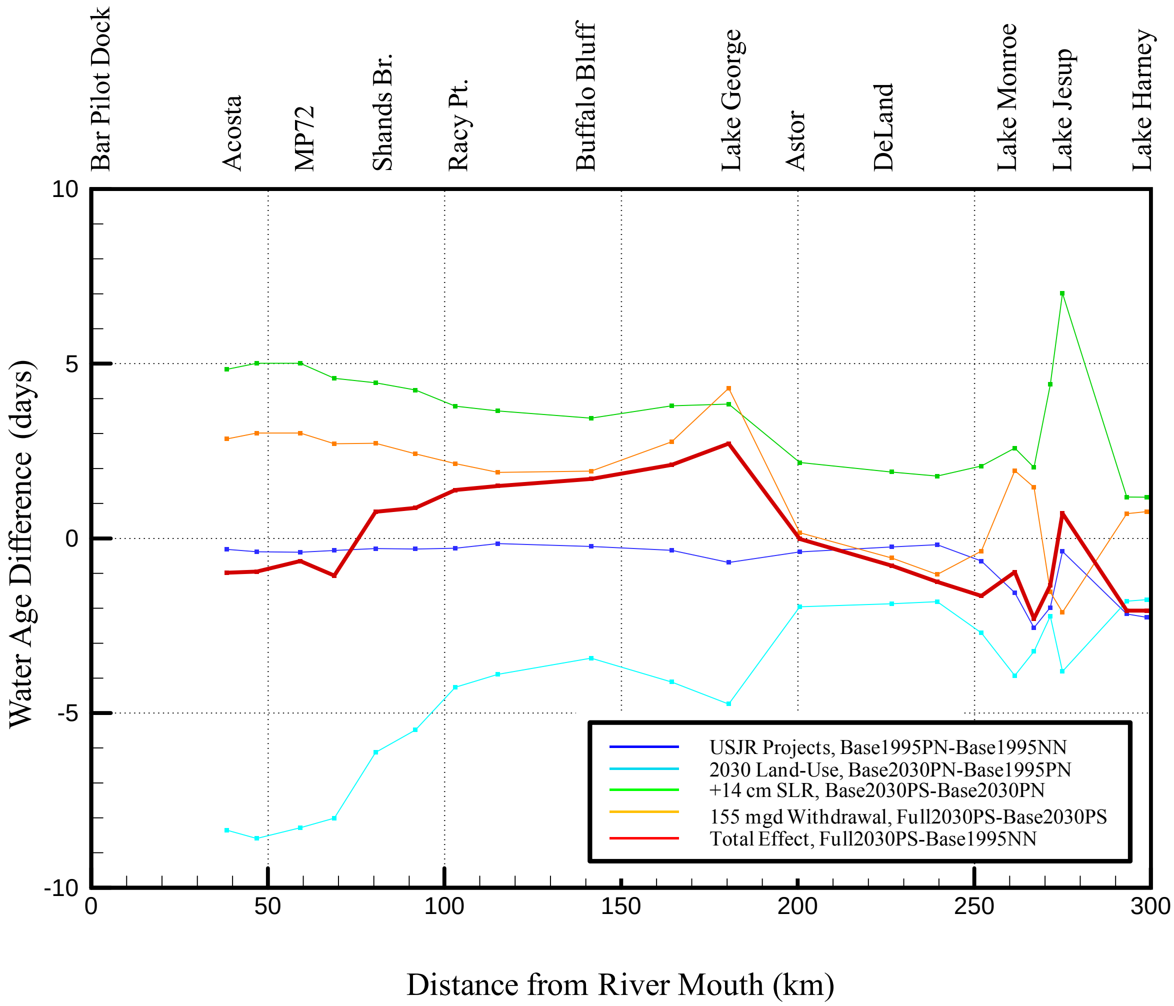

Figure 2–37. Longitudinal plot comparing mean differences in water age between the hindcast scenario (Base1995NN) and selected forecast scenarios. USJR = upper St. Johns River, SLR = sea level rise.

Discharge Difference Plots

Discharge difference plots for water age are shown below for Lake George. Figure 2–38 isolates the effect of a 155-mgd withdrawal, and Figure 2–39 compares 2030 conditions with a 155-mgd (Full2030PS) withdrawal against the hindcast condition (Base1995NN). Thirty-day averaged discharge at DeLand is used as an index of discharge for Lake George.

The greatest increase in water age due to a 155-mgd withdrawal occurs at low flow (Figure 2–38). Water age differences are generally less than 6 days except when discharge is less than approximately 50 m^3s^{-1} (1,140 mgd). For the total effect (Figure 2–39) water age increases 2 to 8 days during low flow periods (discharge < 100 m^3s^{-1}). Water age differences are negligible when discharge exceeds 100 m^3s^{-1} (2,280 mgd).

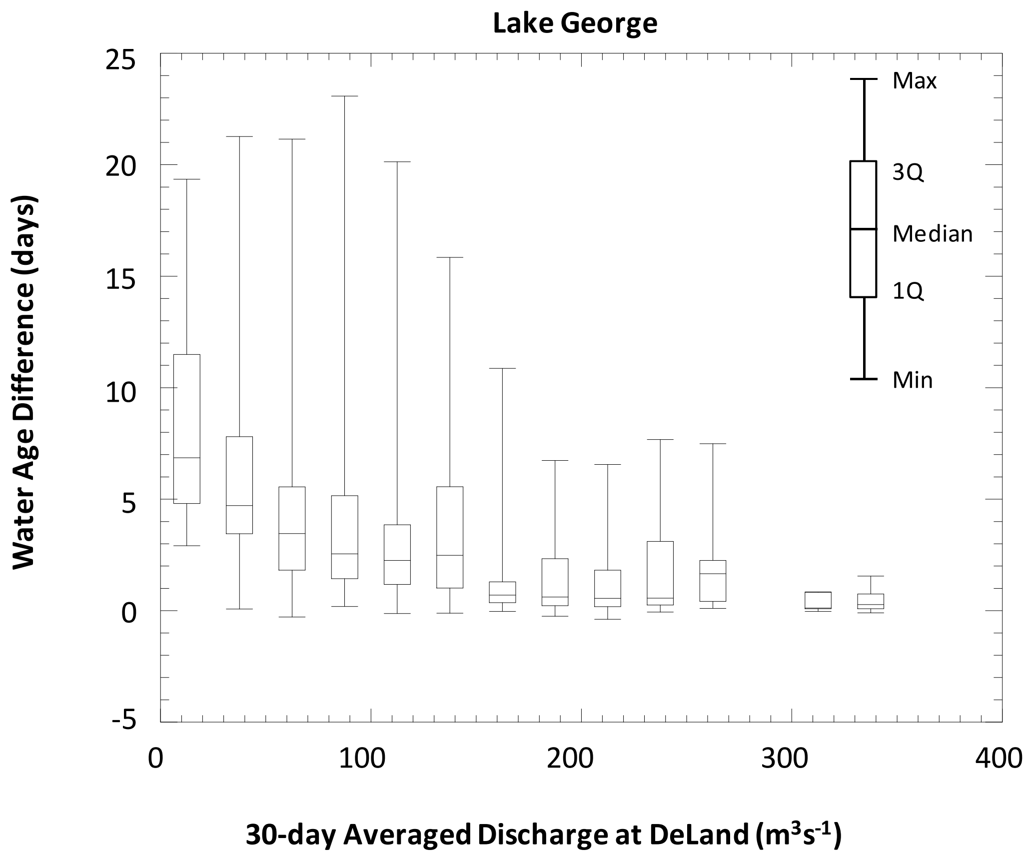

Figure 2–38. Water age differences in Lake George caused by a 155-mgd withdrawal scenario compared with 30-day averaged discharge at DeLand.

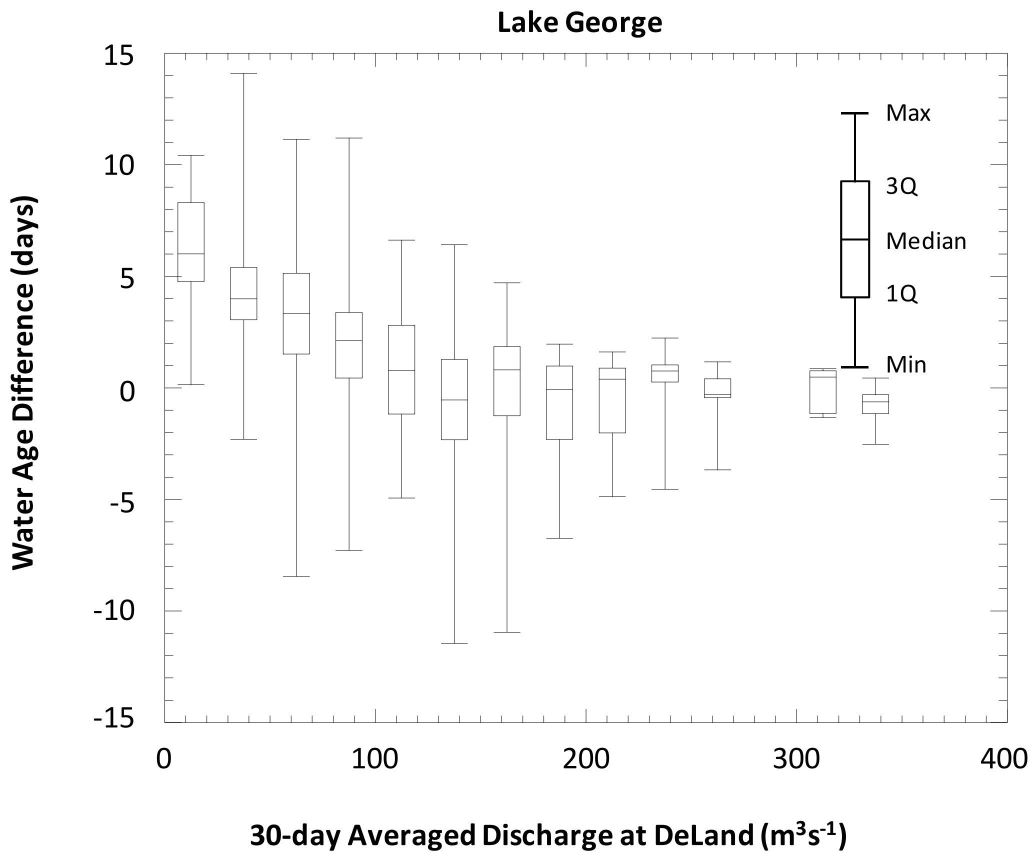

Figure 2–39. Water age differences in Lake George between the Full2030PS and Base1995NN scenarios (total effect) compared with 30-day averaged discharge at DeLand.

Intensity-Frequency-Duration Plots

Intensity-frequency-duration plots are shown below for high water age events in Lake George (Figure 2–40). Maximum water age for the hindcast scenario (black lines, top plot) varies only slightly for durations of 1 to 20 days. Over these durations, water age is approximately 190 days for the 10-yr maximum event, and about 140 days for the 2-yr maximum event.

For 2030 conditions without withdrawal (Base2030PS), water age decreases for the 10-yr event (red line, bottom plot), but water age intensities for the 2-yr event are unchanged (dark blue line, bottom plot). Water ages increase for 2030 conditions with a 155-mgd withdrawal (Full2030PS) for both the 2-yr event (cyan line, bottom plot) and 10-yr event (green line, bottom plot). The change in water age is uniform over a range of durations from 1 day to 1 yr.

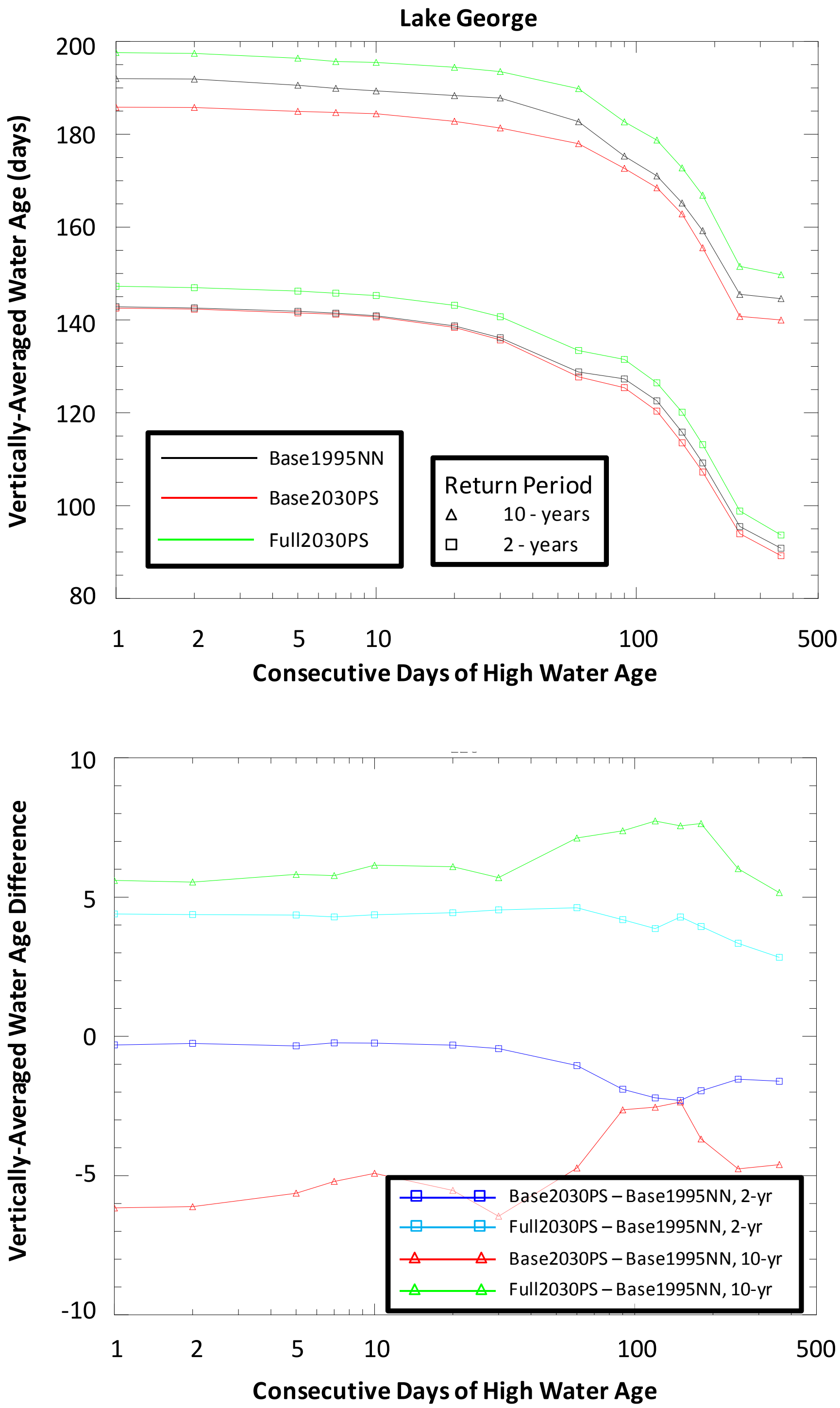

Figure 2–40. High water age duration frequency curves for Lake George. Top: water age for base scenario (Base1995NN), and projected 2030 land use both with (Full2030PS) and without (Base2030PS) a 155-mgd. Bottom: water age differences between scenarios.

2.4.2 FUTURE SCENARIOS

The analysis of hydrodynamic changes for future conditions compares the effects of an additional water withdrawal from the lower Ocklawaha River, reduction of wastewater discharge to the river for reuse, channel deepening in Jacksonville Harbor, and a high rate of sea level rise (Table 2–2). The future changes are referenced against the projected 2030 condition (Base2030PS), not the hindcast scenario (Base1995NN) that was used as the base scenario in the previous section. This choice is made so that these uncertain future conditions can be directly compared against expected forecast conditions.

Linearity of Response

Linearity of response for the future factors is tested by comparison of future scenarios against the Base2030PS scenario. Results show essentially complete linearity of factors for water level (Figure 2–41) and water age (Figure 2–43) at all locations. The response of salinity to future factors, however, is distinctly nonlinear below Racy Point in the estuarine reach (Figure 2–42). For salinity in the estuarine reach, linear superposition of the individual effects of each future factor on salinity underpredicts the total effect.

Figure 2–41 clearly shows the dominance of sea level rise on water level relative to the other future factors. For salinity, the greatest changes occur in the estuarine reach (Acosta, Orange Park, and Shands Bridge). In the estuarine reach, all future factors cause an increase of salinity. Channel deepening dominates the salinity response at Acosta Bridge, but a 262-mgd water withdrawal dominates the salinity response farther upstream at Shands Bridge. The salinity response to the reuse of wastewater is negligible.

The future factors having the greatest effect on water age are a 262-mgd withdrawal and sea level rise.

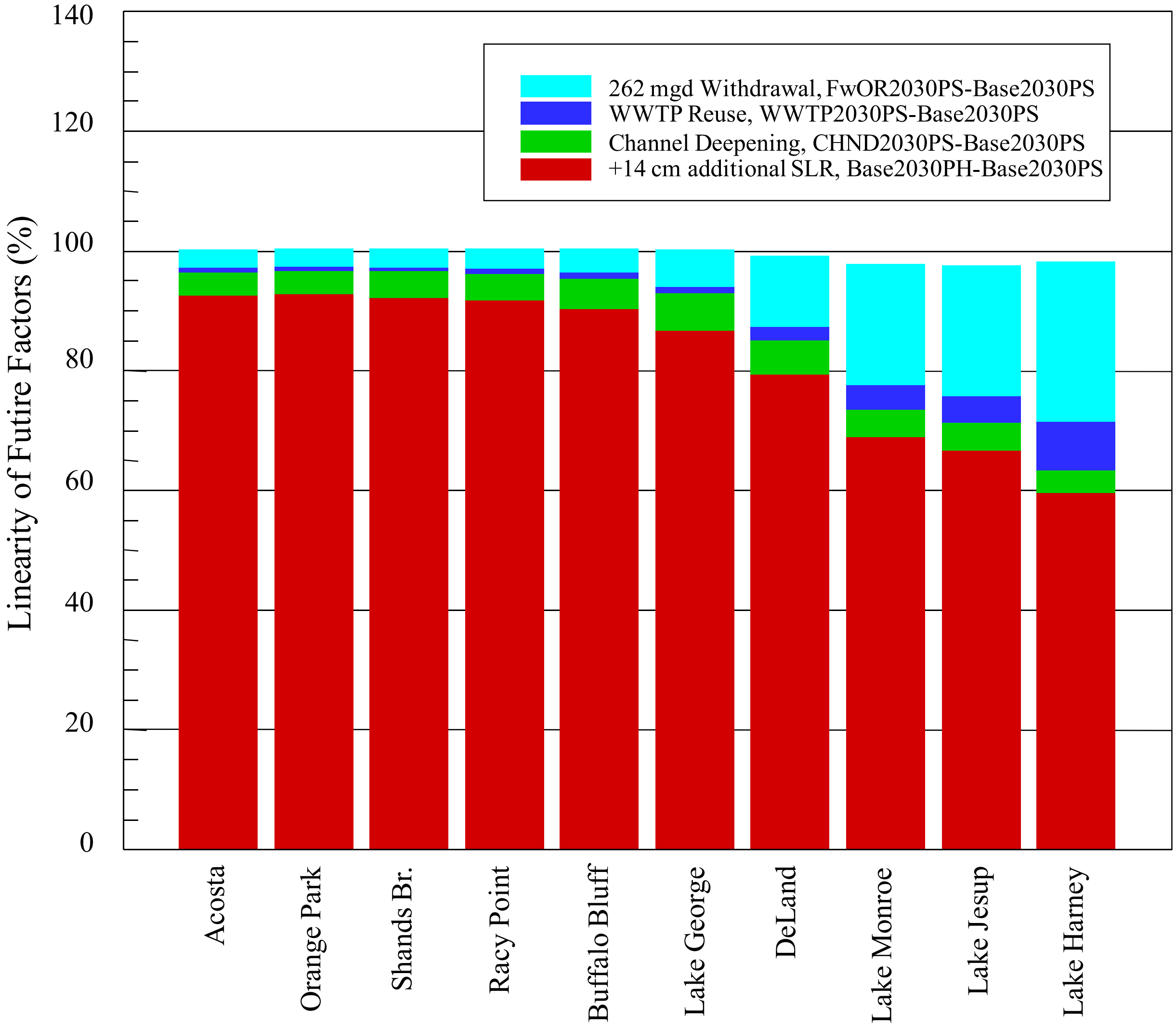

Figure 2–41. Linearity of factors affecting water level for future conditions relative to the Base2030PS scenario. WWTP = wastewater treatment plant, SLR = sea level rise.

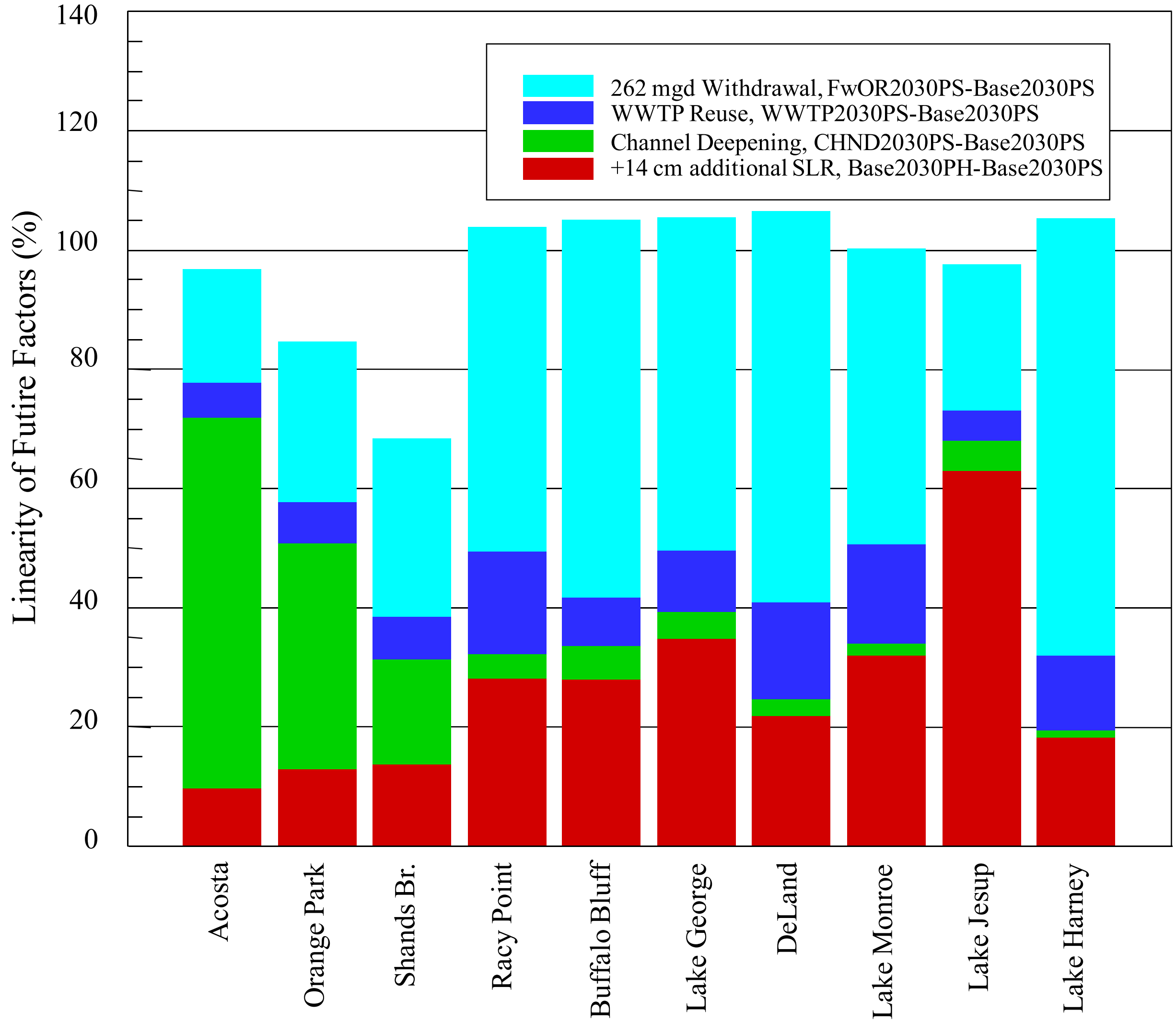

Figure 2–42. Linearity of factors affecting salinity for future conditions relative to the Base2030PS scenario. WWTP = wastewater treatment plant, SLR = sea level rise.

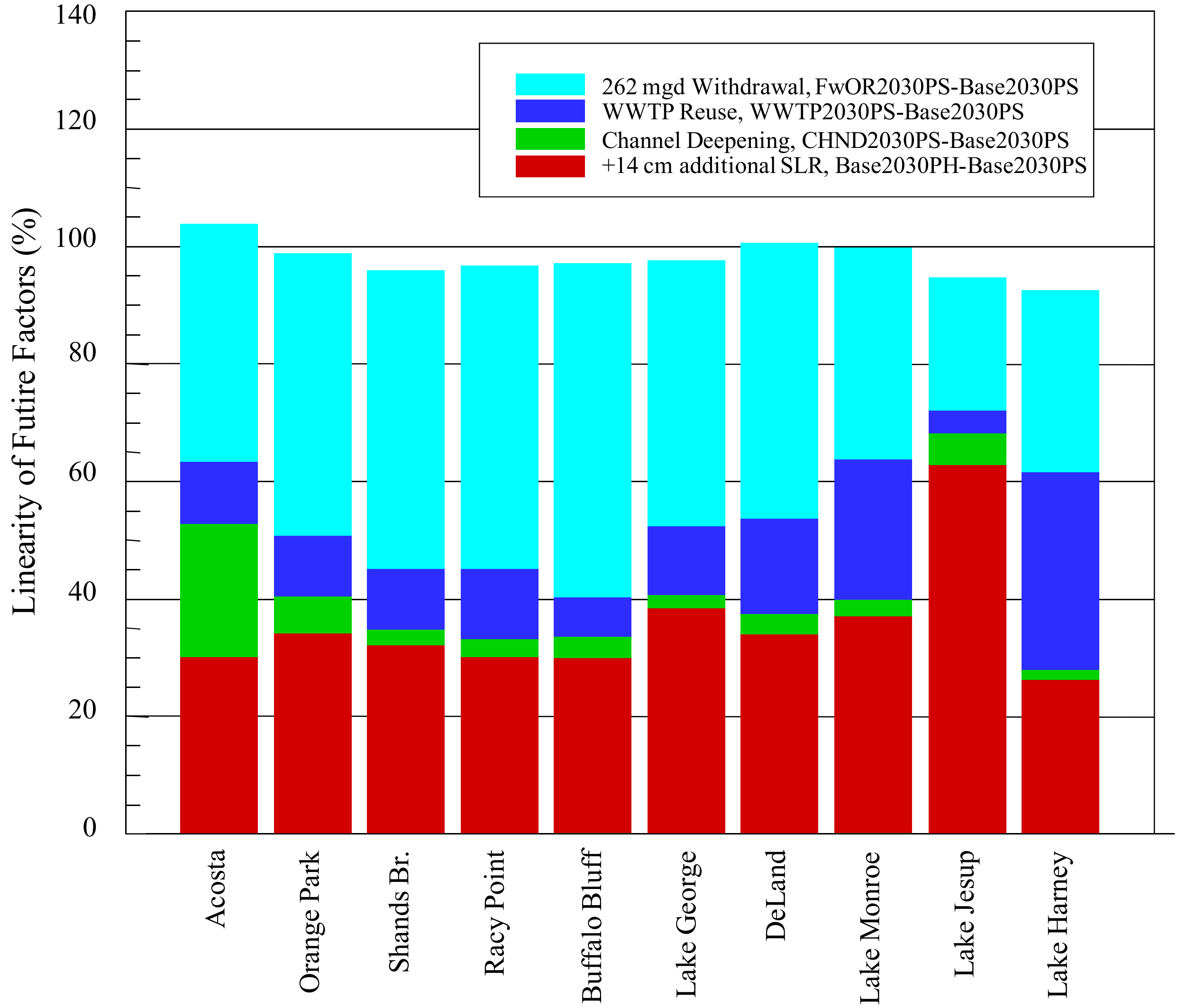

Figure 2–43. Linearity of factors affecting water age for future conditions relative to the Base2030PS scenario. WWTP = wastewater treatment plant, SLR = sea level rise.

Water Level

Time Series Comparisons

Daily time series for water level are shown below for Lake Monroe for the 2030 base scenario (Base2030PS) and future scenarios (Figure 2–44). Water level differences are small between all scenarios.

A plot of water level differences shows that sea level rise dominates the differences in water level among scenarios (Figure 2–45). A 262-mgd water withdrawal reduces water levels in Lake Monroe less than 5 cm, while sea level rise raises water level over 10 cm. Recall that these differences are relative to the Base2030PS scenario that already accounts for an expected 14-cm increase in sea level rise at low flow relative to 1995 conditions. The changes shown in Figure 2–45, then, indicate a possible additional increase in water level for future conditions.

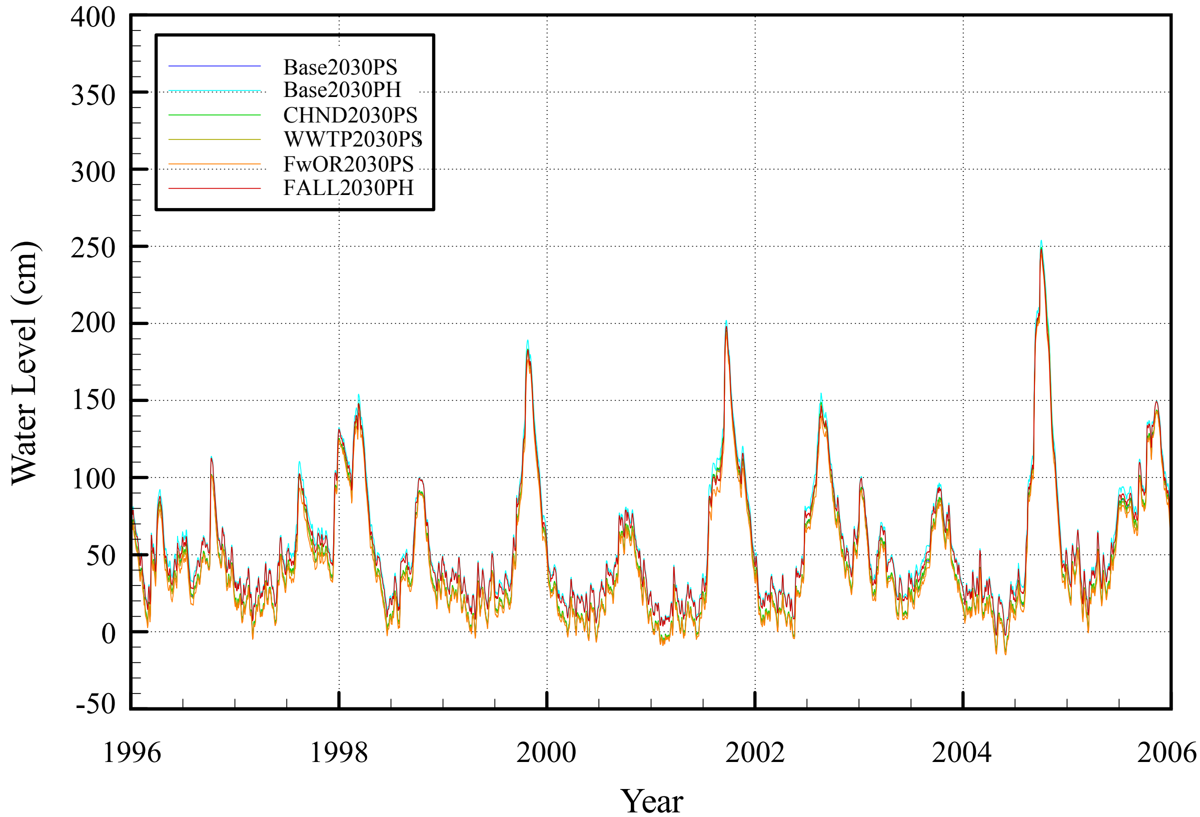

Figure 2–44. Daily averaged water level in Lake Monroe for future scenarios.

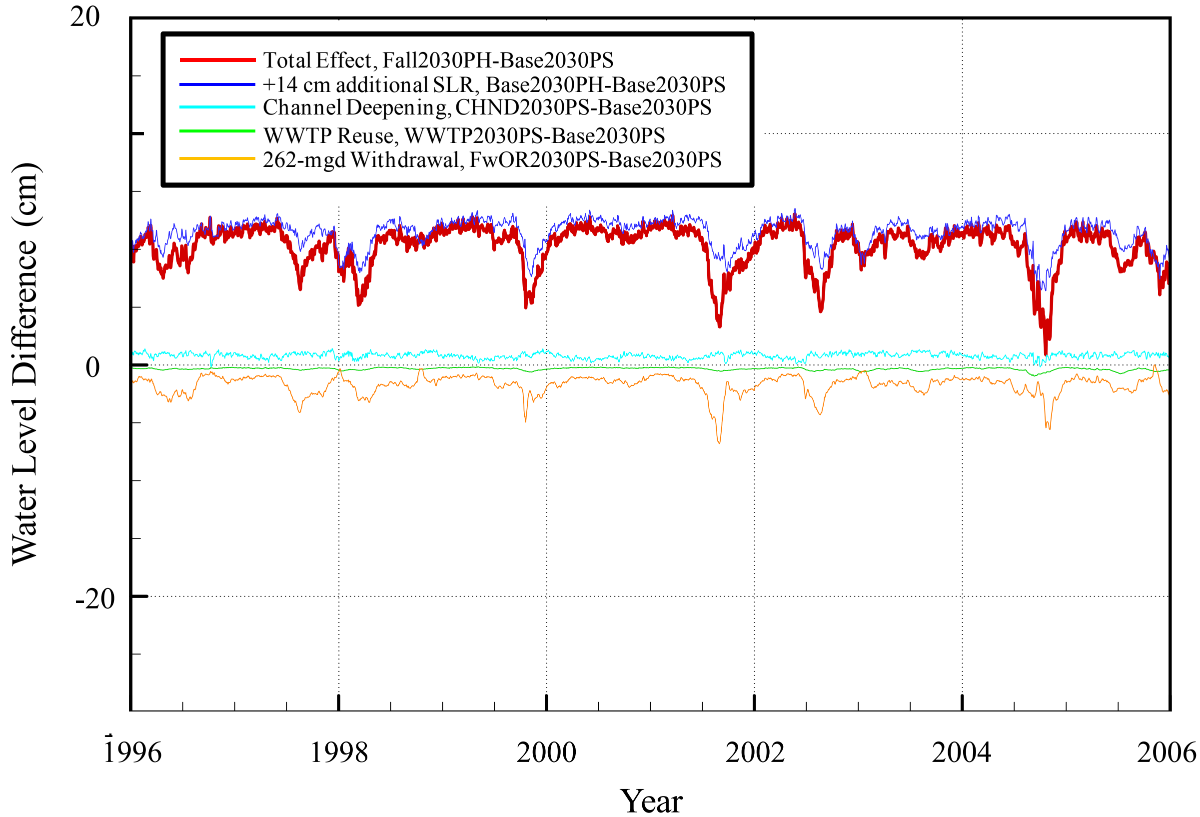

Figure 2–45. Difference of daily averaged water level in Lake Monroe between Base2030PS scenario and five future scenarios. SLR = sea level rise, WWTP = wastewater treatment plant.

Comparative Statistics

Comparative statistics for water level differences between FwOR2030PS and Base2030PS isolate the effect of a 262-mgd withdrawal on water level (Table 2–10). Mean water level differences (*AVRD*) throughout the river are essentially identical to differences calculated for a 155-mgd withdrawal. The lack of sensitivity of water level to the additional water withdrawal is because the withdrawal from the Ocklawaha River affects areas of the St. Johns River downstream of Lake George. Water levels in these areas were previously shown to be insensitive to 155-mgd water withdrawals, and they are similarly insensitive to a 262-mgd withdrawal.

When all future factors are combined (total effect), mean water levels increase 5 to 12 cm throughout the system (Table 2–11). The increased water level is caused by the increased rate of sea level rise.

Table 2–10. Comparative statistics for differences in daily water level between FwOR2030PS and Base2030PS to isolate the effect of a 262-mgd withdrawal.

Station	*NRECS*	r^2	*m*	*b*	*RMSD* (cm)	*AVRD* (cm)	*AVAD* (cm)
Acosta	3,652	1.000	0.999	0.406	0.415	-0.398	0.398
Orange Park	3,652	1.000	0.999	0.427	0.433	-0.415	0.415
Shands Bridge	3,652	1.000	1.000	0.429	0.440	-0.424	0.424
Racy Point	3,652	1.000	1.000	0.455	0.465	-0.449	0.449
Buffalo Bluff	3,652	1.000	1.000	0.565	0.581	-0.560	0.560
Lake George	3,652	1.000	1.000	0.888	0.931	-0.895	0.895
DeLand	3,652	0.999	1.012	1.319	1.922	-1.718	1.718
Lake Monroe	3,652	0.999	1.023	2.057	3.646	-3.105	3.106
Lake Jesup	3,652	0.998	1.022	2.246	3.940	-3.339	3.342
Lake Harney	3,652	0.998	1.017	2.730	5.037	-3.902	4.007

NRECS = Number of paired values
r^2 = Coefficient of determination
m = Slope of the linear regression line
b = Intercept of the linear regression line
RMSD = Root-mean-square difference
AVRD = Average relative difference
AVAD = Average absolute difference

Table 2–11. Comparative statistics for differences in daily water level between FALL2030PS and Base2030PS (total effect).

Station	*NRECS*	r^2	*m*	*b*	*RMSD* (cm)	*AVRD* (cm)	*AVAD* (cm)
Acosta	3,652	0.999	0.996	-11.723	11.818	11.802	11.802
Orange Park	3,652	0.999	0.997	-12.469	12.563	12.549	12.549
Shands Bridge	3,652	0.999	1.000	-12.644	12.668	12.657	12.657
Racy Point	3,652	0.999	1.000	-12.642	12.650	12.639	12.639
Buffalo Bluff	3,652	0.999	1.002	-12.565	12.514	12.504	12.504
Lake George	3,652	0.999	1.005	-12.313	12.144	12.135	12.135
DeLand	3,652	0.998	1.047	-12.384	10.445	10.284	10.284
Lake Monroe	3,652	0.997	1.070	-11.750	8.566	7.736	7.944
Lake Jesup	3,652	0.997	1.071	-11.387	8.178	7.119	7.457
Lake Harney	3,652	0.997	1.064	-9.679	7.298	4.652	6.342

NRECS = Number of paired values
r^2 = Coefficient of determination
m = Slope of the linear regression line
b = Intercept of the linear regression line
RMSD = Root-mean-square difference
AVRD = Average relative difference
AVAD = Average absolute difference

Salinity

Time Series Comparisons

Daily averaged time series of salinity for Shands Bridge show modest changes to salinity for future scenarios (Figure 2–46); differences in salinity among scenarios are barely discernable in the time series graphs. Salinity differences show increases of up to 2 PSS78 during salinity intrusion events at Shands Bridge when all future factors are considered together (red line, Figure 2–47).

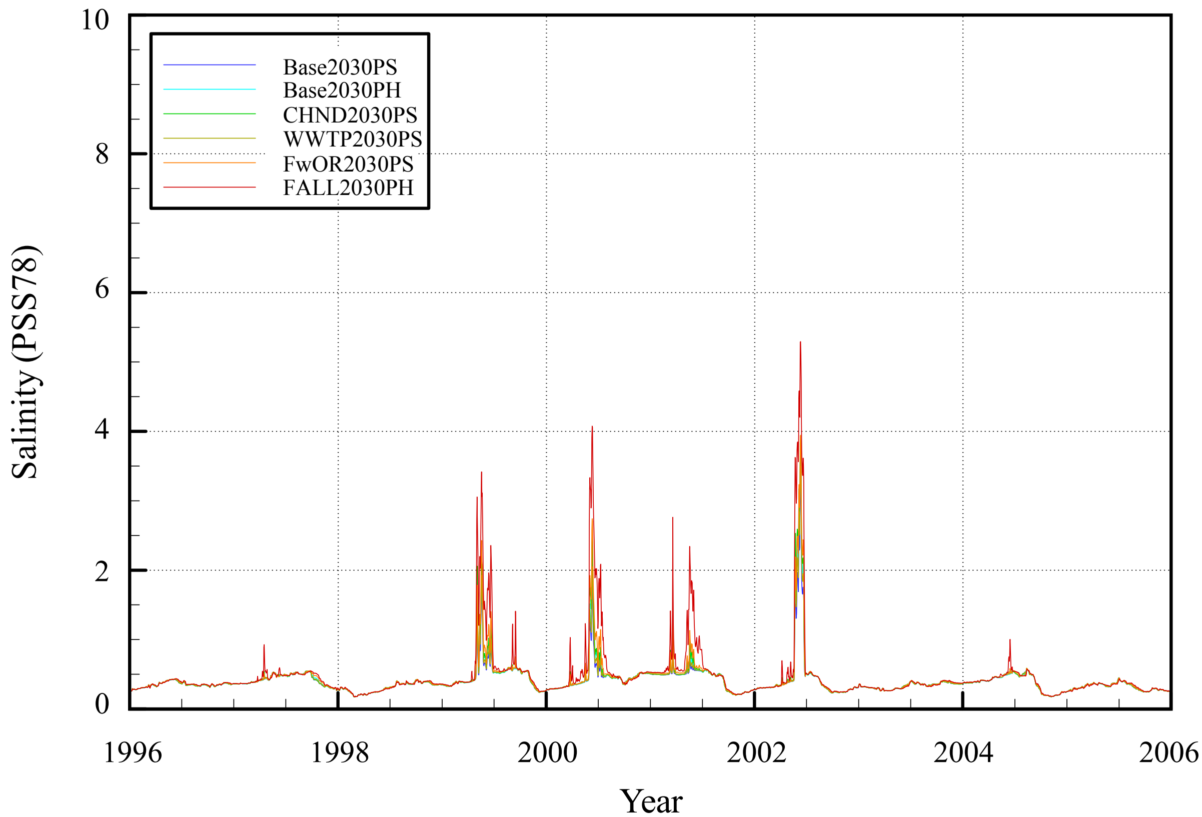

Figure 2–46. Times series of daily averaged salinity at Shands Bridge for future scenarios.

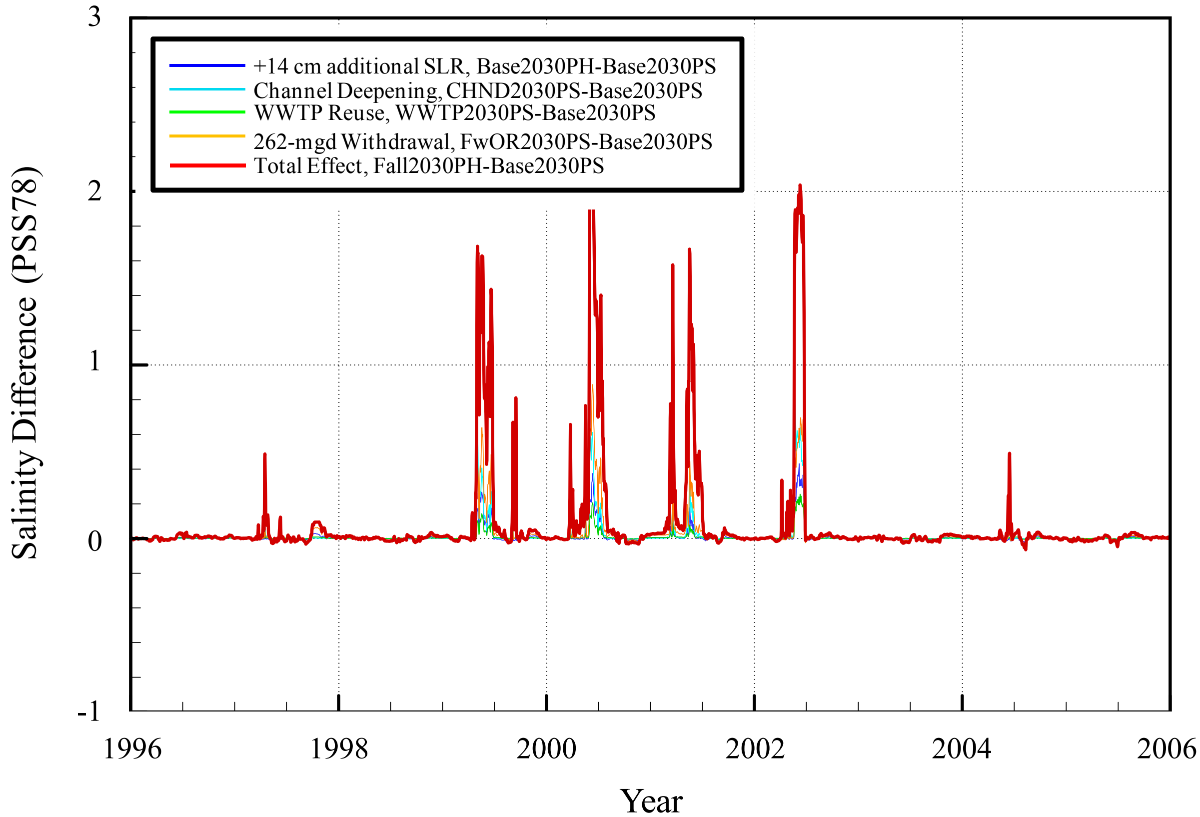

Figure 2–47. Difference of daily averaged salinity at Shands Bridge between Base2030PS and five future condition scenarios. SLR = sea level rise, WWTP = wastewater treatment plant.

Comparative Statistics

Comparative statistics for salinity differences show that future conditions affect only the estuarine reach of the St. Johns River (Acosta to Shands Bridge in the tables below). The individual contribution of future factors to salinity change are shown below for increased sea level rise (Table 2–12), channel deepening (Table 2–13), wastewater reuse (Table 2–14), and a 262-mgd water withdrawal (Table 2–15). The total effect of all four factors (FALL2030PS) relative to the Base2030PS scenario is shown in Table 2–16.

All four individual future factors increase mean salinity. Channel deepening has the greatest effect on salinity at Acosta Bridge (Table 2–13), but water withdrawal has the greatest effect on salinity at Shands Bridge (Table 2–15). Mean salinity increases nearly 3 PSS78 when all future factors are considered together. The increase in mean salinity at Shands Bridge for all future factors, however, is less than 0.1 PSS78 (Table 2–16).

Table 2–12. Comparative statistics for differences in daily salinity between Base2030PH and Base2030PS to isolate the effect of possible increased rate of sea level rise.

Station	*NRECS*	r^2	*m*	*b*	*RMSD*	*AVRD*	*AVAD*
Acosta	3,652	0.999	0.994	-0.226	0.313	0.261	0.264
Orange Park	3,652	0.996	0.944	-0.038	0.199	0.108	0.110
Shands Bridge	3,652	0.990	0.850	0.054	0.043	0.007	0.013
Racy Point	3,652	0.997	1.017	-0.005	0.006	-0.002	0.005
Buffalo Bluff	3,652	0.997	1.021	-0.007	0.007	-0.002	0.005
Lake George	3,652	0.999	1.020	-0.006	0.007	-0.002	0.005
DeLand	3,652	0.999	1.018	-0.006	0.007	-0.002	0.005
Lake Monroe	3,652	0.999	1.034	-0.010	0.011	-0.005	0.007
Lake Jesup	3,652	0.999	1.047	-0.016	0.012	-0.006	0.008
Lake Harney	3,652	0.999	1.017	-0.006	0.008	-0.002	0.005

NRECS = Number of paired values
r^2 = Coefficient of determination
m = Slope of the linear regression line
b = Intercept of the linear regression line
RMSD = Root-mean-square difference
AVRD = Average relative difference
AVAD = Average absolute difference

Table 2–13. Comparative statistics for differences in daily salinity between CHND2030PS and Base2030PS to isolate the effect of channel deepening of Jacksonville Harbor.

Station	*NRECS*	r^2	*m*	*b*	*RMSD*	*AVRD*	*AVAD*
Acosta	3,652	0.984	0.920	-1.157	1.918	1.733	1.733
Orange Park	3,652	0.981	0.827	-0.067	0.589	0.326	0.326
Shands Bridge	3,652	0.976	0.755	0.086	0.077	0.016	0.016
Racy Point	3,652	1.000	1.001	0.000	0.001	0.000	0.001
Buffalo Bluff	3,652	1.000	1.002	-0.001	0.002	0.000	0.001
Lake George	3,652	1.000	1.002	-0.001	0.001	0.000	0.001
DeLand	3,652	1.000	1.001	0.000	0.001	0.000	0.001
Lake Monroe	3,652	1.000	1.001	0.000	0.001	0.000	0.000
Lake Jesup	3,652	1.000	1.003	-0.001	0.001	0.000	0.001
Lake Harney	3,652	1.000	1.001	0.000	0.001	0.000	0.000

NRECS = Number of paired values
r^2 = Coefficient of determination
m = Slope of the linear regression line
b = Intercept of the linear regression line
RMSD = Root-mean-square difference
AVRD = Average relative difference
AVAD = Average absolute difference

Table 2–14. Comparative statistics for differences in daily salinity between WWTP2030PS and Base2030PN to isolate the effects of reuse of wastewater.

Station	*NRECS*	r^2	*m*	*b*	*RMSD*	*AVRD*	*AVAD*
Acosta	3,652	1.000	0.983	-0.062	0.196	0.159	0.159
Orange Park	3,652	0.999	0.958	-0.007	0.115	0.059	0.059
Shands Bridge	3,652	0.997	0.907	0.032	0.025	0.006	0.007
Racy Point	3,652	0.999	0.991	0.001	0.004	0.003	0.003
Buffalo Bluff	3,652	1.000	1.004	-0.002	0.002	0.000	0.002
Lake George	3,652	1.000	1.002	-0.001	0.002	0.000	0.002
DeLand	3,652	0.998	1.012	-0.005	0.006	-0.001	0.003
Lake Monroe	3,652	0.999	1.016	-0.006	0.007	-0.001	0.004
Lake Jesup	3,652	1.000	1.000	0.000	0.001	0.000	0.001
Lake Harney	3,652	0.999	1.002	-0.002	0.007	0.001	0.003

NRECS = Number of paired values
r^2 = Coefficient of determination
m = Slope of the linear regression line
b = Intercept of the linear regression line
RMSD = Root-mean-square difference
AVRD = Average relative difference
AVAD = Average absolute difference

Table 2–15. Comparative statistics for differences in daily salinity between FwOR2030PS and Base2030PS to isolate the effects of a 262-mgd withdrawal.

Station	*NRECS*	r^2	*m*	*b*	*RMSD*	*AVRD*	*AVAD*
Acosta	3,652	0.998	0.945	-0.201	0.672	0.534	0.534
Orange Park	3,652	0.990	0.860	-0.035	0.442	0.230	0.232
Shands Bridge	3,652	0.960	0.711	0.098	0.097	0.025	0.028
Racy Point	3,652	0.985	0.968	0.007	0.014	0.006	0.009
Buffalo Bluff	3,652	0.986	0.960	0.007	0.018	0.010	0.012
Lake George	3,652	0.995	0.989	-0.001	0.012	0.006	0.008
DeLand	3,652	0.980	1.018	-0.011	0.023	0.004	0.014
Lake Monroe	3,652	0.992	1.020	-0.013	0.019	0.004	0.011
Lake Jesup	3,652	1.000	0.991	0.003	0.004	0.001	0.003
Lake Harney	3,652	0.989	0.973	-0.002	0.030	0.014	0.018

NRECS = Number of paired values
r^2 = Coefficient of determination
m = Slope of the linear regression line
b = Intercept of the linear regression line
RMSD = Root-mean-square difference
AVRD = Average relative difference
AVAD = Average absolute difference

Table 2–16. Comparative statistics for differences in daily salinity between FALL2030PS and Base2030PS (total effect).

Station	*NRECS*	r^2	*m*	*b*	*RMSD*	*AVRD*	*AVAD*
Acosta	3,652	0.967	0.861	-1.629	3.067	2.777	2.777
Orange Park	3,652	0.923	0.646	-0.141	1.455	0.858	0.860
Shands Bridge	3,652	0.844	0.399	0.207	0.315	0.084	0.090
Racy Point	3,652	0.966	0.969	0.005	0.020	0.007	0.014
Buffalo Bluff	3,652	0.972	0.980	0.001	0.021	0.007	0.015
Lake George	3,652	0.988	1.009	-0.007	0.017	0.003	0.011
DeLand	3,652	0.966	1.038	-0.018	0.030	0.001	0.018
Lake Monroe	3,652	0.979	1.070	-0.028	0.033	-0.003	0.020
Lake Jesup	3,652	0.999	1.041	-0.014	0.011	-0.005	0.006
Lake Harney	3,652	0.982	0.989	-0.008	0.035	0.013	0.020

NRECS = Number of paired values
r^2 = Coefficient of determination
m = Slope of the linear regression line
b = Intercept of the linear regression line
RMSD = Root-mean-square difference
AVRD = Average relative difference
AVAD = Average absolute difference

Longitudinal Plots

Longitudinal plots of mean salinity for future scenarios show that salinity is only appreciably affected in the estuarine reach of the river (Figure 2–48).

For clarity, a longitudinal plot of salinity differences among future scenarios focuses on the estuarine reach and shows salinity differences for only the lower 100 km of river (Figure 2–49). Mean salinity between river km 20 and 30 increases more than 3 PSS78 when all future factors are considered together (red line, total effect). The predominant factor affecting this change is channel deepening (cyan line). In the upper reaches of the estuarine reach (Buckman to Shands bridges), the effects of channel deepening and the mean increase in salinity for the total effect is less than 0.5 PSS78.

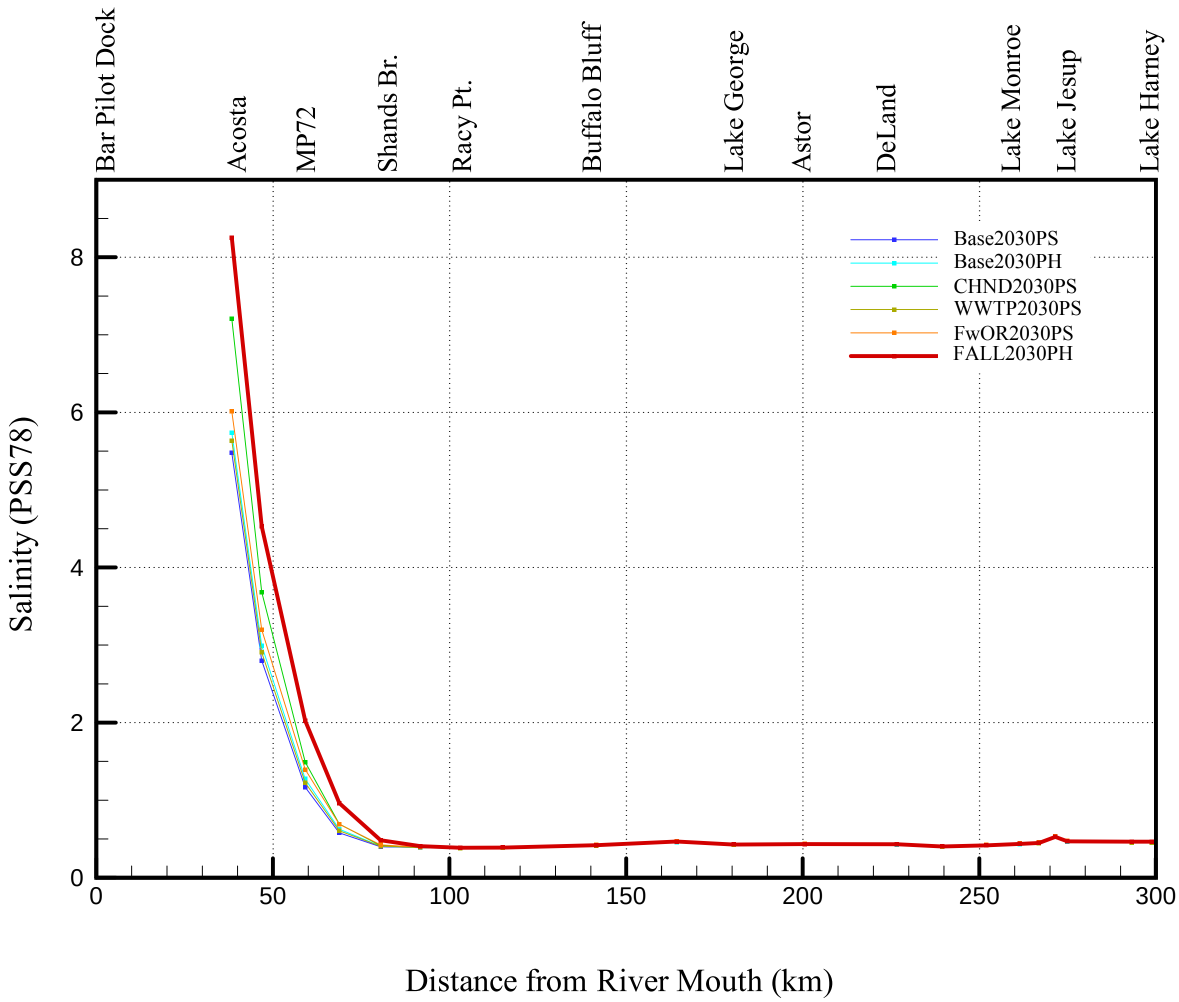

Figure 2–48. Longitudinal distribution for mean salinity comparing future scenarios (1996 to 2006).

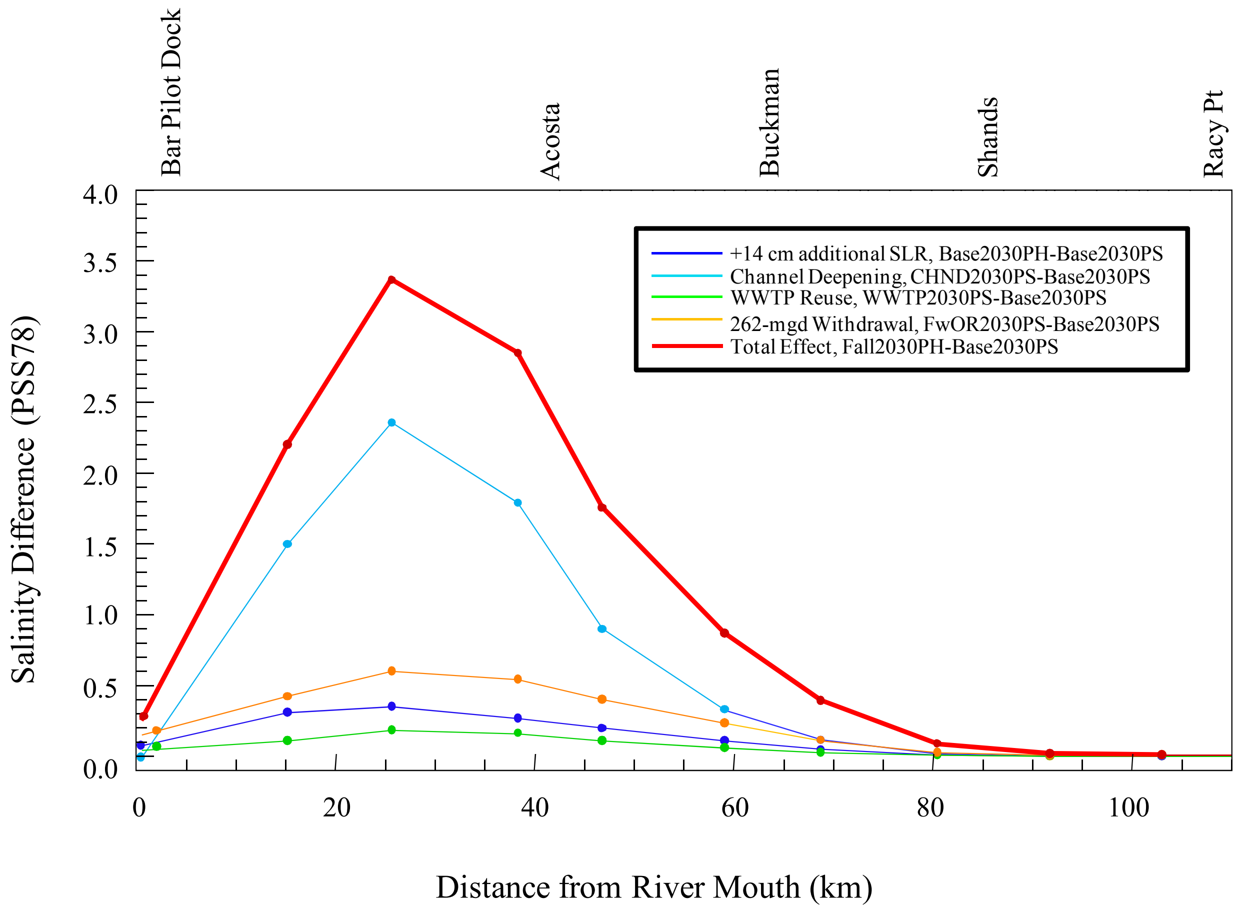

Figure 2–49. Longitudinal distribution for the difference in mean salinity between Base2030PS and future scenarios. SLR = sea level rise, WWTP = wastewater treatment plant.

Contour Plots

Contours of mean salinity differences (Figure 2–50) and 1-day maximum salinity differences (Figure 2–51) for future scenarios relative to Base2030PS are shown below. Channel deepening has the greatest effect on mean salinity with the greatest differences occurring in areas in and surrounding the navigational channel serving Jacksonville Harbor. Mean salinity increases approximately 3 PSS78 downstream of Acosta Bridge when considering all future conditions together (total effect, Figure 2–50).

The greatest differences for a 1-day maximum salinity event over the 10-yr model simulation period are also approximately 3 PSS78 (total effect, Figure 2–51). One-day maximum salinity increases of 3 PSS78 extend far upstream, past Doctors Lake to near the confluence of the St. Johns River and Black Creek. Channel deepening and a 262-mgd withdrawal are the most important contributions to the salinity increase. Reuse of wastewater (WWTP Reuse in figures) has no appreciable effect on salinity.

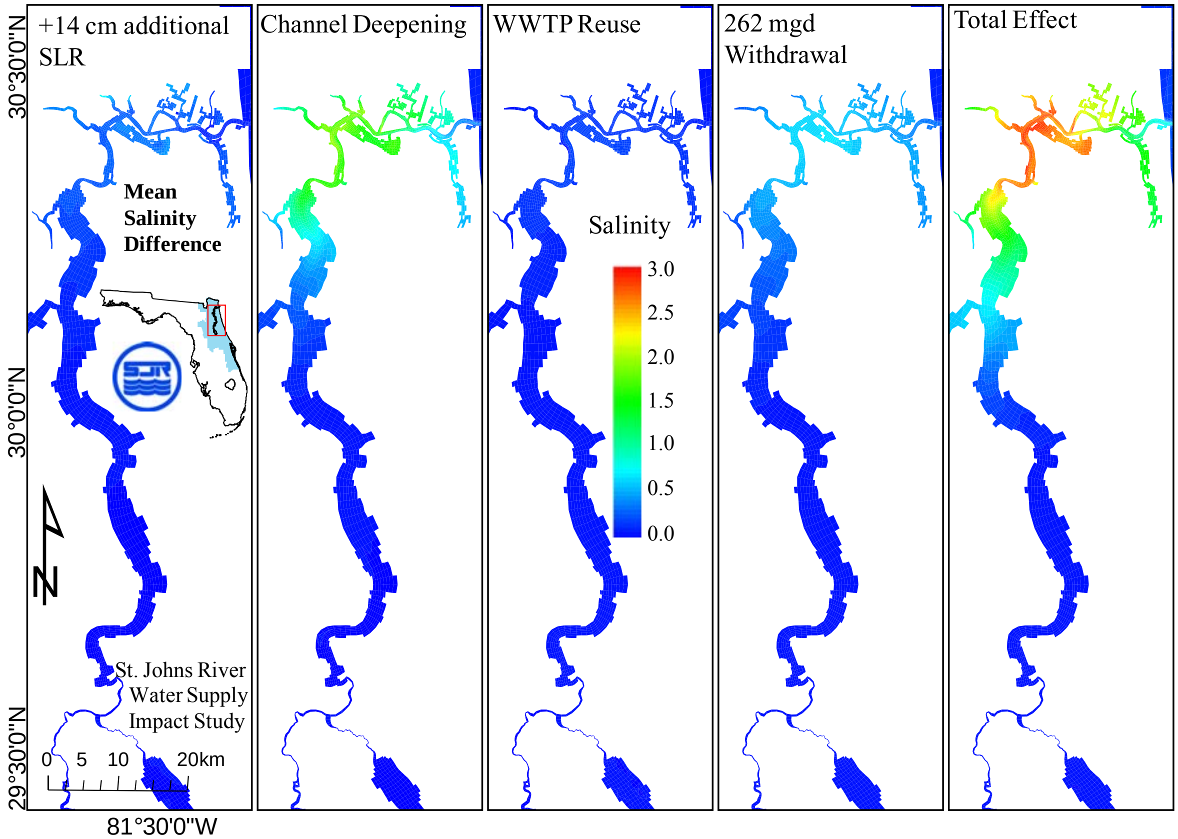

Figure 2–50. Contour plot of mean difference in salinity for future scenarios relative to Base2030PS scenario. SLR = sea level rise, WWTP = wastewater treatment plant.

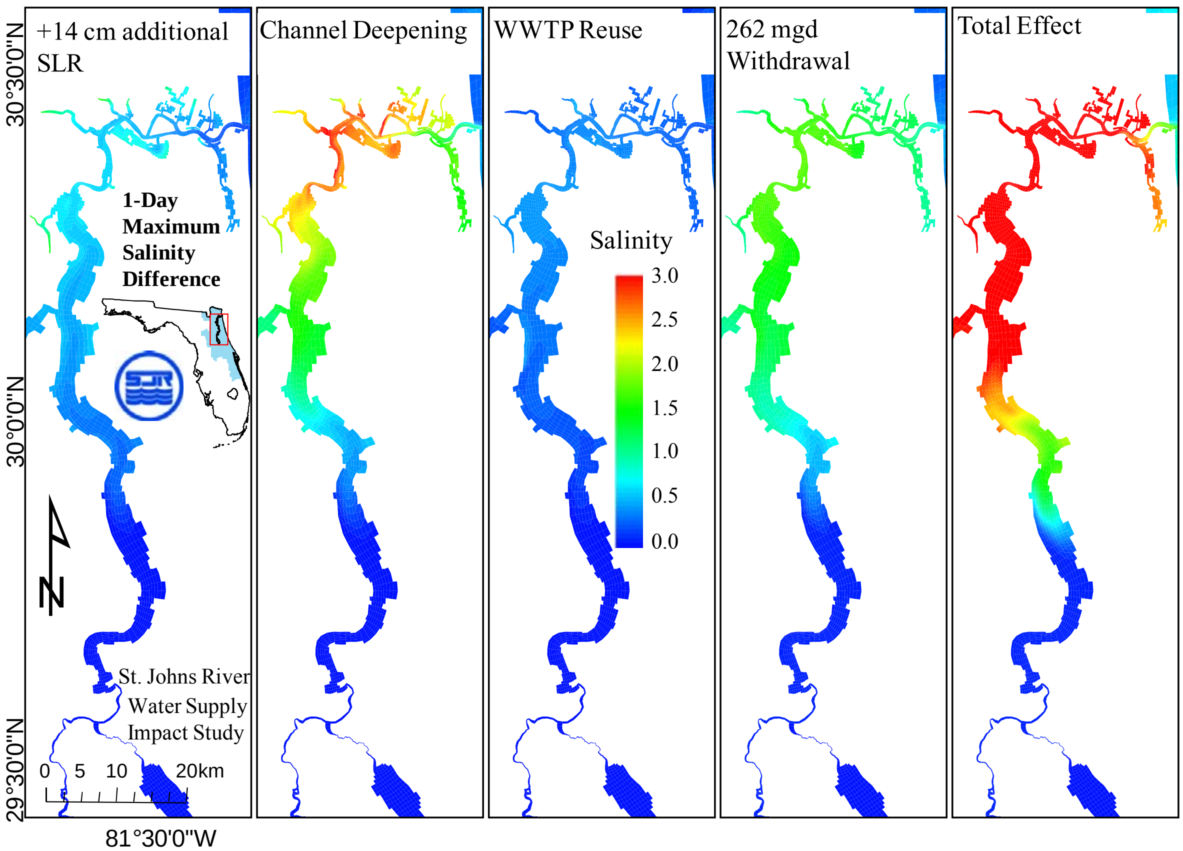

Figure 2–51. Contour plot of maximum 1-day difference in salinity for future scenarios relative to Base2030PS scenario. SLR = sea level rise, WWTP = wastewater treatment plant.

Water Age

Time Series Comparisons

Daily averaged time series of water age for Lake George compare water age for future scenarios (Figure 2–52). The difference among scenarios is only apparent when water age is high.

A plot of water age differences among scenarios shows that water age in Lake George is most affected by water withdrawal and sea level rise (Figure 2–53), whereas the effects of channel deepening and wastewater reuse on water age are negligible.

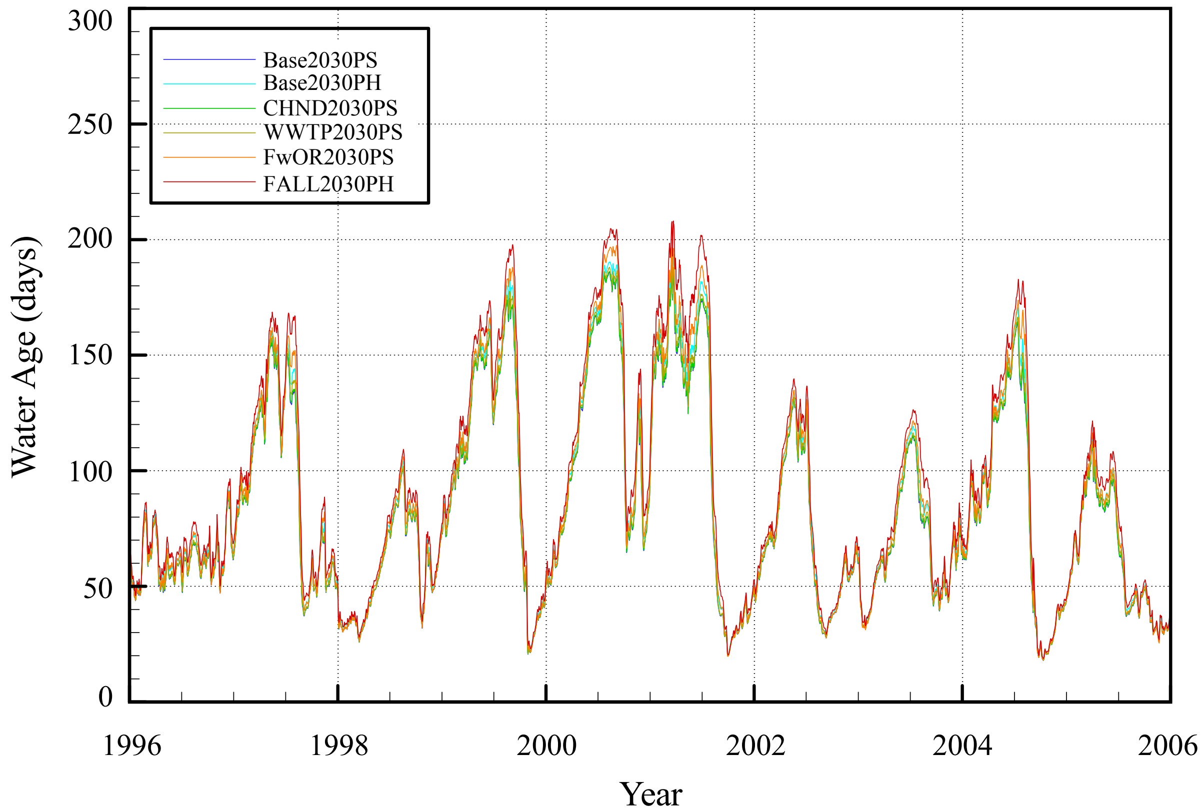

Figure 2–52. Times series of daily averaged water age in Lake George for future scenarios.

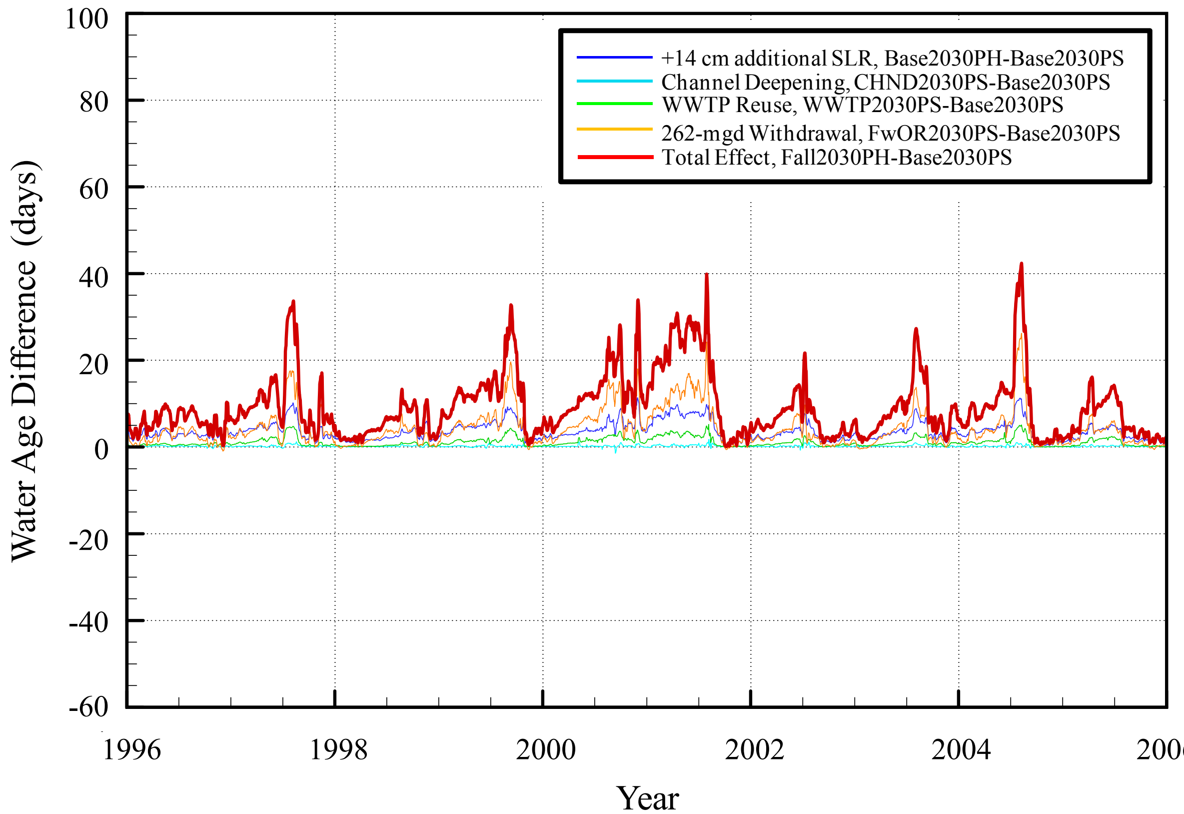

Figure 2–53. Difference of daily averaged water age between Base2030PS and future scenarios. Lake George. SLR = sea level rise, WWTP = wastewater treatment plant.

Comparative Statistics

The total effect of all the future factors (FALL2030PH minus Base2030PS) results in an increase in mean water age of 3.6 to 14 days. The greatest differences occur in the lower St. Johns River and Lake George.

Table 2–17. Comparative statistics for differences in daily water age between FALL2030PS and Base2030PS (total effect).

Station	*NRECS*	r^2	*m*	*b*	*RMSD* (days)	*AVRD* (days)	*AVAD* (days)
Acosta	3,652	0.987	0.960	-8.420	15.540	14.371	14.372
Orange Park	3,652	0.988	0.880	2.708	15.994	13.648	13.648
Shands Bridge	3,652	0.982	0.863	3.606	15.770	13.014	13.020
Racy Point	3,652	0.963	0.847	4.560	15.275	11.385	11.600
Buffalo Bluff	3,652	0.967	0.843	3.531	13.856	10.269	10.439
Lake George	3,652	0.988	0.876	1.930	11.937	9.322	9.322
DeLand	3,652	0.865	0.886	2.462	6.918	1.697	4.291
Lake Monroe	3,652	0.979	0.893	-0.184	8.625	5.990	6.062
Lake Jesup	3,652	0.998	0.936	2.770	5.851	4.680	4.682
Lake Harney	3,652	0.964	0.806	0.627	6.033	3.563	3.571

NRECS = Number of paired values
r^2 = Coefficient of determination
m = Slope of the linear regression line
b = Intercept of the linear regression line
RMSD = Root-mean-square difference
AVRD = Average relative difference
AVAD = Average absolute difference

Longitudinal Plots

A longitudinal plot of mean water age shows the general trend of increasing water age proceeding downstream (Figure 2–54). One exception is Lake Jesup. It has high water age, because it is off the main stem of the river and experiences less flushing than adjacent mainstem locations. The greatest differences among scenarios occur between Lake George and Acosta.

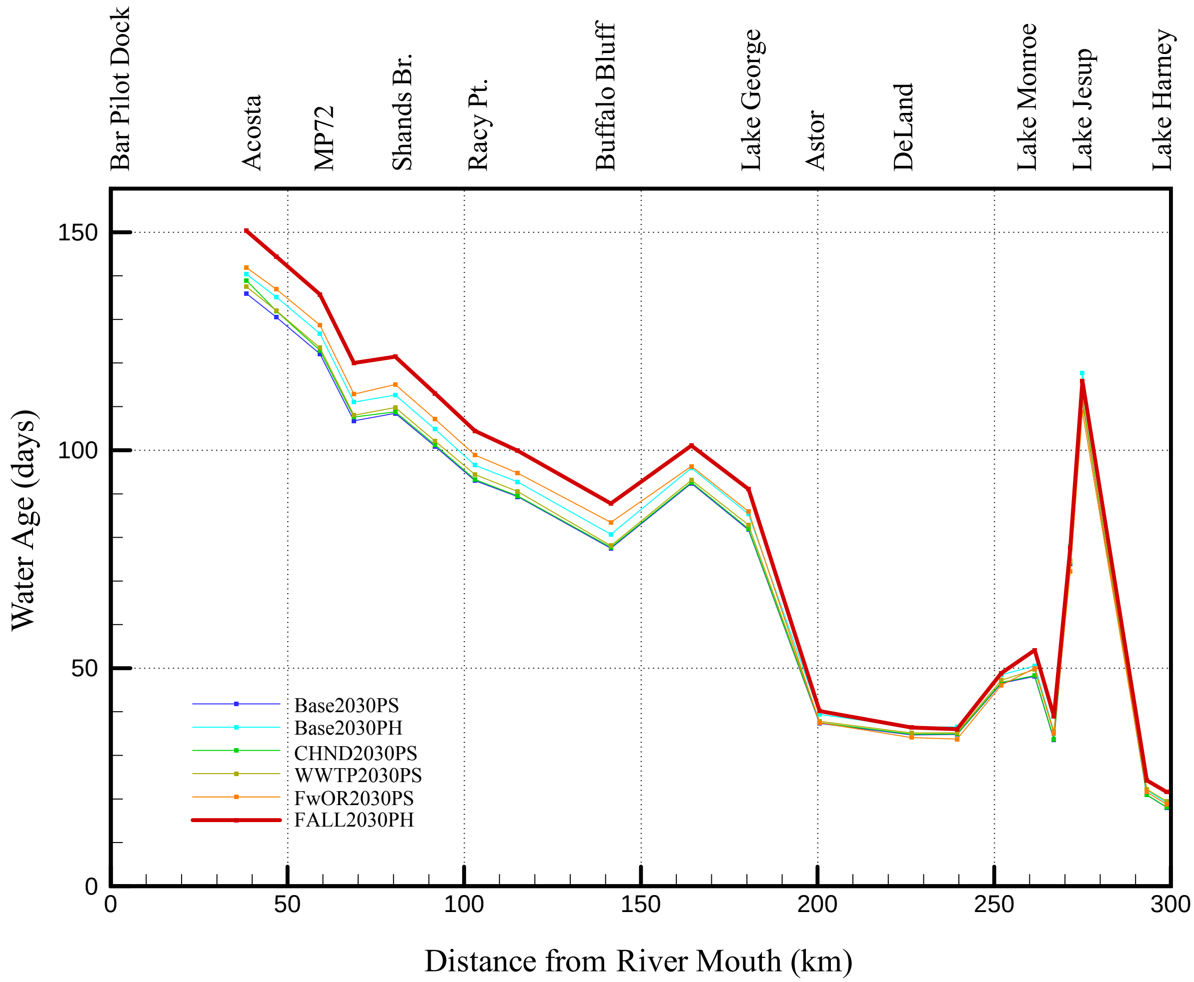

Figure 2–54. Longitudinal distribution of mean water age for future scenarios.

A longitudinal plot of mean water age differences among future scenarios clearly shows the greater change in water age for areas downstream of Astor (Figure 2–55). The greater increase in water age in the downstream reach is caused by the greater sensitivity of this reach compared to upstream areas to a 262-mgd withdrawal (FwOR2030PS). The greater sensitivity to water withdrawal of the downstream reach is largely due to the water withdrawals from the Ocklawaha River, which enters the St. Johns River below Lake George (orange line). Sea level rise (Base2030PH) increases mean water age 3 to 5 days throughout the model area (dark blue line). Channel deepening (CHND2030PS) and wastewater reuse (WWTP2030PS) have a negligible effect on water age.

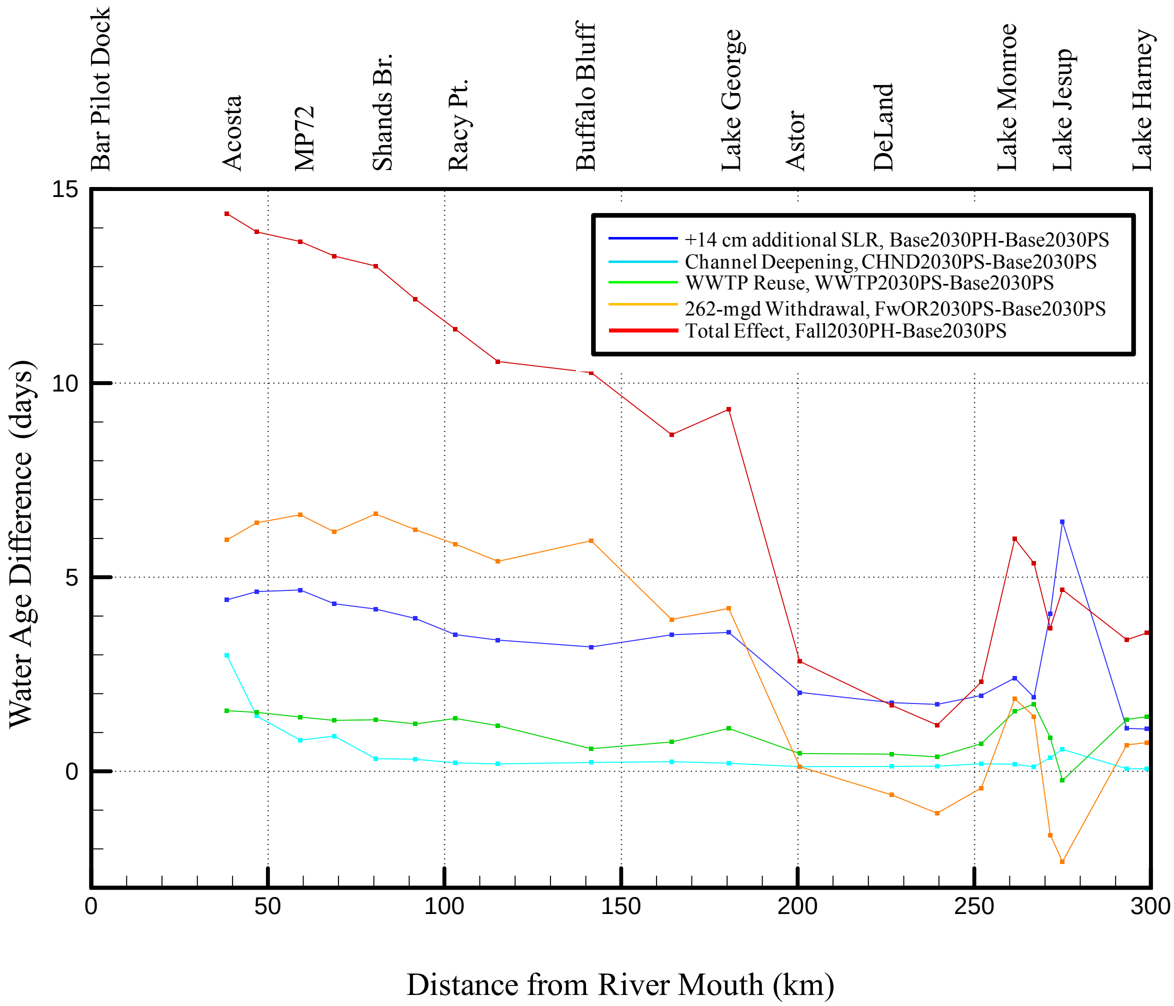

Figure 2–55. Longitudinal distribution of difference in mean water age among future scenarios. SLR = sea level rise, WWTP = wastewater treatment plant.

2.5 SUMMARY

Forecast scenarios consider factors affecting river hydrodynamics likely to occur during the period 1995 through 2030. These factors include structural changes to the USJRB, urbanization of watersheds, sea level rise, and a 155-mgd withdrawal. Water level changes expected under forecast conditions are dominated by sea level rise. Even with a 155-mgd withdrawal, mean water levels throughout the lower St. Johns River, Lake George, and middle St. Johns River are expected to rise at least 12 to 14 cm. Sea level rise has less effect on middle St. Johns River locations during periods of high flow, but under these conditions an increase in runoff due to increased urbanization of watersheds is expected to increase water levels also.

Future scenarios consider possible hydrodynamic changes caused by greater rates of sea level rise due to global climate change, channel dredging, wastewater reuse, and additional water withdrawal from the Ocklawaha River. For future conditions, only sea level rise has an appreciable effect on water levels. The consideration of possible increased future sea level rise increases the overall expectation of future water level increase throughout the system.

Salinity changes upstream of the estuarine reach of the river are negligible for both forecast and future conditions. Salinity in the estuarine reach is increased by water withdrawals, sea level rise, and channel dredging; and decreased by structural changes to the USJRB and urbanization of watersheds. For forecast conditions, the net change to mean salinity is negligible, and maximum salinity levels of high salinity events increase only slightly. Future conditions predict an increasing trend of salinity in the estuarine reach with channel deepening and water withdrawal being the most important factors. Even when taking into account an improbable combination of future conditions (FALL2030PH), however, the salinity regime of the lower St. Johns River is unlikely to change by the year 2030.

Water age changes for forecast conditions are greatest in Lake George. Water age changes for both forecast and future conditions, however, are small relative to the large variability of water age.

3 Hydrodynamic Uncertainty Analysis

3.1 Introduction

Uncertainty analysis refers to a general procedure to document, usually in a qualitative way, the confidence placed by scientists and engineers in their results and conclusions (Intergovernmental Panel on Climate Change 2005), and to specific, quantitative analyses designed to determine confidence in the output of a numerical model. We term the former procedure qualitative uncertainty analysis and the latter procedure model uncertainty analysis. The primary goal of both these types of uncertainty analyses is the same: to provide resource managers with the information necessary to make informed decisions. The fact that uncertainty exists does not mean that policy decisions cannot be made or management strategies adopted, but rather that responsible decisions and sound strategies take a certain level of uncertainty into account.

In this section, the qualitative uncertainty for EFDC hydrodynamic modeling is presented first (Section 3.2), followed by the model uncertainty analysis (Section 3.3). The qualitative uncertainty analysis incorporates the results of the model uncertainty analysis, as well as all other aspects of uncertainty considered relevant to the hydrodynamic study. As such, the qualitative uncertainty analysis both integrates and summarizes all aspects of uncertainty for the hydrodynamic modeling results. The qualitative uncertainty analysis is presented before the model uncertainty analysis to provide the reader a broad overview of hydrodynamic uncertainty without the necessity of reading the technically complex section on model uncertainty (Section 3.3).

In general, predicted model output from the EFDC hydrodynamic model has very low or low uncertainty. Specific areas of the model have greater uncertainty under certain conditions. These include (a) water level in Lake Harney under flood conditions, (b) daily fluctuations of discharge through the mouth of Lake Jesup, (c) salinity at the leading edge of ocean salinity intrusions, and (d) salinity in Lake Woodruff. These model outputs have medium uncertainty, although salinity in Lake Woodruff has high uncertainty.

3.2 Qualitative Uncertainty Analysis

This section summarizes qualitative uncertainty of the EFDC hydrodynamic model results with the implicit goal of informing the decision process so that the model can be a useful tool for decision makers. Qualitative uncertainty is evaluated and reported according to the general WSIS guidelines. These guidelines are derived from an approach outlined by the Intergovernmental Panel on Climate Change (2005) that assigns uncertainty to five categories based on evaluation of three types of evidence: weight of supporting evidence (SE), strength of predictive models (PM), and degree of understanding of mechanisms (UM) (Table 3–1).

Table 3–1. Criteria used to assign qualitative categories of uncertainty for WSIS.

Category of Uncertainty	Criteria
Very Low	Strong— Weight of supporting evidence (SE) Strength of predictive model (PM) Degree of understanding of mechanisms (UM)
Low	Strong— Strength of predictive model Weight of supporting evidence ***or*** Degree of understanding of mechanisms
Medium	Strong— Strength of predictive model ***or*** Weight of supporting evidence and Degree of understanding of mechanisms
High	Strong— Weight of supporting evidence ***or*** Degree of understanding of mechanisms
Very High	Weak— Weight of supporting evidence Strength of predictive model Degree of understanding of mechanisms

3.2.1 Methods

Application of the three criteria to the evaluation of qualitative uncertainty for hydrodynamic modeling requires association of the criteria with specific areas of uncertainty identified by the hydrodynamic modeling process. Within the context of hydrodynamic modeling, understanding of mechanisms is associated with the uncertainty of the model structure, or the relationships among the variables characterizing the system (Beck 1987). The strength of the predictive model is associated with model identification, or the parameters and model inputs used to define the system's behavior during model calibration. Finally, the weight of supporting evidence is associated with the measured data and data analyses used to understand the physical processes. Measurement uncertainty considers not only measurement error, but also the completeness of observations deemed necessary for building and assessing the model and defining the initial model state.

Model Structure

In general, we do not examine the uncertainty of the EFDC hydrodynamic model structure, particularly regarding assessment of the adequacy of the constituent hypotheses. Because of its documented history of use, we accept that the EFDC hydrodynamic model is an appropriate model for our application. The EFDC hydrodynamic model is a highly mechanistic model, built on the well-established Navier–Stokes equations describing the physical laws governing fluid motion. For practical application to large-scale surface water systems, these equations include simplifying assumptions that we accept as appropriate for our system. Beck (1987) also accepts this premise, pointing out "cause and effect in hydrology are unambiguously related, although…the precise mathematical form of this relationship can be extremely difficult to identify." The degree of understanding of mechanisms, then, is implicitly considered strong for EFDC hydrodynamic modeling.

Model Identification

Uncertainty analysis for EFDC hydrodynamic modeling is primarily focused on model identification, the setting of model parameters, and the description of external forces that drive the model prediction. Uncertainty in model identification can arise from definition of the model grid resolution, accuracy of bathymetry and bathymetric interpolation, placement of model boundaries defining the model domain, choice of spatial and temporal resolution of boundary forces, or selection of model parameters. Quantification of the aggregate uncertainty inherent throughout model identification is embedded in statistical comparison of observed and simulated variables during calibration. Hydrologic model results from the HSPF hydrologic model (see Chapter 3. Watershed Hydrology) were assigned uncertainty categories by reliance on Nash–Sutcliffe statistics developed during calibration of that model for WSIS (Table 3–2).

Table 3–2. Relationship between Nash–Sutcliffe statistic and WSIS uncertainty categories.

Nash–Sutcliffe Statistic (N – S)	WSIS Uncertainty Categories
0.75 < N–S ≤ 1.0	Very low
0.65 < N–S ≤ 0.75	Low
0.50 < N–S ≤ 0.65	Medium
N–S ≤ 0.50	High

For the EFDC hydrodynamic modeling, uncertainty categories are not completely determined by Nash–Sutcliffe statistics, although these statistics are used to demonstrate the strength of the predictive model. Uncertainty of supporting evidence is considered here as well. Unlike the HSPF hydrologic models, uncertainty of the EFDC hydrodynamic model output depends heavily on complex interactions among model boundary conditions, including ocean tide, wind, inflows, rainfall, and evaporation. The question of how uncertainty of the model boundary conditions propagates through the model to the model output addresses the supporting evidence criteria. This question is addressed formally in Section 3.3. The results of Section 3.3 are used here, in Section 3.2, to provide the reader with a complete assessment of the qualitative uncertainty without the need to first read the longer and technically complex Section3.3 on model uncertainty.

3.2.2 Results

Nash–Sutcliffe Statistics

Nash–Sutcliffe statistics are calculated for water level (Table 3–3), discharge (Table 3–4), and salinity (Table 3–5) at locations representative of each of the six WSIS river reaches contained within the lower and middle St. Johns River. Observed discharge is not available for all river reaches, but Main Street Bridge is strongly tidal and considered representative of both river reaches 1 and 2, while Buffalo Bluff is considered representative of river reaches 3 and 4 (see Chapter 5, River Hydrodynamics Calibration). For water level and discharge, Nash–Sutcliffe statistics are calculated using daily averaged values. For salinity, Nash–Sutcliffe statistics are calculated using 1-, 7-, and 30-day averages.

Table 3–3. Nash–Sutcliffe statistics for hydrodynamic response to daily water level representative of WSIS river reaches.

River Reach	Station	Station ID	Nash–Sutcliffe
1	Dames Point	FDEP 872-0219	0.96
2	Main Street Bridge	FDEP 872-0226	0.92
3	Shands Bridge	FDEP 872-0503	0.92
4	Buffalo Bluff	FDEP 872-0767	0.93
5	DeLand	USGS 02236000	0.98
6	Sanford	USGS 02234500	0.96

Table 3–4. Nash–Sutcliffe statistics for hydrodynamic response to daily discharge representative of WSIS river reaches.

River Reach	Station	Station ID	Nash–Sutcliffe
1, 2	Main Street Bridge	USGS 02246500	0.84
3, 4	Buffalo Bluff	USGS 02244040	0.88
5	DeLand	USGS 02236000	0.95
6	Sanford	USGS 02234500	0.96

Table 3–5. Nash–Sutcliffe statistics for hydrodynamic response to 1-, 7-, and 30-day salinity representative of WSIS river reaches.

River Reach	Station	Station ID	1-day Nash–Sutcliffe	7-day Nash–Sutcliffe	30-day Nash–Sutcliffe
1	Dames Point	USGS 302309081333001	0.79	0.80	0.84
2	Main Street Bridge	USGS 02246500	0.89	0.90	0.90
3	Shands Bridge	USGS 295856081372301	0.58	0.57	0.57
4	Buffalo Bluff	USGS 02244040	0.75	0.79	0.82
5	DeLand	USGS 02236000	0.82	0.86	0.92
6	Sanford	USGS 02234500	0.86	0.89	0.92

The Nash–Sutcliffe statistics show that the strength of predictive models is generally strong for the hydrodynamic model. Nash–Sutcliffe equals or exceeds 0.75 in all river reaches and for all variables except salinity at Shands Bridge (river reach 3). A strong predictive model coupled with the implicit assumption of strong understanding of mechanisms for the hydrodynamic model classifies most model output as having very low to low uncertainty. Salinity at Shands Bridge is examined further below, as well as other exceptions determined through consideration of model calibration, model uncertainty analysis (section 3.3), and the adequacy of observed data.

Consideration of Hydrodynamic Model Calibration

Hydrodynamic model calibration (see Chapter 5. River Hydrodynamics Calibration) identified four areas of elevated uncertainty: (a) the strength of the leading edge of marine salinity intrusion in river reach 3, (b) water level in Lake Harney (river reach 6) during extreme high river discharge, (c) Lake Woodruff salinity (river reach 5), and (d) discharge through the mouth of Lake Jesup.

The Nash–Sutcliffe statistics for salinity at Shands Bridge in river reach 3 are low because the model underpredicted a few of the highest salinity events. For several events, the model underpredicted the magnitude of salinity at the leading edge of upstream salinity intrusions. The model, however, predicted the timing and duration of these intrusion events well. In addition, this underprediction of salinity did not extend to the entire river river reach, but only to those times and locations where salinity is elevated above the background level of the normal oligohaline condition. These times and locations are identified by salinity between 1 and 3 PSS78. For salinity either above or below this range, the model is strongly predictive in this river reach (river reach 3). Because of the weaker predictive capability of the model, uncertainty of salinity is considered medium in the immediate zone of transition between upstream oligohaline waters and a salinity contour level of 3 PSS78.

Although the model is a strong predictor of water level throughout the model area, the model is shown to overpredict water level in Lake Harney for periods of extreme high discharge when water levels exceed 2 m NAVD88. The cause of the overprediction is likely due to the lack of flood plain storage in our set-up of the EFDC hydrodynamic model. For high flow conditions, then, predicted water level in Lake Harney has medium uncertainty.

Model calibration showed that the model prediction of salinity in Lake Woodruff was unacceptable. In addition, available observed data are presently inadequate to address the cause of this problem. Therefore, model predictions of salinity in Lake Woodruff and areas east of the lake have high uncertainty.

Monthly discharge at the mouth of Lake Jesup (river reach 6) had a Nash–Sutcliffe statistic of 0.60. This location is accordingly assigned medium uncertainty.

Consideration of Model Uncertainty Analysis

Model uncertainty analysis is used below (section 3.3) to propagate the estimated uncertainty of model boundary conditions and parameters (bottom roughness) through the modeled system to the predicted output. This analysis shows that water level and discharge in the middle St. Johns River (river reaches 5 and 6) are sensitive to tributary discharge under certain hydrologic conditions. Under these conditions, uncertainty for these variables should be linked to the uncertainty of the tributary discharges driving the response. The hydrodynamic uncertainty, then, should not be lower than the hydrologic uncertainty.

Uncertainty for water level becomes dependent on hydrologic uncertainty when river stage exceeds 0.25 m NAVD88 in river reach 5 (Figure 3–29) and 0.5 m NAVD88 in river reach 6 (Figure 3–31). For river reach 5 these are water levels above the 37th percentile. For river reach 6 these are water levels above the 75th percentile. Under these conditions, uncertainty is raised from very low to low to match hydrologic uncertainty (see Chapter 3. Watershed Hydrology).

Uncertainty for discharge becomes dependent on hydrologic uncertainty in river reaches 5 and 6 when river discharge at DeLand exceeds 2,282 mgd (100 m^3s^{-1}) (Figure 3–41). These are discharges above the 75th percentile. Under these conditions, uncertainty is raised from very low to low.

Adequacy of Observed Data

Salinity dynamics in the partially stratified portions of the lower St. Johns River depend on complex interactions among tides, freshwater discharges, stratification, and estuarine circulation. At present, there are no direct observations of residual two-layer circulation in this area to directly confirm the model’s dynamic response. There is also no comprehensive set of synoptic salinity measurements that show the dynamic response of salinity and stratification at tidal scales. Although the model predicts salinity at fixed locations well (strong predictive model), and the model structure is well established for this flow dynamic (strong understanding of mechanisms), uncertainty for salinity in river reaches 1 and 2 is raised from very low to low due to the inadequacy of observed data.

Spatial Grid Resolution

One additional aspect of hydrodynamic model uncertainty to be considered is the appropriateness of the model’s spatial resolution to a given question. The hydrodynamic model resolves the system at about a 100-m spatial scale. System properties, then, are aggregated to conform to this minimum resolution. Subgrid scale features, such as narrow submersed aquatic vegetation beds for example, are not resolved and uncertainty is introduced if the larger scale features of the model do not appropriately represent a subgrid scale feature.

Uncertainty of Differences Between Model Scenarios

The primary use of the model is for prediction of the relative change between a base condition and a scenario. The uncertainty inherent in the prediction of relative change, then, is of importance to WSIS.

The uncertainty of relative change is examined in Section 0. This analysis indicates that relative change remains constant throughout the range of uncertainty of the model input. This result indicates that perturbations to, or uncertainty of, the base condition does not affect the predicted change wrought by the scenario. At Shands Bridge, for example, the absolute predictions were assigned a medium uncertainty for salinity between 1 and 3 PSS78. Predicted change of salinity at this location for this salinity range, however, varies only ±0.25 PSS78 due to uncertainty in model inputs. The predicted differences among model scenarios, then, have a very low uncertainty for all river reaches and all output variables. The exceptions are salinity in Lake Woodruff, where the lack of prediction of absolute salinity makes prediction of scenario differences meaningless, and water level in Lake Harney during high flow events when the model overpredicts the change between scenarios.

Uncertainty of Water Age

The uncertainty of water age is not directly assessed above because water age is a synthetic model output variable with no real world observations. Water age, however, follows the response of the model to advection and diffusion. Its uncertainty, then, is assumed to follow the combined uncertainty of discharge and salinity. We conservatively assign water age the higher uncertainty level between discharge and salinity.

3.2.3 Summary of Qualitative Uncertainty

Hydrodynamic uncertainty is summarized in four tables below. Uncertainty categories are assigned for each river reach and for output variables of water level (Table 3–6), discharge (Table 3–7), salinity (Table 3–8), and water age (Table 3–9). Exceptions are noted in each table.

Table 3–6. Summary of hydrodynamic model uncertainty for water level.

WSIS River Reach	Uncertainty Category	Exceptions
1	Very low	None
2	Very low	None
3	Very low	None
4	Very low	None
5	Very low	Low for H > 0.25 m NAVD88
6	Very low	Low for H > 0.5 m NAVD88 Medium for H > 2.0 m NAVD88

H = Depth.

Table 3–7. Summary of hydrodynamic model uncertainty for discharge.

WSIS River Reach	Uncertainty Category	Exceptions
1	Very low	None
2	Very low	None
3	Very low	None
4	Very low	None
5	Very low	Low for discharge exceeding 75th percentile at DeLand
6	Very low	Medium in Lake Jesup mouth Low for discharge exceeding 75th percentile at Sanford

Table 3–8. Summary of hydrodynamic model uncertainty for salinity.

WSIS River Reach	Uncertainty Category	Exceptions
1	Low	None
2	Low	None
3	Low	Medium when 1 < S < 3 PSS78
4	Very low	None
5	Very low	High in Lake Woodruff and areas east
6	Very low	None

Table 3–9. Summary of hydrodynamic model uncertainty for water age.

WSIS River Reach	Uncertainty Category	Exceptions
1	Low	None
2	Low	None
3	Low	Moderate when 1 < S < 3 PSS78
4	Very low	None
5	Very low	Low for discharge exceeding 75th percentile at DeLand High in Lake Woodruff and areas east
6	Very low	Medium in Lake Jesup mouth Low for discharge exceeding 75th percentile at Sanford

3.3 Model Uncertainty Analysis

Model uncertainty analysis provides a means to assess how much variability in the model output is due to uncertainty in the model inputs. This assessment allows the placement of confidence intervals about the simulated model output. In addition, model uncertainty analysis provides a means for assessing the numerical model's ability to predict future conditions for "what-if" scenarios.

The model uncertainty analysis described here examines EFDC hydrodynamic model responses to estimated uncertainty in model input variables. The following input variables are considered:

- Wind, rain, and evaporation
- Tidal and subtidal ocean water level
- Freshwater inflows derived from hydrologic modeling
- Bathymetry
- Salinity of surface water, groundwater, and ocean inflows
- Bottom roughness

3.3.1 Comparison of Model Uncertainty Analysis Methods

Model uncertainty analysis is an evaluation methodology that can provide additional information about the sources of model uncertainty. Model uncertainty analysis generally includes sensitivity analysis, assignment of variance to individual model variables and parameters, and determination of how the defined uncertainty of the model inputs affects the model outputs (Matott, et al. 2009). Beck (1987) and Matott et al. (2009) provide reviews of the wide range of model evaluation categories and analysis techniques that fall into the discipline of model uncertainty analysis. We compare here three broad and commonly used categories: sensitivity analysis, first order error analysis (FOEA), and Monte Carlo simulation (MCS).

Sensitivity analysis is a simple assessment used to determine the relative effect each model input variable or parameter has on the simulated model results. Although simple, sensitivity analysis is useful for calibration and for insight into how a modeled system responds to alteration of individual model boundary conditions that may be difficult to separate by in situ observation.

FOEA includes sensitivity analysis but also accounts for variance of individual model inputs and propagates uncertainty from the model inputs to the model outputs using linear combination (Zhang and Yu 2004). FOEA, therefore, provides (a) the relative sensitivity of each variable, (b) the relative contribution of each variable to model uncertainty, and (c) error bounds on model output. In addition, FOEA can estimate the expected increase in model performance from an expected improvement to an input variable (Blumberg and Georgas 2008), for example, additional monitoring, helping to determine the efficacy of proposed data collection plans.

Zhang and Yu (2004) consider the main limitation of FOEA to be the dependence on the results of the system performance function linearization at the central values of the input variables (where the central values are at the calibrated state.) This assumption is inappropriate for nonlinear models where values deviate far from the central state. Blumberg and Georgas (2008) also note the weakness of the assumption of zero correlation among input variables.

MCS is a category of model uncertainty analysis that describes model input variables and parameters as probability density functions. In MCS, output uncertainty is evaluated using multivariate combinations of model inputs. The result of MCS is quite powerful in that the aggregation of model uncertainty is expressed as complete probability density functions of the model output.

There are two disadvantages to MCS: computational burden and the difficulty of assigning probability density functions to uncertain input variables and parameters. The class of three-dimensional hydrodynamic models used for this study is computationally intensive and, as expressed by Martin and McCutcheon (1999), “the computational burden of making thousands of simulations practically limits the application (of MCS) to simpler water quality models.” Uncertainty in model inputs and parameters often includes lack of knowledge regarding their probability distributions. This important aspect of MCS then requires subjective estimation. When such lack of knowledge exists, the advantage of MCS over simpler methods, such as FOEA, is reduced. For these reasons model uncertainty for the EFDC hydrodynamic model was evaluated using FOEA.

3.3.2 METHODS

First Order Error Analysis

The theoretical development of FOEA is described by Blumberg and Georgas (2008). Only the key elements of the practical application of the method are presented here.

Let $F(\mathbf{X})$ = a model output variable with $\mathbf{X} = (x_1, x_2, \ldots, x_p)$, where x_i is a model input parameter. If σ_F = standard deviation of the output variable, and σ_i= the standard deviation of the input parameter x_i, then the FOEA method estimates the relationship between the output variance and input variances by the relation:

$$\sigma_F^2 = \sum_{i=1}^{p} [(\frac{\partial F(x_i = x_{io})}{\partial x_i} \sigma_i]^2 \tag{3–1}$$

The notation for the derivative is meant to indicate that the derivative is estimated at the unperturbed model state for which $x_i = x_{io}$. The input variables for the unperturbed state are those used for the model calibration, or model base scenario.

This equation can be expressed in the following equivalent nondimensional form:

$$[C_v(F)]^2 = \sum_{i=1}^{p} (S_i^{F_{x_i}=x_{io}})^2 [C_v(x_i)]^2 \tag{3–2}$$

where

C_v(F) $= \frac{\sigma_F}{F_0}$ = coefficient of variation of the output variable

$C_v(x_i)$ $= \frac{\sigma_i}{x_{io}}$ = coefficients of variation of the model input parameters

$S_i^{F_{x_i}=x_{io}}$ = a dimensionless sensitivity coefficient (*DSC*).

Equation 3-2 indicates that the total variance of the model output can be estimated from the individual variances of the model input variables and a set of calculated sensitivity coefficients. One useful result of FOEA is that the sensitivity of model output variables to each input variable is readily available.

The *DSC*s are estimated numerically by a simple forward difference by the following equation:

$$S_i = \frac{\frac{F(x_{io} + \Delta x_i) - F(x_{io})}{F(x_{io})}}{\frac{\Delta x_i}{x_{io}}} \tag{3–3}$$

where

$F(x_{io})$ = the model base state

$F(x_{io}+\Delta x_i)$ = the perturbed model state with the i-th input variable varied from its base value by a fixed percentage.

In practice, the magnitude of the variation of each input variable must be large enough to effect a discernible change in the output, but not so large that the estimation of the derivative about the unperturbed state deviates significantly from the assumed linear approximation. Note that the calculation of a *DSC* requires only one additional model simulation in addition to the base simulation. If there are *N* output variables and *P* input variables, FOEA requires $N \cdot P + 1$ model simulations. This can be a considerable savings in computational effort over MCS, which requires in the order of 100 to 1,000 model simulations.

The *DSC*s calculated by Equation 3–3 represent the percent change in the output variable for a unit 1% change in an input variable. For example, a value of 1.0 for a *DSC* indicates that the coefficient of variation of an input variable (as a percentage) will contribute that identical percentage of uncertainty to the output variable. *DSC* values, then, can be presented as either absolute or relative values. Relative values of *DSC*s show the percentage of contribution of each *DSC* to the total model uncertainty, assuming equal uncertainty of each model input variable, and are a useful way to classify the relative sensitivity of model output variables to various model inputs.

Because *DSC*s are calculated for all combinations of output and input variables, they are generally notated with a superscript identifying the output variable and a subscript identifying the input variable. For example, the *DSC* for the sensitivity of model salinity to wind would be notated as S_W^{Sal}.

Because F(**X**) in Equation 3–3 is a function of both space and time, the calculated *DSC*s are also. This means that Equation 3–2 could be used to establish confidence limits about the model output for each individual model cell and each output time interval. In practice, the spatially and temporally varying *DSC*s are sampled over specified regions and time periods, usually by selection of a single median value (Blumberg and Georgas 2008). This simplification follows the general goal of making the uncertainty analysis understandable and useful, and this method has been shown to produce reasonable results for FOEA.

Finally, Equation 3–2 can be used to calculate a total variance for model output using the calculated *DSC*s in conjunction with estimated variances of the model input variables. For this step, model input variances are selected by the modeler based on observation, literature values, or professional judgment. The total variance for the model output can then be used to calculate error bars about the simulated time series generated as model output.

Application of First Order Error Analysis to the EFDC Hydrodynamic Model

The FOEA for the EFDC hydrodynamic model estimates the uncertainty of three principle hydrodynamic output variables to eleven input variables. The output variables considered are water level (η), current speed (V), and salinity (Sal). The input variables are listed in Table 3–10 along with the symbol used for designating each variable, range of values used in the model, and units of range values.

Table 3–10. Input variables used for application of FOEA to EFDC hydrodynamic model (excluding ocean cells).

Input Variable	Symbol	Model Range	Units
Depth	H	0.8 to 20.6	m
Bottom roughness	Z_0	0.0001 to 0.025	m
Wind speed	W	0.0 to 25.2	m s^{-1}
Tributary discharge	Q	1,011 (44.3) to 49,901 (2,186.3)	mgd (m^3 s^{-1})
Ocean tide	η_T	Tidal range of 1.4	m
Ocean non-tide	η_{NT}	Quasi-periodic range of 20 to 40	cm
Rain	Rn	0 to 32	cm day^{-1}
Evaporation	Ev	0.06 to 0.83	cm day^{-1}
Tributary salinity	Sal_Q	0.01 to 3.4	PSS78
Ocean salinity	Sal_O	35.5	PSS78
Groundwater salinity	Sal_{GW}	0.36 to 2.5	PSS78

*DSC*s were calculated within 12 model sub-domains (Figure 3–1) distributed through the model domain. *DSC*s were calculated for the year 2001 for each of 8,760 hourly values and for each model cell. The median *DSC* was then estimated for each sub-domain and month as the estimate of overall sensitivity.

The *DSC*s were calculated using a forward difference (Equation 3–3), where each input variable was increased by 10% of the unperturbed state. For spatially varying input variables (depth and bottom roughness), values in all model cells were increased by an equal percentage. For all time series, except η_T and η_{NT}, each value in the series was increased by 10%. For ocean water level variation (η_T and η_{NT}), each value in the series was increased 10%, but relative to the mean so that MSL was left unaltered and only the range of water level about the mean was altered.

Coefficients of variation (C_v) for input variables are required to estimate total model uncertainty using Equation 3–2. Zhang and Yu (2004) report typical ranges of C_v for hydraulic variables of 5% to 15%. Our estimates of C_v for the input variables (Table 3–10) were generally within this range except for tributary salinity (Sal_Q), groundwater salinity (Sal_{GW}), and bottom roughness (Z_0), which were increased above 15%; and ocean salinity (Sal_O), which was regarded as having very low uncertainty. We classified the uncertainty of the remaining input variables as either low (5%), median (10%), or high (15%).

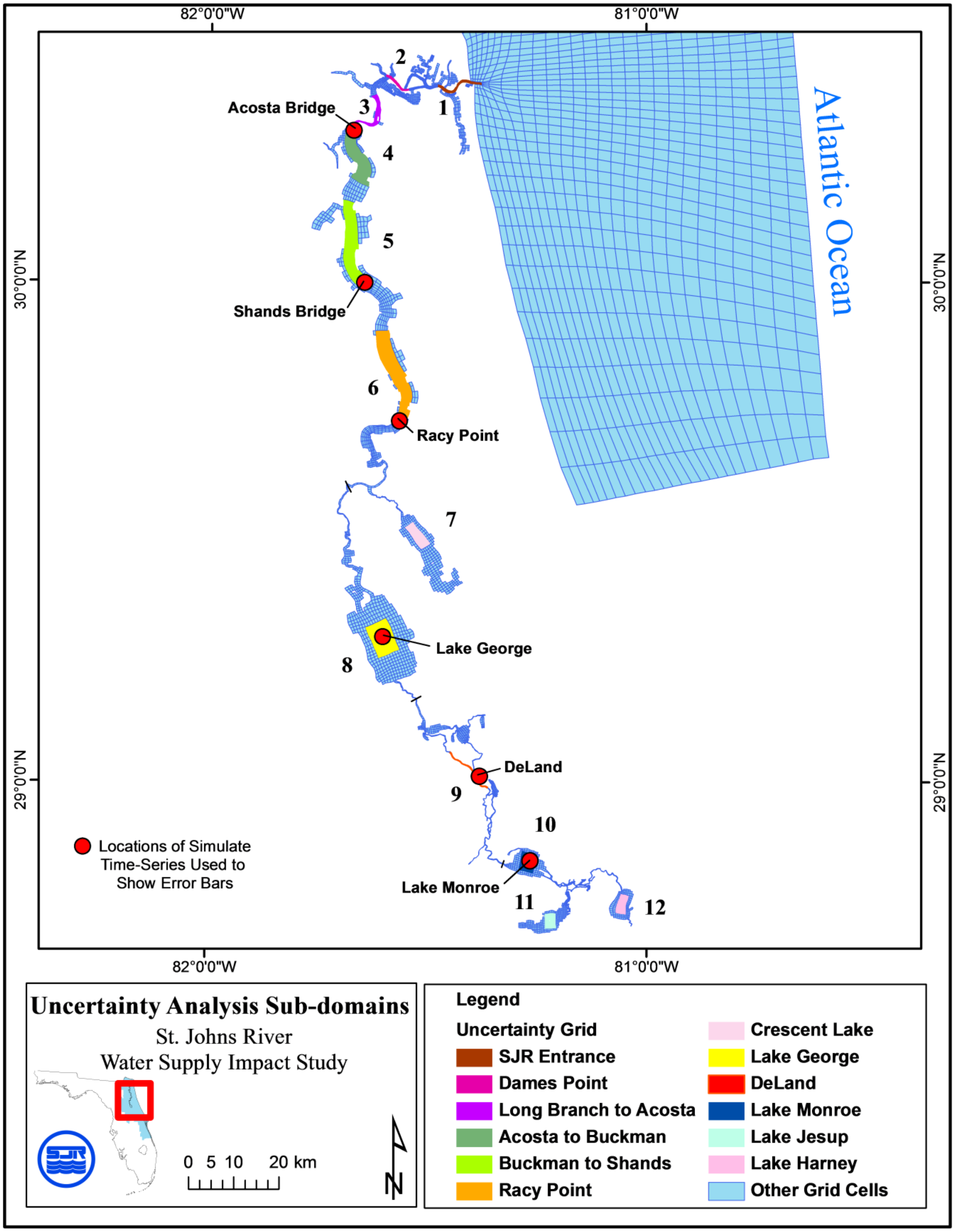

Figure 3–1. Sub-domains within EFDC hydrodynamic model grid used for uncertainty analysis. SJR = St. Johns River.

Depth (H) and ocean water level (η_T and η_{NT}) were classified as low uncertainty. Although there is considerable uncertainty for a single depth measurement in the field, the model depths are determined from many thousands of observations, and we had good bathymetric coverage throughout the model domain. We assume that the model depths, then, have low uncertainty because of the spatial averaging. A conservative range of error for global depth is ±15 cm and, because the mean depth of the non-ocean cells is 2.86 m, this translates to about a 5% uncertainty.

Ocean water level was based on hourly water level observations at Bar Pilot Dock that spanned the entire model simulation period and have subcentimeter accuracy. We moved the boundary offshore, however, and manually adjusted the offshore tide against predicted tide at Bar Pilot Dock, which resulted in an offshore, principle lunar semidiurnal (M_2) tide of 65.9 cm. As a check, an independent estimate of M_2 tide predicted from a western Atlantic tide model (Hagen and Parrish 2004) along our open model boundary was 64.5 cm, a deviation of 2%.

The C_v of mean wind speeds at eight sites throughout the region was 16% and wind was thus classified as high (15%) uncertainty. Tributary discharge (Q), rain (Rn), and evaporation (Ev) were classified as having median (10%) uncertainty to follow literature estimates (Zhang and Yu 2004) and recognizing that considerable effort was put into minimizing bias in hydrologic data through the HSPF hydrologic modeling process (see Chapter 3. Watershed Hydrology).

Variation of mean ocean salinity is considered small, although the salinity on the shelf along the southern Atlantic Bight can be affected by large regional discharge events. SJRWMD monitoring of salinity in this shelf region during March through October 2007 showed a mean salinity of 35.9, with essentially no salinity stratification. The observations were within 1% of the model input of 35.5. Therefore, we use a C_v of 1% for ocean salinity.

The uncertainty of tributary salinity and groundwater salinity was set at 20% and is greater than the high classification based on observed relationships between discharge and salinity within tributaries. The mean residual error for these relationships was generally about 10%. However, a chloride budget of the middle St. Johns River between Lake Harney and DeLand showed errors of 20%, where much of the chloride flux was generated from a steady state groundwater simulation. Based on this result, we increased the C_v for both tributary and groundwater salinity to 20%.

Finally, the C_v for bottom roughness (Z_0) was also increased above the high classification to 20% based on the judgment of the modelers when considering global adjustments of bottom roughness that would still lie within acceptable model calibration criteria. The C_v for all input variables is summarized in Table 3–11.

We recognize that the estimation of uncertainty for input variables is ad hoc. However, testing of alternate values of uncertainty using FOEA is straightforward; and assessments of the importance of uncertainty range of input variables to the overall model uncertainty can be quickly grasped by simple examination of the *DSC*s.

Table 3–11. Summary of EFDC hydrodynamic model input variable uncertainties.

Input Variable	Coefficient of Variation (%)
Depth (H)	5
Bottom roughness (Z_o)	20
Wind speed (W)	15
Tributary discharge (Q)	10
Ocean tide (η_T)	5
Ocean non-tide (η_{NT})	5
Rain (Rn)	10
Evaporation (Ev)	10
Tributary salinity (S_Q)	20
Ocean salinity(Sal_O)	1
Groundwater salinity (Sal_{GW})	20

3.3.3 RESULTS

Dimensionless Sensitivity Coefficients

Dimensionless Sensitivity Coefficients (*DSC*s) for the output variables were calculated for each of 12 sub-domains (Figure 3–1) and for each month of the year 2001. The *DSC*s show the sensitivity of model output to an equal percent change in input. Examination of *DSC*s for the 12 sub-domains illustrates how model sensitivity changes throughout the model domain, while examination of *DSC*s for each month illustrates how model sensitivity changes over time. *DSC*s at some locations exhibit seasonal variability in response to seasonal discharge variability.

Results of the *DSC* calculations are presented below for water level (S^{η}), current speed (S^{V}), and salinity (S^{Sal}) as a series of time series plots. The y-axes are on a log scale. Values of *DSC*s near 1.0 or greater indicate large sensitivity, values near 0.1 indicate low sensitivity, and values of 0.01 or less indicate insensitivity.

Water Elevation

Not surprisingly, the tidal portion of the St. Johns River is sensitive to ocean tide. However, ocean tide exhibits a dominant sensitivity on water level only in the area near the river entrance (Figure 3–2). In sub-domains 2 and 3, between Dames Point and Acosta Bridge, water level is most sensitive to depth and secondarily to ocean tide (Figure 3–3).

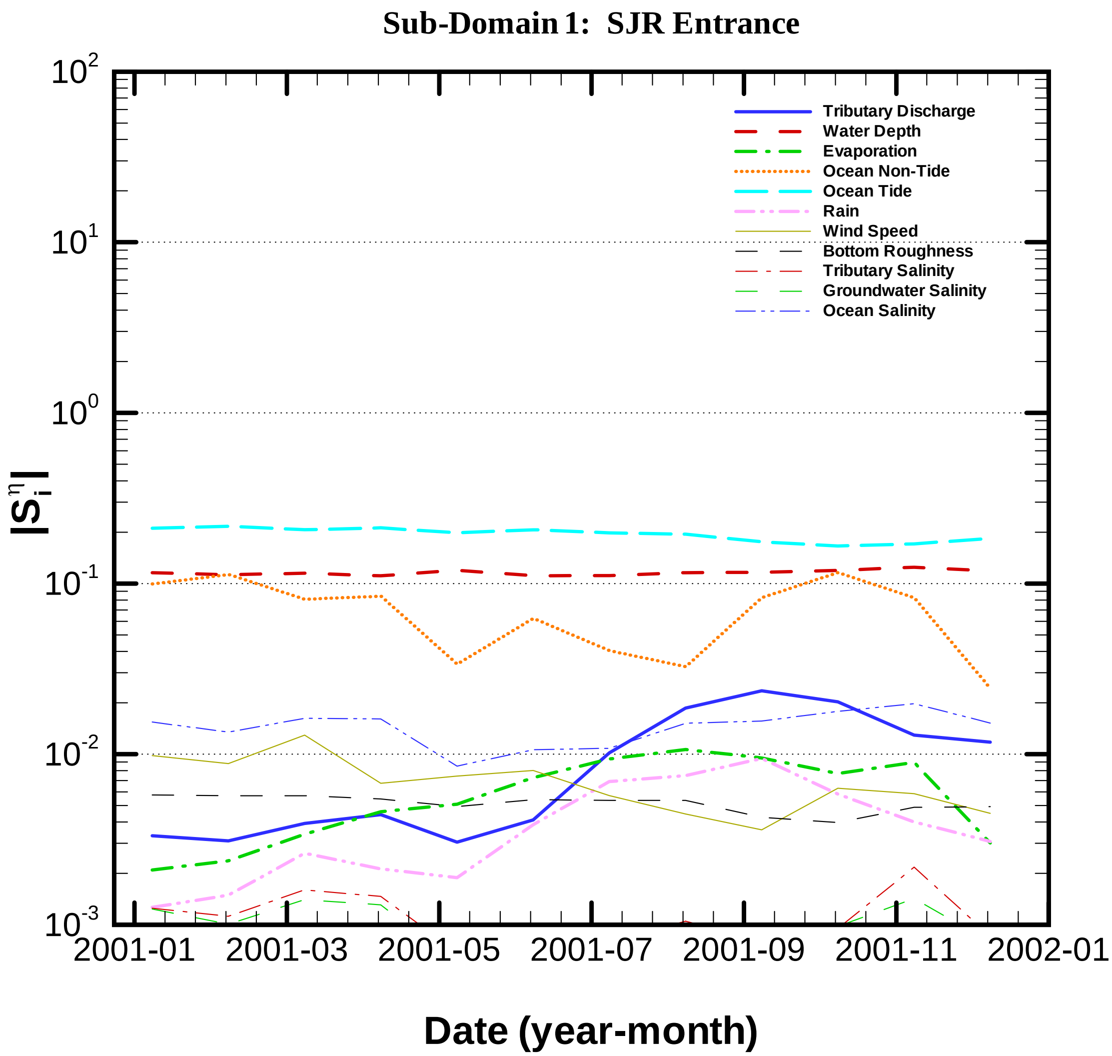

Figure 3–2. Median monthly dimensionless sensitivity coefficients (S^{η}) of water level to all tested input variables in sub-domain 1, St. Johns River entrance. SJR = St. Johns River.

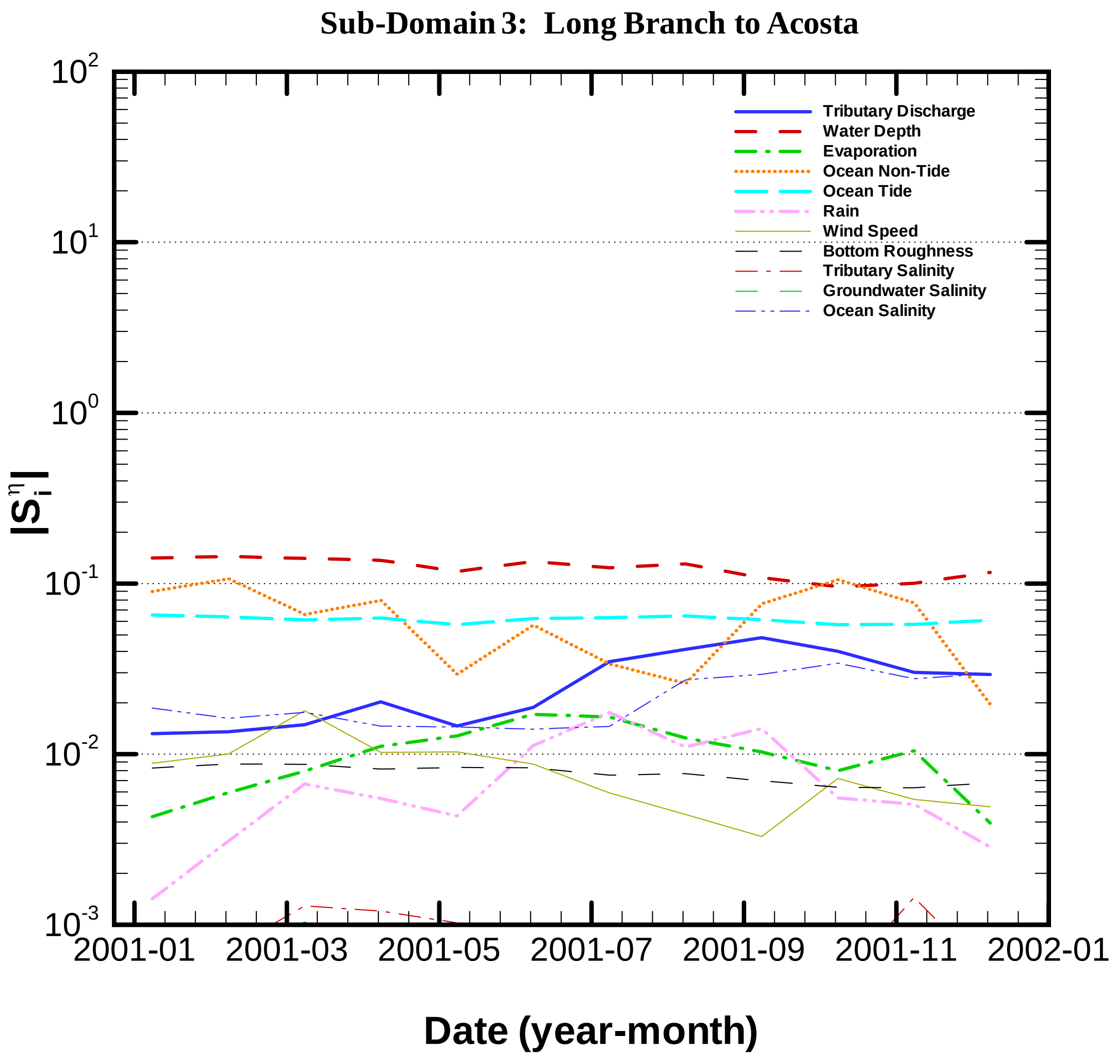

Figure 3–3. Median monthly dimensionless sensitivity coefficients (S^η) of water level to all tested input variables in sub-domain 3, Long Branch to Acosta. (Sub-domain 2 showed similar results.)

In sub-domains 4 through 6 (the freshwater tidal portion of the St. Johns River) depth, ocean tide, and ocean non-tide all exhibit nearly equivalent sensitivity on water level (Figure 3–4). Water level in Lakes Crescent and George shows similar sensitivity as sub-domains 4 through 6 in the first half of 2001 (the dry period). The sensitivity of water level shifts in the fall (the wet period) to include tributary discharge (Figure 3–5).

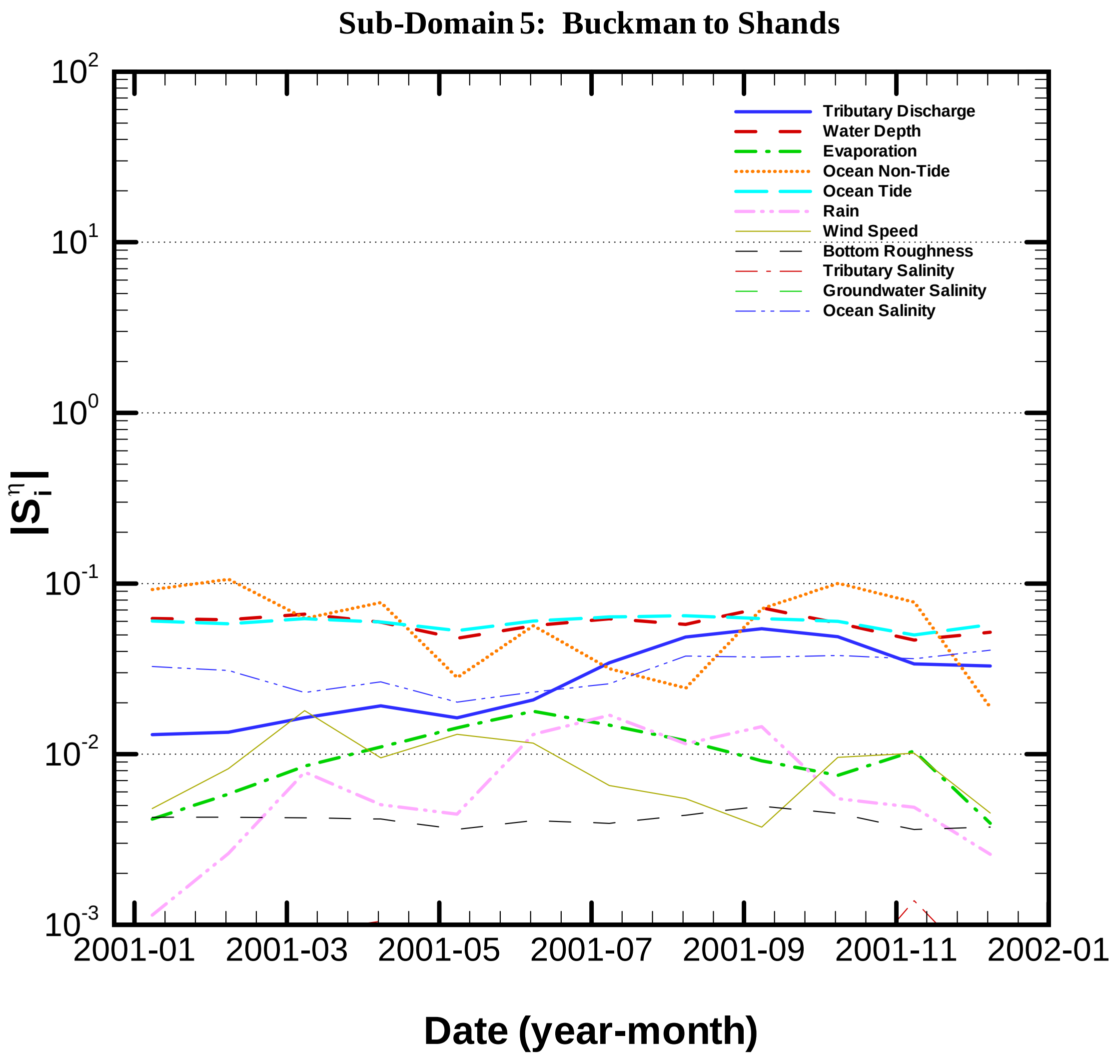

Figure 3–4. Median monthly dimensionless sensitivity coefficients (S^{η}) of water level to all tested input variables in sub-domain 5, Buckman to Shands. (Sub-domains 4 and 6 showed similar results.)

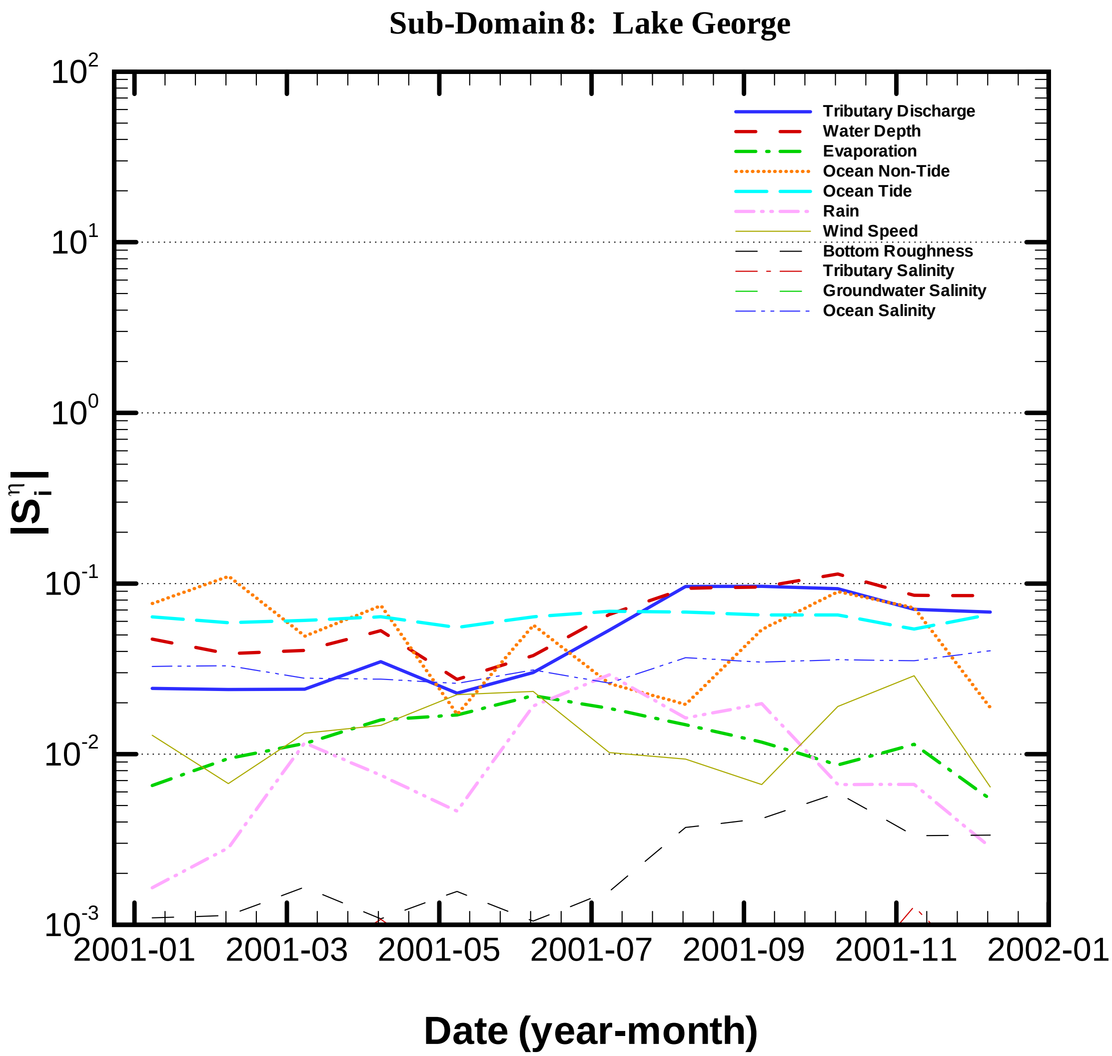

Figure 3–5. Median monthly dimensionless sensitivity coefficients (S^η) of water level to all tested input variables in sub-domain 8, Lake George. (Sub-domain 7 showed similar results.)

Sub-domains 9 through 12 (the middle St. Johns River) exhibit similar sensitivity for water level (Figure 3–6). As for the downstream tidal areas, water levels in the middle St. Johns River are sensitive to depth, ocean tidal, and ocean non-tidal forces in the dry season. The sensitivity of middle St. Johns River water level to ocean tide is an indication that ocean tide does influence this area during periods of low discharge. During the wet season, and in contrast to areas further downstream, water levels in the middle St. Johns River are sensitive to both depth and discharge. This sensitivity is indicative of a strong relationship between discharge and stage during periods of high discharge.

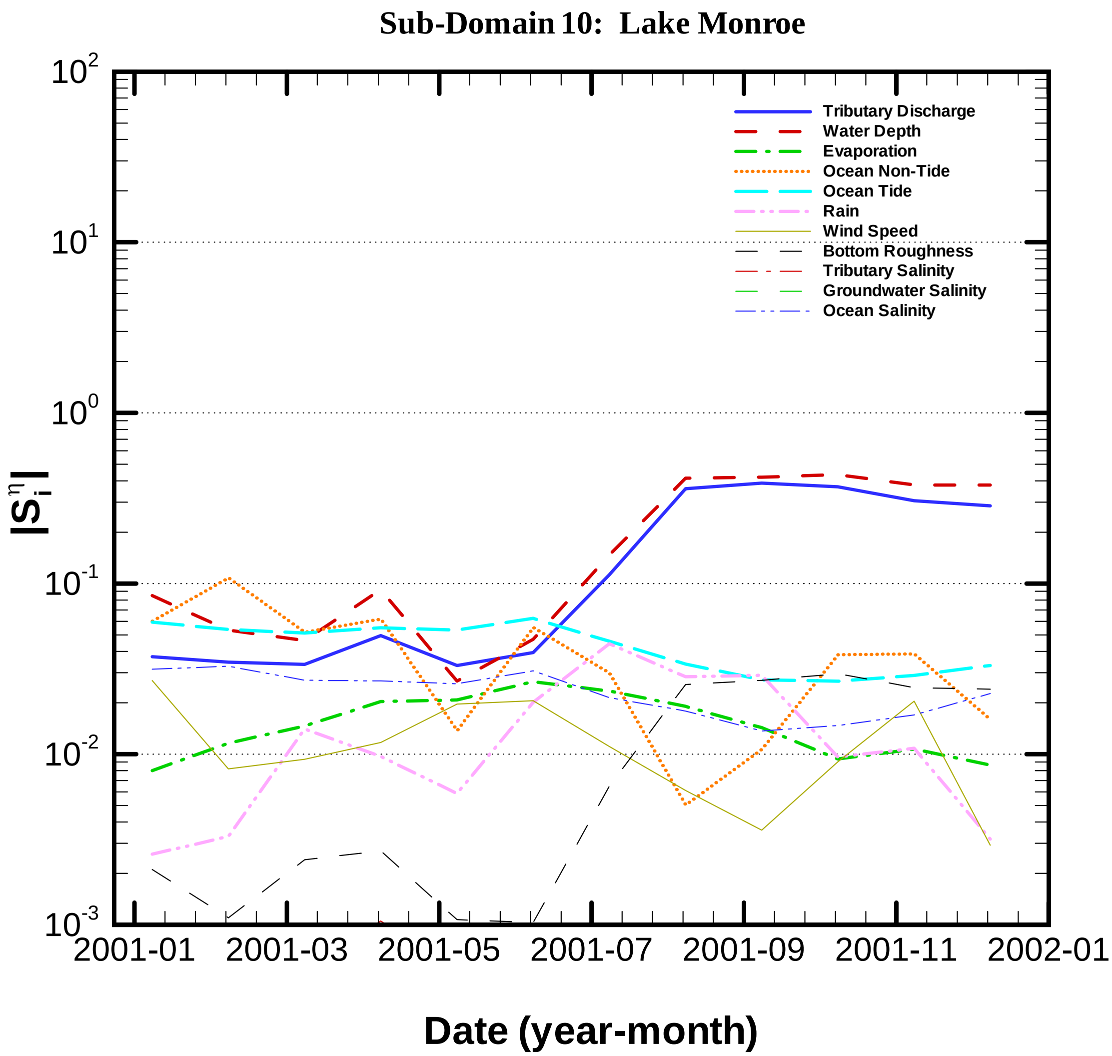

Figure 3–6. Median monthly dimensionless sensitivity coefficients (S^η) of water level to all tested input variables in sub-domain 10, Lake Monroe. (Sub-domains 9, 11, and 12 showed similar results.)

Current Speed

In sub-domains 1 and 2 (the river entrance to Dames Point) tidal currents are very strong, and current speed is sensitive to both ocean tide and depth (Figure 3–7). Throughout the remaining lower St. Johns River and Lake George, with the exception of Crescent Lake, current speed is primarily sensitive to depth alone (Figure 3–8). Throughout these areas, S_H^V is consistently near 1, indicating that a given percent uncertainty in depth leads to an equivalent percent uncertainty in current speed.

Sub-Domain 1: SJR Entrance

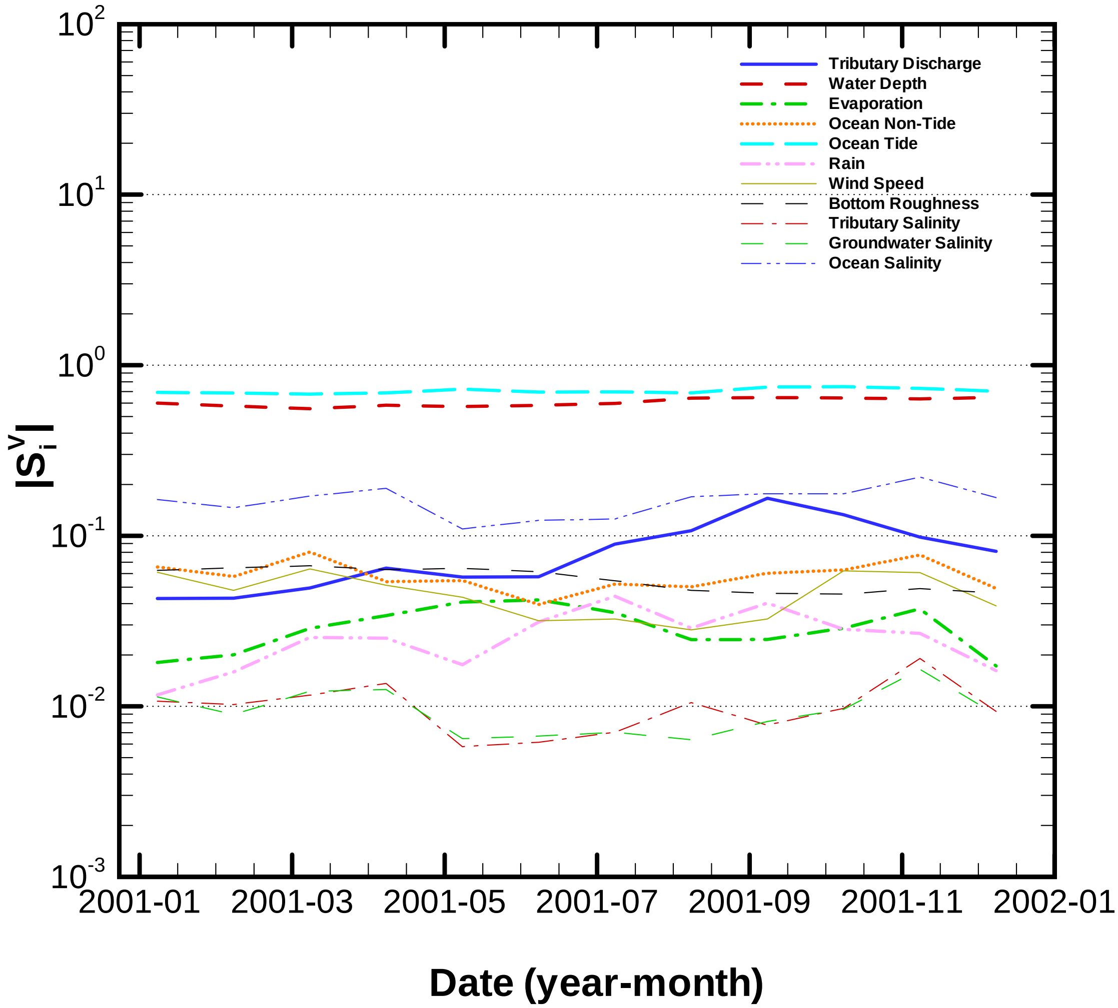

Figure 3–7. Median monthly dimensionless sensitivity coefficients (S^V) of current speed to all tested input variables in sub-domain 1, St. Johns River entrance. (Sub-domain 2 showed similar results.) SJR = St. Johns River.

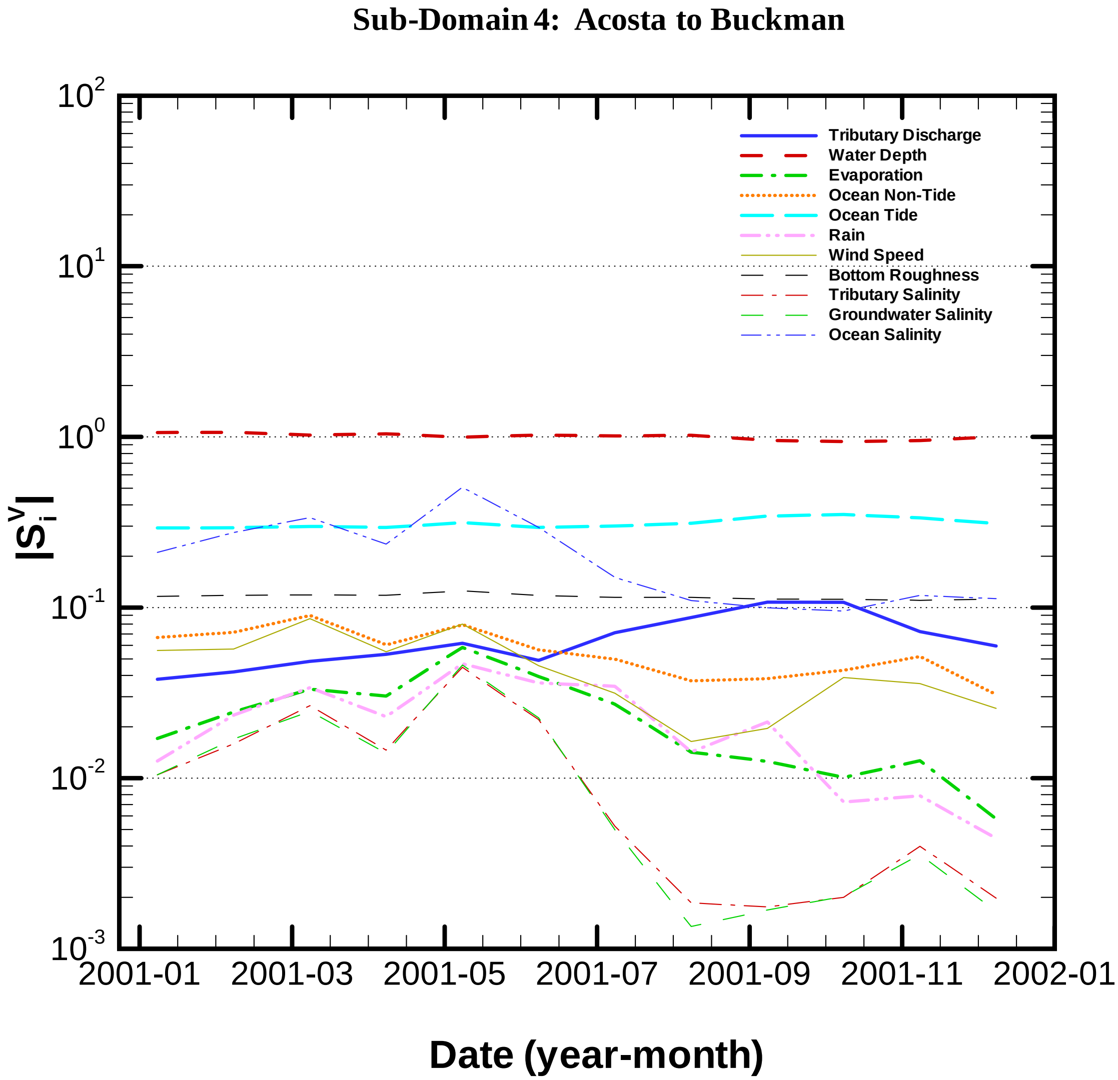

Figure 3–8. Median monthly dimensionless sensitivity coefficients (S^V) of current speed to all tested input variables in sub-domain 4, Acosta to Buckman. (Sub-domains 3, 5, 6, and 8 showed similar results.)

Current speed in Crescent Lake is also sensitive to depth, but wind is of equal importance (Figure 3–9). The sensitivity of both wind and depth on current speed is fairly strong in Crescent Lake with S_W^V = 0.5 to 1.0 and S_H^V = 0.6 to 1.0.

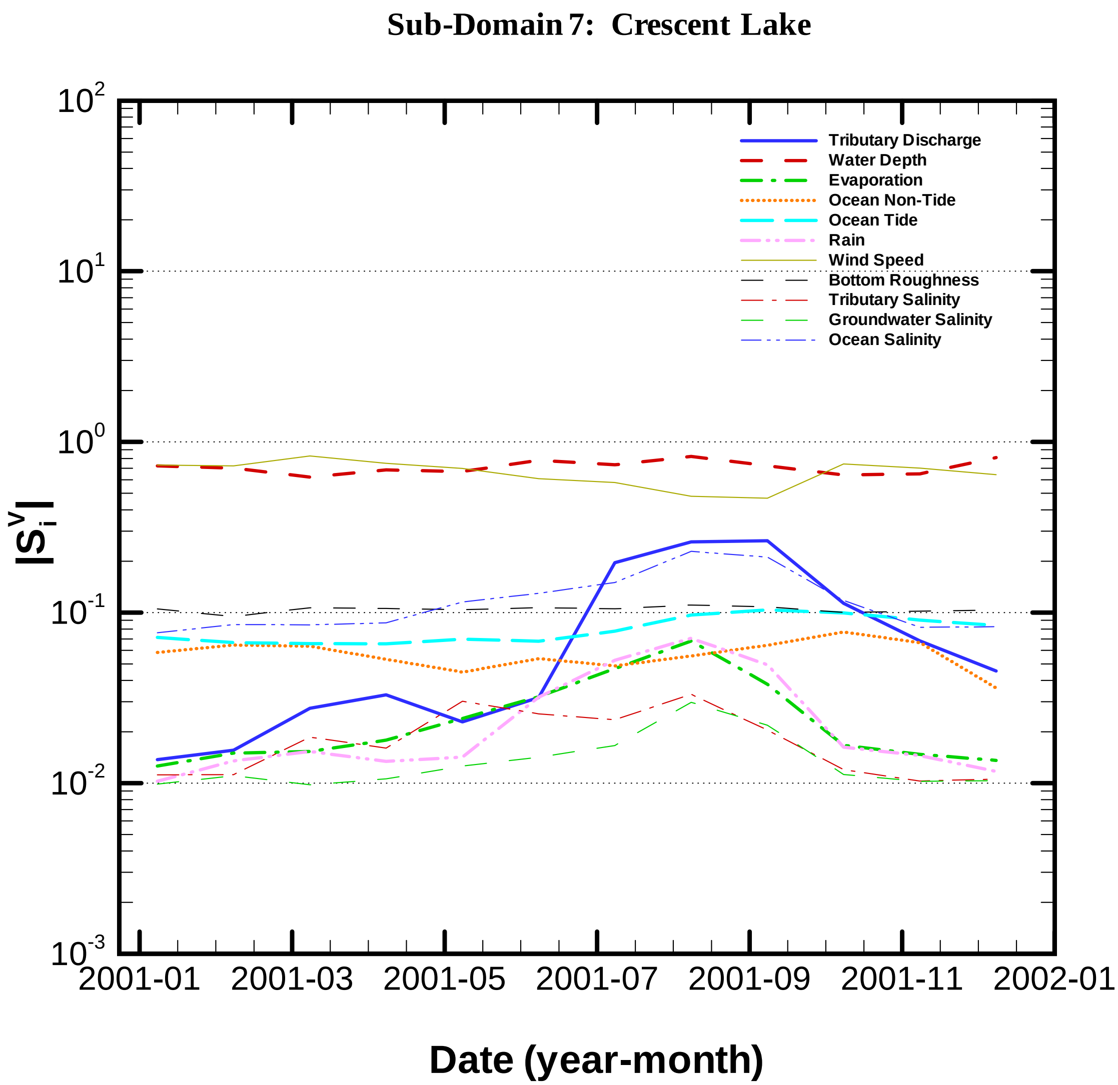

Figure 3–9. Median monthly dimensionless sensitivity coefficients (S^V) of current speed to all tested input variables in sub-domain 7, Crescent Lake.

Depth remains the most sensitive variable for current speed at DeLand (Figure 3–10) during the dry season with S_H^V near 1. DeLand exhibits a shift in the dominant sensitive variable between dry and wet seasons, and tributary discharge becomes most dominant in the wet season with S_Q^V = 0.7 to 0.8. The sensitivity of current speed on depth remains high during the wet period, however, with S_H^V = 0.5 to 0.8.

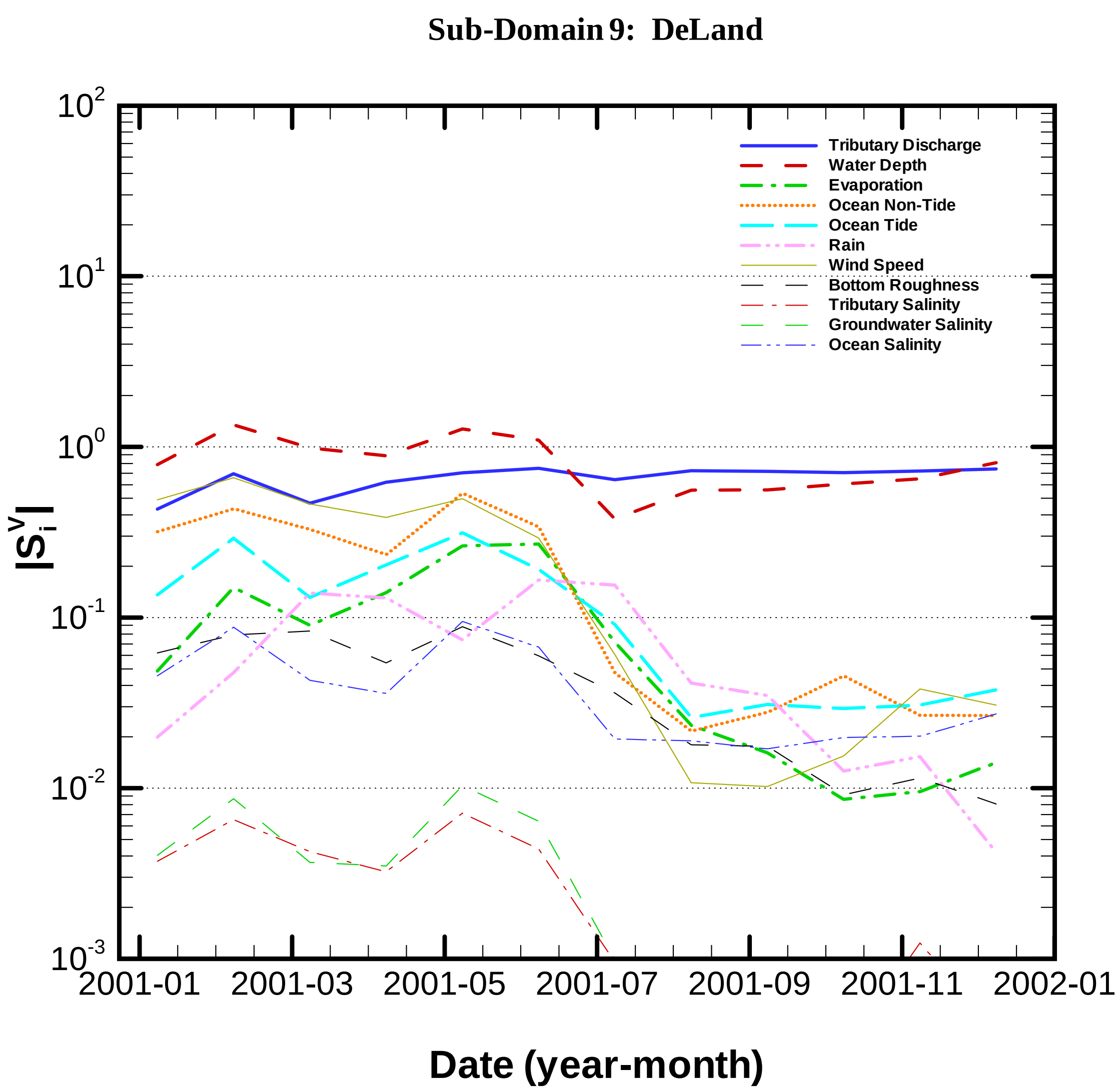

Figure 3–10. Median monthly dimensionless sensitivity coefficients (S^V) of current speed to all tested input variables in sub-domain 9, DeLand.

Sensitivity of current speeds in sub-domains 10 (Lake Monroe) and 12 (Lake Harney) exhibit a seasonal variability, with wind being the most sensitive variable in the dry season. Three variables (wind, tributary discharge, and depth) are of almost equal importance to sensitivity on current speed in the wet season (Figure 3–11).

Lake Jesup also exhibits a strong sensitivity to wind in the dry season; but, in contrast to the flow-through lakes Monroe and Harney, current speed in the wet season does not show sensitivity to tributary discharge (Figure 3–12).

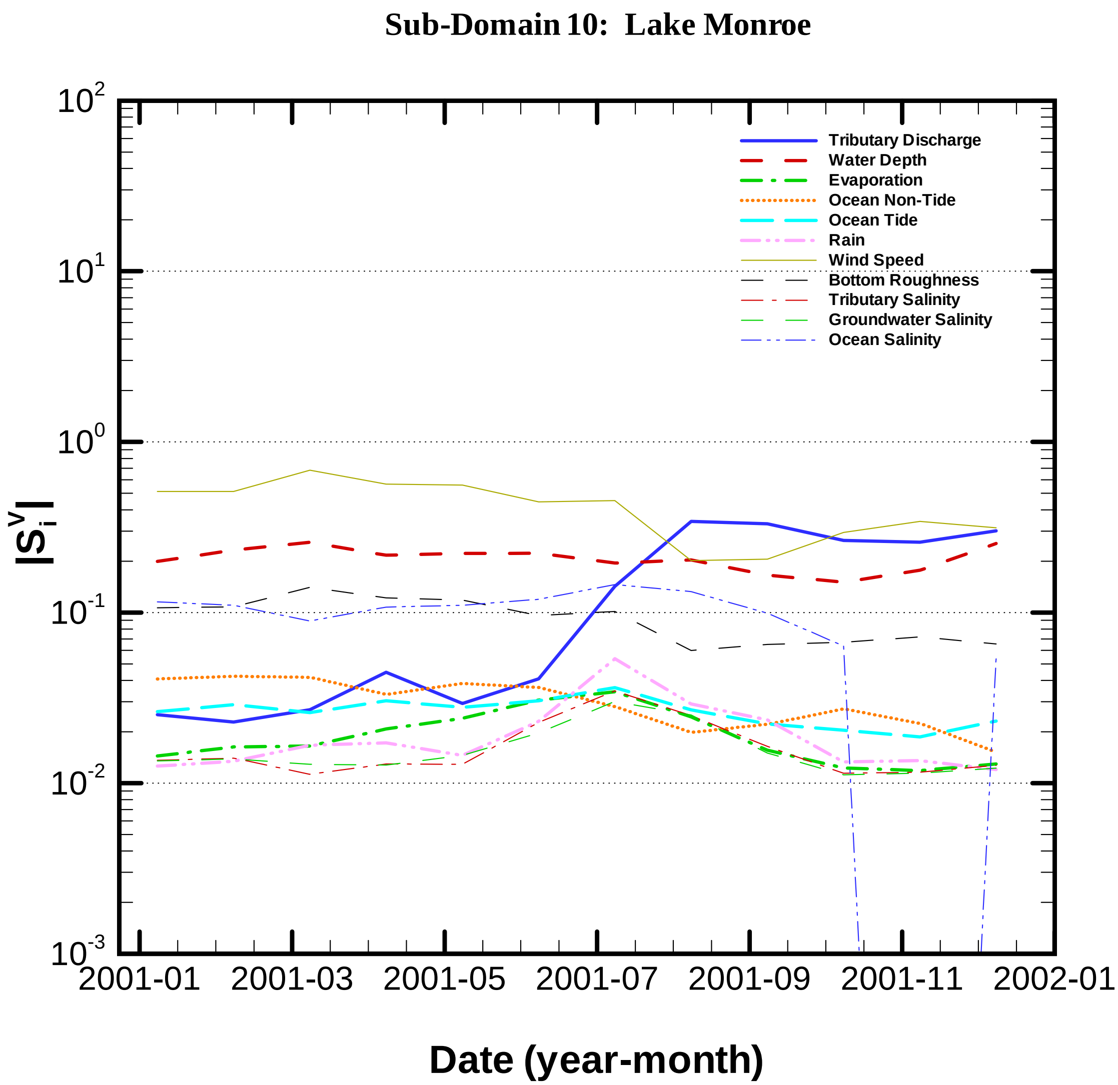

Figure 3–11. Median monthly dimensionless sensitivity coefficients (S^V) of current speed to all tested input variables in sub-domain 10, Lake Monroe. (Sub-domain 12 showed similar results.)

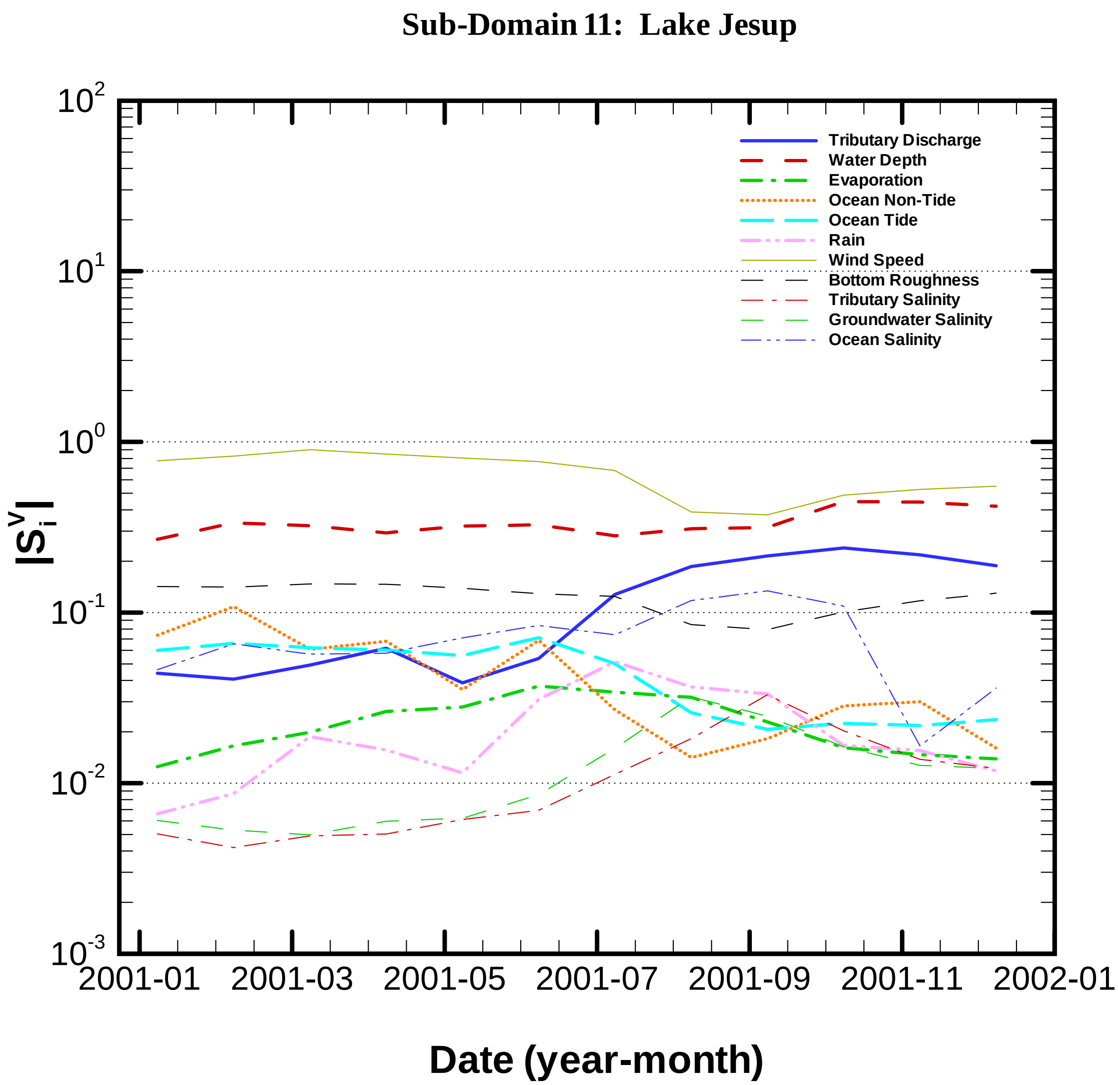

Figure 3–12. Median monthly dimensionless sensitivity coefficients (S^V) of current speed to all tested input variables in sub-domain 11, Lake Jesup.

Salinity

Sub-domains 1 and 2 are nearest to the ocean, and salinity in these areas is sensitive to specification of ocean salinity at the open ocean boundary (Figure 3–13). In sub-domains 3 and 4 (from Long Branch to Buckman Bridge) the sensitivity of salinity to depth becomes equivalent to ocean salinity in the dry season and dominant in the wet season (Figure 3–14). The sensitivity of salinity to depth is extreme during the wet season in these areas with $S_H^{Sal} = 6$ to 8.

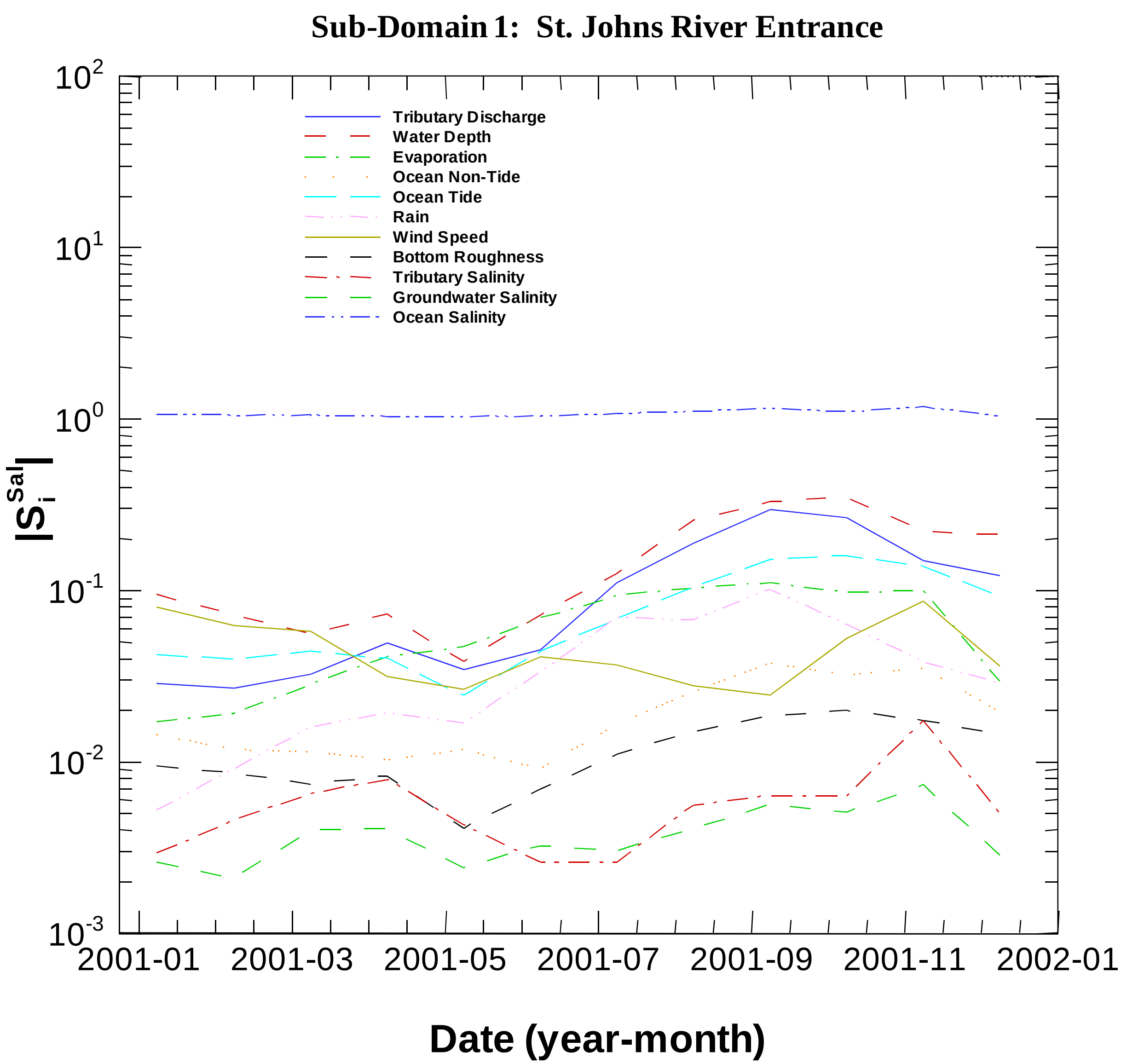

Figure 3–13. Median monthly dimensionless sensitivity coefficients (S^{Sal}) of salinity to all tested input variables in sub-domain 1, St. Johns River entrance. (Sub-domain 2 showed similar results.)

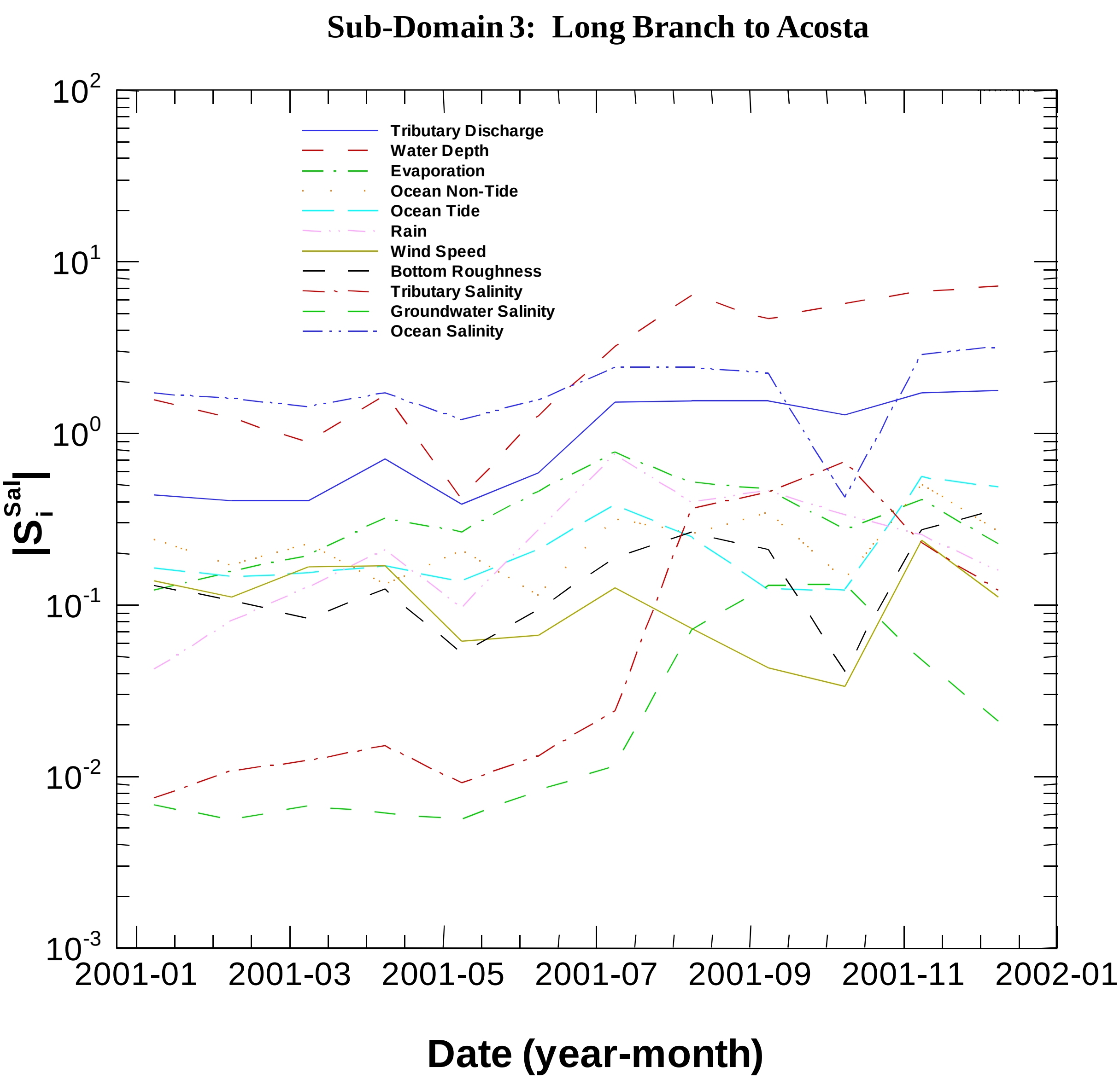

Figure 3–14. Median monthly dimensionless sensitivity coefficients (S^{Sal}) of salinity to all tested input variables in sub-domain 3, Long Branch to Acosta. Sub-domain 4 showed similar results.

In sub-domain 5 (between Buckman Bridge and Shands Bridge), salinity is influenced by ocean water during dry periods and by freshwater inflows during wet periods. As a result, salinity is quite sensitive to depth during dry periods, but most sensitive to tributary salinity during wet periods (Figure 3–15). Farther upstream, in sub-domains 6 and 8 (from Racy Point through Lake George), salinity sensitivity is dominated by tributary salinity in all seasons (Figure 3–16).

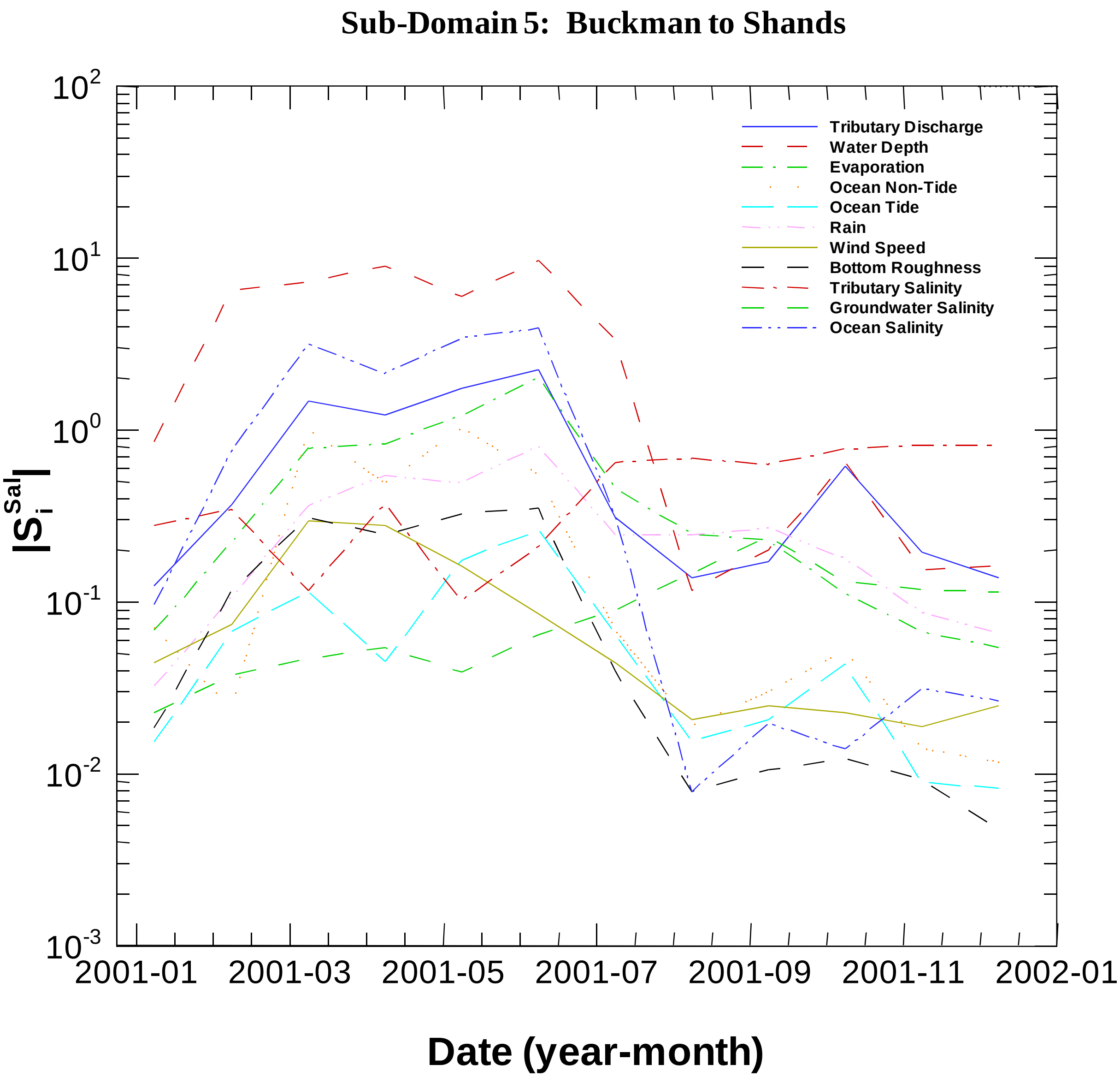

Figure 3–15. Median monthly dimensionless sensitivity coefficients (S^{Sal}) of salinity to all tested input variables in sub-domain 5, Buckman to Shands.

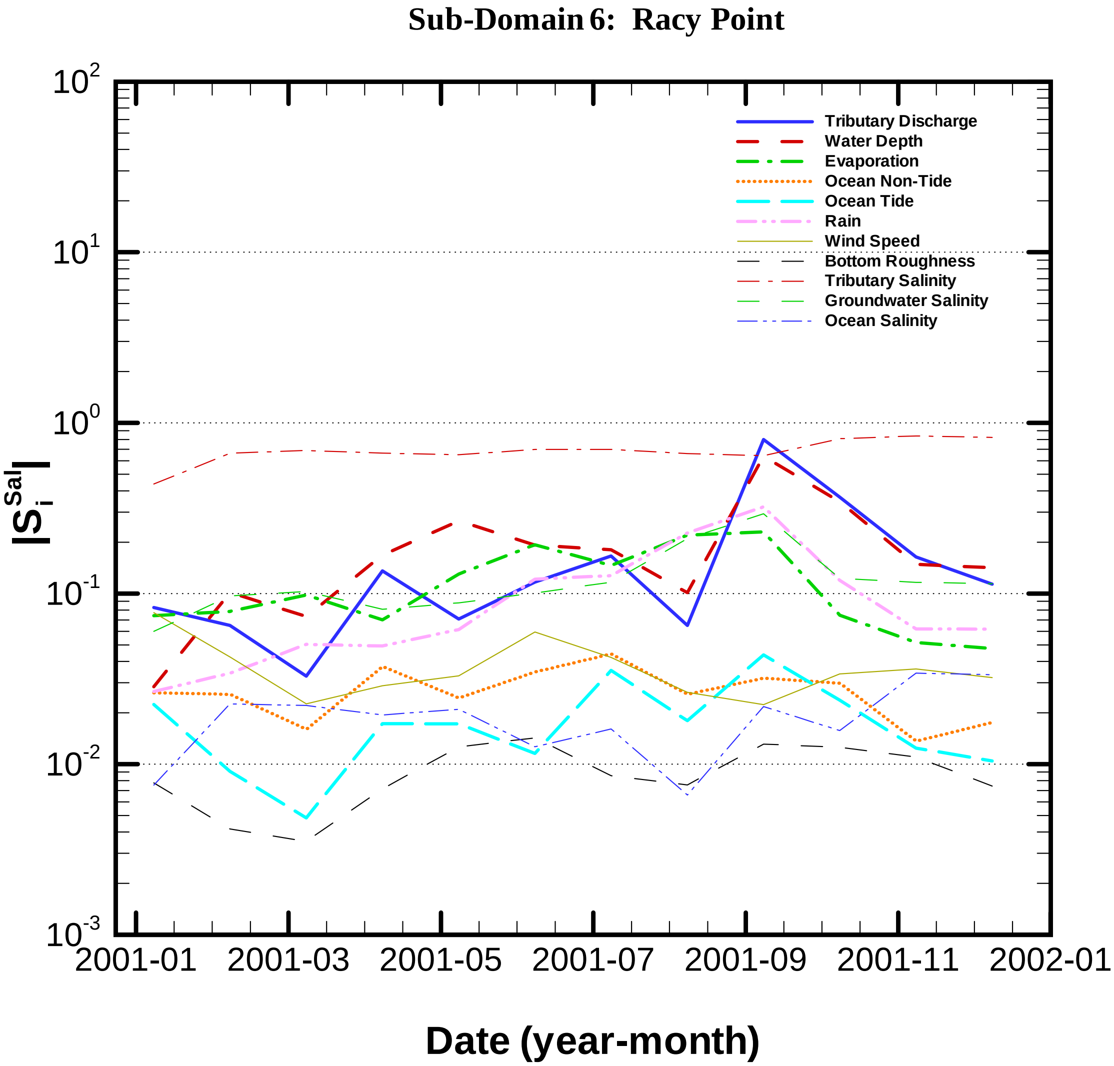

Figure 3–16. Median monthly dimensionless sensitivity coefficients (S^{Sal}) of salinity to all tested input variables in sub-domain 6, Racy Point. (Sub-domain 8 showed similar results.)

The sensitivity of salinity to depth is not as pronounced in sub-domain 7 (the off-line Crescent Lake) as it is in neighboring flow-through areas (Figure 3–17). During dry periods, salinity in Crescent Lake is about equally sensitive to depth, tributary discharge, and evaporation. The longer residence time of water in Crescent Lake, compared with Lake George, enhances sensitivity to local water budget terms. During the wet season, Crescent Lake salinity is almost equally sensitive to depth and tributary discharge.

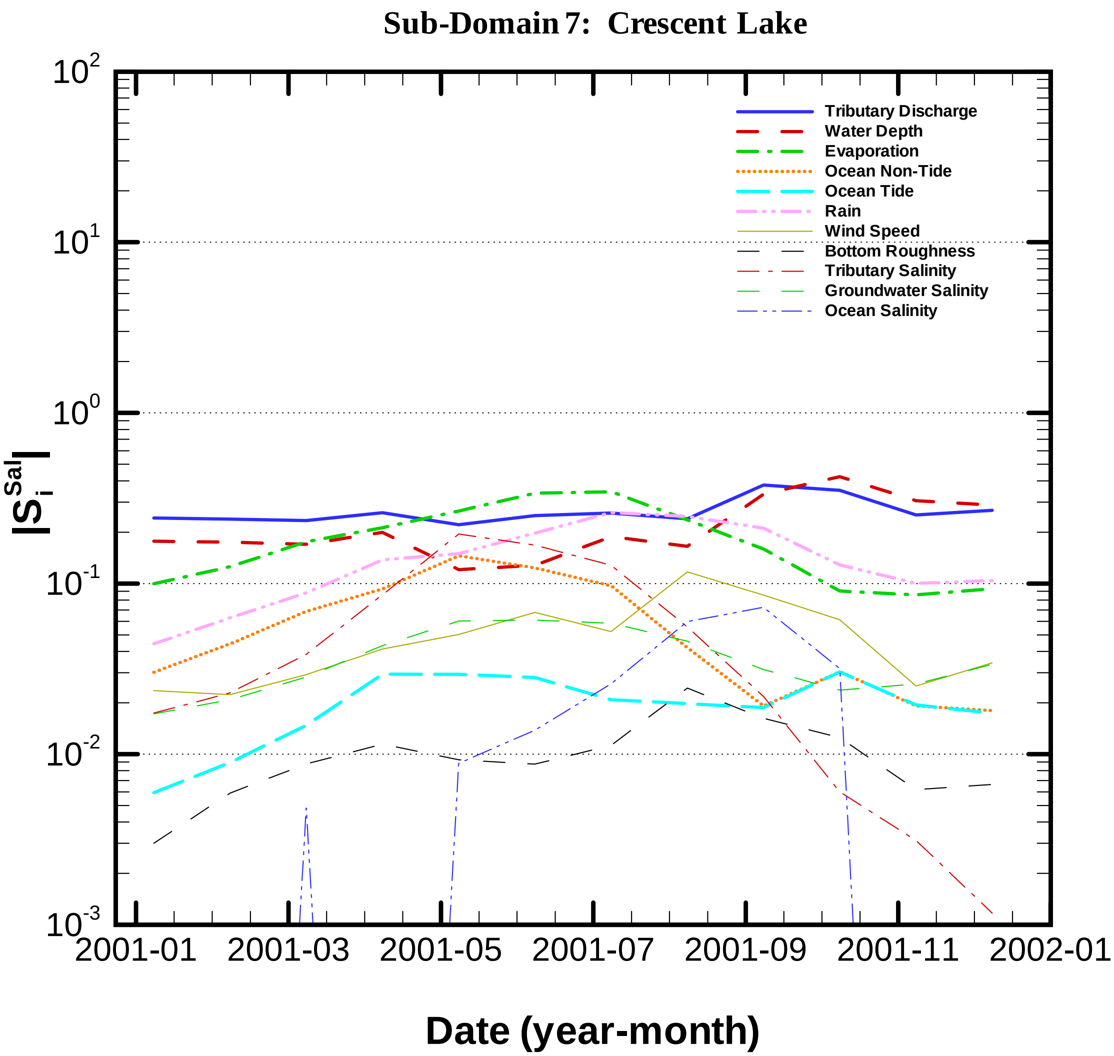

Figure 3–17. Median monthly dimensionless sensitivity coefficients (S^{Sal}) of salinity to all tested input variables in sub-domain 7, Crescent Lake.

Salinity in both sub-domain 9 (DeLand) and 10 (Lake Harney) show a dominant sensitivity to tributary salinity (Figure 3–18). For DeLand, this effect likely reflects the importance of the Wekiva River system and Blue Spring on salinity. For Lake Harney, this effect simply means that lake salinity closely follows the imposed salinity boundary condition at the upstream model boundary.

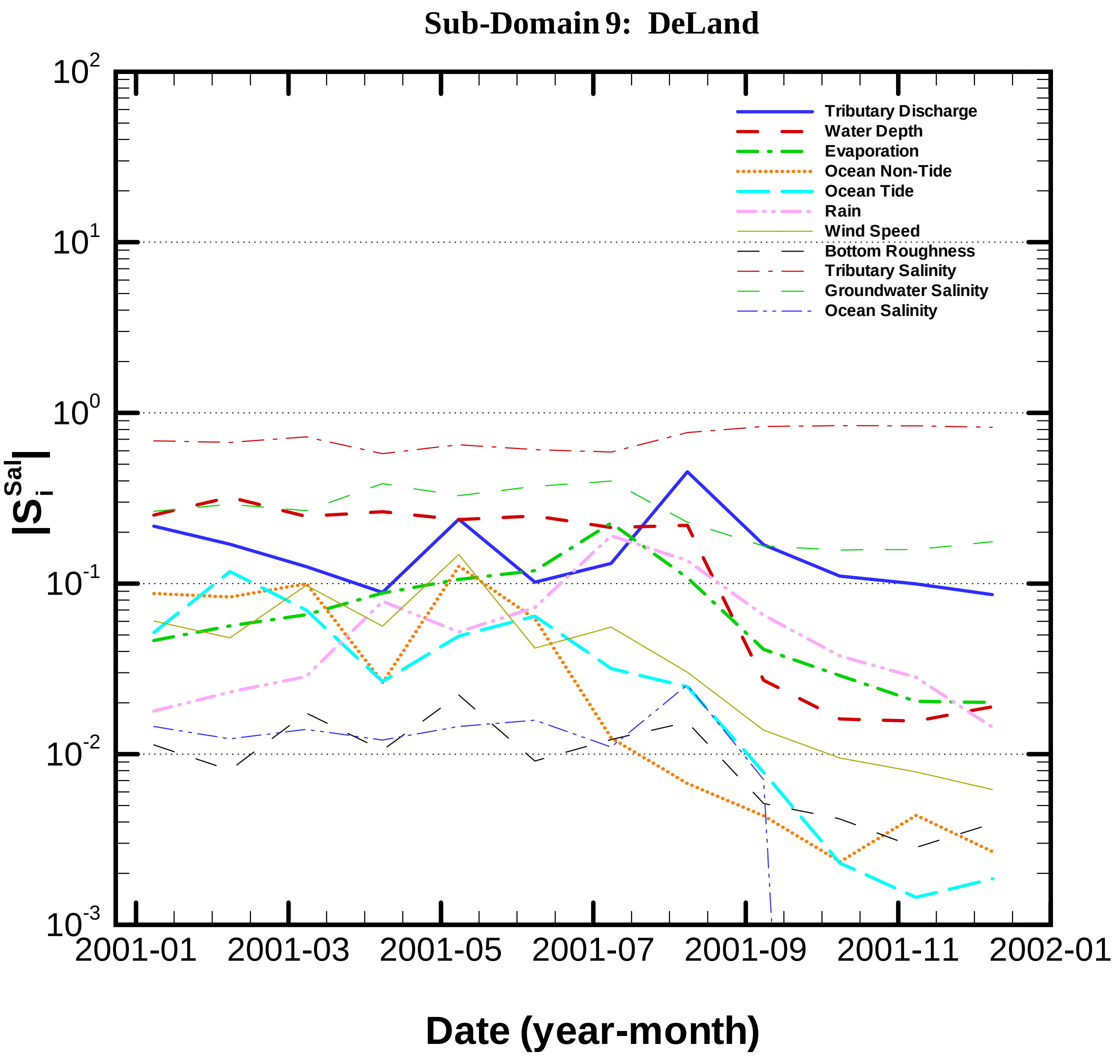

Figure 3–18. Median monthly dimensionless sensitivity coefficients (S^{Sal}) of salinity to all tested input variables in sub-domain 9, DeLand. (Sub-domain 12 showed similar results.)

Similarly to DeLand, salinity in sub-domain 10 (Lake Monroe) also exhibits a strong sensitivity to tributary salinity, but only during the wet period. During dry periods, salinity in the lake is equally affected by tributary salinity, depth, and groundwater salinity.

Sub-domain 11 (Lake Jesup, an off-line lake) similarly to Crescent Lake, exhibits sensitivity of salinity to evaporation during dry periods. Unlike Crescent Lake, salinity in Lake Jesup during dry periods is also sensitive to groundwater salinity. During wet periods, salinity in Lake Jesup shows sensitivity to tributary salinity in accordance with the other freshwater areas.

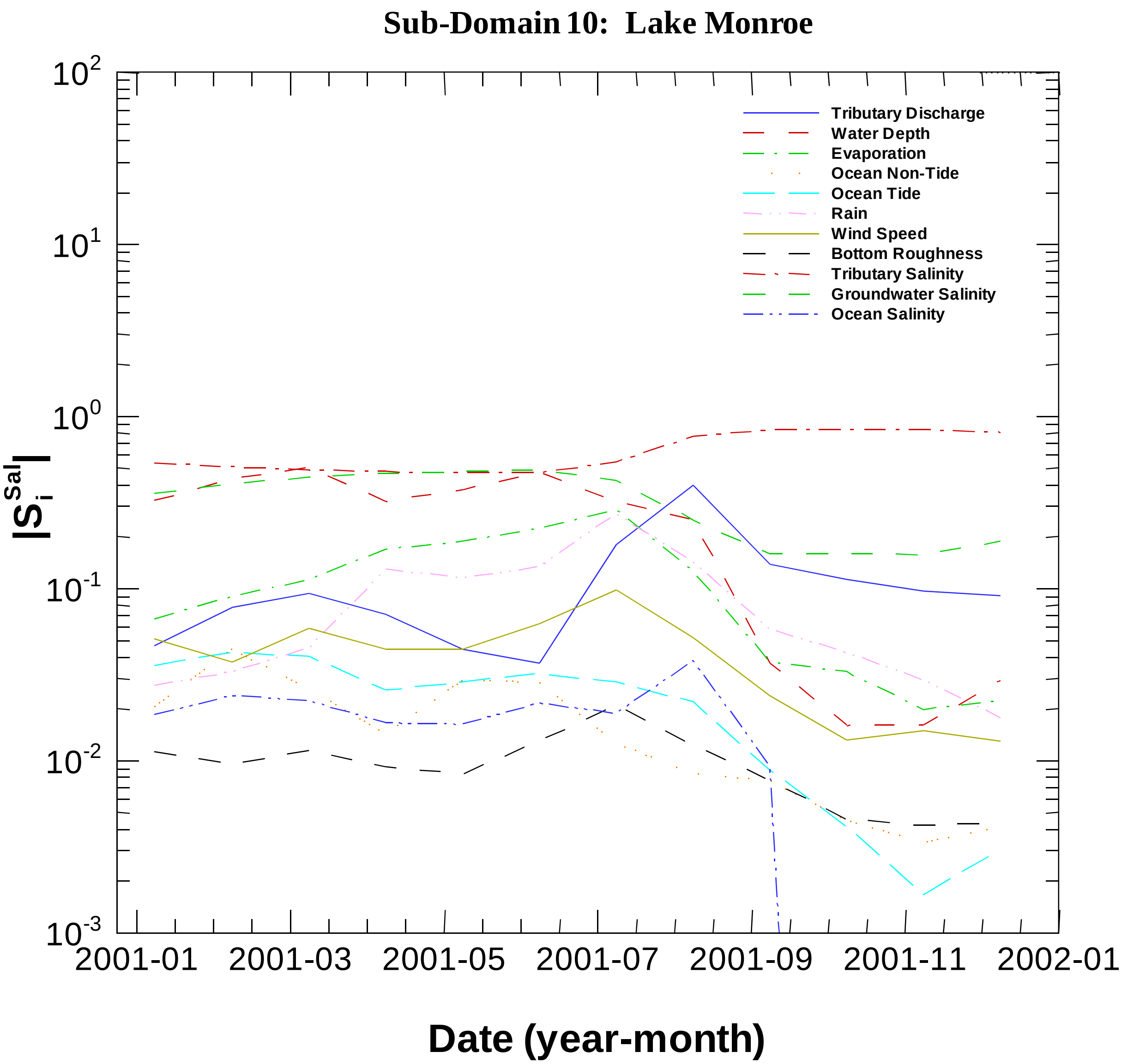

Figure 3–19. Median monthly dimensionless sensitivity coefficients (S^{Sal}) of salinity to all tested input variables in sub-domain 10, Lake Monroe.

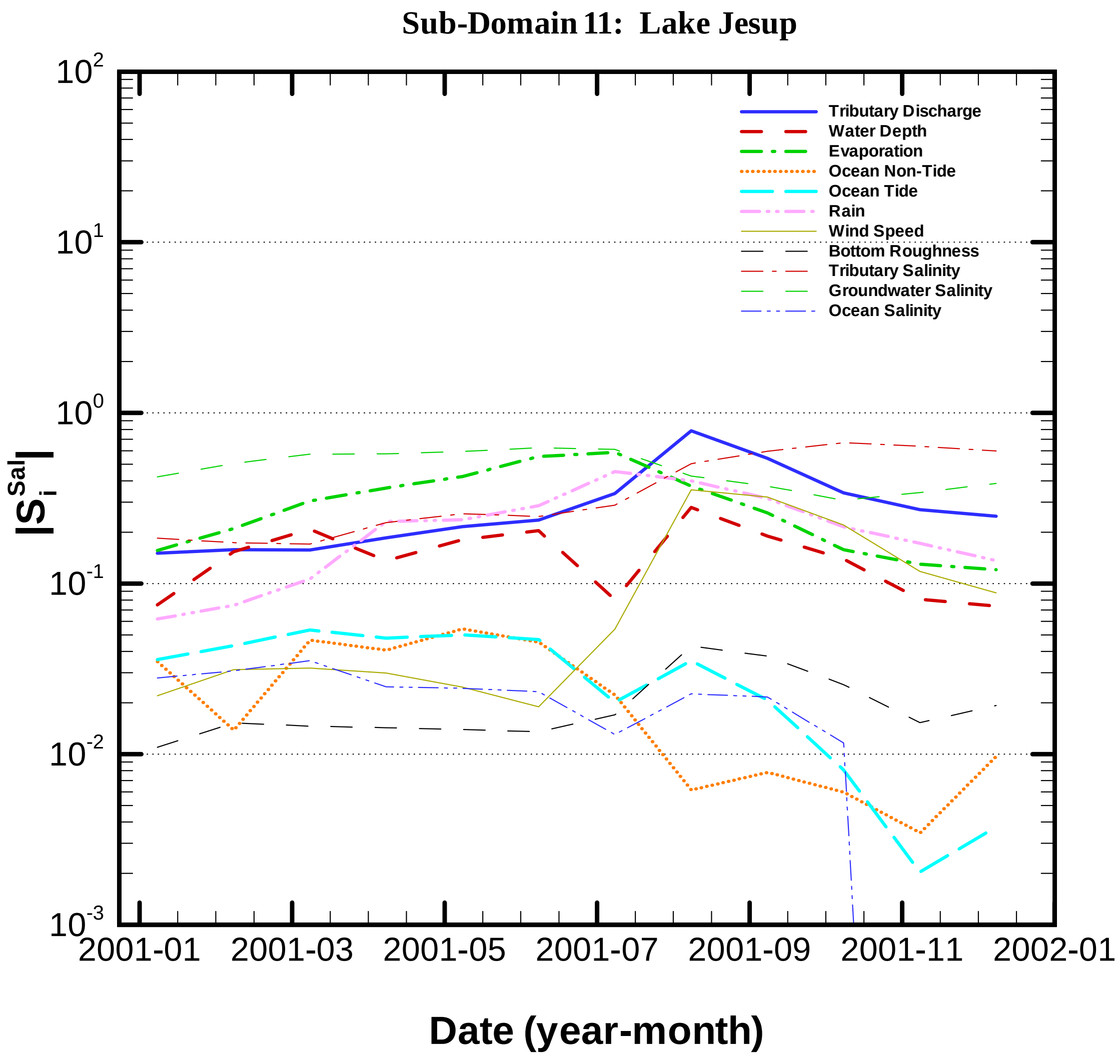

Figure 3–20. Median monthly dimensionless sensitivity coefficients (S^{Sal}) of salinity to all tested input variables in sub-domain 11, Lake Jesup.

Confidence Intervals for Simulated Time Series

The *DSC*s shown above can be combined with estimates of input uncertainty (Table 3–11) to estimate total uncertainty of the model output variables using Equation 3–2. Total uncertainty of model output was calculated at the six representative locations shown in Figure 3–1. Total uncertainty is expressed as a standard deviation for each output variable for each month. Assuming uncertainties are normally distributed about the central tendency of the model output, the standard deviation is used to assign confidence intervals to the simulated output.

The figures in the sections below show confidence intervals for ±1 standard deviation (labeled as the 68% confidence interval) and ±1.96 standard deviation (labeled as the 95% confidence interval). Although 95% confidence levels (or higher) are common in tests of statistical significance, this high level of confidence is not necessarily most appropriate here because of the conservative nature of global alteration of input variables. Zhang and Yu (2004), for example, used ±1 standard deviation (68% confidence interval) for setting a margin of safety on simulated water quality variables for a total maximum daily load application.

Following each time series plot of an output variable with confidence intervals are time series plots showing the percent contribution of each input variable to the total uncertainty. These plots are useful to quickly grasp which input variable or combination of variables cause the degree of uncertainty seen in the accompanying output time series. The percent contribution to total uncertainty (r_i) includes the coefficient of variation of each input variable as well as the *DSC*s. This definition of r_i follows that of Brown and Barnwell (1987), but differs from that of Blumberg and Georgas (2008) where r_i is calculated assuming constant coefficient of variation for all input parameters.

Water Elevation

Predicted water elevation within the tidal portion of the St. Johns River is fairly robust with respect to model uncertainty. This portion of the river is represented by stations at Acosta Bridge (Figure 3–21), Shands Bridge (Figure 3–23), and Racy Point (Figure 3–25); and input uncertainties alter predicted tidal amplitudes by only a few centimeters. For all these stations, depth dominates the uncertainty of predicted water level (Figure 3–22, Figure 3–24, and Figure 3–26).

Total uncertainty is also low in Lake George for water level (Figure 3–27). In this non-tidal area of the river, depth is no longer a controlling factor for water level uncertainty. The dominant input variable affecting uncertainty for water level during the wet season is tributary discharge (Figure 3–28).

At DeLand and Lake Monroe, the two middle basin stations, water level uncertainty is low in the dry season but becomes high in the wet season (Figure 3–29 and Figure 3–31). Simulated peak water level during the wet season in Lake Monroe, for example, was 1.8 m NAVD88 with a 95% confidence interval of ±30 cm. Seventy-five percent of the uncertainty for water level during these periods is caused by uncertainty of tributary discharge, and about 20% is caused by uncertainty of depth (Figure 3–30 and Figure 3–32).

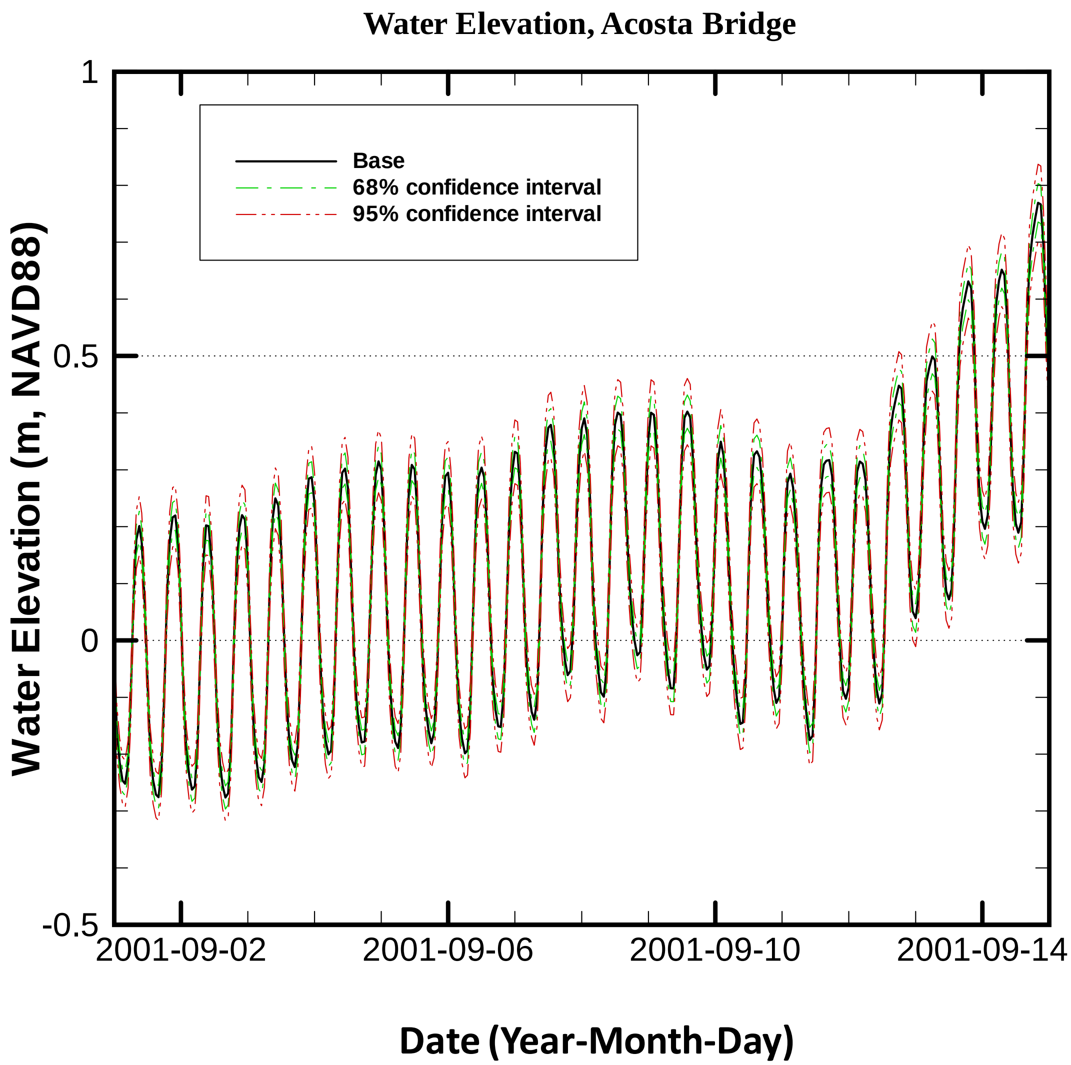

Figure 3–21. Simulated water level at Acosta Bridge with confidence intervals for the year 2001. (The base scenario is the calibrated model.)

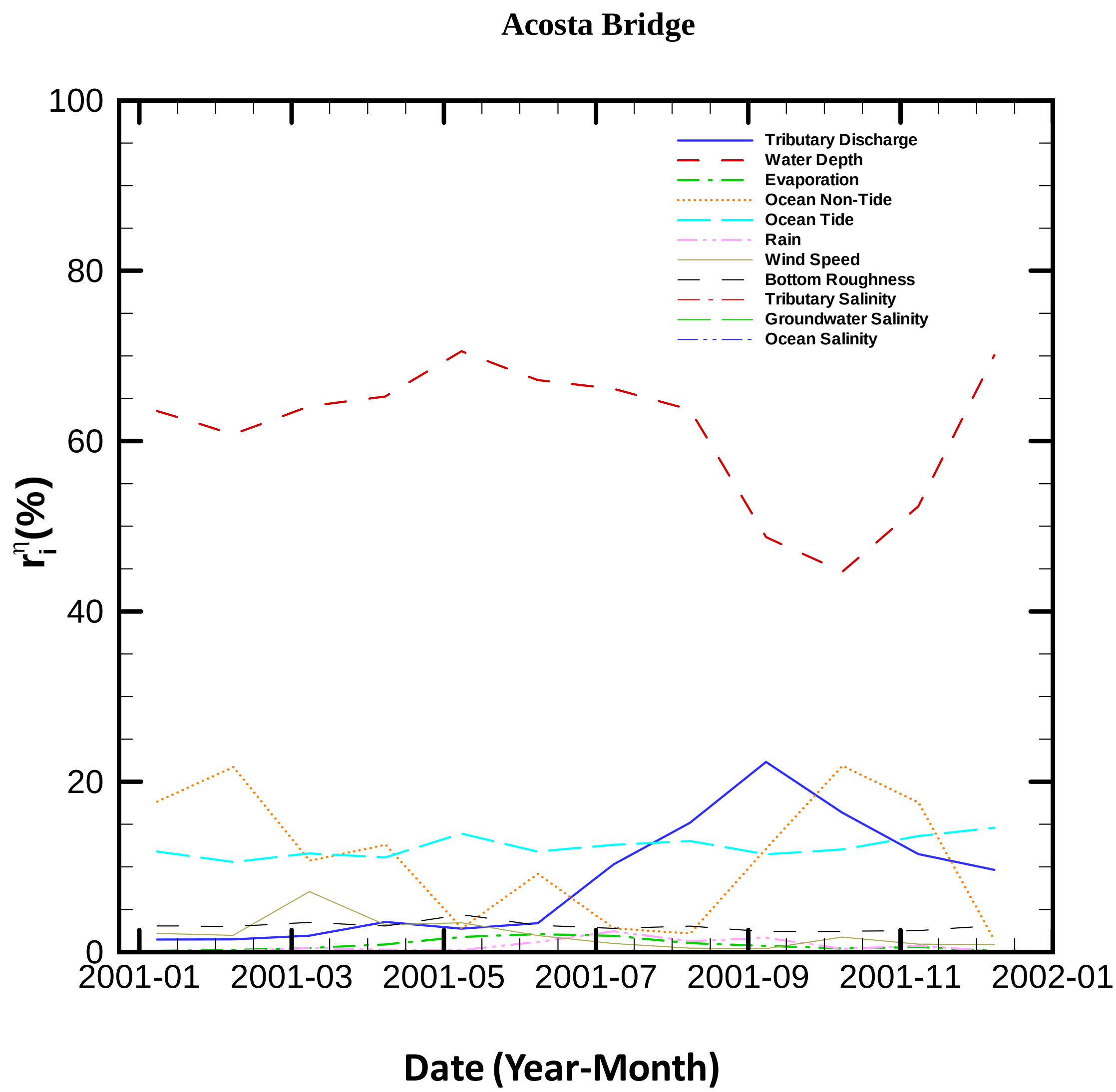

Figure 3–22. Percent contribution of input variables to the total uncertainty of water level (r^η) at Acosta Bridge.

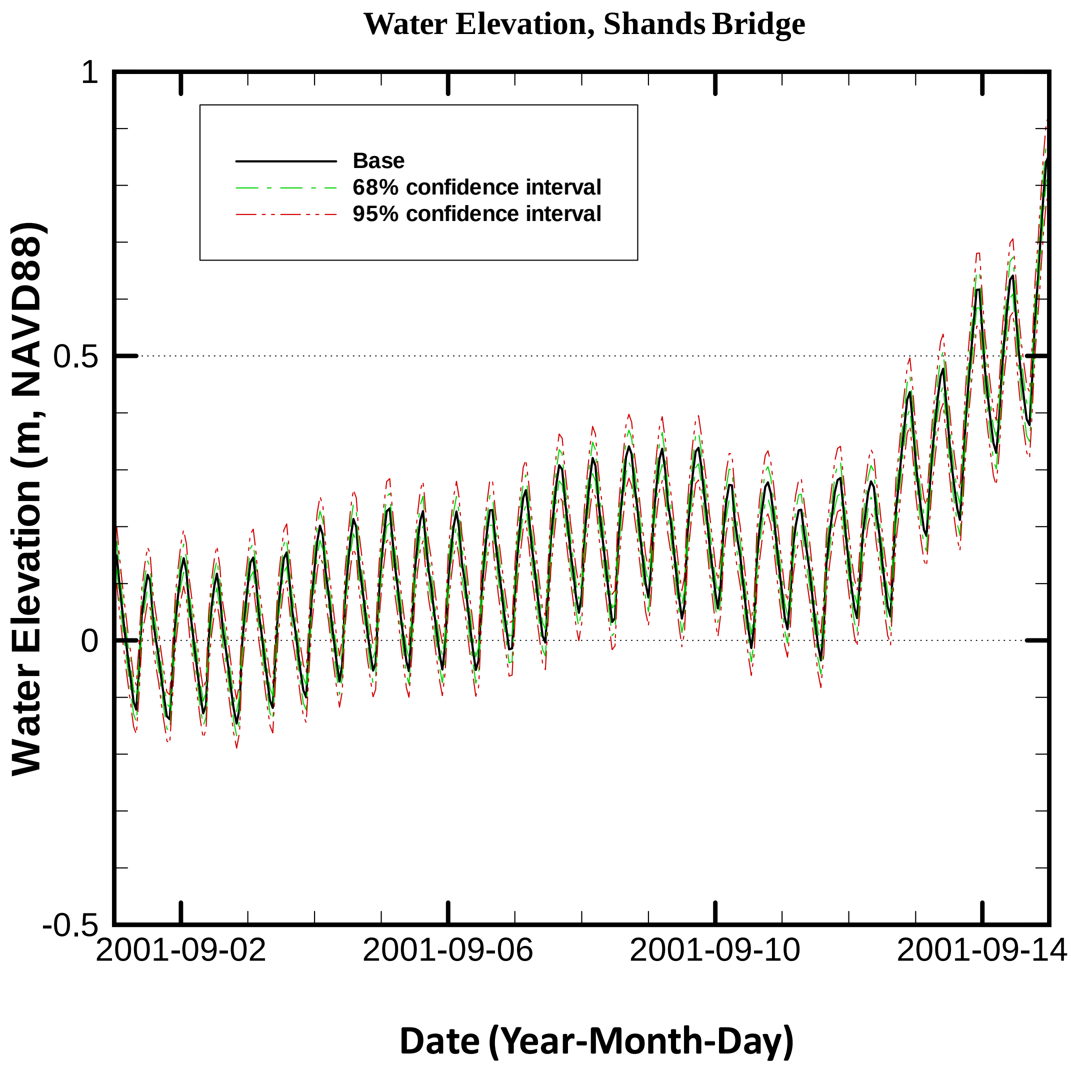

Figure 3–23. Simulated water level at Shands Bridge with confidence intervals for the year 2001. (The base scenario is the calibrated model.)

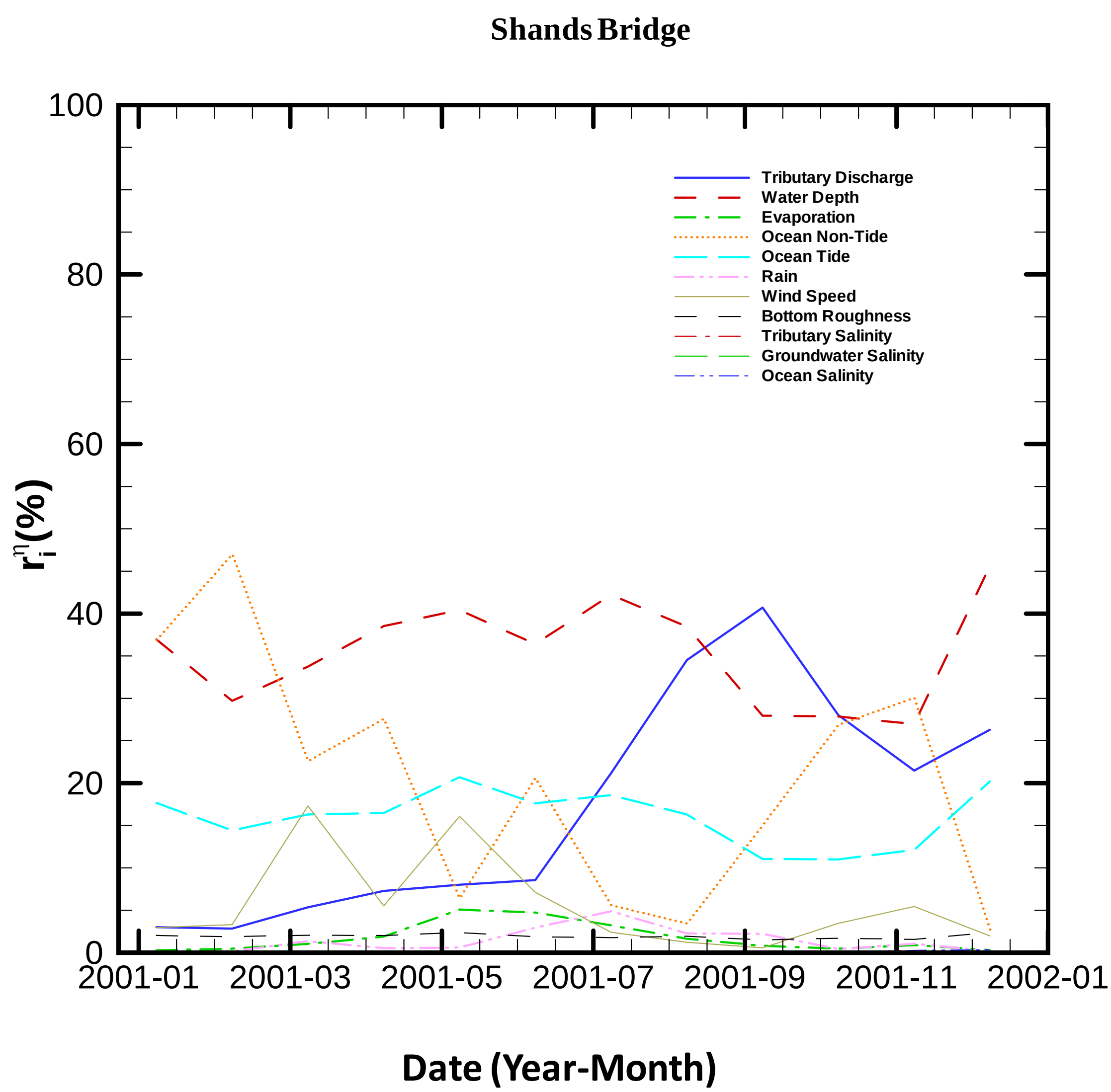

Figure 3–24. Percent contribution of input variables to the total uncertainty of water level (r^η) at Shands Bridge.

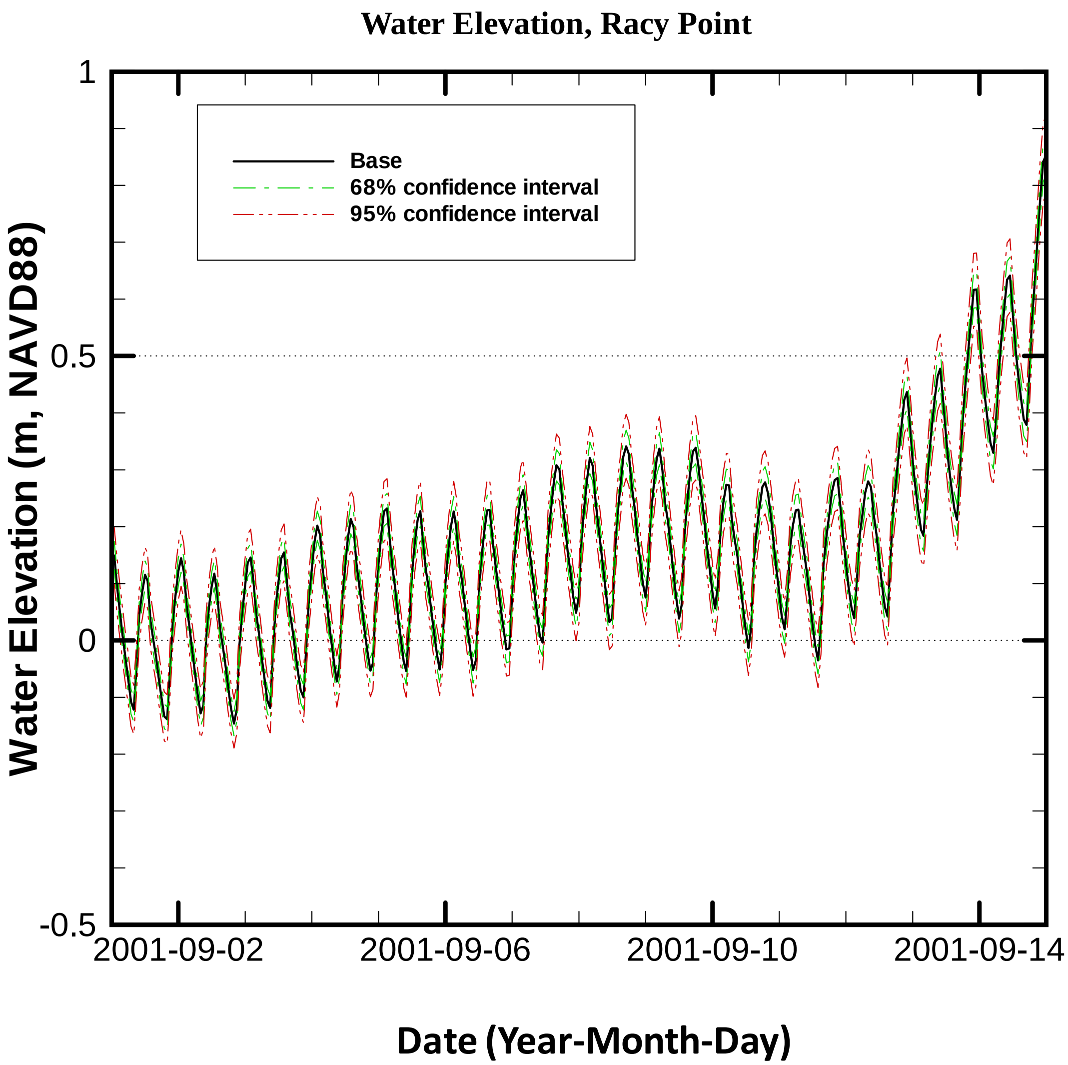

Figure 3–25. Simulated water level at Racy Point with confidence intervals for the year 2001. (The base scenario is the calibrated model.)

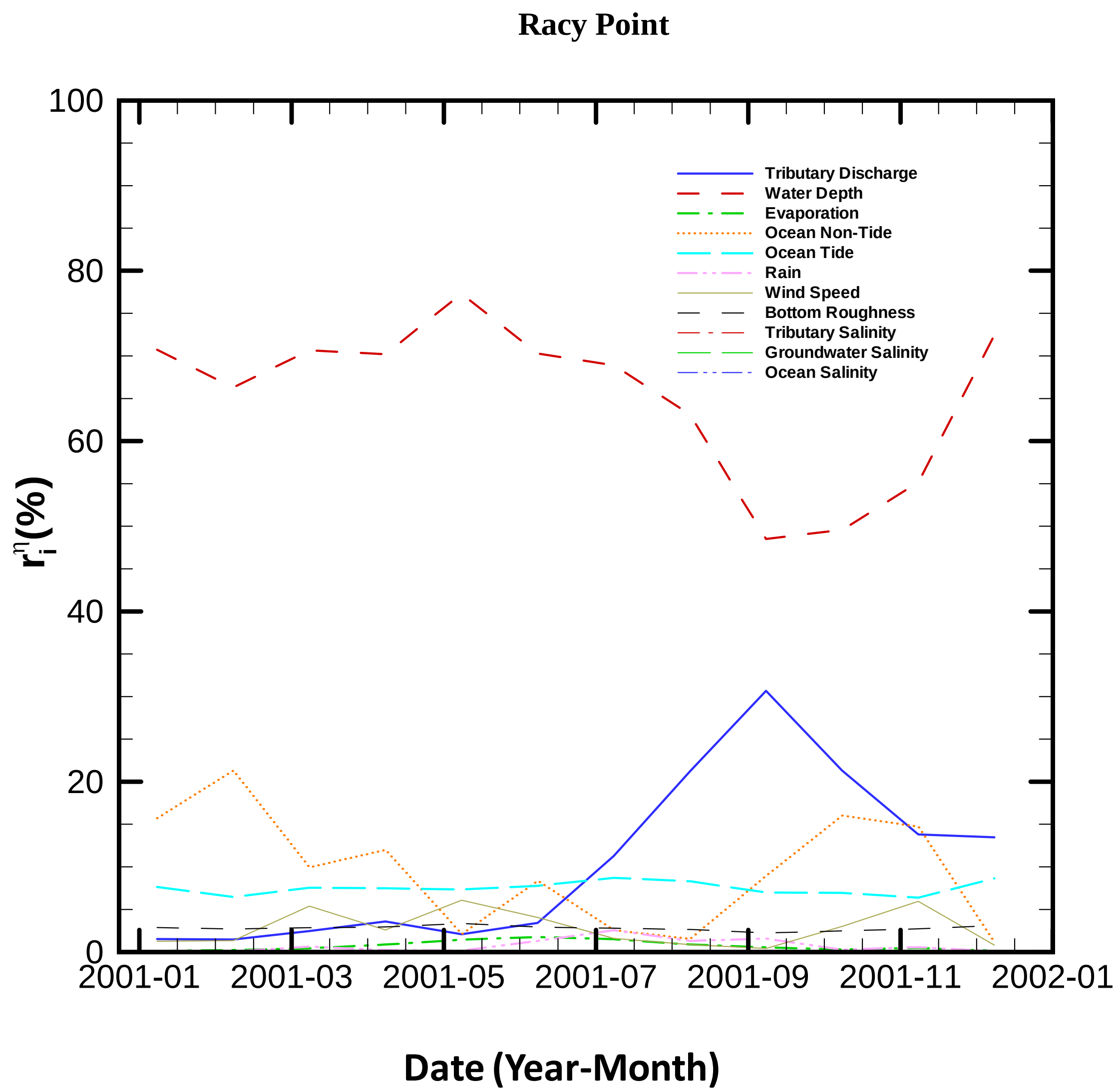

Figure 3–26. Percent contribution of input variables to the total uncertainty of water level (r^{η}) at Racy Point.

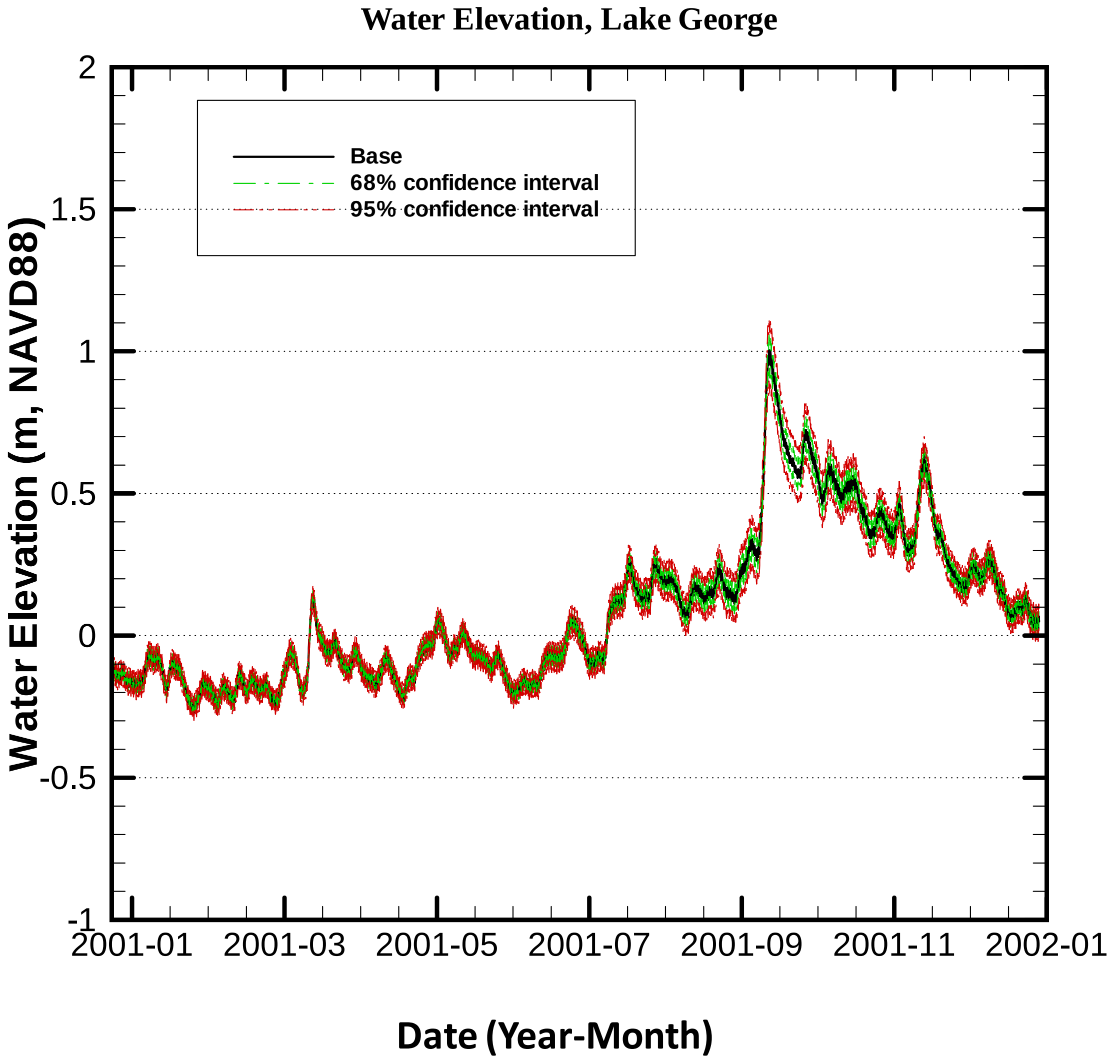

Figure 3–27. Simulated water level at Lake George with confidence intervals for the year 2001. (The base scenario is the calibrated model.)

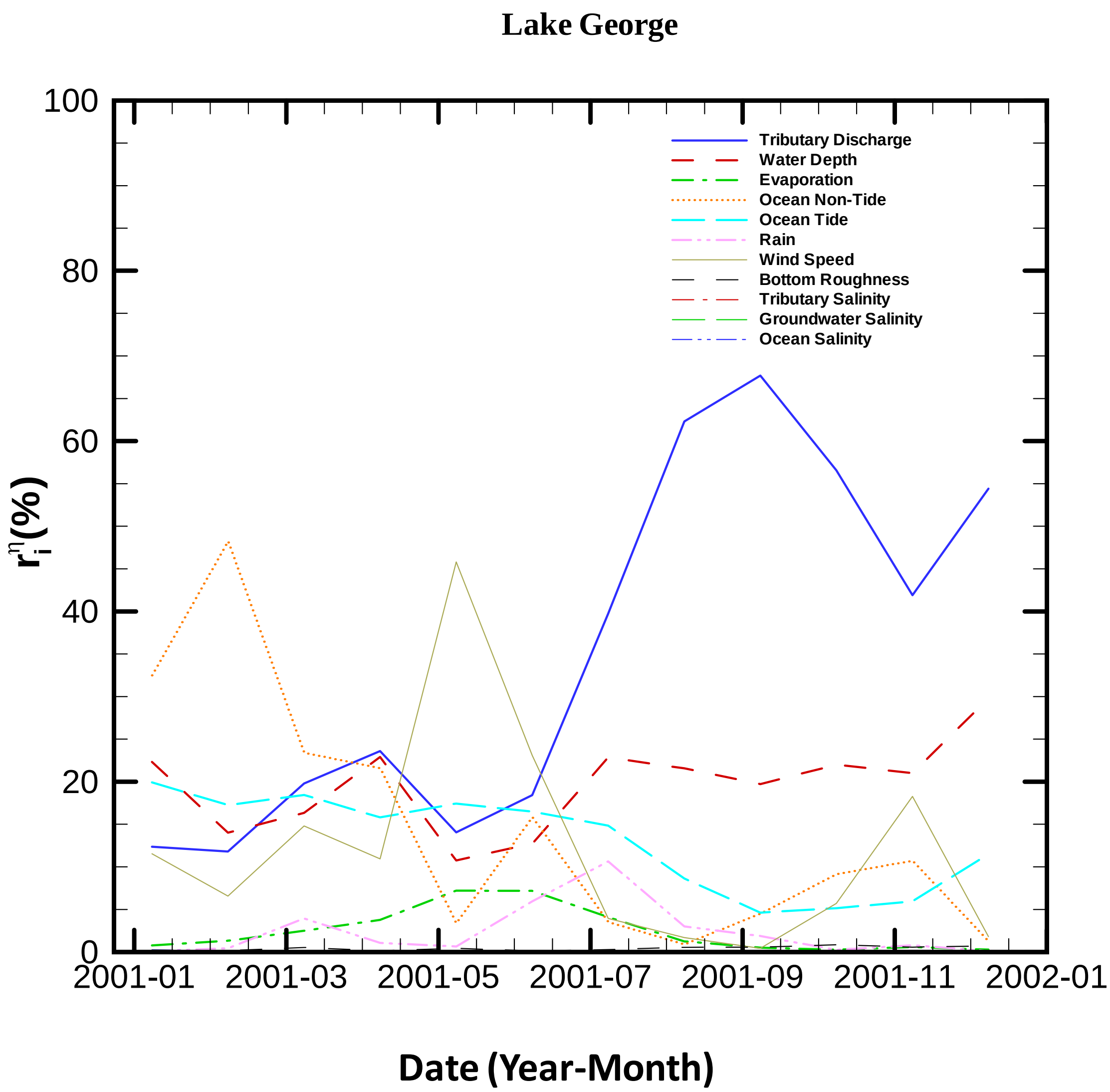

Figure 3–28. Percent contribution of input variables to the total uncertainty of water level (r^η) at Lake George.

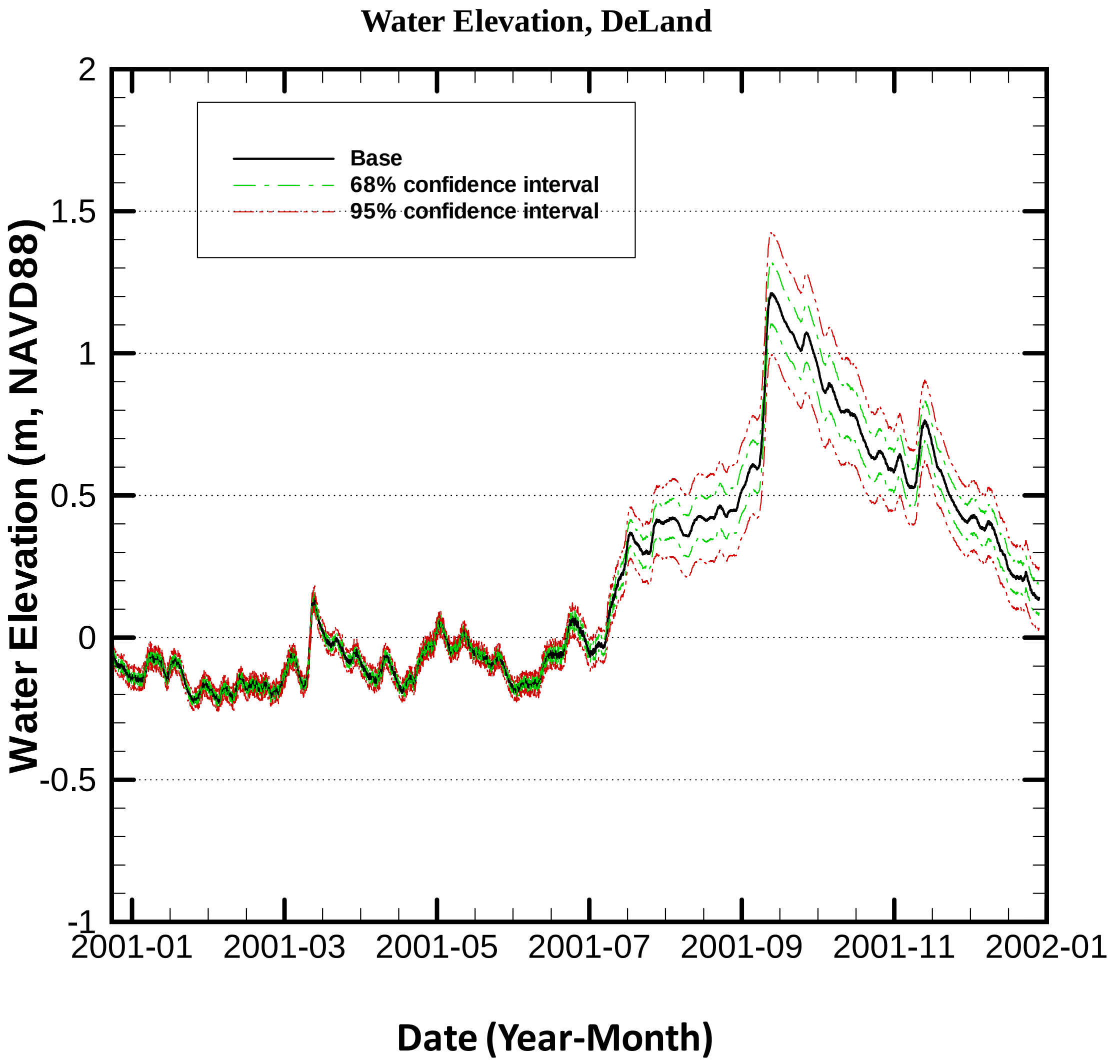

Figure 3–29. Simulated water level at DeLand with confidence intervals for the year 2001. (The base scenario is the calibrated model.)

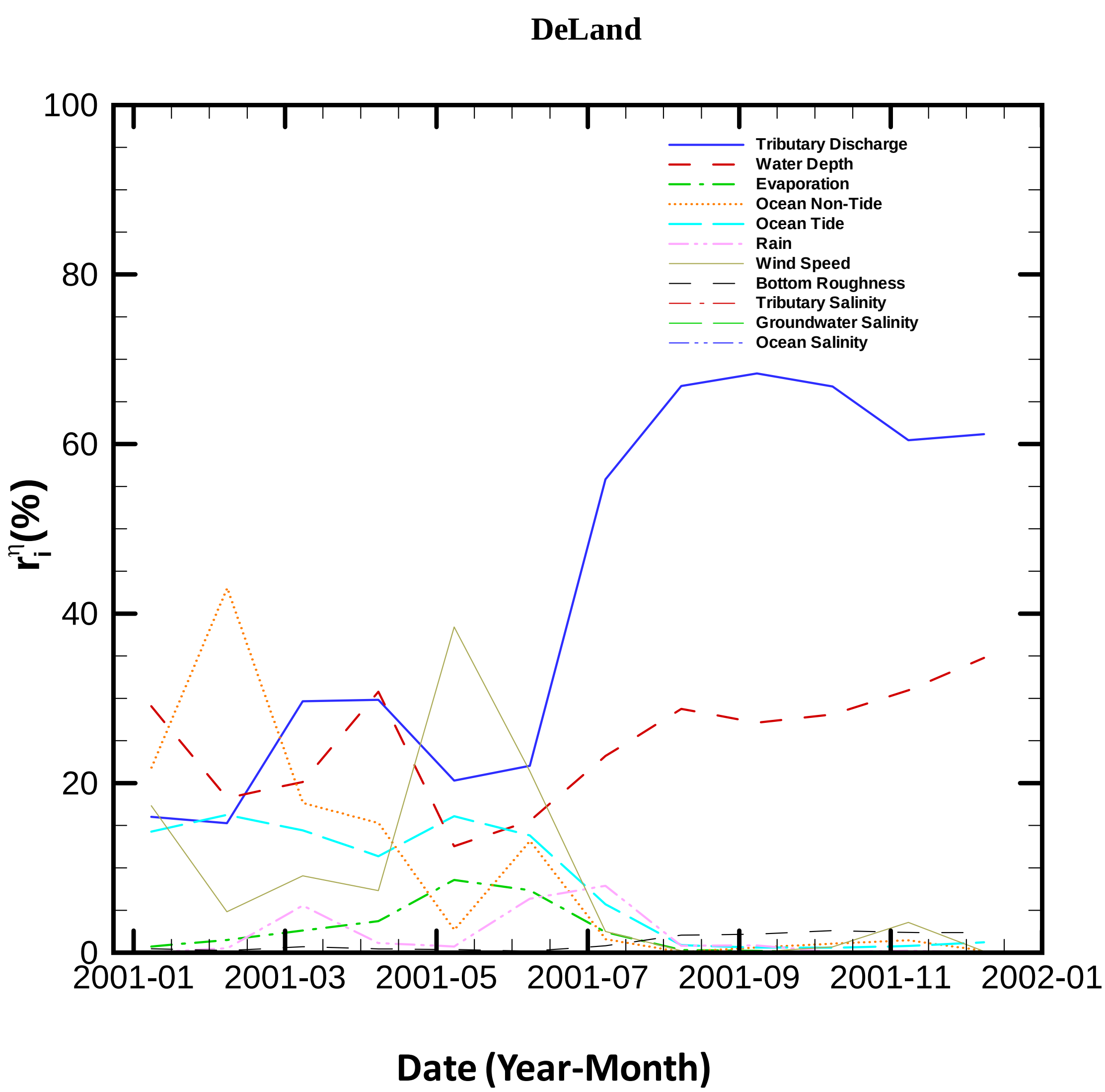

Figure 3–30. Percent contribution of input variables to the total uncertainty of water level (r^η) at DeLand.

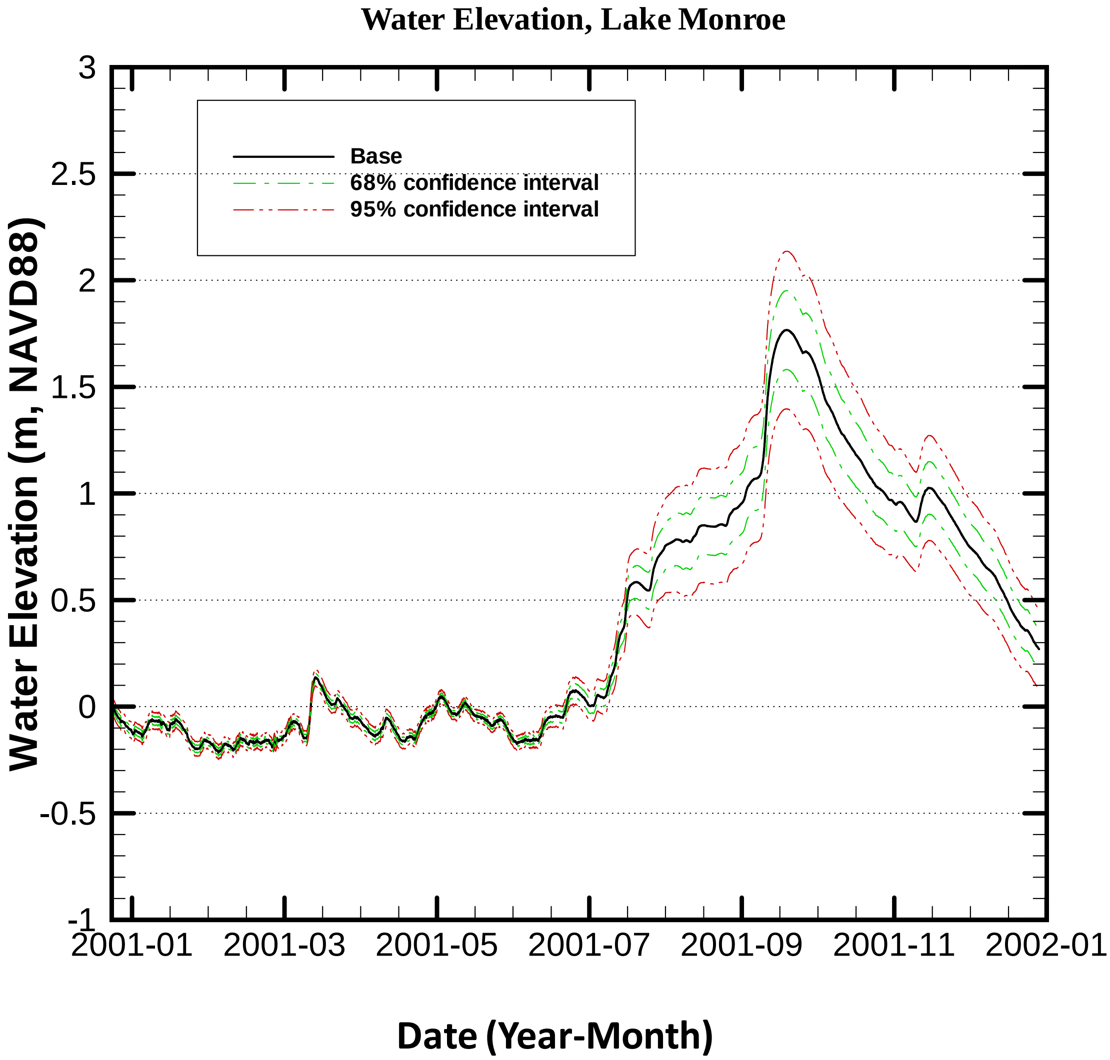

Figure 3–31. Simulated water level at Lake Monroe with confidence intervals for the year 2001. (The base scenario is the calibrated model.)

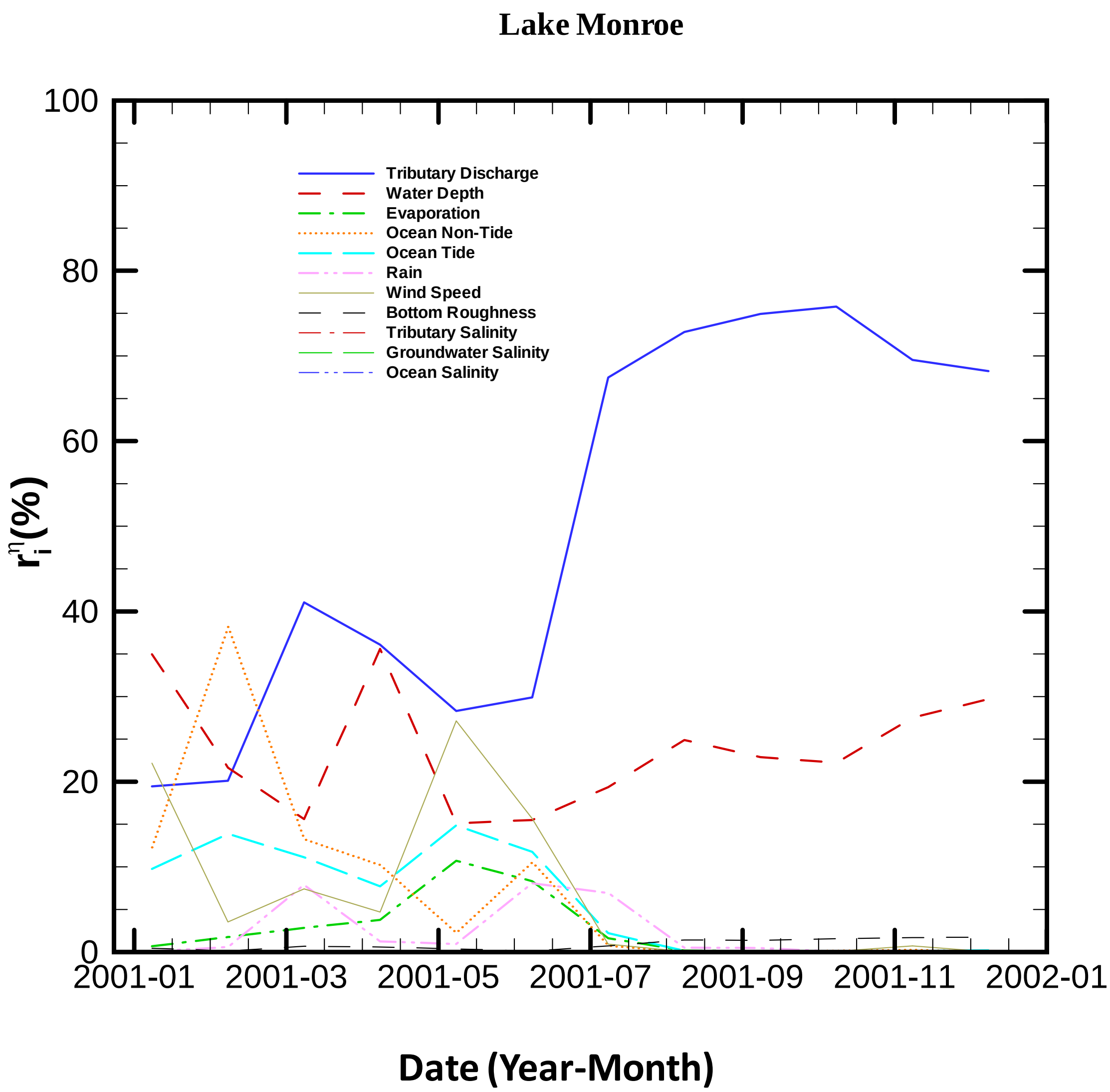

Figure 3–32. Percent contribution of input variables to the total uncertainty of water level (r^η) at Lake Monroe.

Current Speed

Uncertainty for current speed throughout the lower St. Johns River and Lake George is dominated by uncertainty in depth (Figure 3–34, Figure 3–36, Figure 3–38, and Figure 3–40). The total output uncertainty for peak velocities in the tidal reaches is 20% to 30% (Figure 3–33, Figure 3–35, Figure 3–37, and Figure 3–39).

Total uncertainty for velocity is low during the dry periods in the middle St. Johns River (Figure 3–41), and for all periods within the lakes (for example, Figure 3–43). In the restricted channels of the middle St. Johns River, represented by DeLand (Figure 3–41), uncertainty for velocity is near 25% when current speeds approach about 40 cm s^{-1}. Similarly to uncertainty for water level, uncertainty for velocity during these wet periods and in the river channels is primarily dominated by uncertainty in tributary discharge and secondarily by uncertainty in depth (Figure 3–42). Uncertainty of current speed in Lake Monroe is dominated by uncertainty in wind (Figure 3–44).

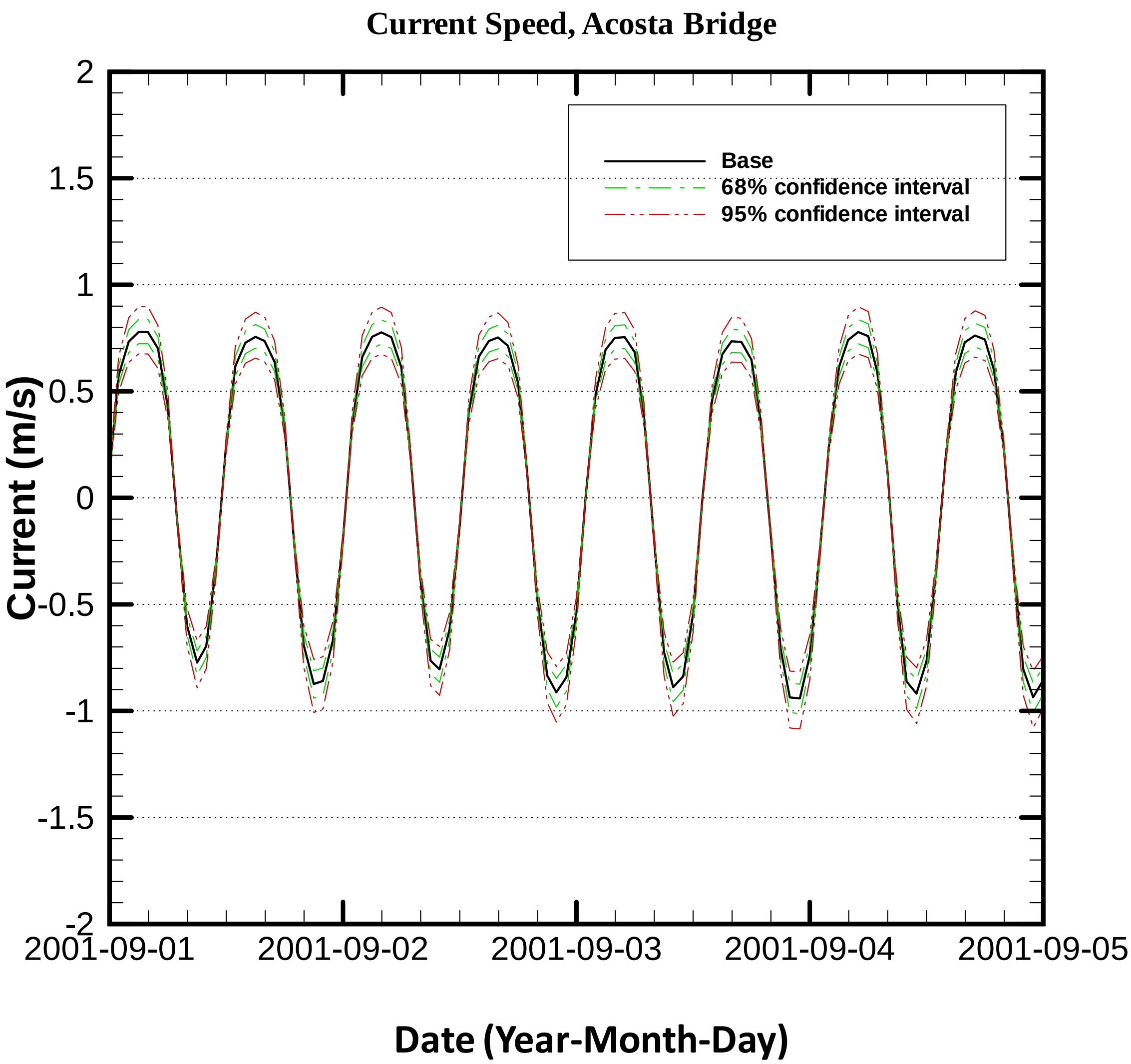

Figure 3–33. Simulated current speed at Acosta Bridge with confidence intervals for the year 2001. (The base scenario is the calibrated model Base1995NN.)

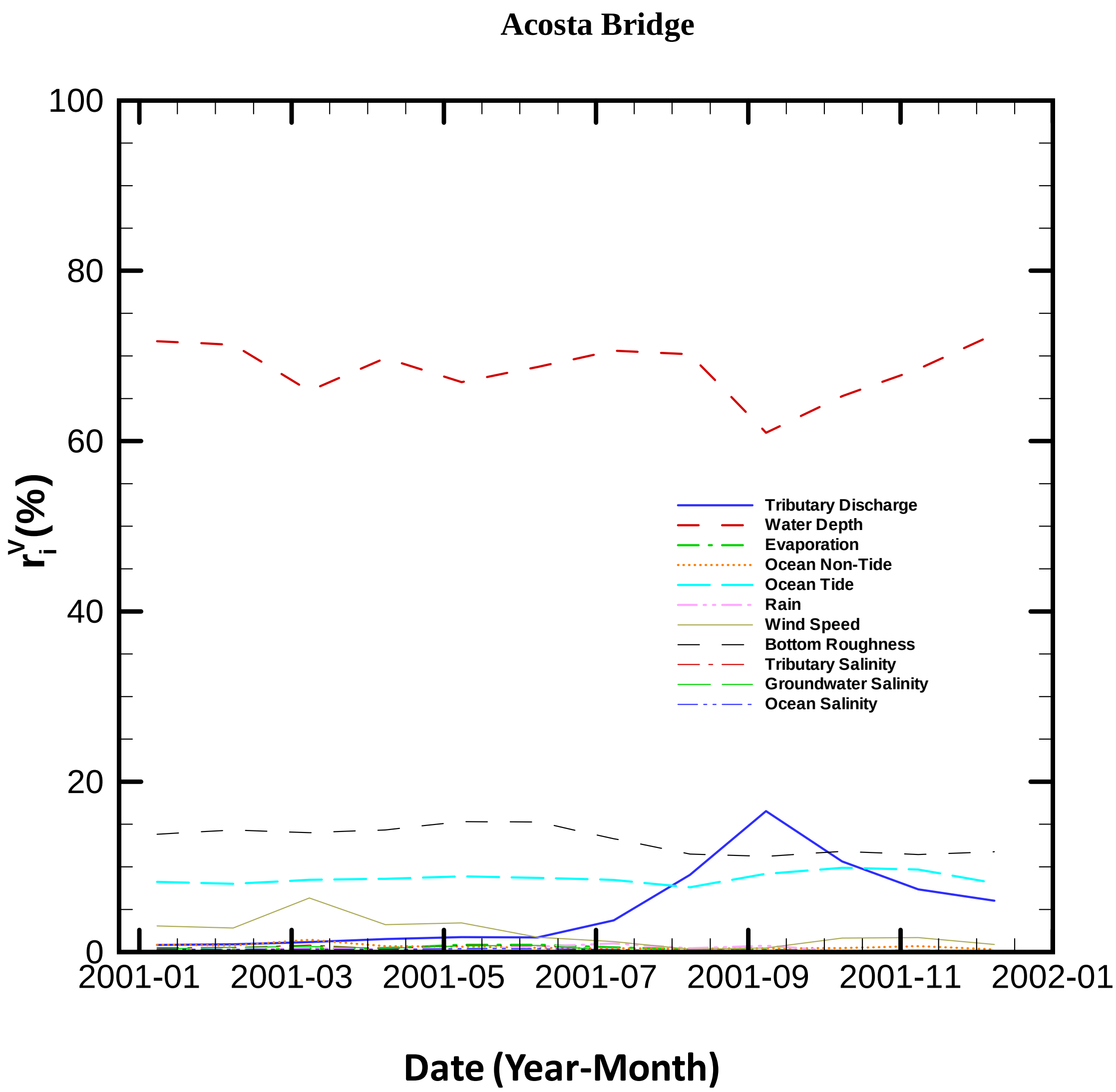

Figure 3–34. Percent contribution of input variables to the total uncertainty of current speed (r^V) at Acosta Bridge.

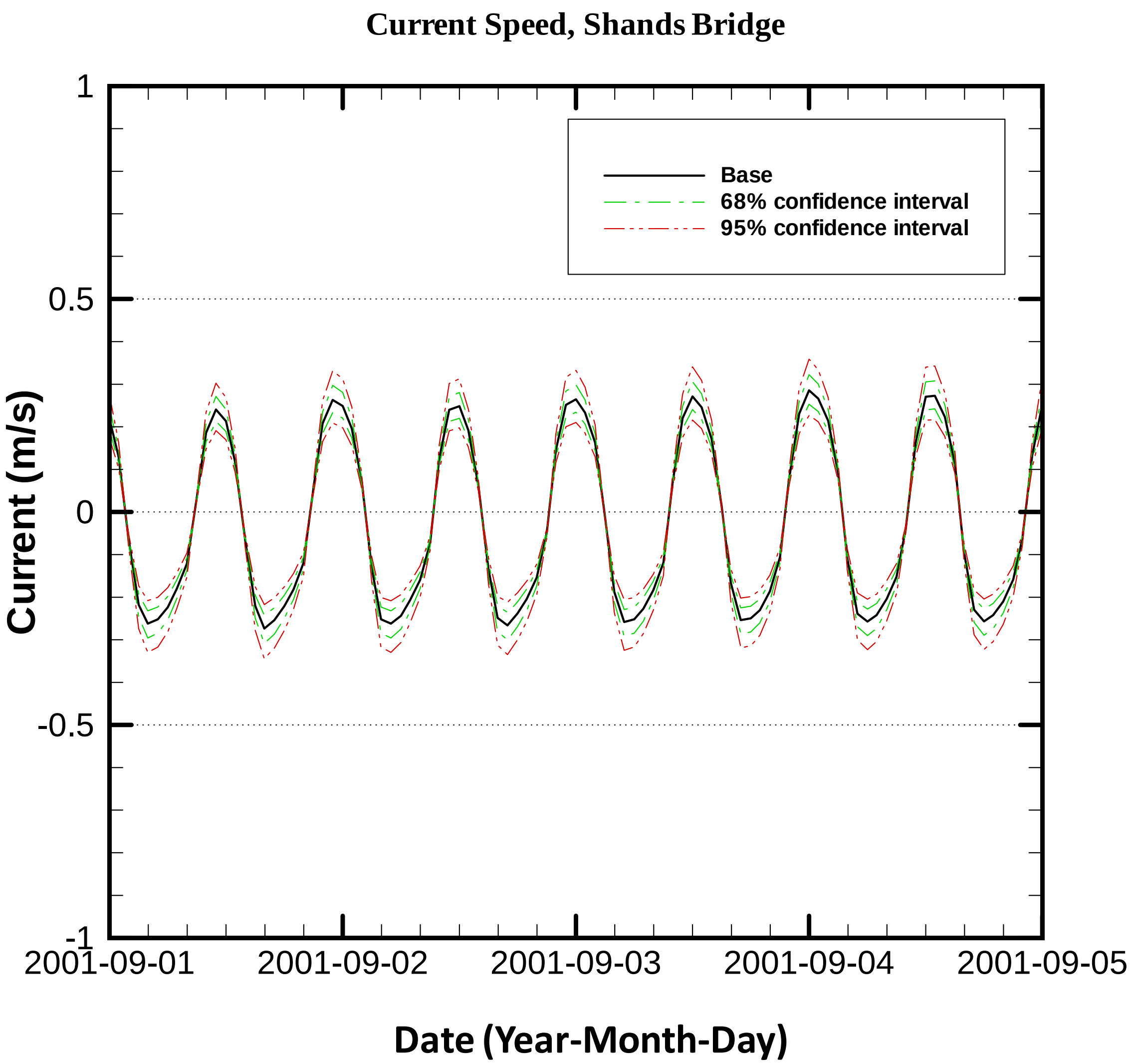

Figure 3–35. Simulated current speed at Shands Bridge with confidence intervals for the year 2001. (The base scenario is the calibrated model Base1995NN).

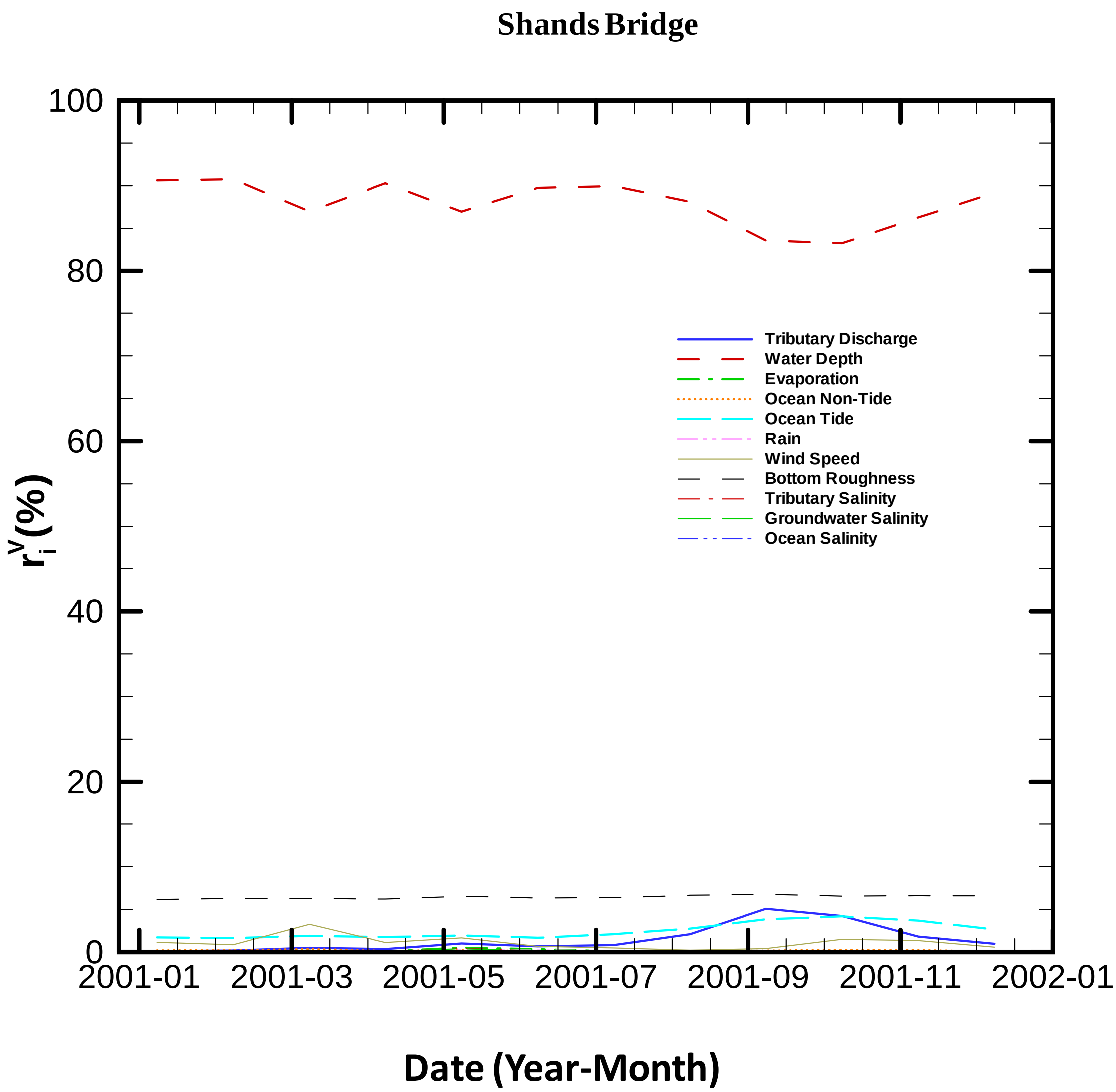

Figure 3–36. Percent contribution of input variables to the total uncertainty of current speed (r^V) at Shands Bridge.

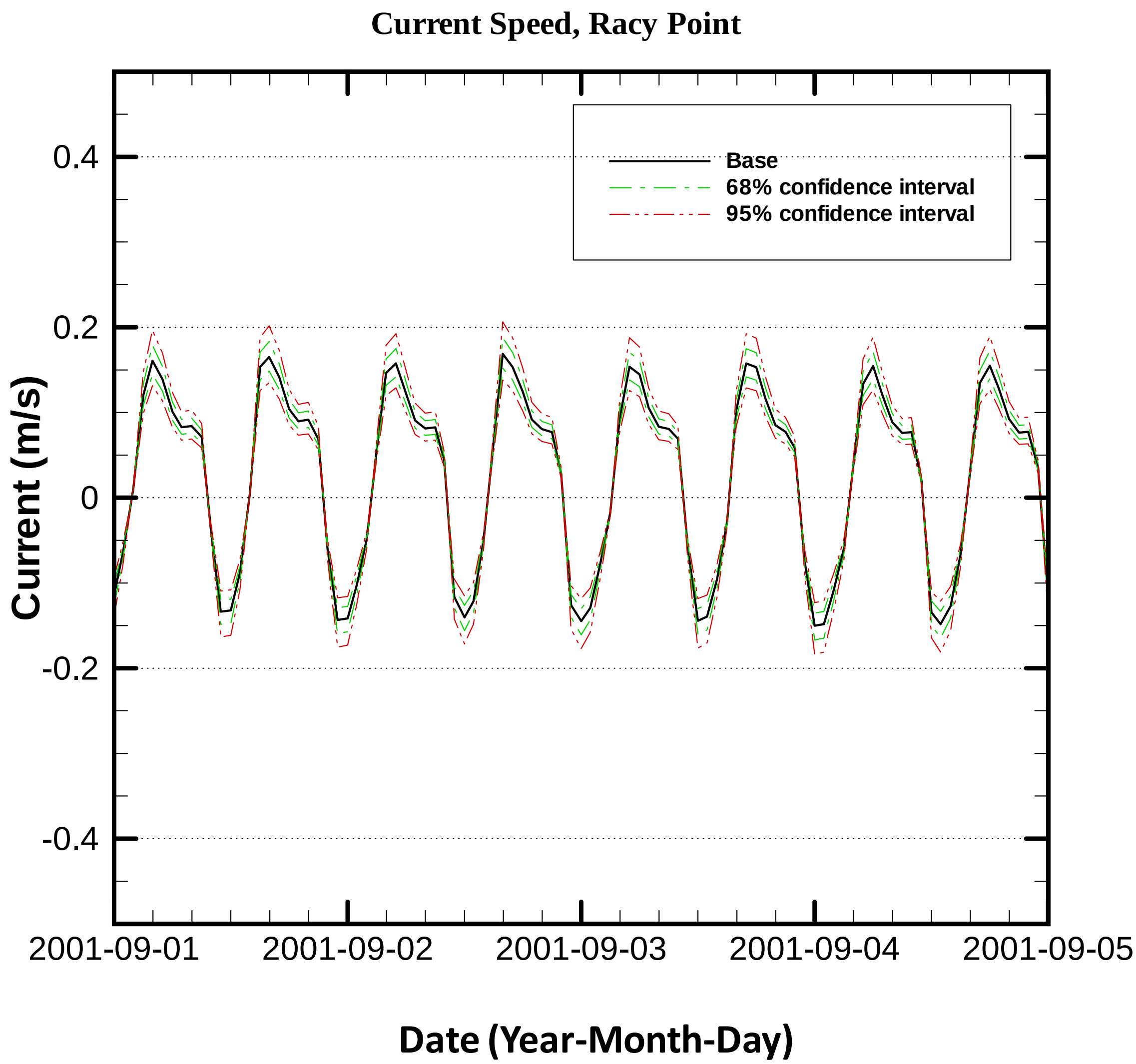

Figure 3–37. Simulated current speed at Racy Point with confidence intervals for the year 2001. (The base scenario is the calibrated model Base1995NN).

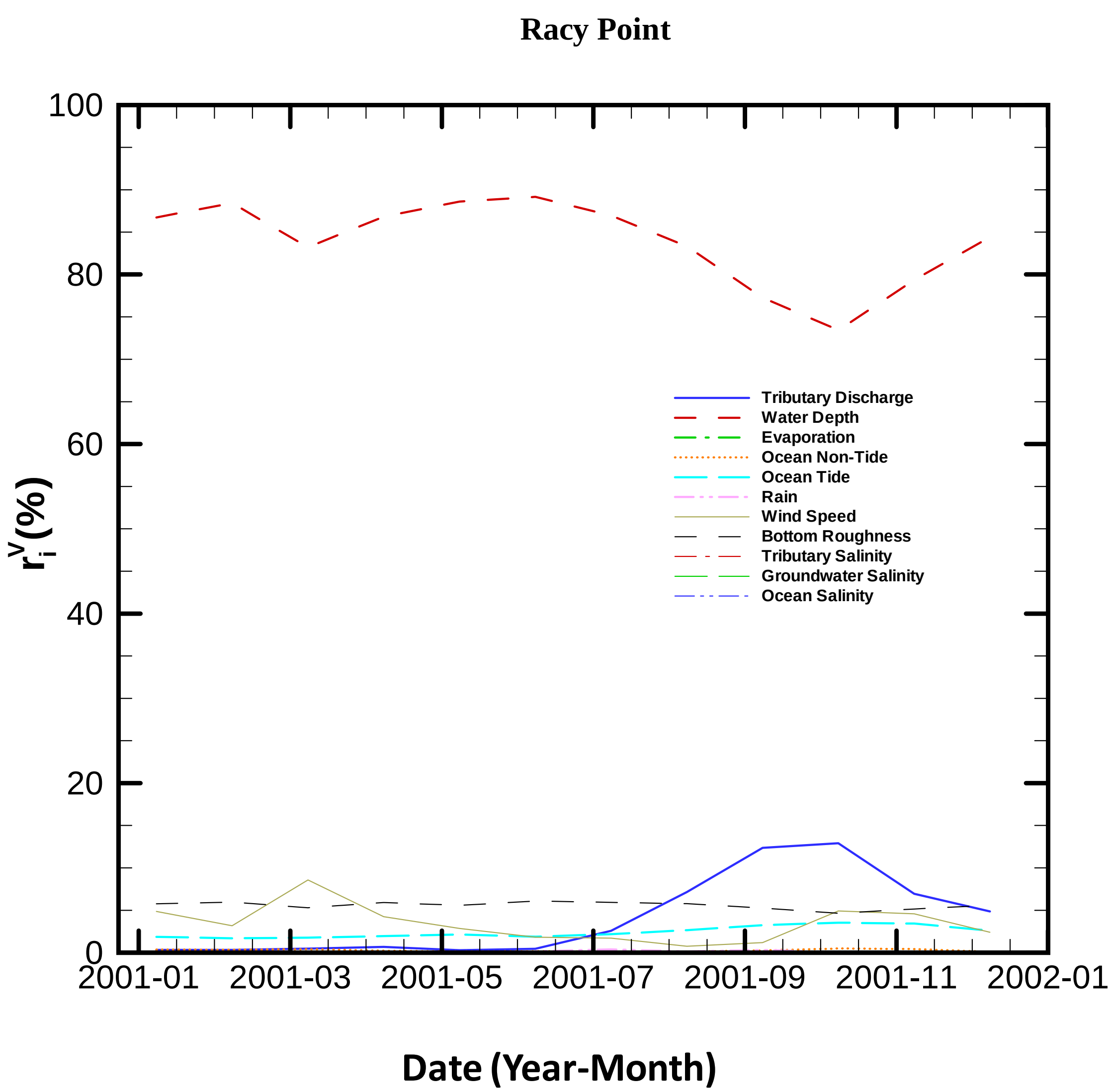

Figure 3–38. Percent contribution of input variables to the total uncertainty of current speed (r^V) at Racy Point.

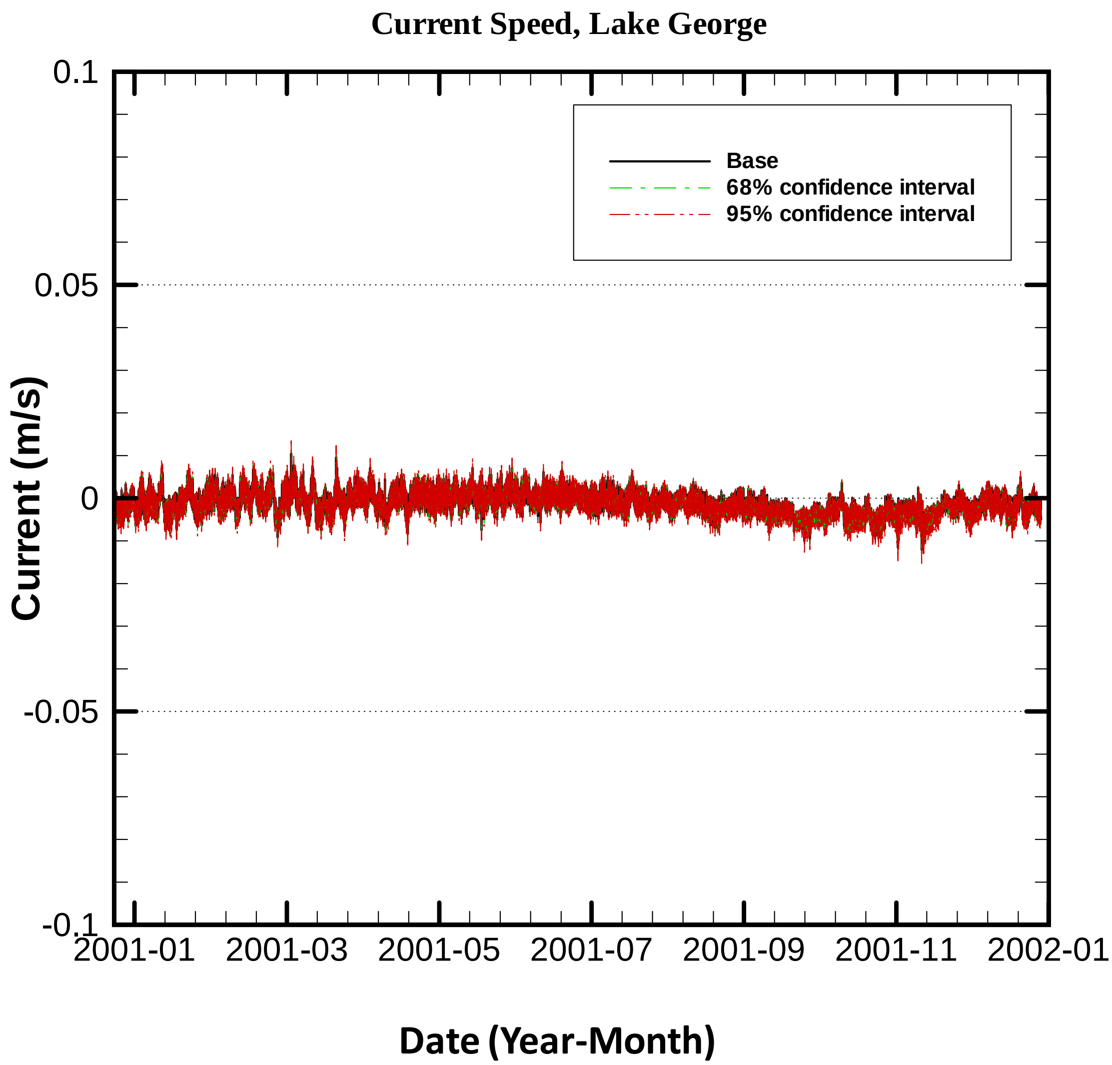

Figure 3–39. Simulated current speed at Lake George with confidence intervals for the year 2001. (The base scenario is the calibrated model Base1995NN).

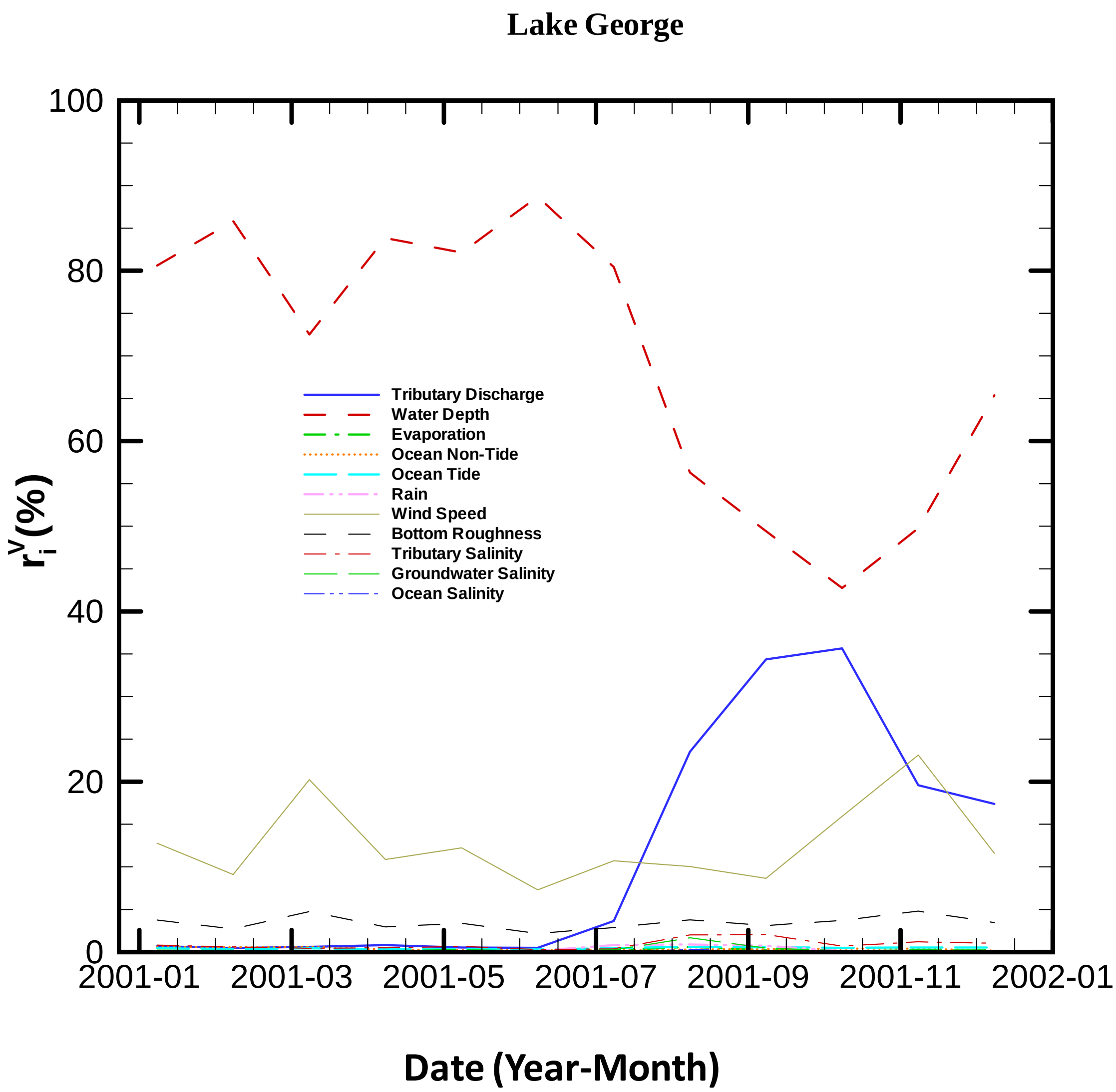

Figure 3–40. Percent contribution of input variables to the total uncertainty of current speed (r^V) at Lake George.

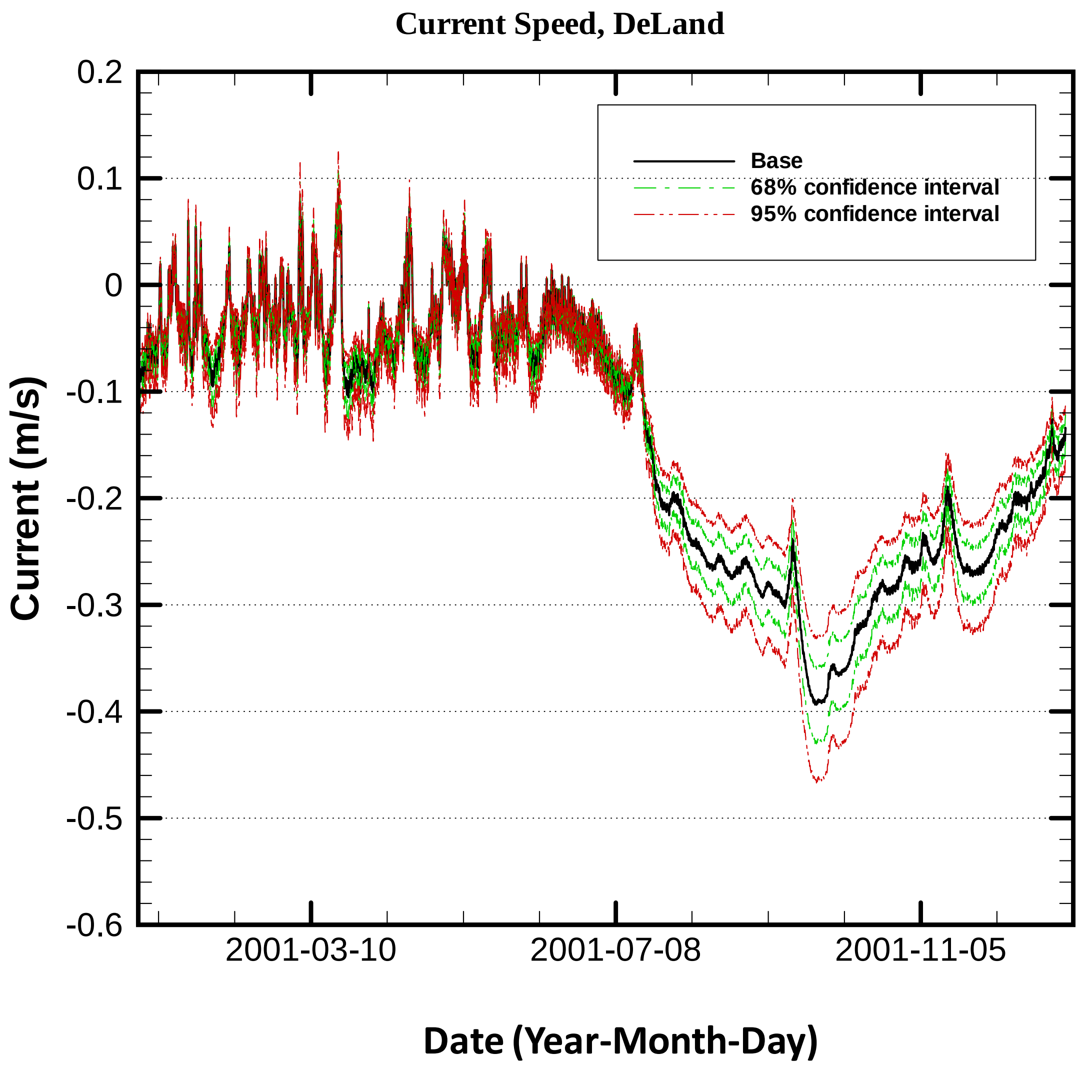

Figure 3–41. Simulated current speed at DeLand with confidence intervals for the year 2001. (The base scenario is the calibrated model Base1995NN).

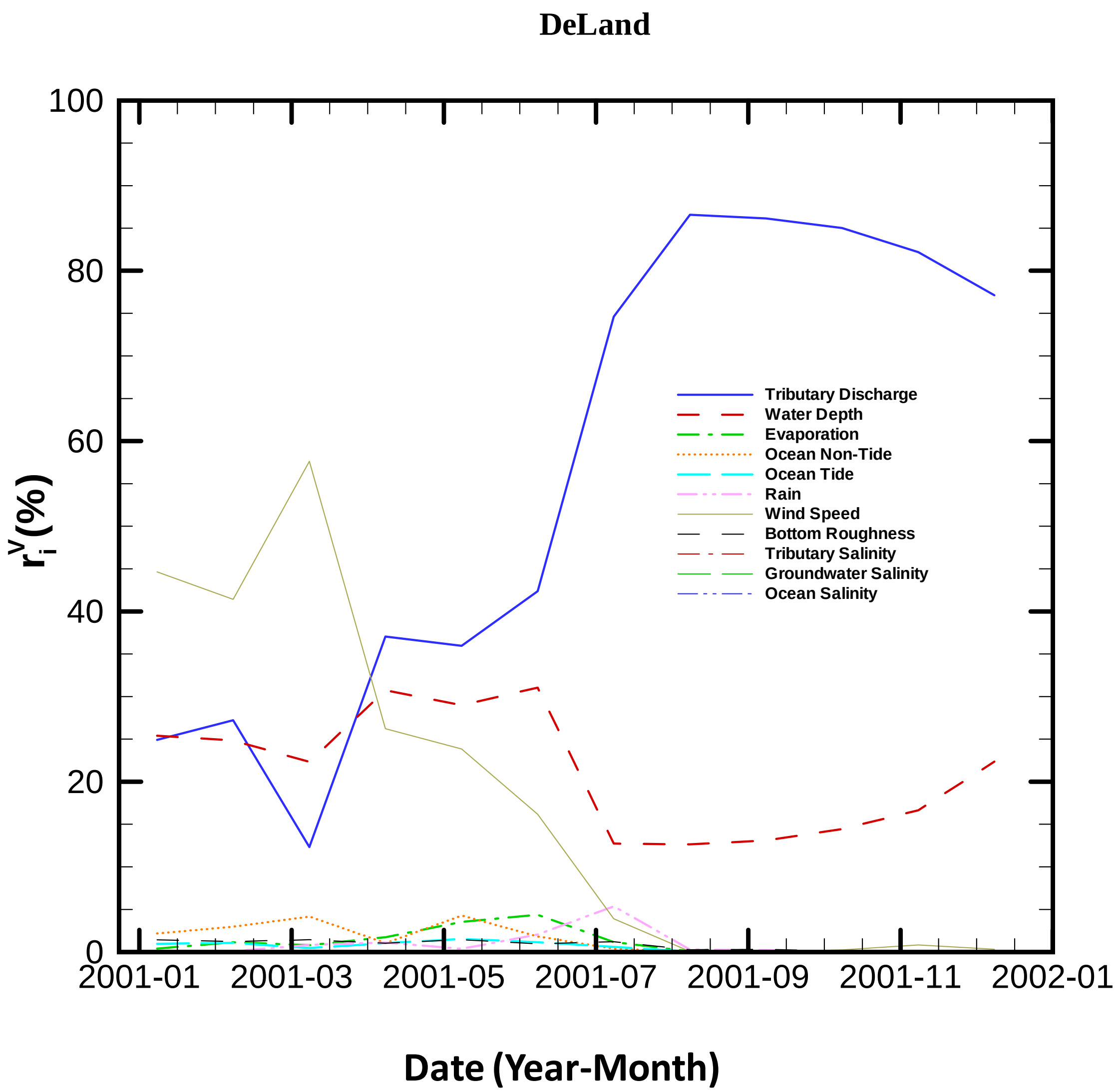

Figure 3–42. Percent contribution of input variables to the total uncertainty of current speed (r^V) at DeLand.

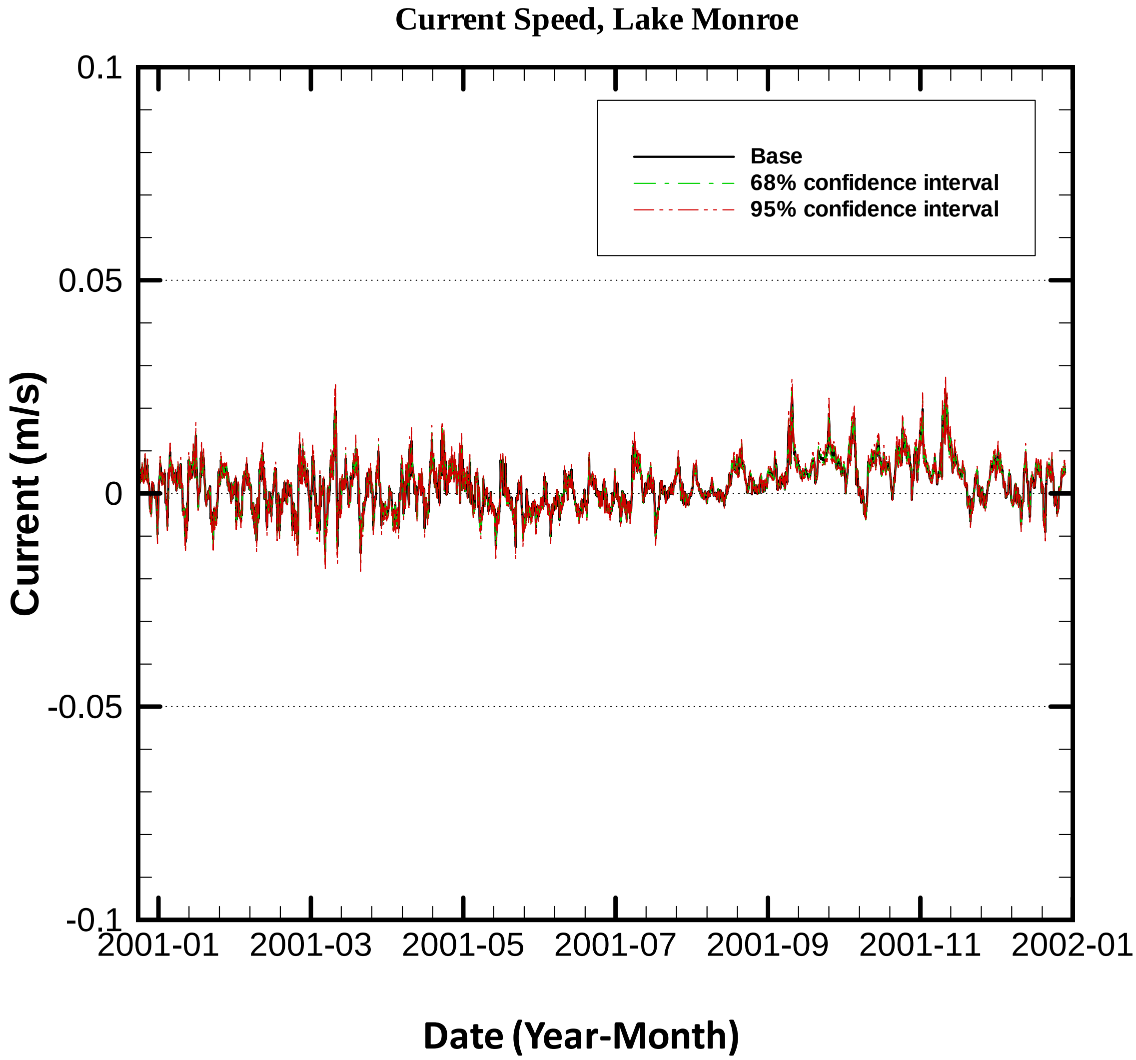

Figure 3–43. Simulated current speed at Lake Monroe with confidence intervals for the year 2001. (The base scenario is the calibrated model Base1995NN).

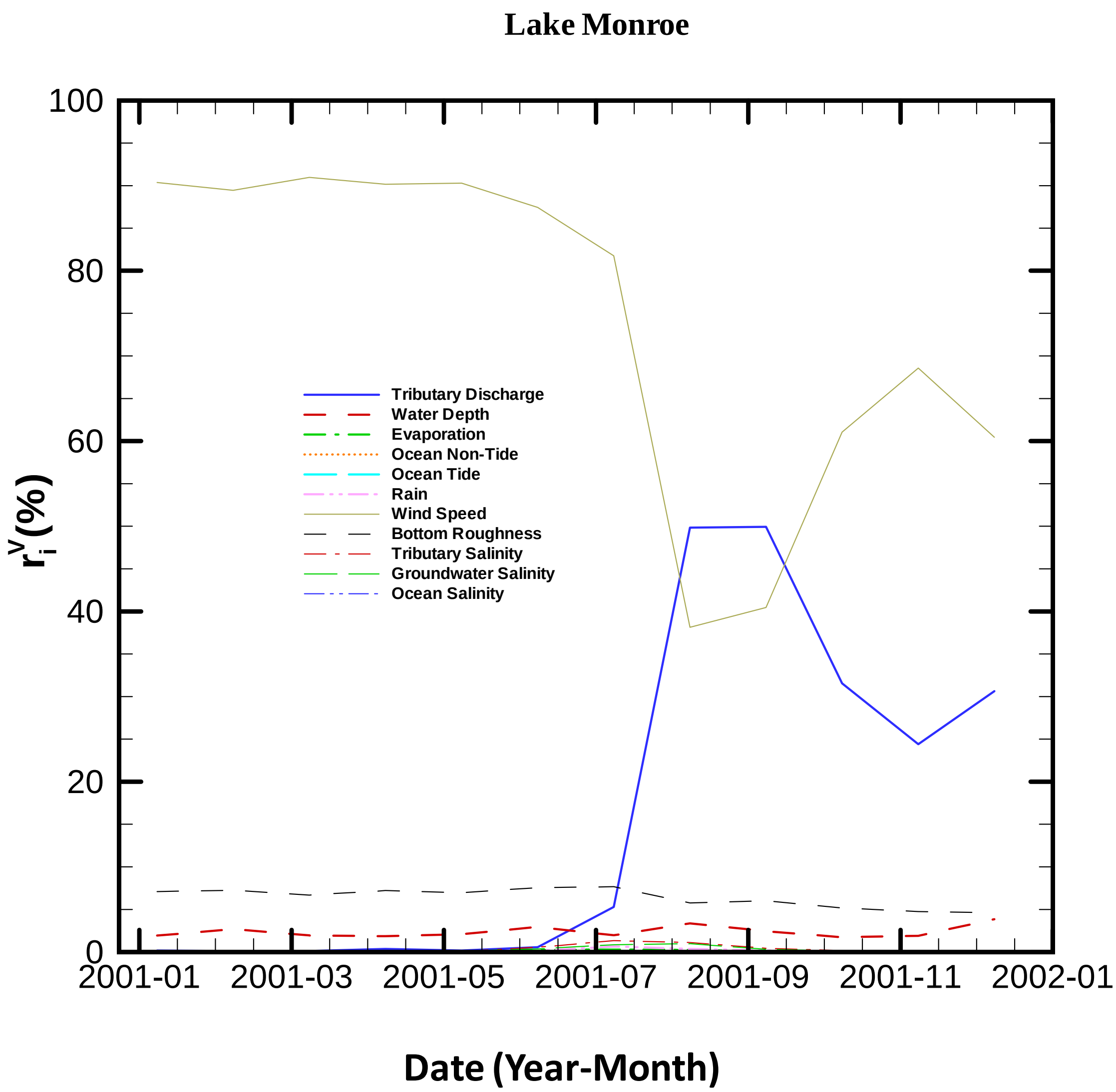

Figure 3–44. Percent contribution of input variables to the total uncertainty of current speed (r^V) at Lake Monroe.

Salinity

Uncertainty for salinity can be quite high during certain periods and in portions of the lower St. Johns River affected by ocean salinity. At Acosta Bridge during June 2001, for example, the 95% confidence interval is nearly 50% of the predicted salinity (Figure 3–45). At Shands Bridge during May 2001 (Figure 3–47), the predicted peak salinity was about 0.6 PSS78, and the 95% confidence interval extended to 1.2 PSS78. This illustrates the large uncertainty inherent in predicting absolute levels of salinity near salinity fronts. At Acosta Bridge and Shands Bridge during the dry season, salinity uncertainty is dominated by uncertainty of depth and secondarily by uncertainty in discharge (Figure 3–46 and Figure 3–48).

For all freshwater areas upstream of Shands Bridge, the absolute uncertainty in salinity is fairly small, less than 0.2 PSS78 (Figure 3–49, Figure 3–51, Figure 3–53, and Figure 3–55). This result also applies to Shands Bridge (Figure 3–47) during the wet season. At these locations the uncertainty in salinity is dominated by uncertainty in tributary salinity (Figure 3–48, Figure 3–50, Figure 3–52, and Figure 3–54) with the exception of Lake Monroe during the dry season when uncertainty in groundwater salinity is equal in importance to tributary salinity (Figure 3–56).

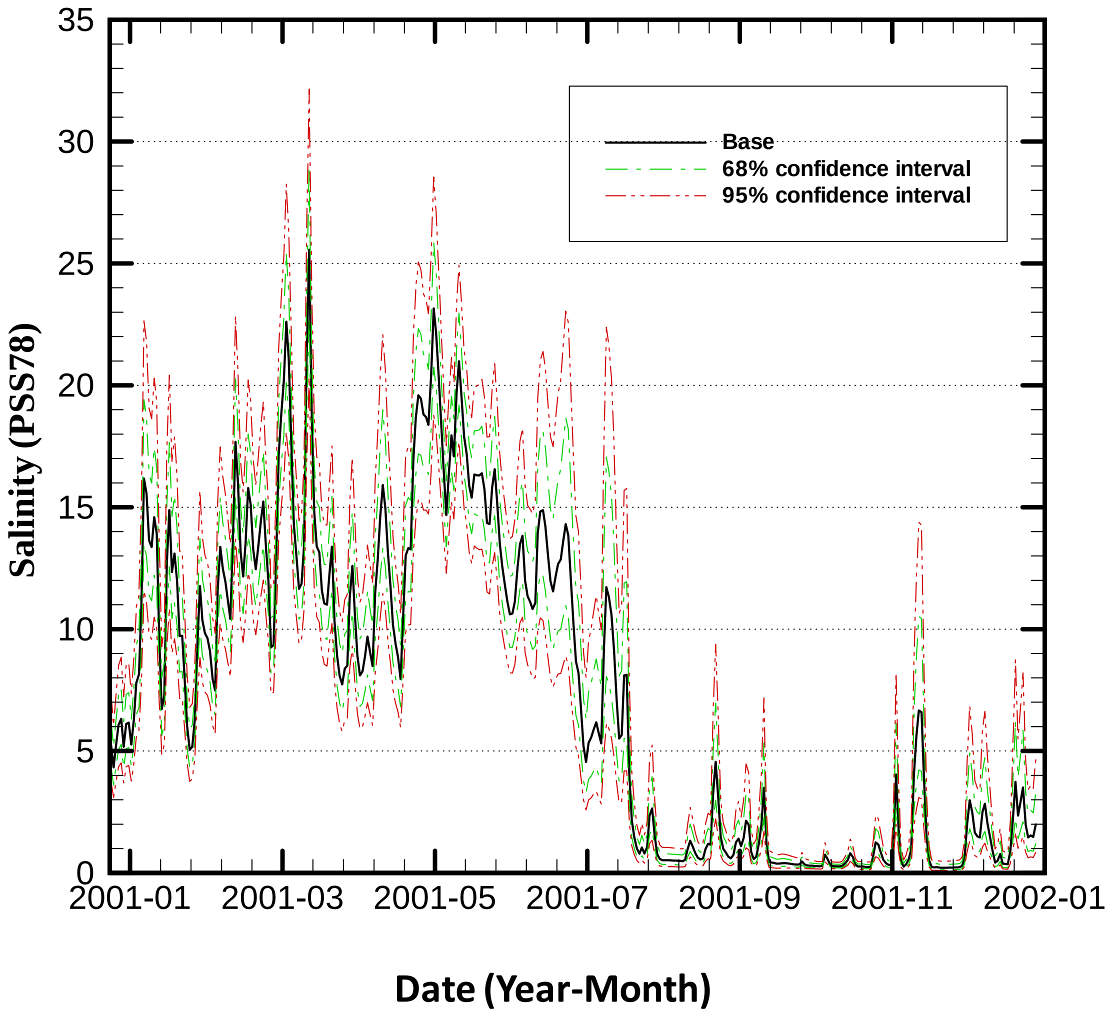

Figure 3–45. Simulated salinity at Acosta Bridge with confidence intervals for the year 2001. (The base scenario is the calibrated model).

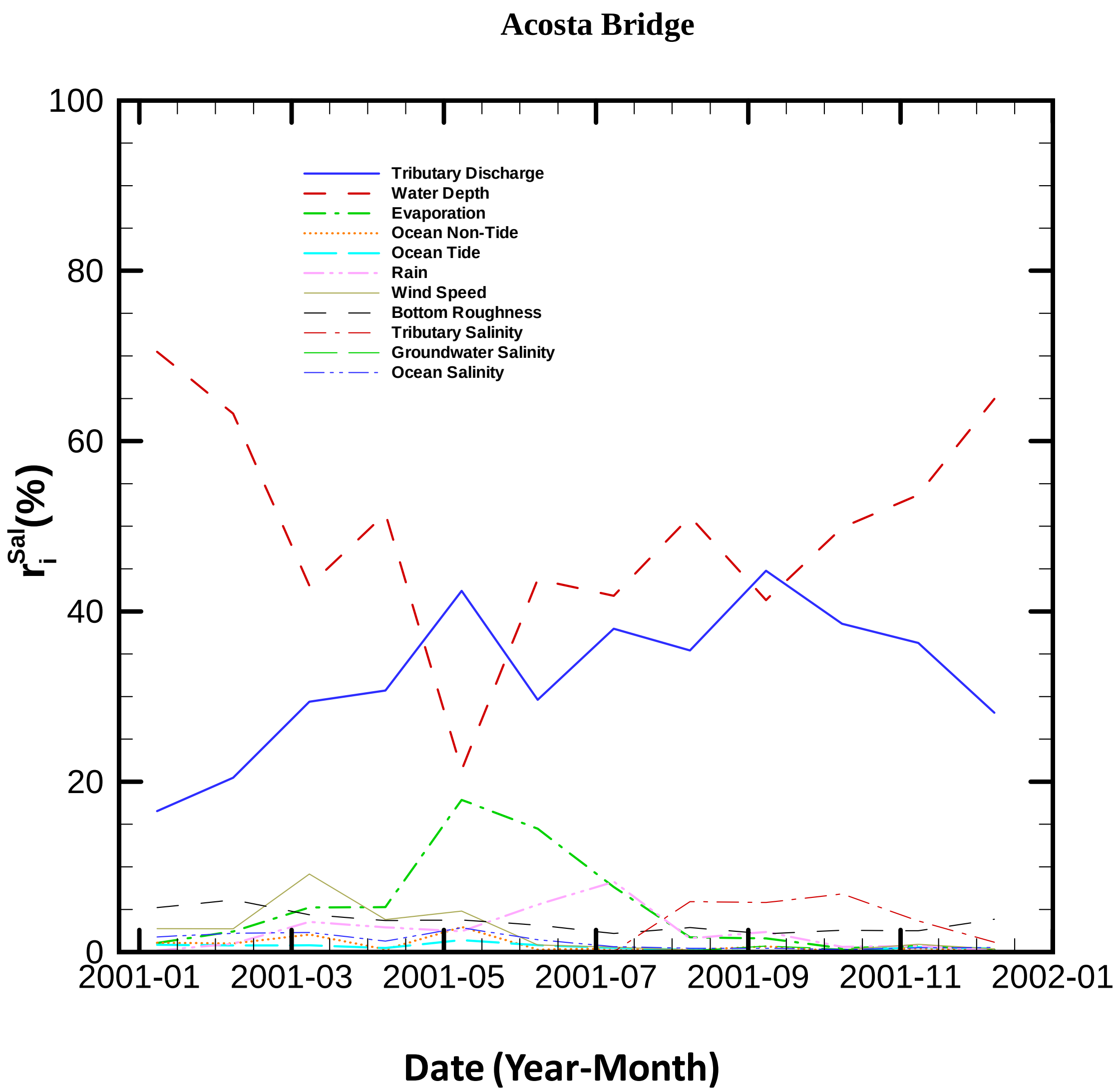

Figure 3–46. Percent contribution of input variables to the total uncertainty of salinity (r^{Sal}) at Acosta Bridge.

Figure 3–47. Simulated salinity at Shands Bridge with confidence intervals for the year 2001. (The base scenario is the calibrated model.)

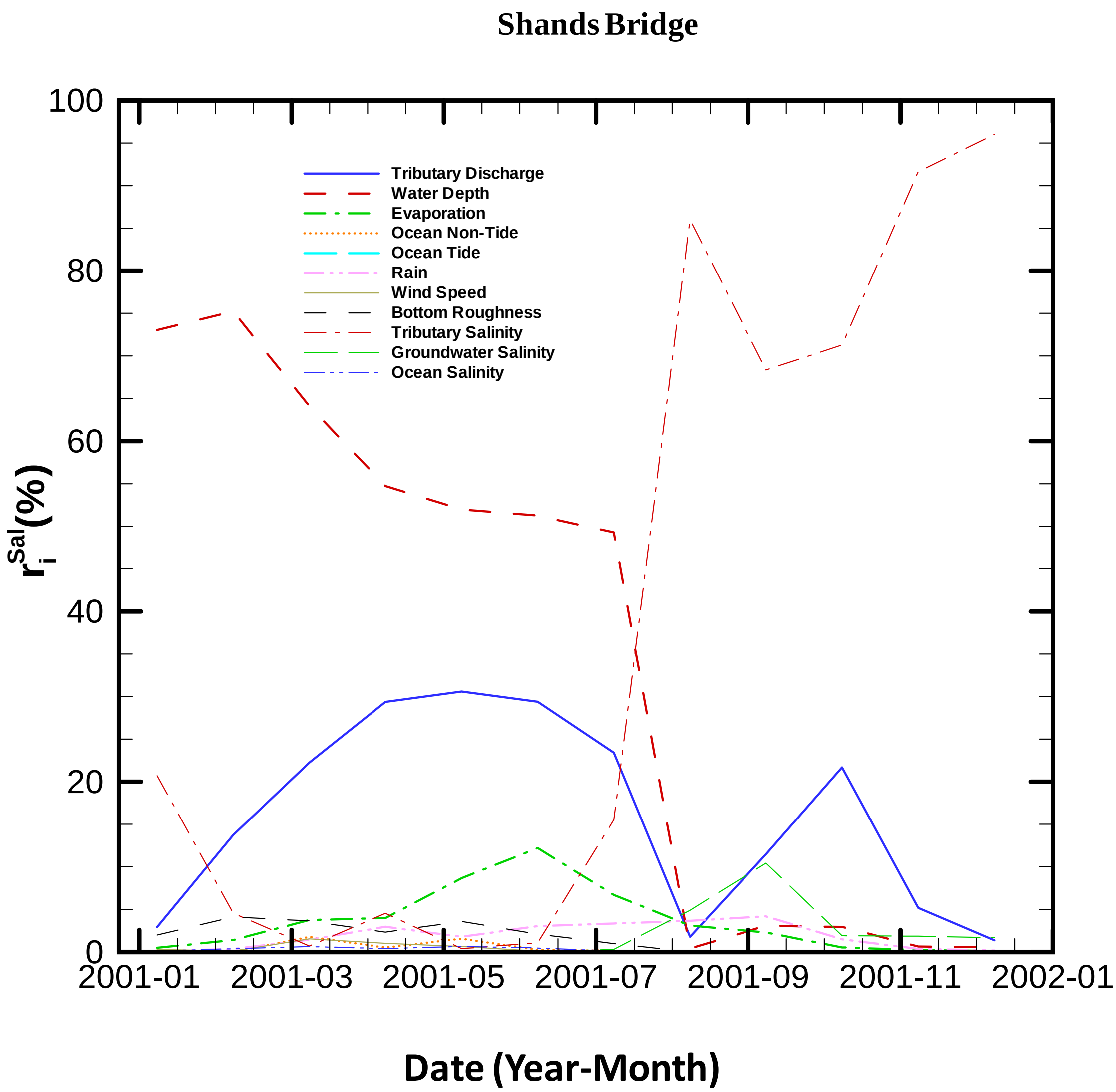

Figure 3–48. Percent contribution of input variables to the total uncertainty of salinity (r^{Sal}) at Shands Bridge.

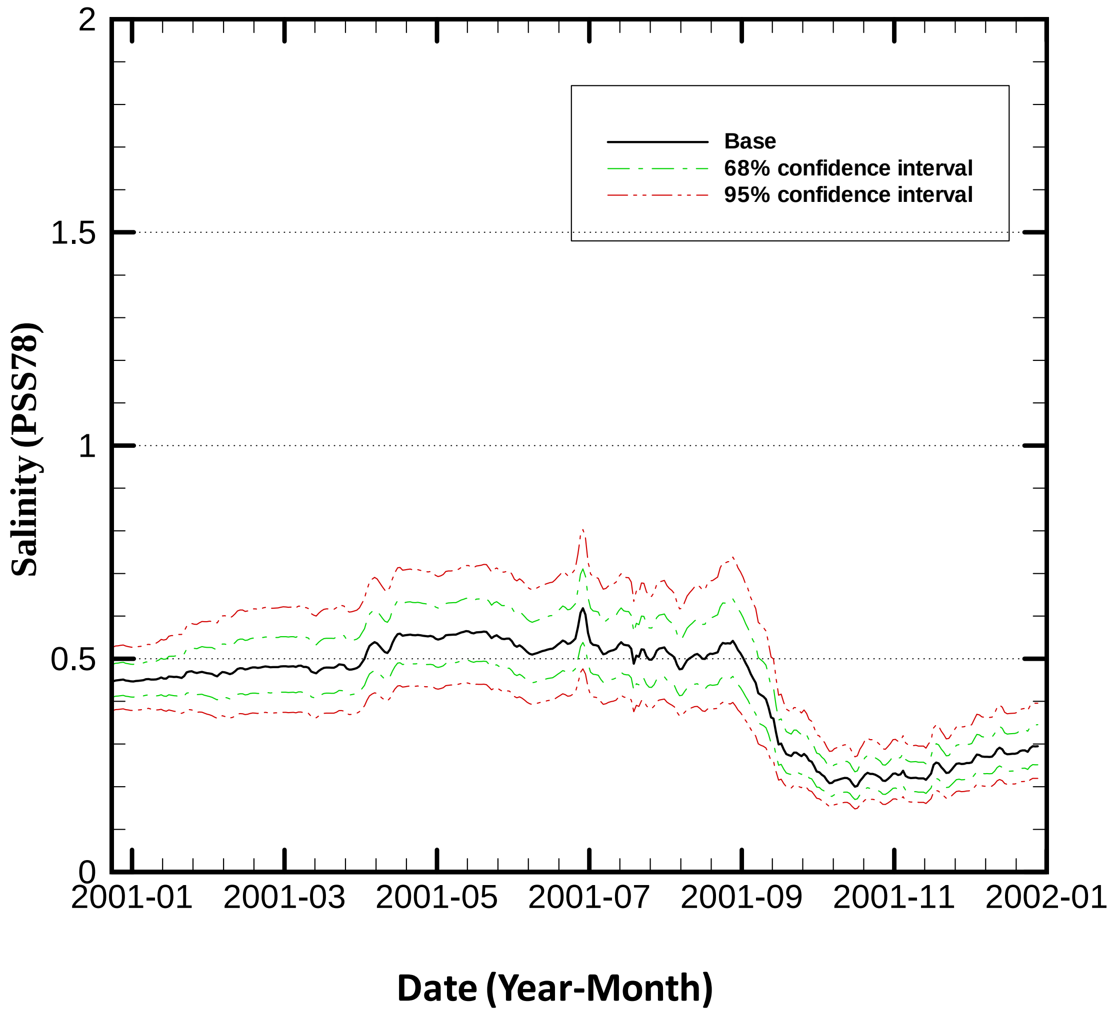

Figure 3–49. Simulated salinity at Racy Point with confidence intervals for the year 2001. (The base scenario is the calibrated model.)

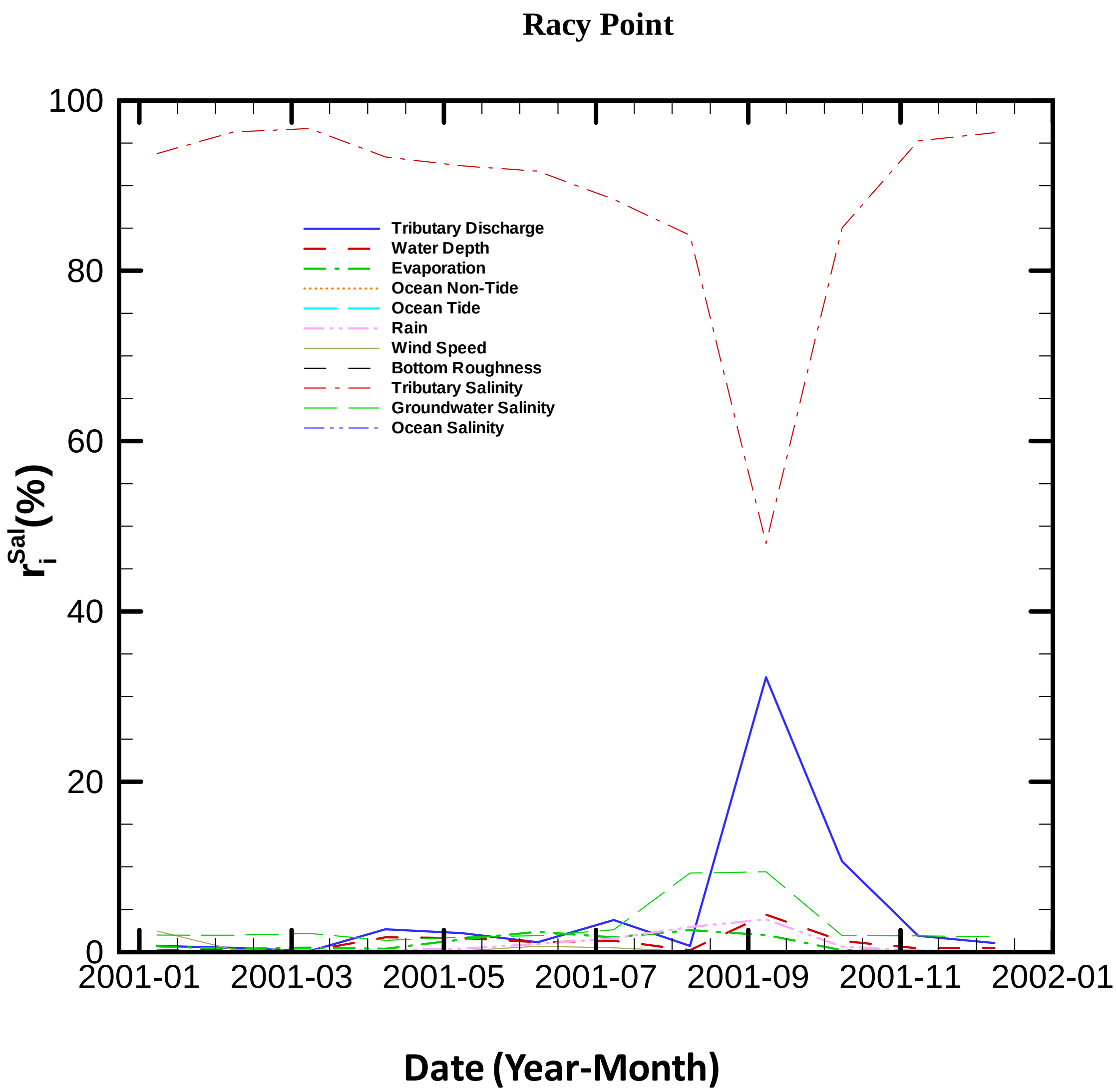

Figure 3–50. Percent contribution of input variables to the total uncertainty of salinity (r^{Sal}) at Racy Point.

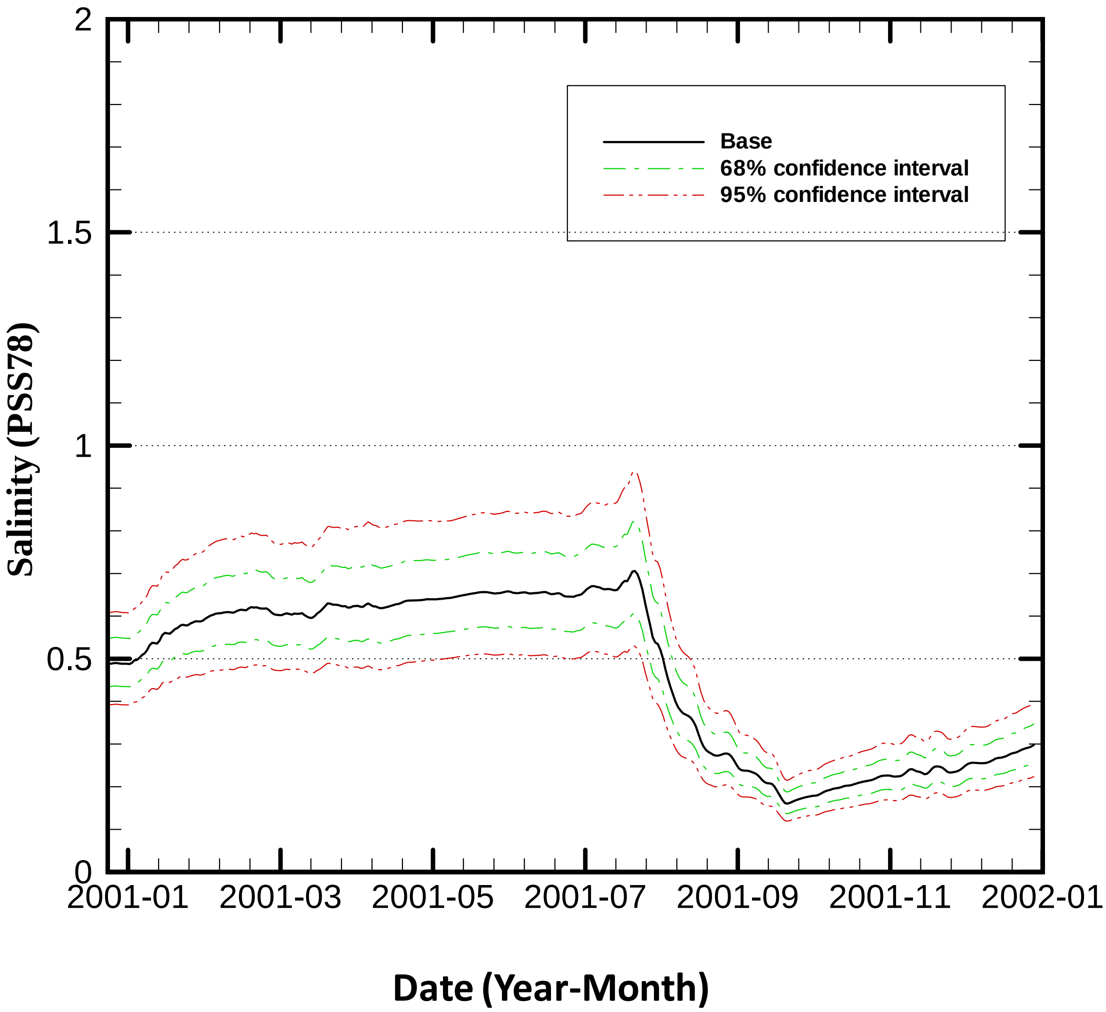

Figure 3–51. Simulated salinity at Lake George with confidence intervals for the year 2001. (The base scenario is the calibrated model.)

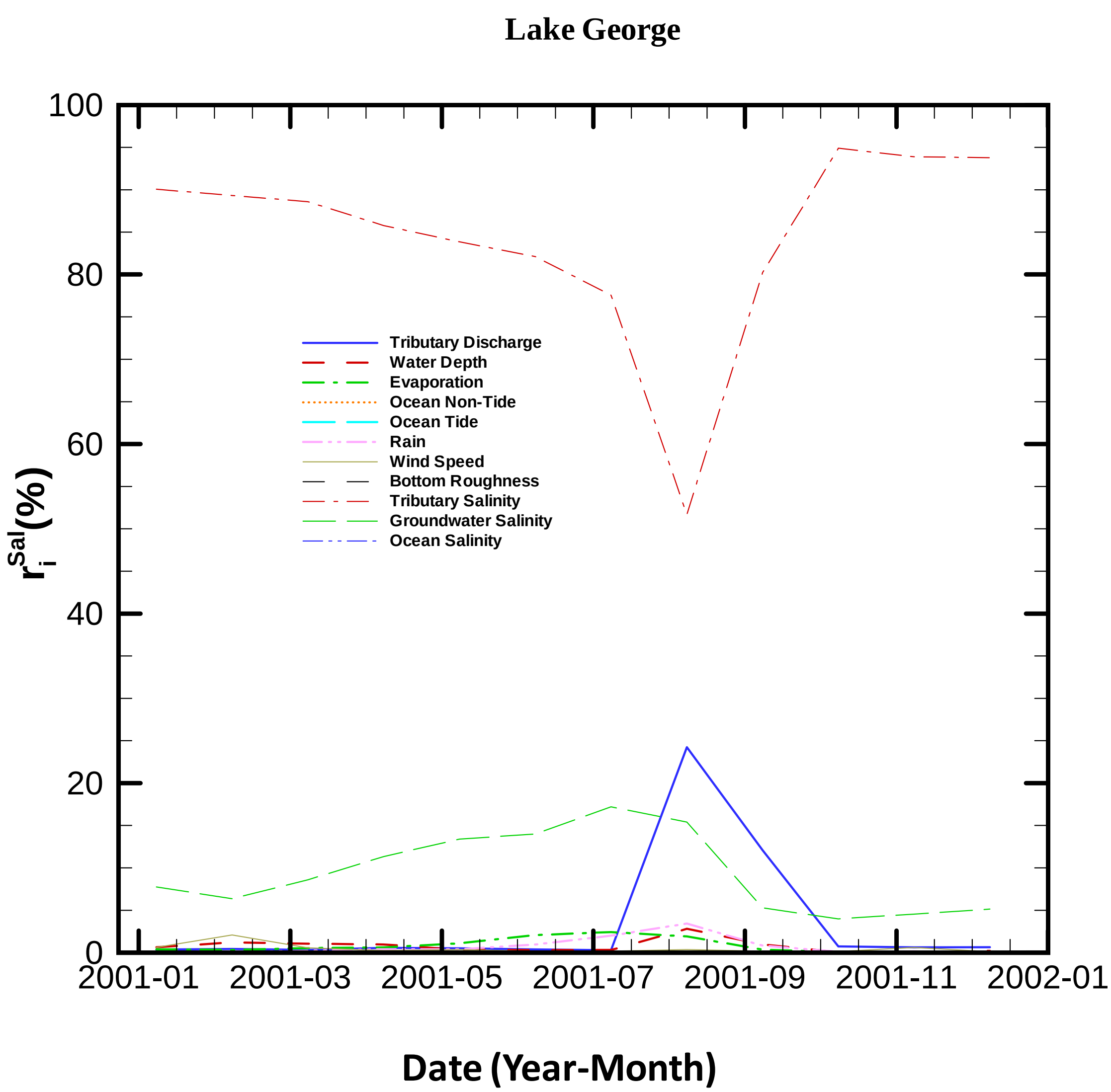

Figure 3–52. Percent contribution of input variables to the total uncertainty of salinity (r^{Sal}) at Lake George.

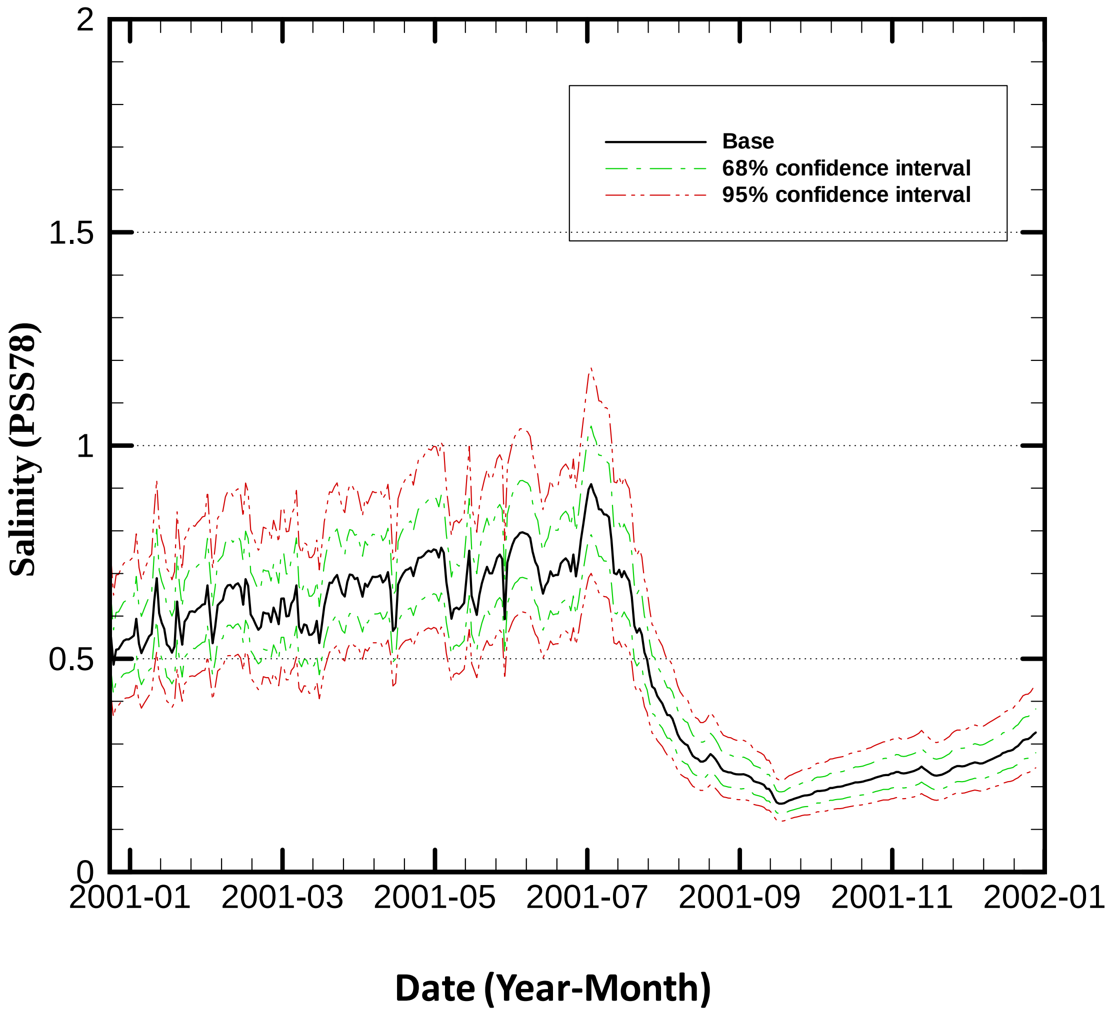

Figure 3–53. Simulated salinity at DeLand with confidence intervals for the year 2001. (The base scenario is the calibrated model.)

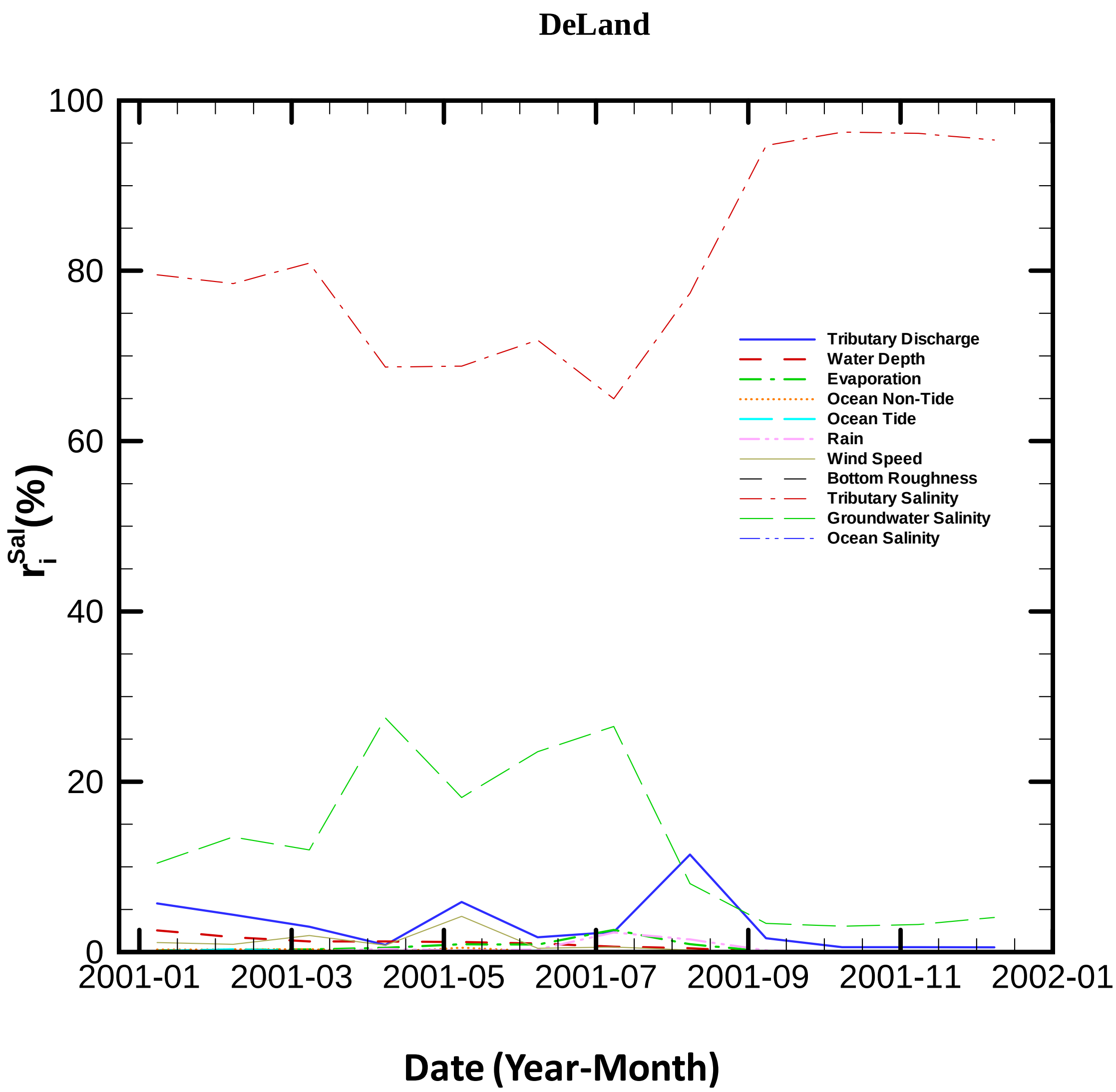

Figure 3–54. Percent contribution of input variables to the total uncertainty of salinity (r^{Sal}) at DeLand.

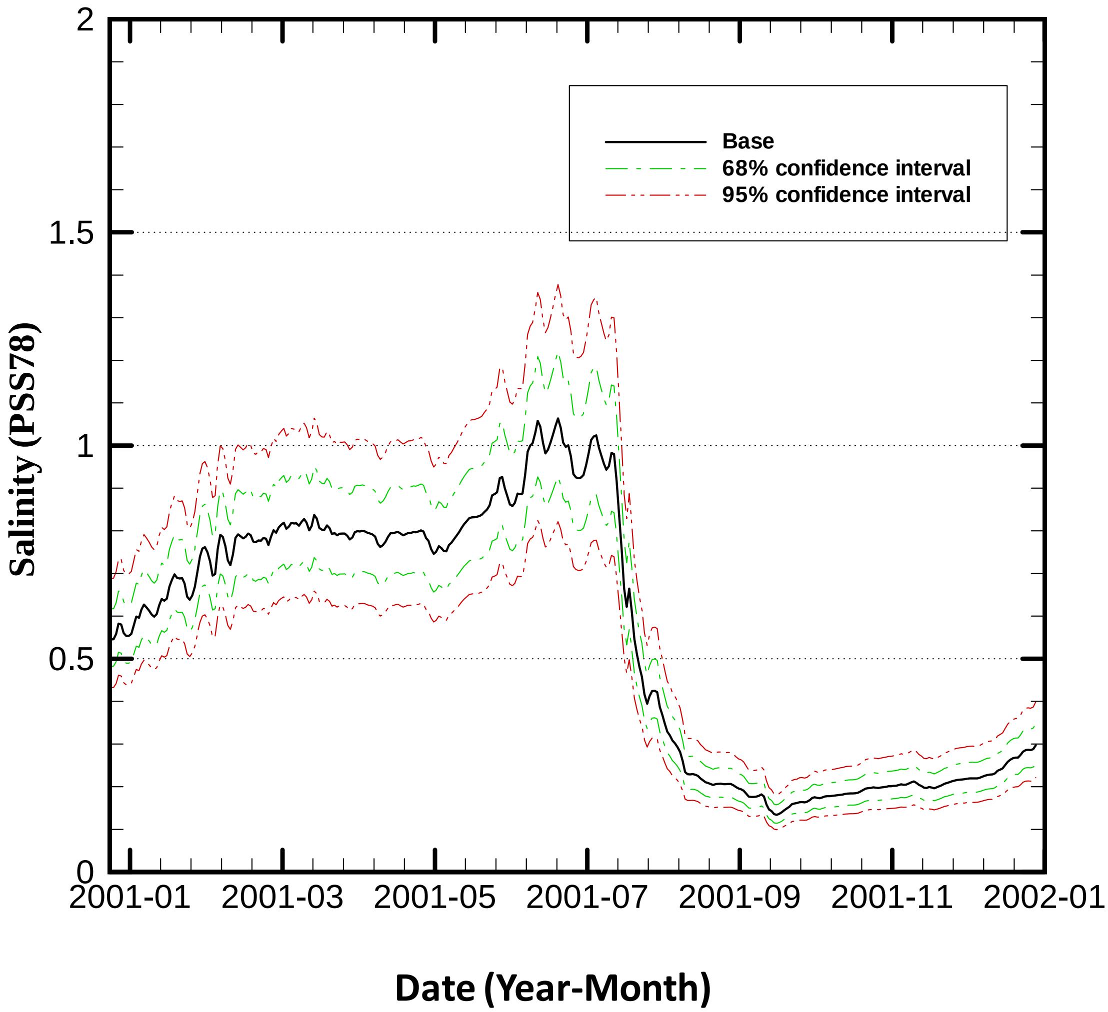

Figure 3–55. Simulated salinity at Lake Monroe with confidence intervals for the year 2001. (The base scenario is the calibrated model.)

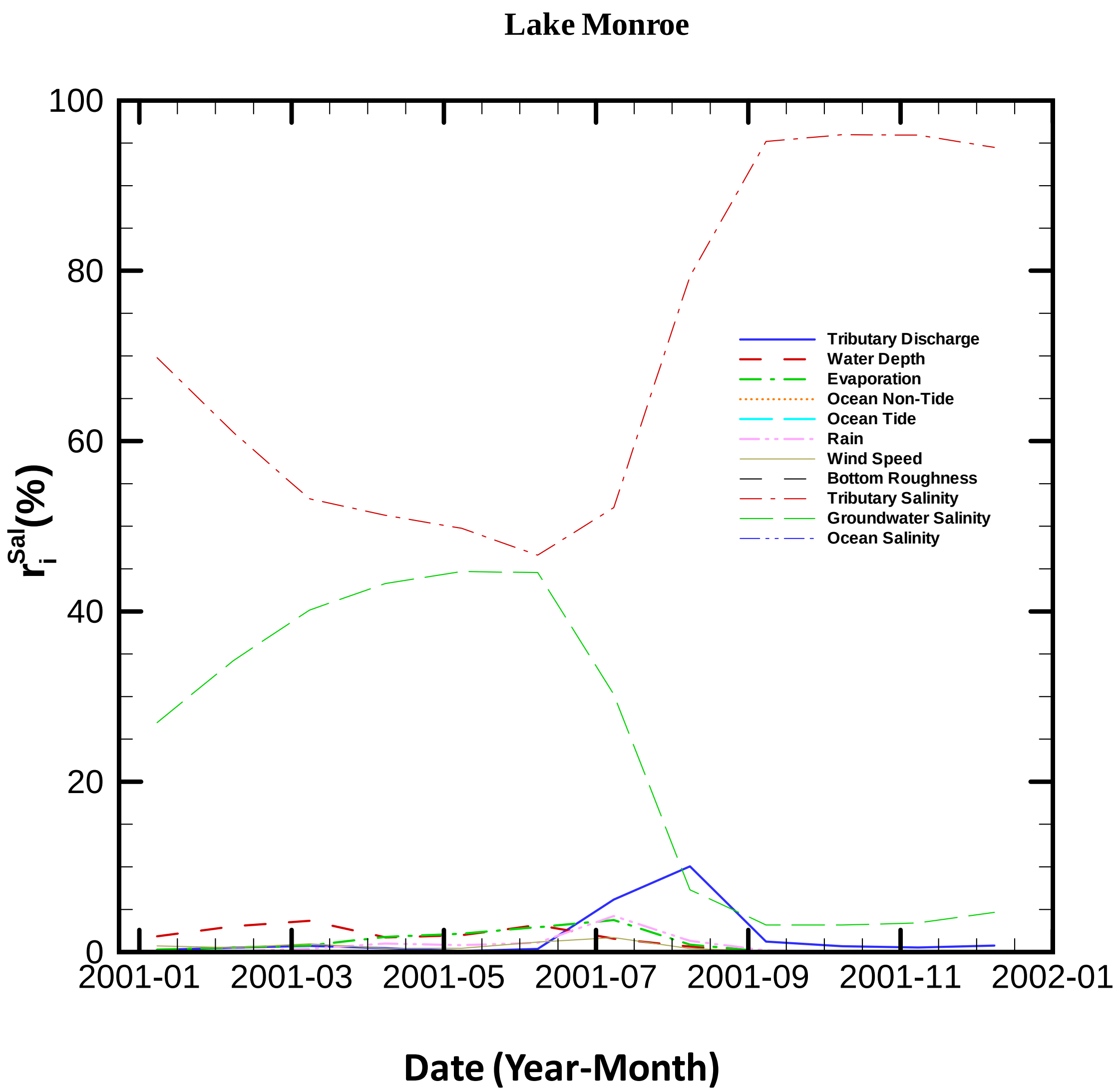

Figure 3–56. Percent contribution of input variables to the total uncertainty of salinity (r^{Sal}) at Lake Monroe.

Uncertainty of Predicted Differences to Water Withdrawal Scenarios

This section focuses on the question "what is the uncertainty of predicted differences in output variables, obtained by differencing two model scenarios, due to uncertainty in model inputs?" This question is addressed by using FOEA to propagate the uncertainty of model inputs through a calculation of differences between output variables for a base scenario (Base1995NN) and a change scenario (Full2030PS). Recall that the Base1995NN scenario represents a hindcast of the period 1996 to 2005, and the Full2030PS scenario represents a forecast of the likely state of the river in the year 2030 in conjunction with a 155-mgd surface water withdrawal.

The application of FOEA to simulated differences is identical, in principle, to its application to simulated output. The model is simply run twice, once for the base case and once for the change scenario. The outputs from these two runs are then differenced. The FOEA is then performed using the time series of differences in place of the time series of absolute values. In short, the function F(**X**) of Equation 3–3 is defined to be the difference between simulated output from the Base1995NN and Full2030PS scenarios.

In the plots below, differences are always shown for Base1995NN minus Full2030PN. Positive differences thus indicate a decrease in value from Base1995NN to Full2030PN. A decrease in water level from the Base1995NN to the Full2030PN scenario, then, is indicated by a positive difference. Because sea level rise is generally the predominant effect between the scenarios, water level differences shown are generally negative, indicating that water level has risen between the scenarios. Note also that an increase in salinity between scenarios, of particular concern in the lower St. Johns River, is indicated by a negative difference.

Water Level

The uncertainty for water level differences is insignificantly small in the tidal portion of the lower St. Johns River (Figure 3–57, Figure 3–59, and Figure 3–61). The absolute difference of water level in these areas is completely dominated by the 14-cm rise in sea level between the scenarios. The confidence limits are very small, indicating a low degree of uncertainty for the predicted water level changes at these locations. The dominant variable affecting the uncertainty of water level difference is depth (Figure 3–58, Figure 3–60, and Figure 3–62).

Uncertainty for water level differences in Lake George is also small, ±0.5 cm (Figure 3–63). Depth remains the dominant factor affecting uncertainty in the dry season, but tributary discharge increases in importance during the wet season (Figure 3–64).

Uncertainty of water level differences at DeLand is equivalent to Lake George during the dry season (Figure 3–65) and is dominated by uncertainty in depth (Figure 3–66). Uncertainty of water level differences increases during the wet season, however, and was ±2 cm during November and December 2001. During this period of greatest uncertainty in water level differences, the uncertainty is about equally attributed to depth and tributary discharge.

Uncertainty for water level differences in the wet season increases at Lake Monroe to ±4 cm (Figure 3–67), and is dominated by uncertainty in tributary discharge (Figure 3–68).

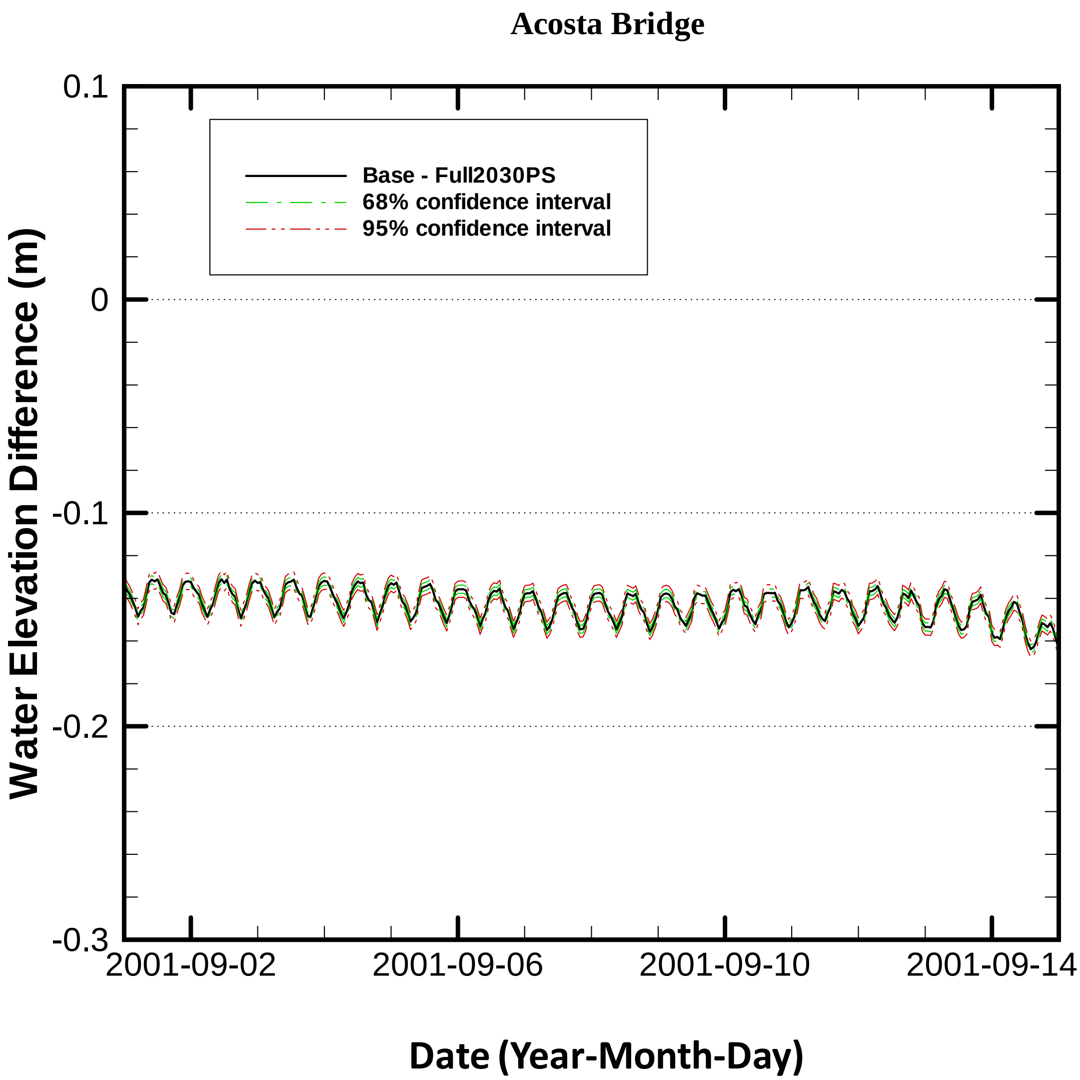

Figure 3–57. Simulated difference in hourly water level between the Base1995NN and Full2030PS scenarios at Acosta Bridge with confidence intervals for the year 2001.

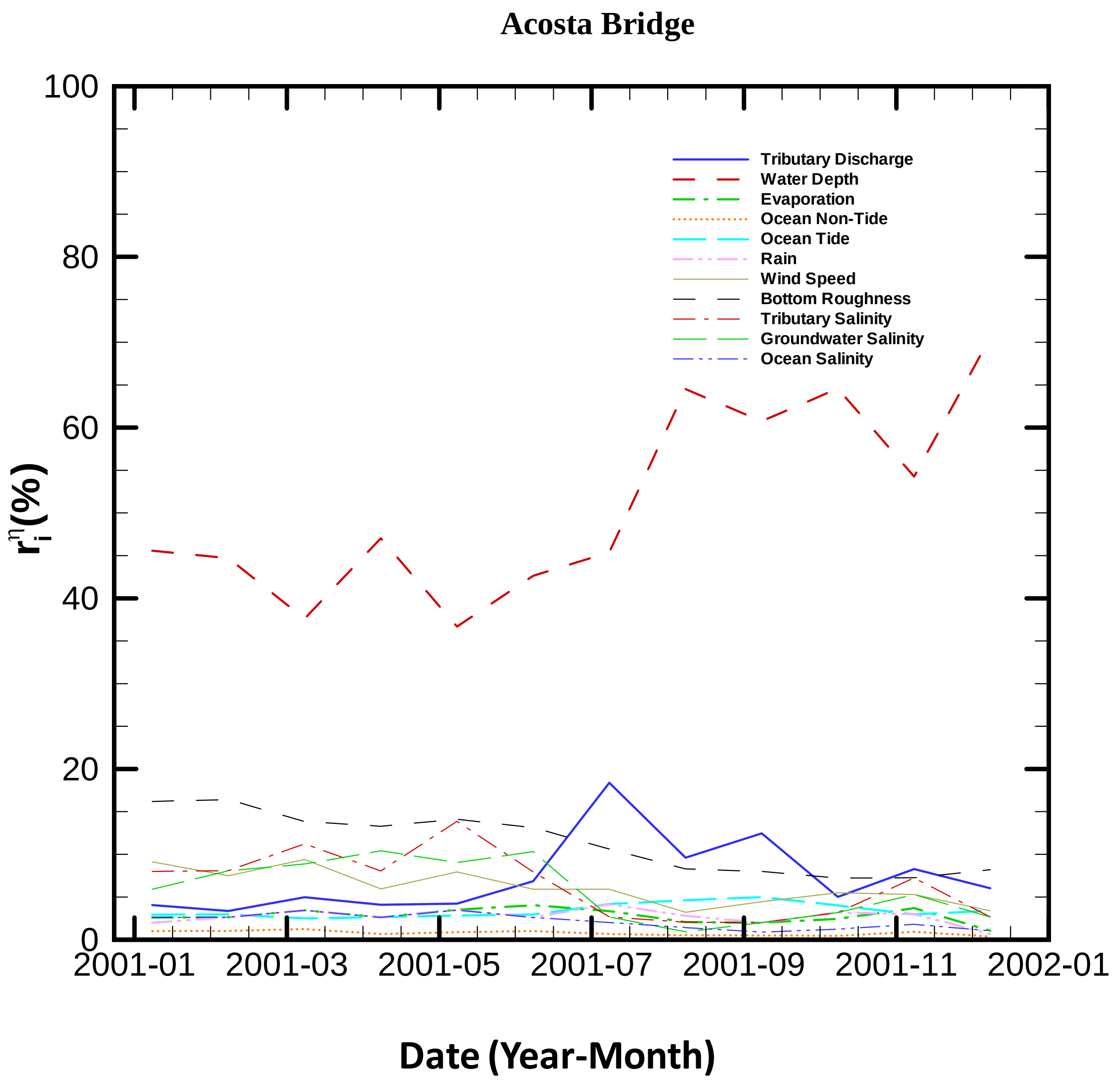

Figure 3–58. Percent contribution of input variables to the total uncertainty of predicted water level change (r^η) at Acosta Bridge.

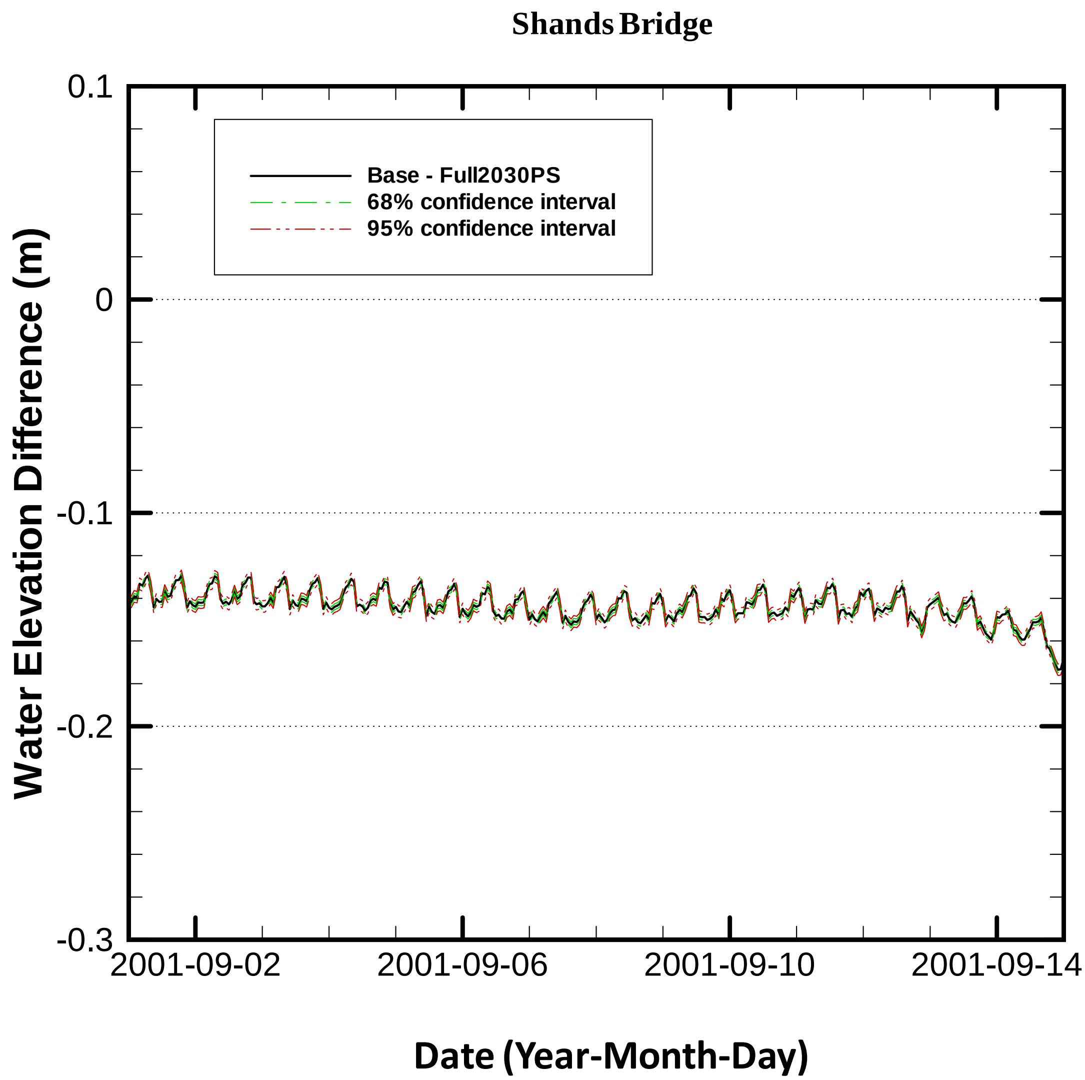

Figure 3–59. Simulated difference in hourly water level between the Base1995NN and Full2030PS scenarios at Shands Bridge, with confidence intervals for the year 2001.

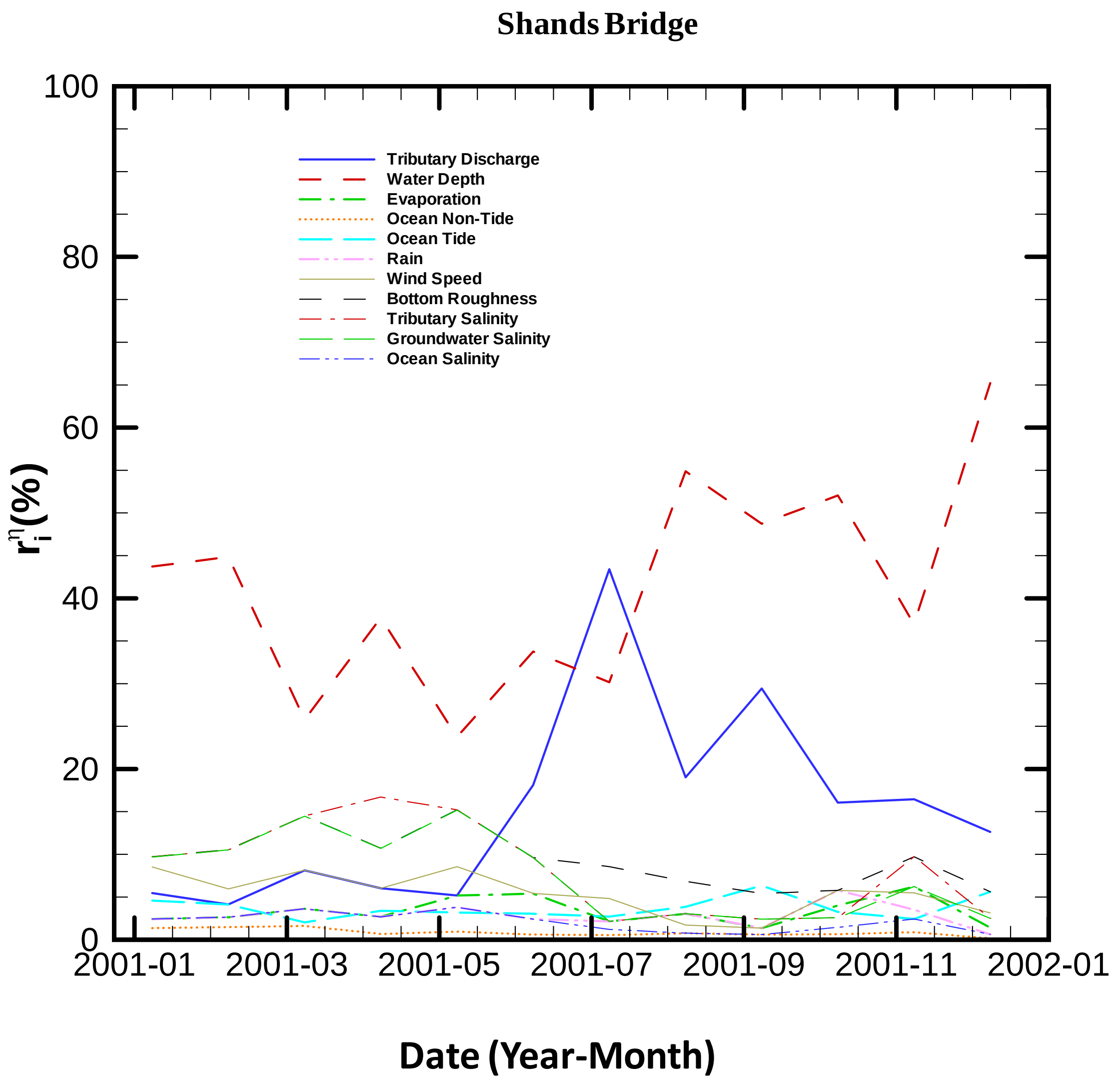

Figure 3–60. Percent contribution of input variables to the total uncertainty of predicted water level change (r^{η}) at Shands Bridge.

Figure 3–61. Simulated difference in hourly water level between the Base1995NN and Full2030PS scenarios at Racy Point, with confidence intervals for the year 2001.

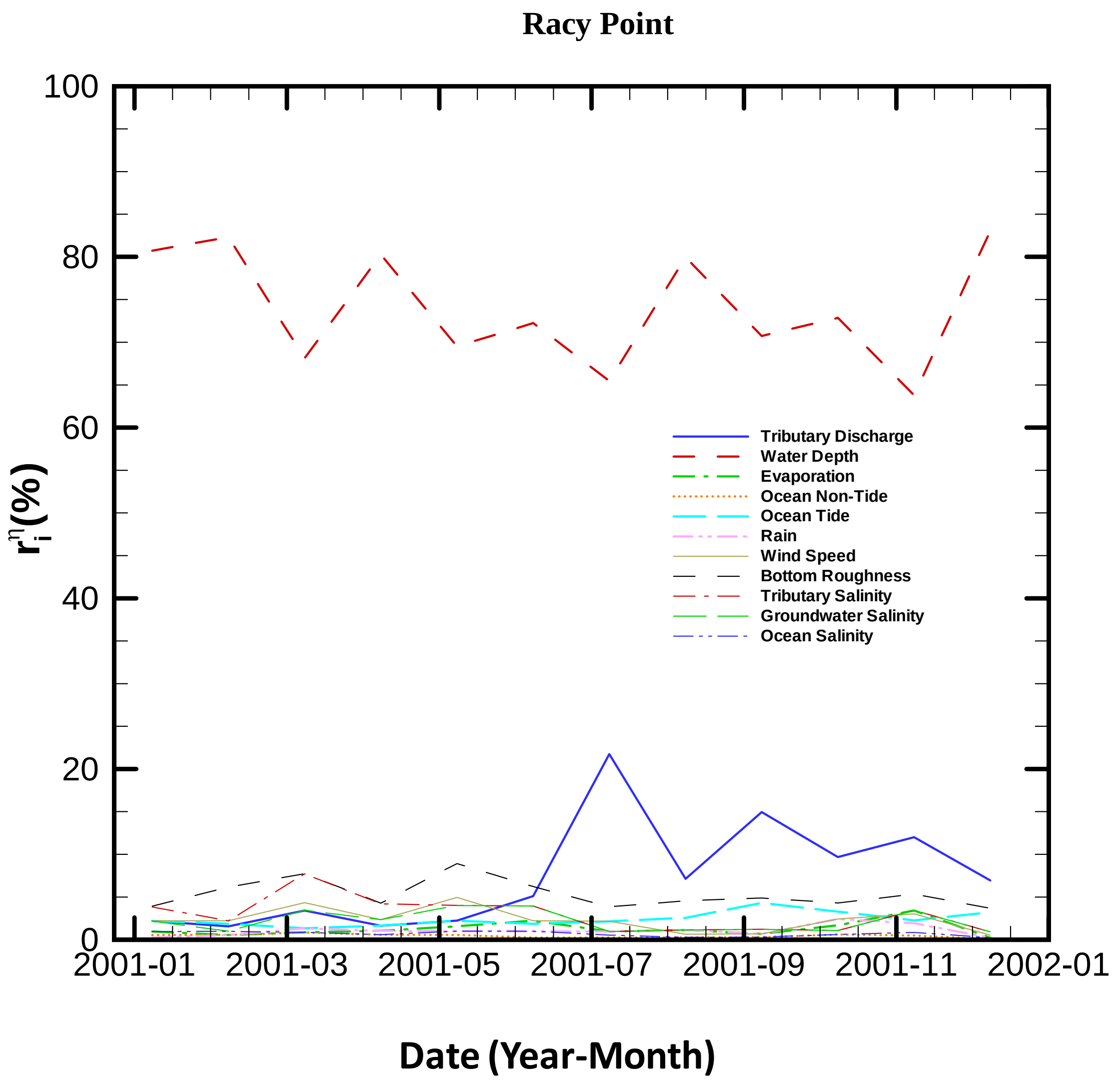

Figure 3–62. Percent contribution of input variables to the total uncertainty of predicted water level change (r^η) at Racy Point.

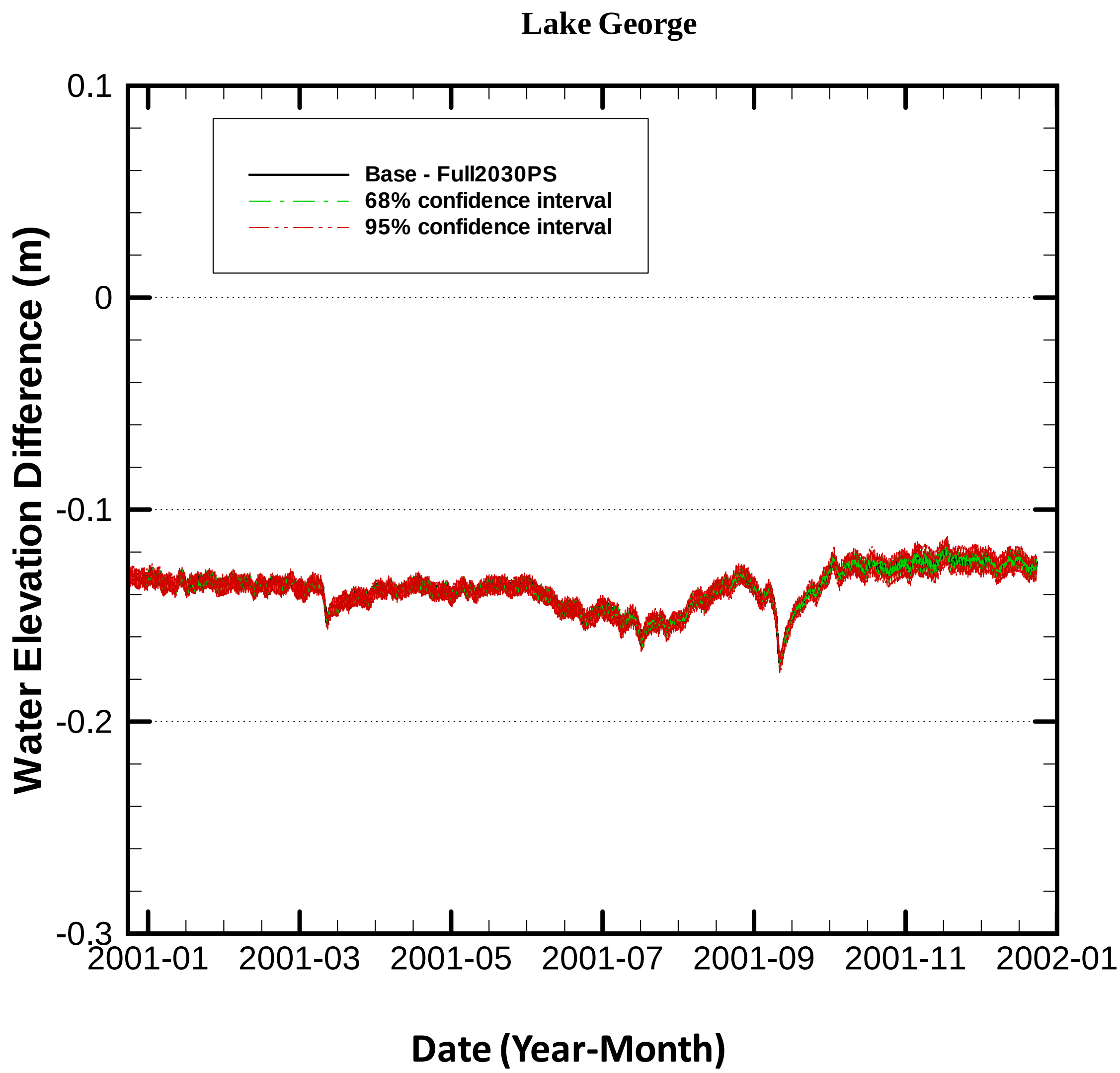

Figure 3–63. Simulated difference in hourly water level between the Base1995NN and Full2030PS scenarios at Lake George with confidence intervals for the year 2001.

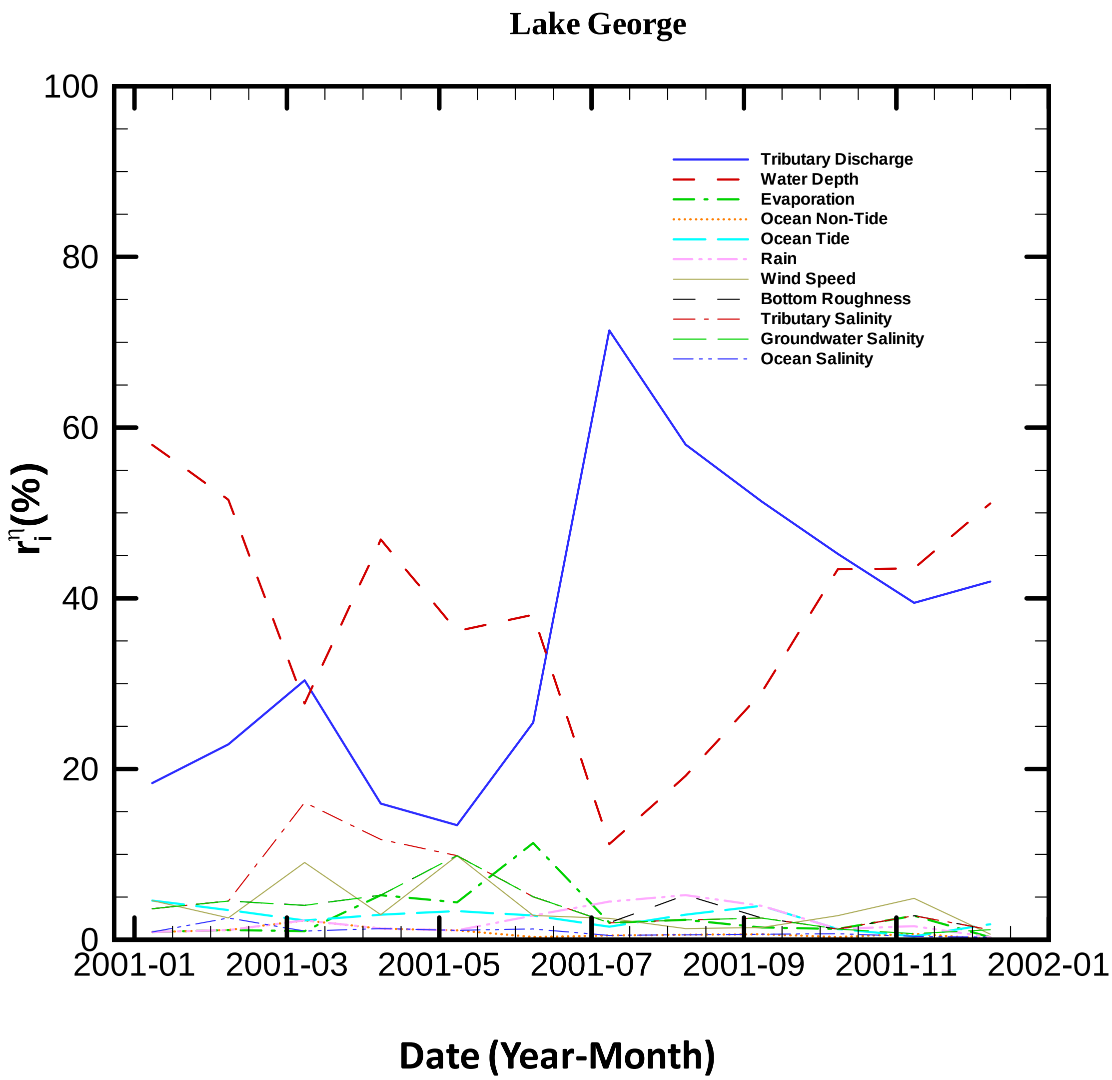

Figure 3–64. Percent contribution of input variables to the total uncertainty of predicted water level (r^η) at Lake George.

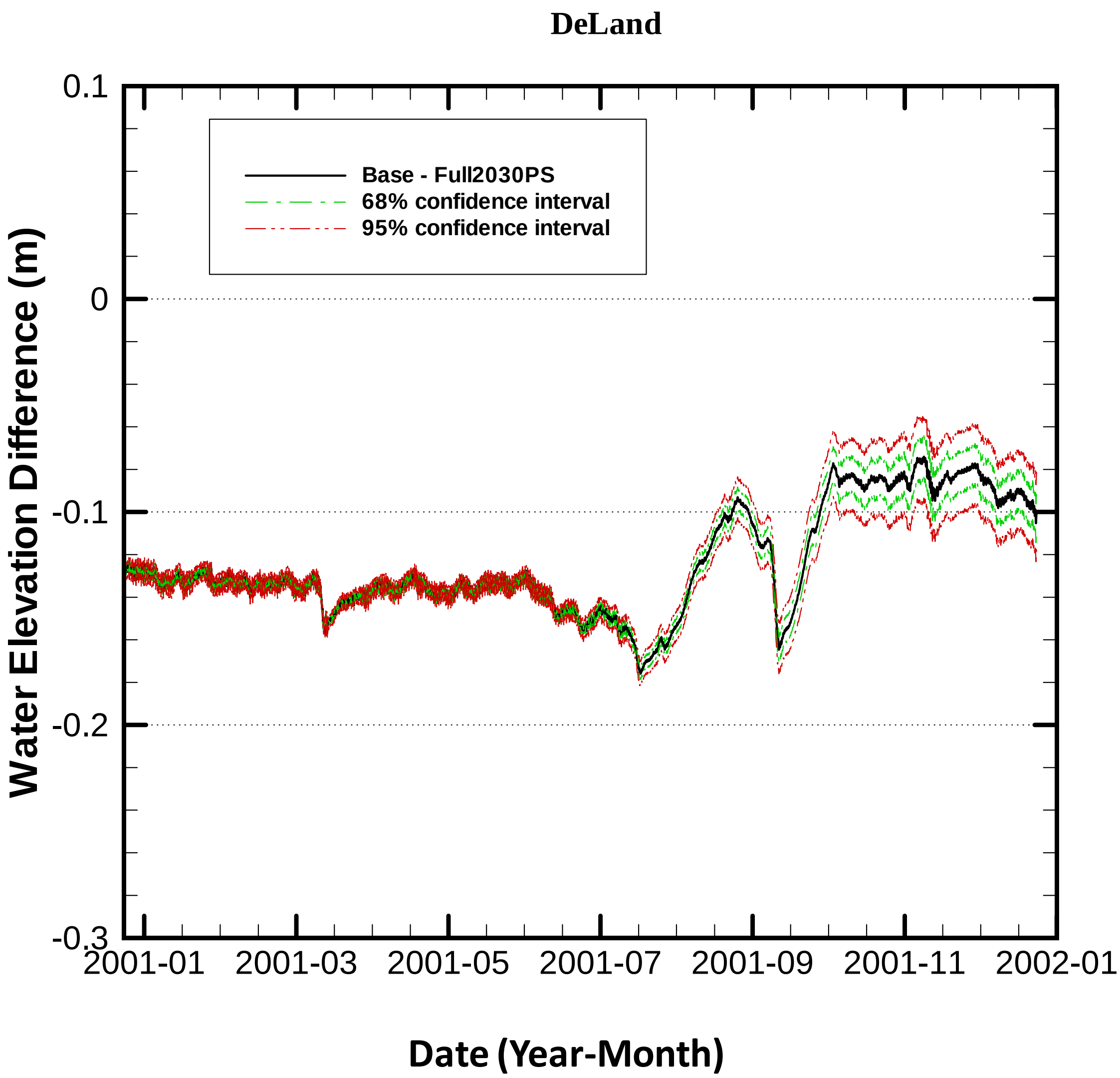

Figure 3–65. Simulated difference in hourly water level between the Base1995NN and Full2030PS scenarios at DeLand, with confidence intervals for the year 2001.

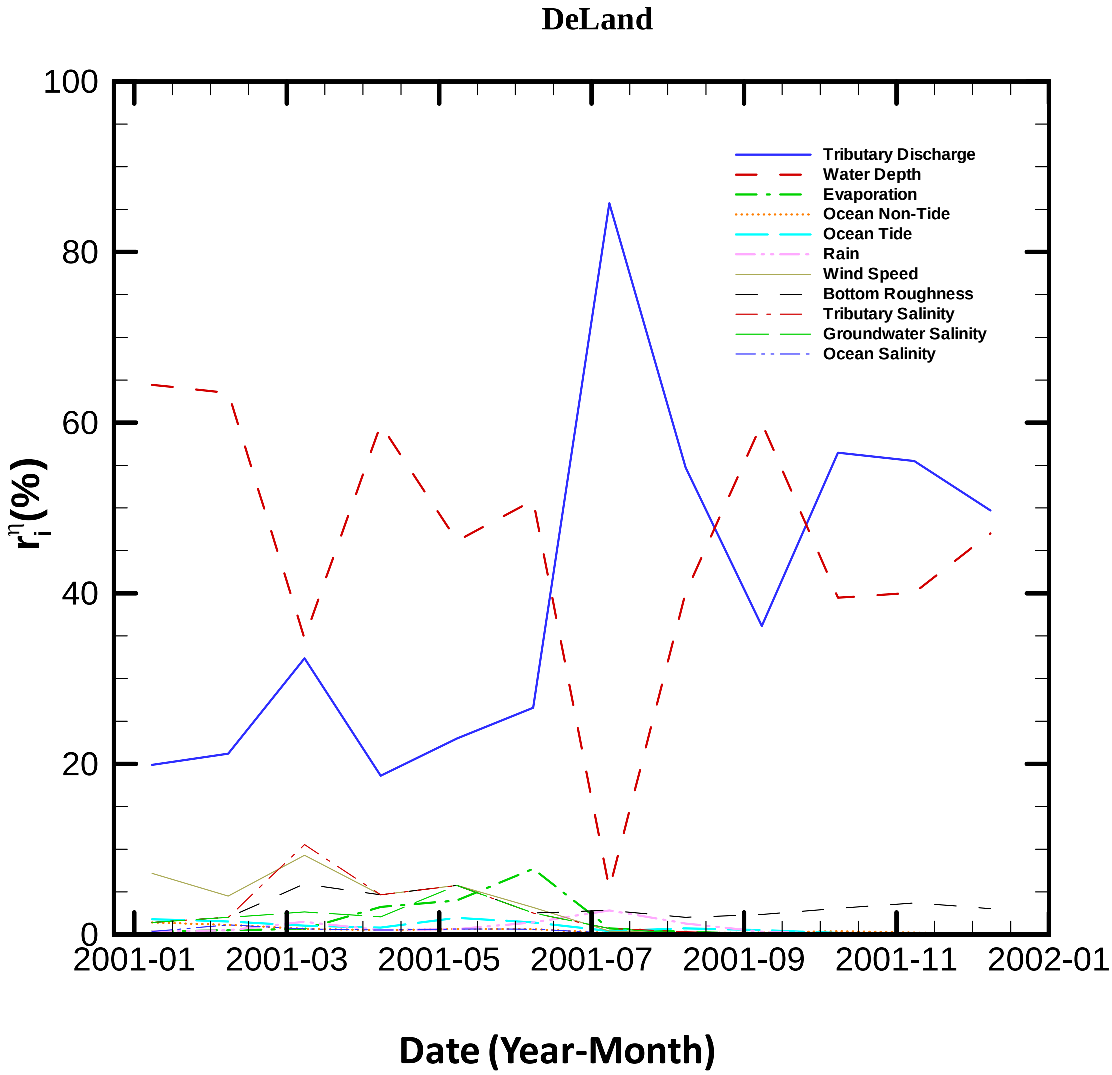

Figure 3–66. Percent contribution of input variables to the total uncertainty of predicted water level (r^η) at DeLand.

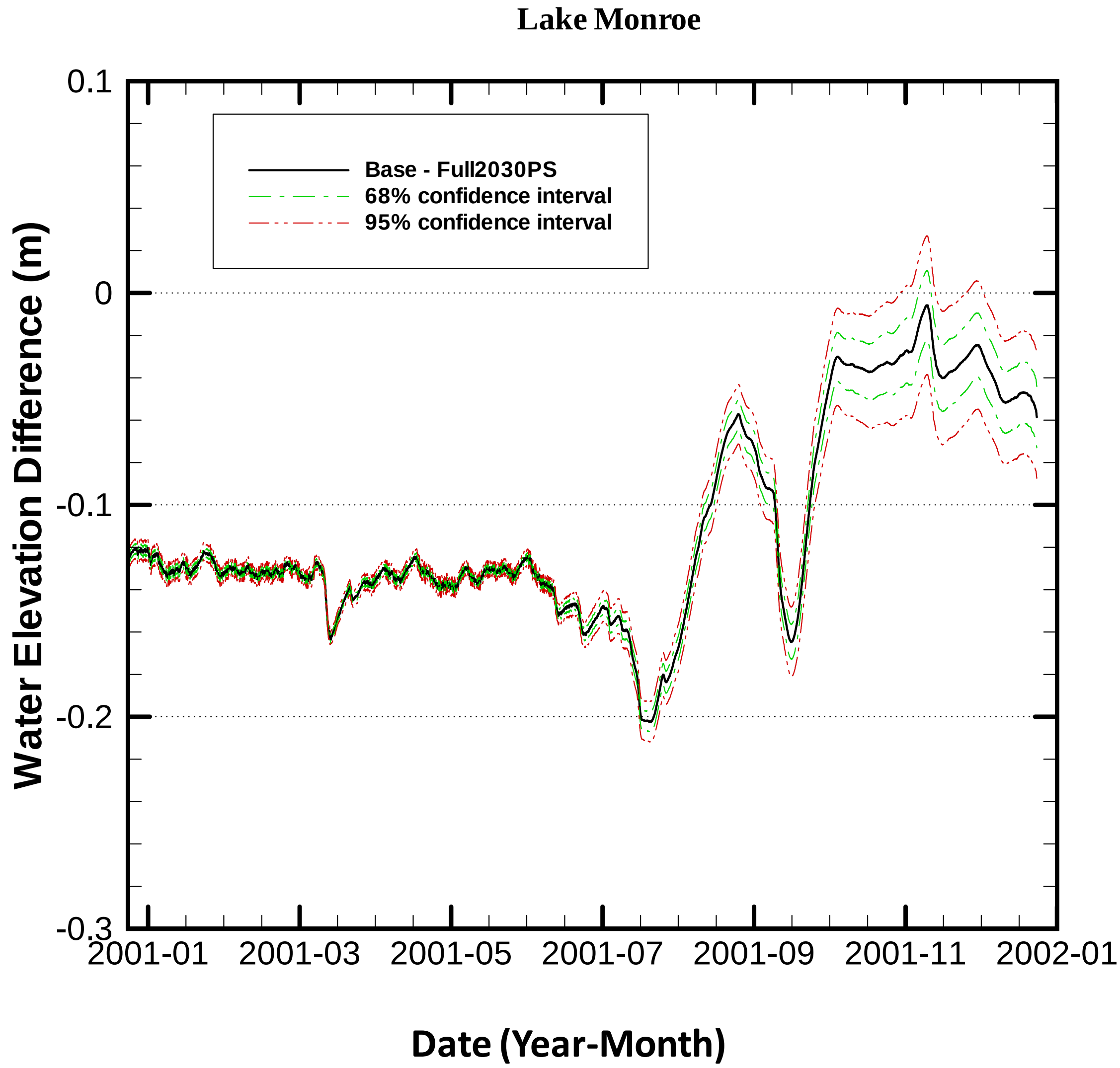

Figure 3–67. Simulated difference in hourly water level between the Base1995NN and Full2030PS scenarios at Lake Monroe with confidence intervals for the year 2001.

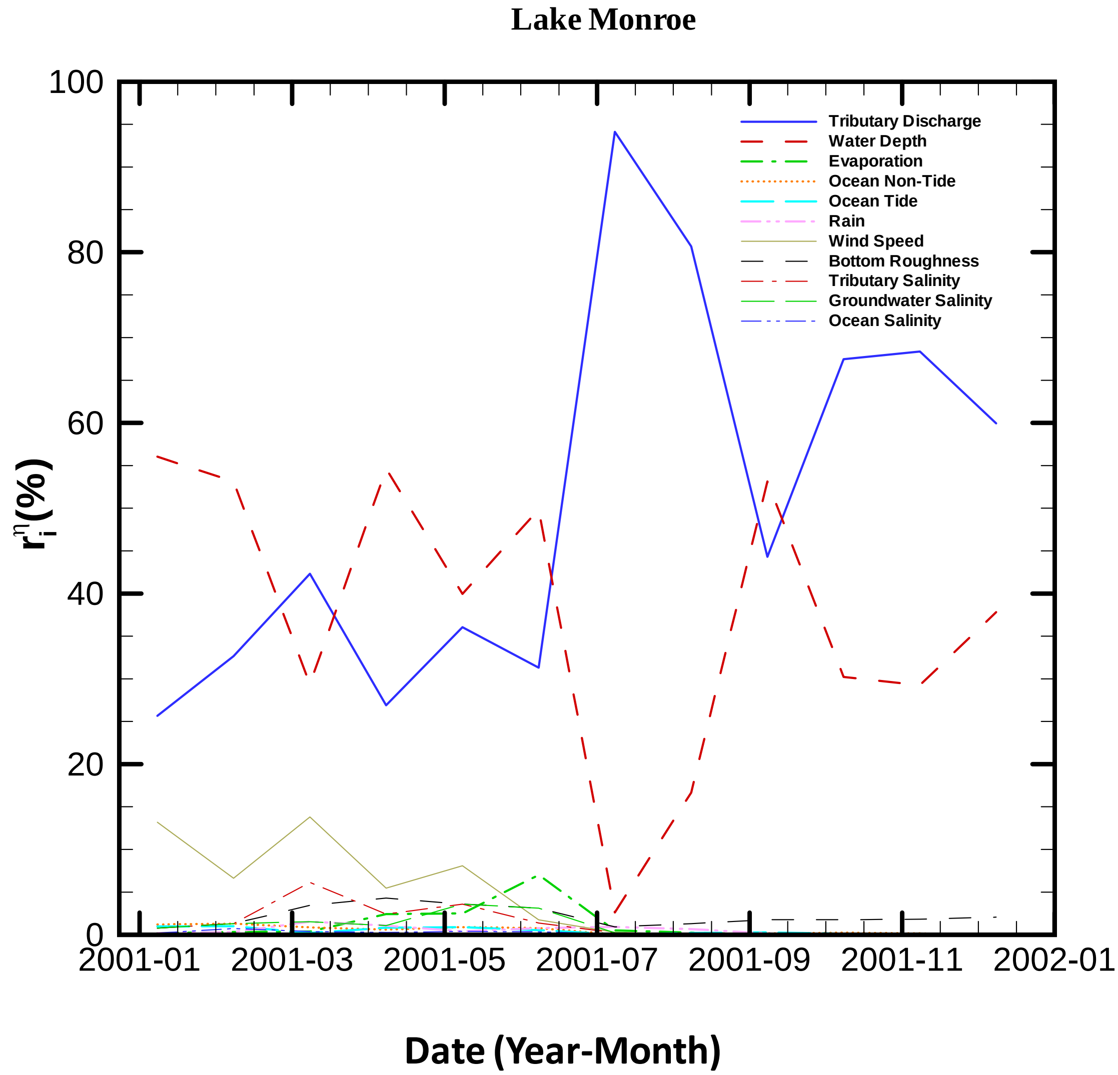

Figure 3–68. Percent contribution of input variables to the total uncertainty of predicted water level change (r^{η}) at Lake Monroe.

Current Speed

The uncertainty of simulated differences of current speed to uncertainty in model input is very low throughout the model domain. Only two stations are shown here, Shands Bridge (in the tidal portion of the river) and DeLand (in the non-tidal reach). Current speed differences at both locations are less than 2 cm s^{-1} and within a few mm s^{-1} for the 95% confidence interval (Figure 3–69 and Figure 3–71). The uncertainty in current speed differences is mostly attributed to uncertainty in depth at Shands Bridge (Figure 3–70) in all seasons and at DeLand in the dry season (Figure 3–71). Uncertainty at DeLand in the wet season is mostly attributed to uncertainty in river discharge.

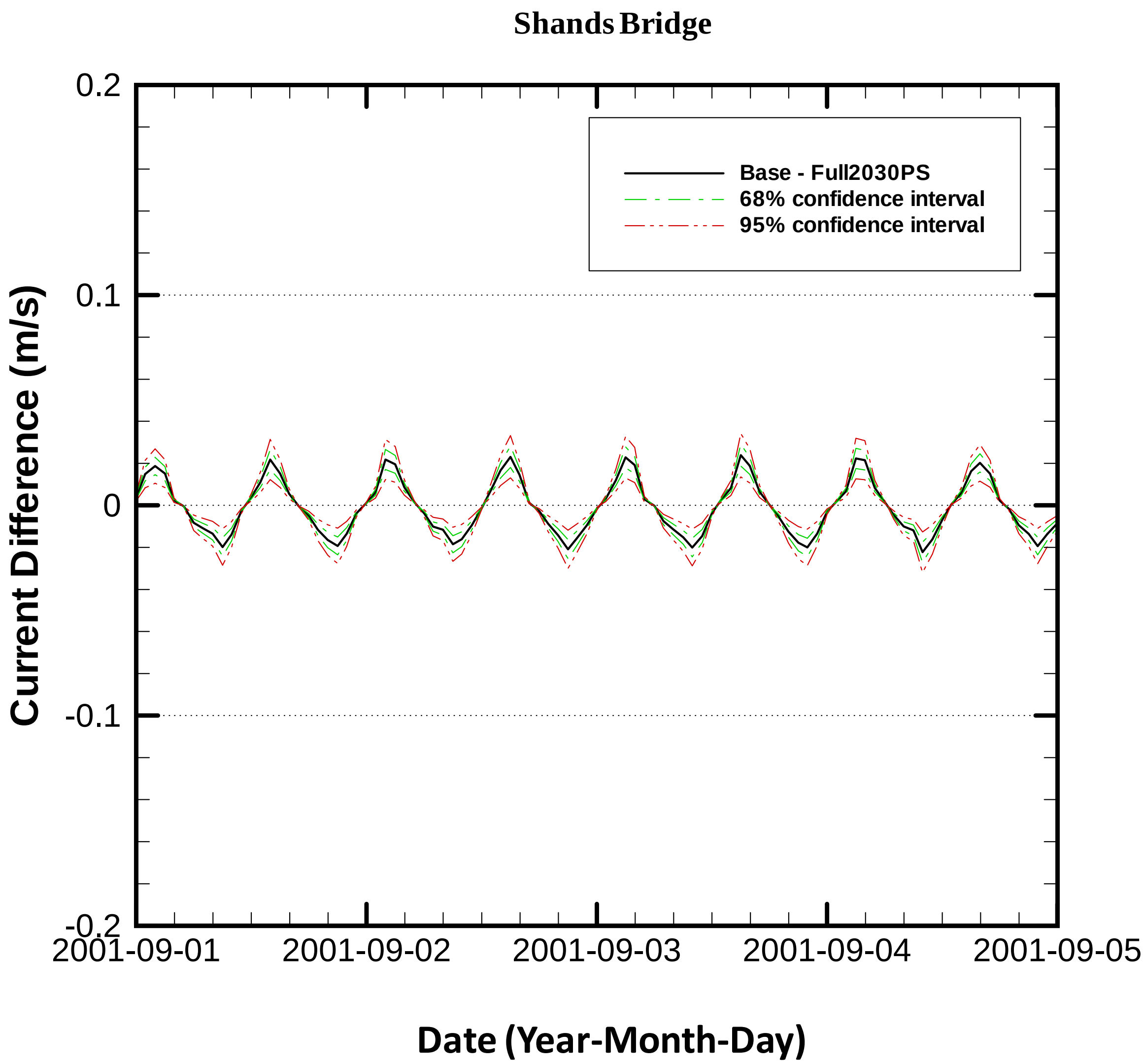

Figure 3–69. Simulated difference in hourly current speed between the Base1995NN and Full2030PS scenarios at Shands Bridge with confidence intervals for the year 2001.

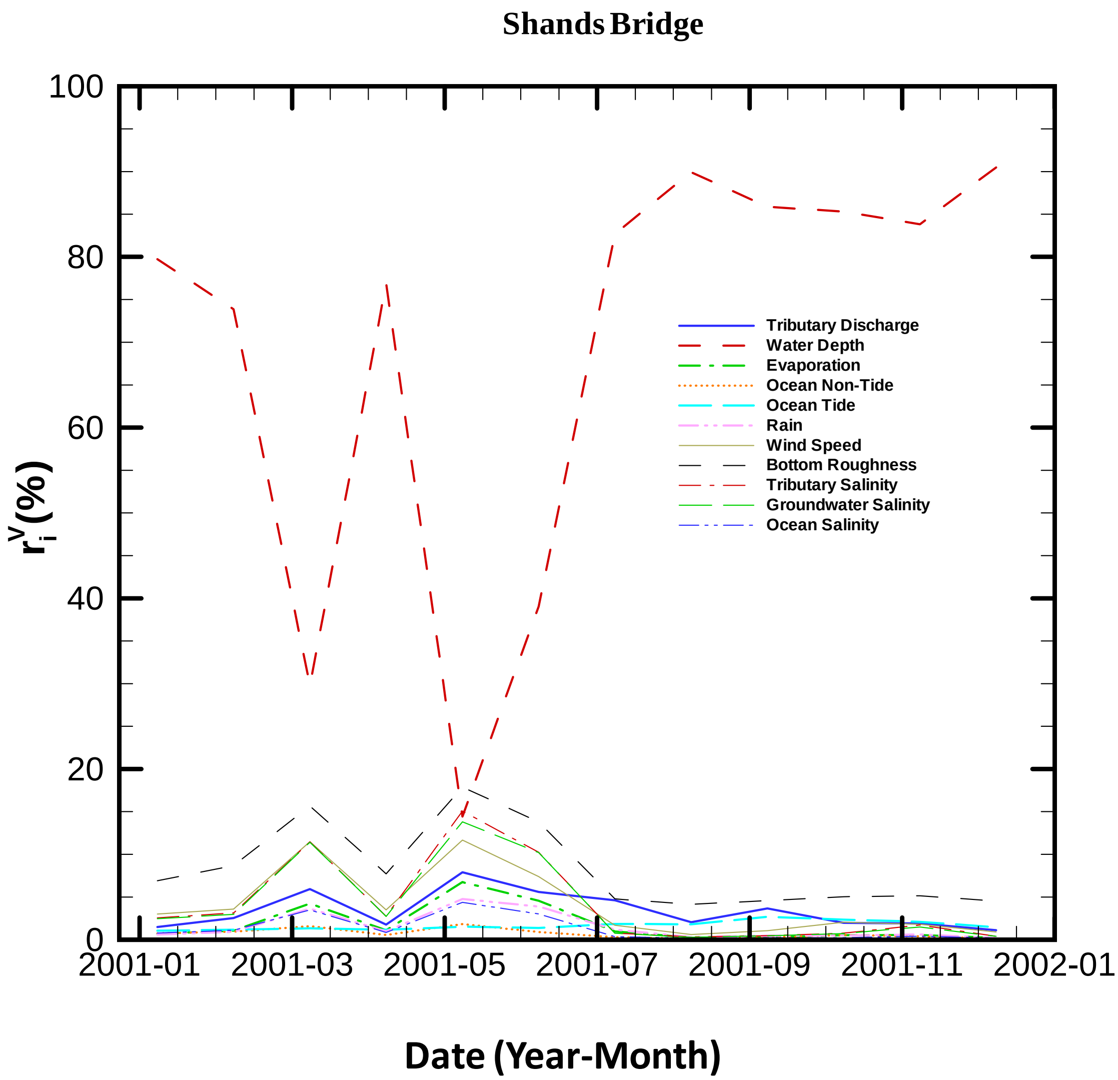

Figure 3–70. Percent contribution of input variables to the total uncertainty of predicted current speed (r^V) at Shands Bridge.

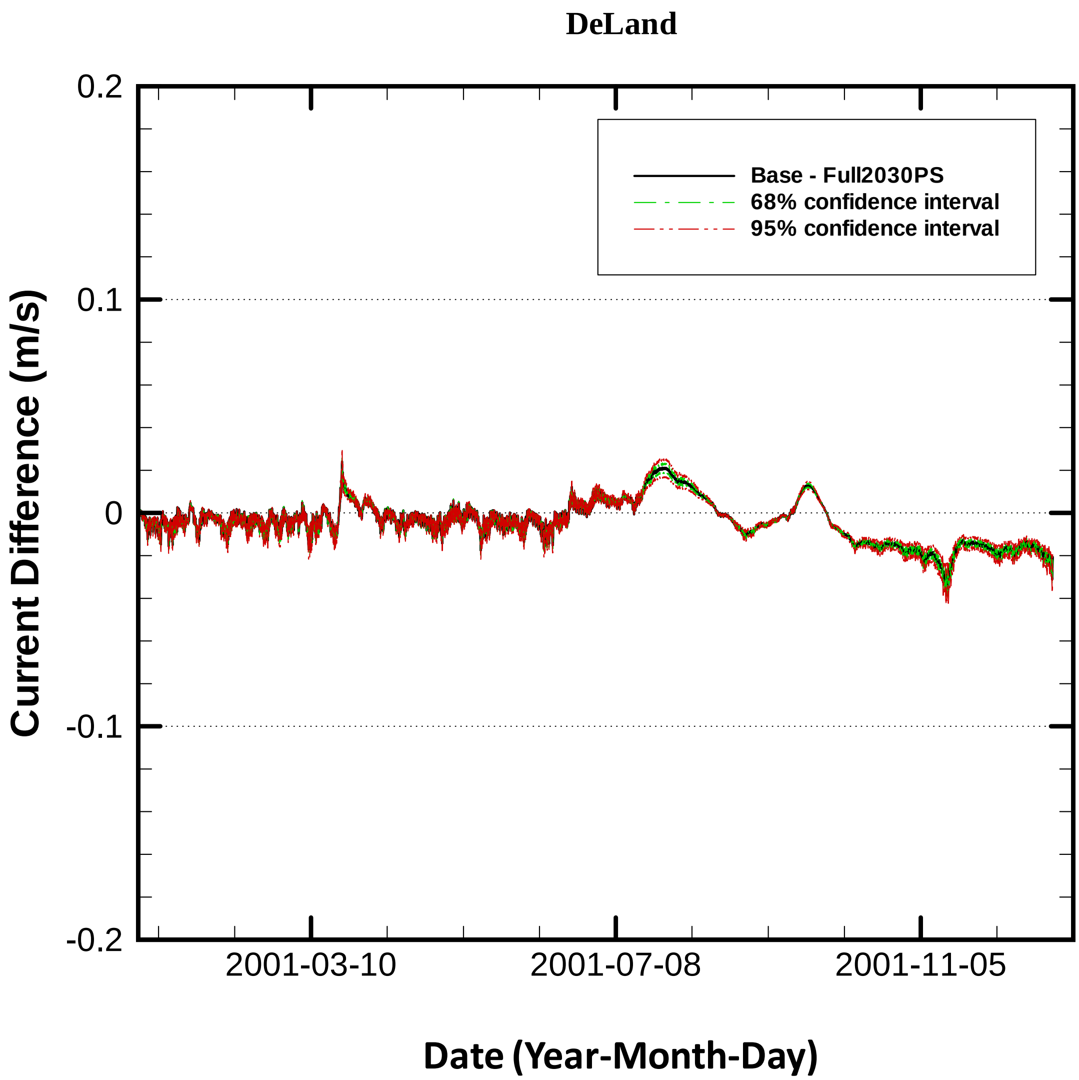

Figure 3–71. Simulated difference in hourly current speed between the Base1995NN and Full2030PS scenarios at DeLand with confidence intervals for the year 2001.

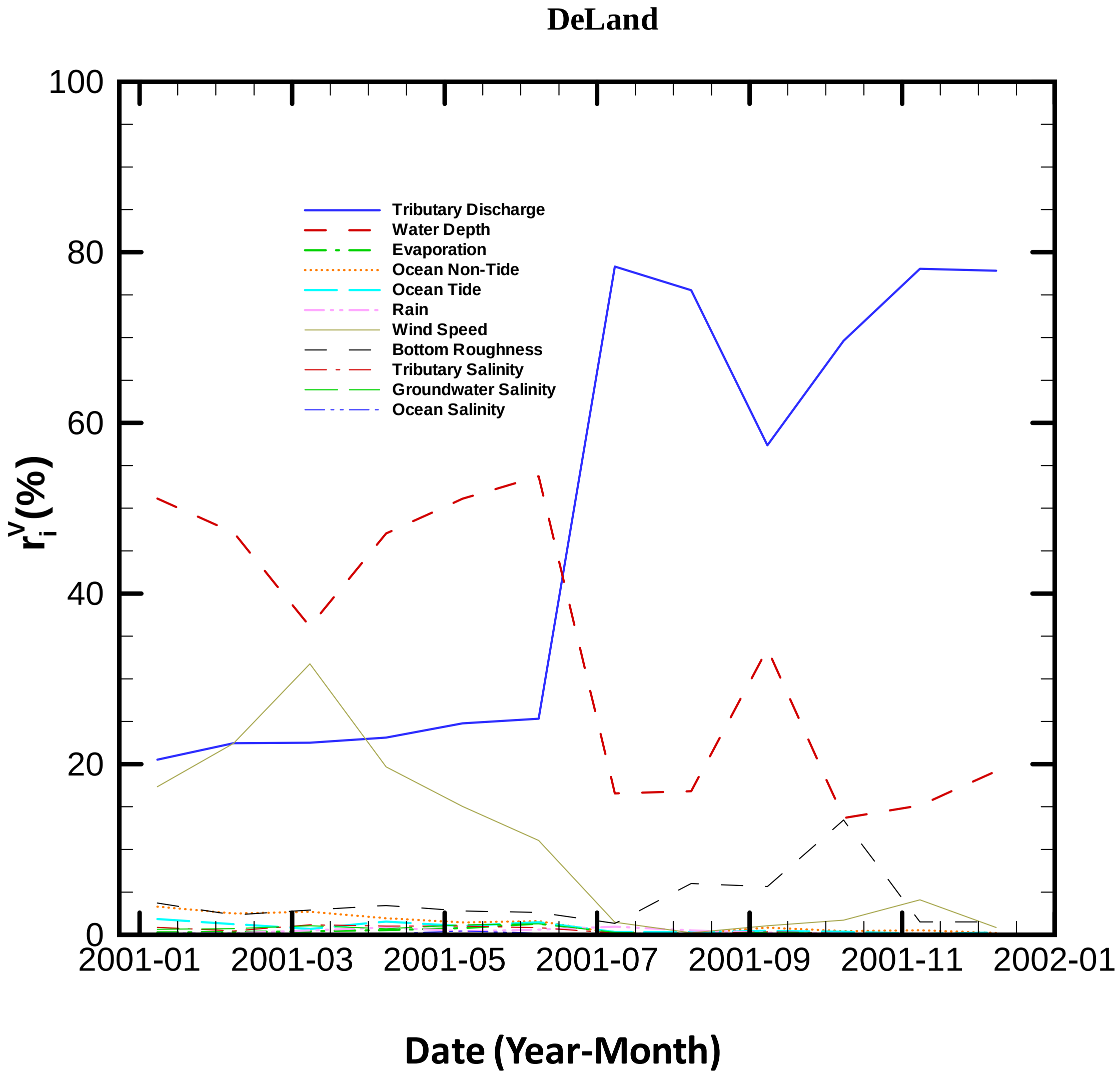

Figure 3–72. Percent contribution of input variables to the total uncertainty of predicted current speed change (r^V) at DeLand.

Salinity

Uncertainty in prediction of salinity differences from the river entrance to Shands Bridge in the lower St. Johns River was greater than for prediction of either water level or current speed and is likely indicative of difficulties inherent in numerical prediction of salinity near steep gradients and salinity fronts. At Acosta Bridge, the uncertainty of the prediction of salinity differences was generally less than 0.25 PSS78 but ranged as high as 1.5 PSS78 for the 95% confidence interval. The greatest salinity difference at this location occurred during July, when salinity was about 1.5 PSS78 lower for Full2030PS compared with the Base1995NN (Figure 3–73). During July, the 95% confidence interval was 0 to 3 PSS78. At Shands Bridge, near the upstream extent of ocean salinity intrusions, the confidence in prediction of salinity differences is high, and the 95% confidence level for salinity differences is generally less than 0.25 PSS78 (Figure 3–75).

During dry periods, the uncertainty of salinity differences between Acosta Bridge and Shands Bridge is primarily attributable to uncertainty in depth (Figure 3–74 and Figure 3–76). During wet periods, uncertainty in tributary discharge becomes of equal importance at Acosta Bridge, and is the dominant factor at Shands Bridge.

In the freshwater sections of the river, upstream of Shands Bridge, predicted salinity differences are small and uncertainty is low (Figure 3–77, Figure 3–79, Figure 3–81, and Figure 3–83). Uncertainty of predicted salinity differences is primarily caused by uncertainty in depth and tributary discharge (Figure 3–78, Figure 3–80, Figure 3–82, and Figure 3–84).

The greatest uncertainty (although small) for predicted salinity differences occurs at DeLand during the dry season, where salinity is influenced by reverse flows.

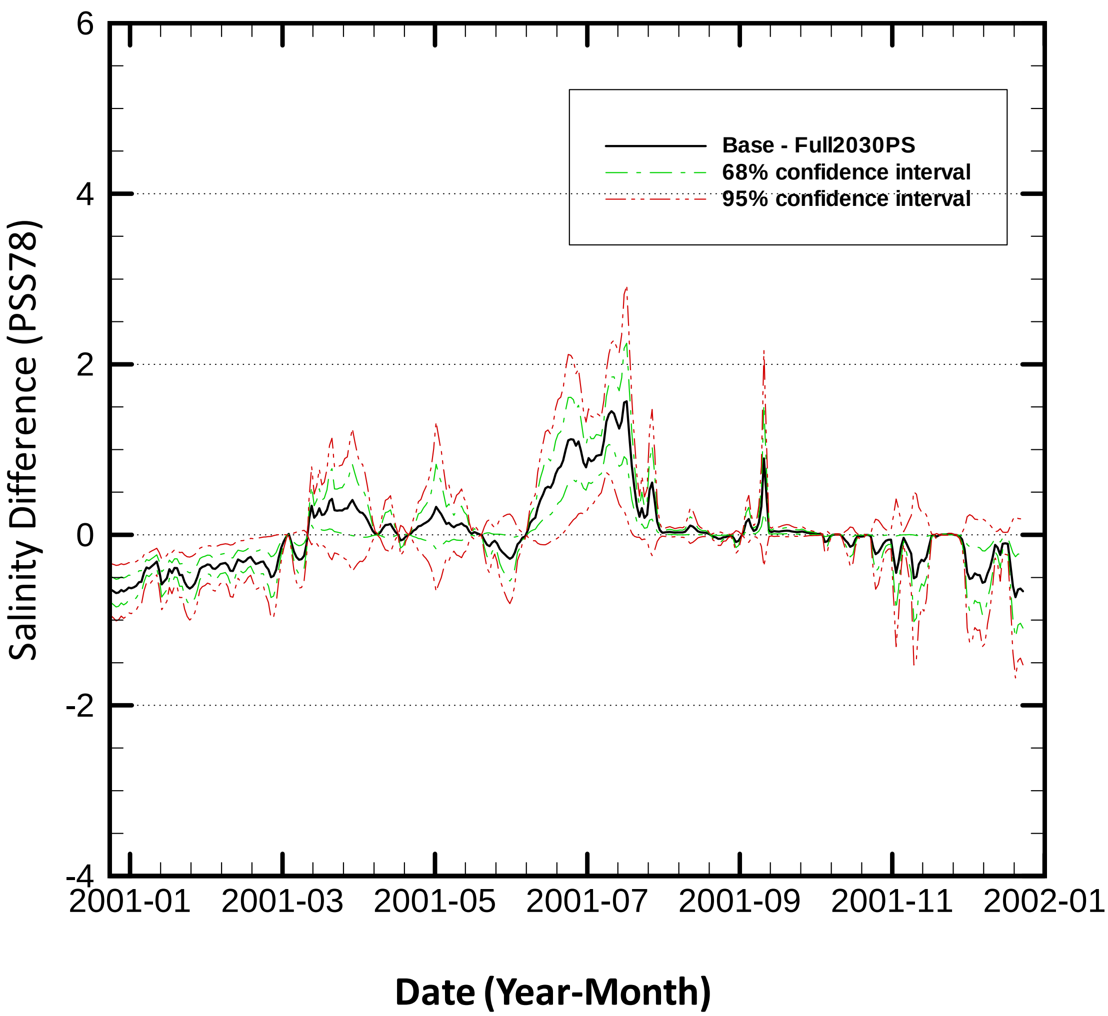

Figure 3–73. Simulated difference in hourly salinity between the Base1995NN and Full2030PS scenarios at Acosta Bridge with confidence intervals for the year 2001.

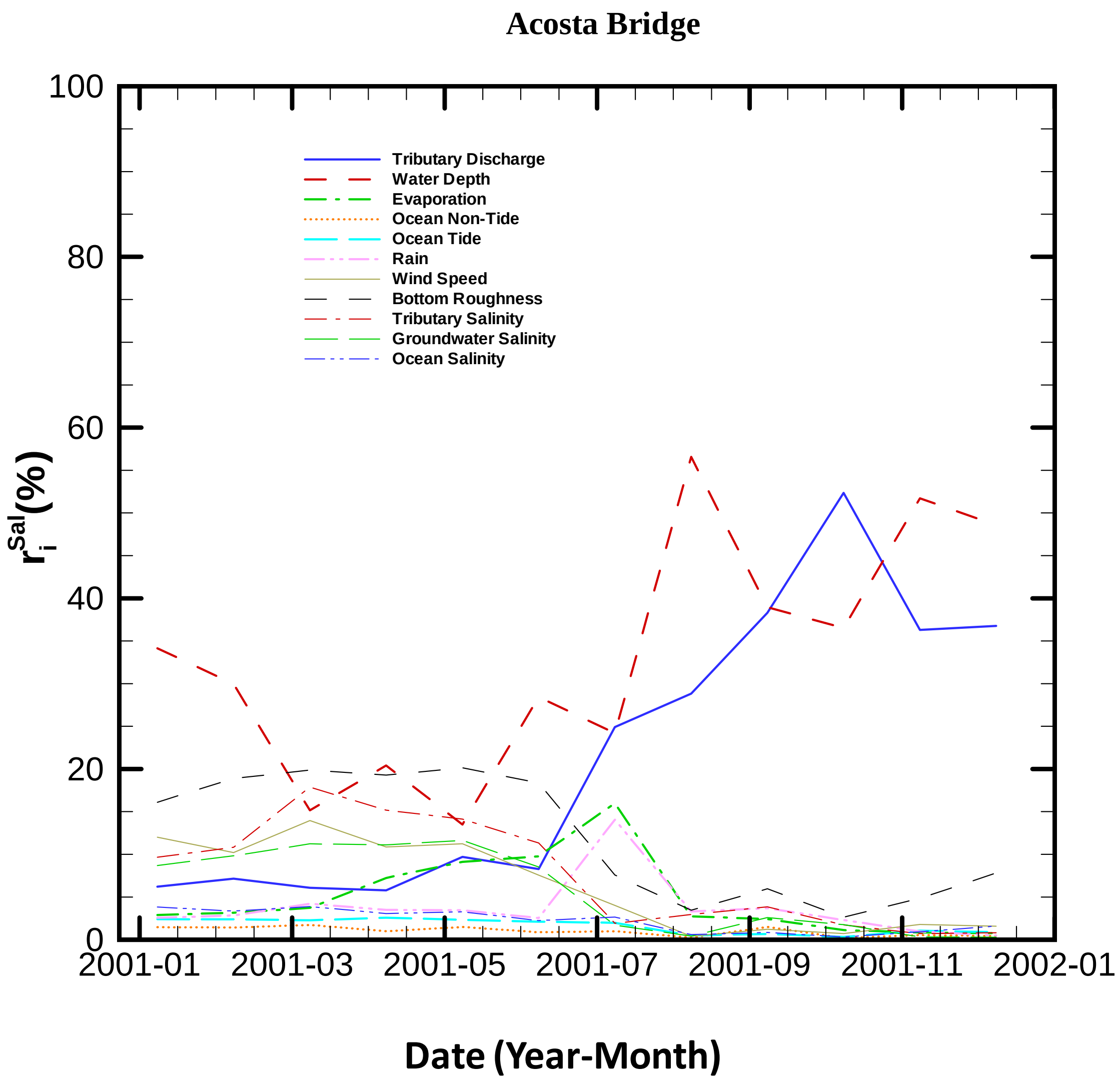

Figure 3–74. Percent contribution of input variables to the total uncertainty of predicted salinity change (r^{Sal}) at Acosta Bridge.

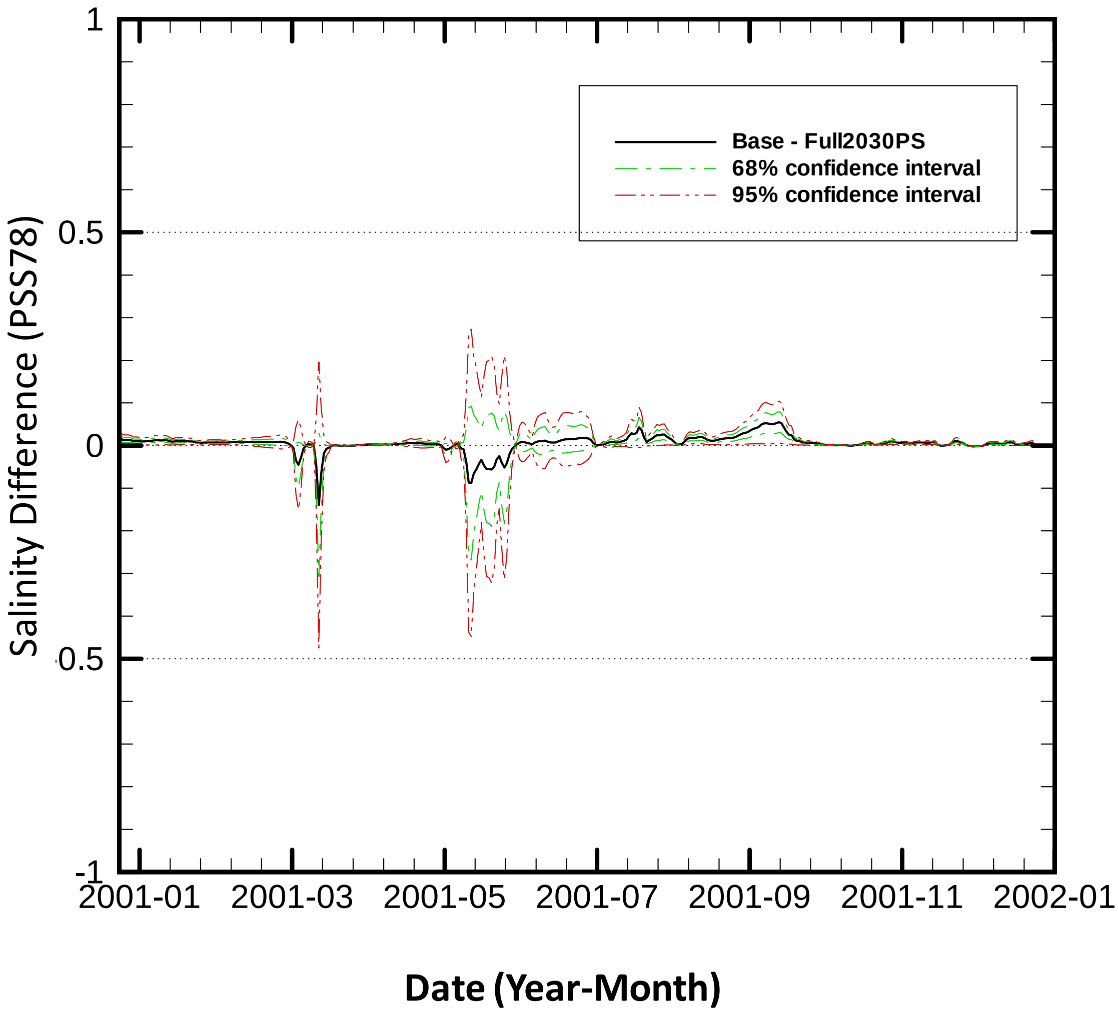

Figure 3–75. Simulated difference in hourly salinity between the Base1995NN and Full2030PS scenarios at Shands Bridge, with confidence intervals for the year 2001.

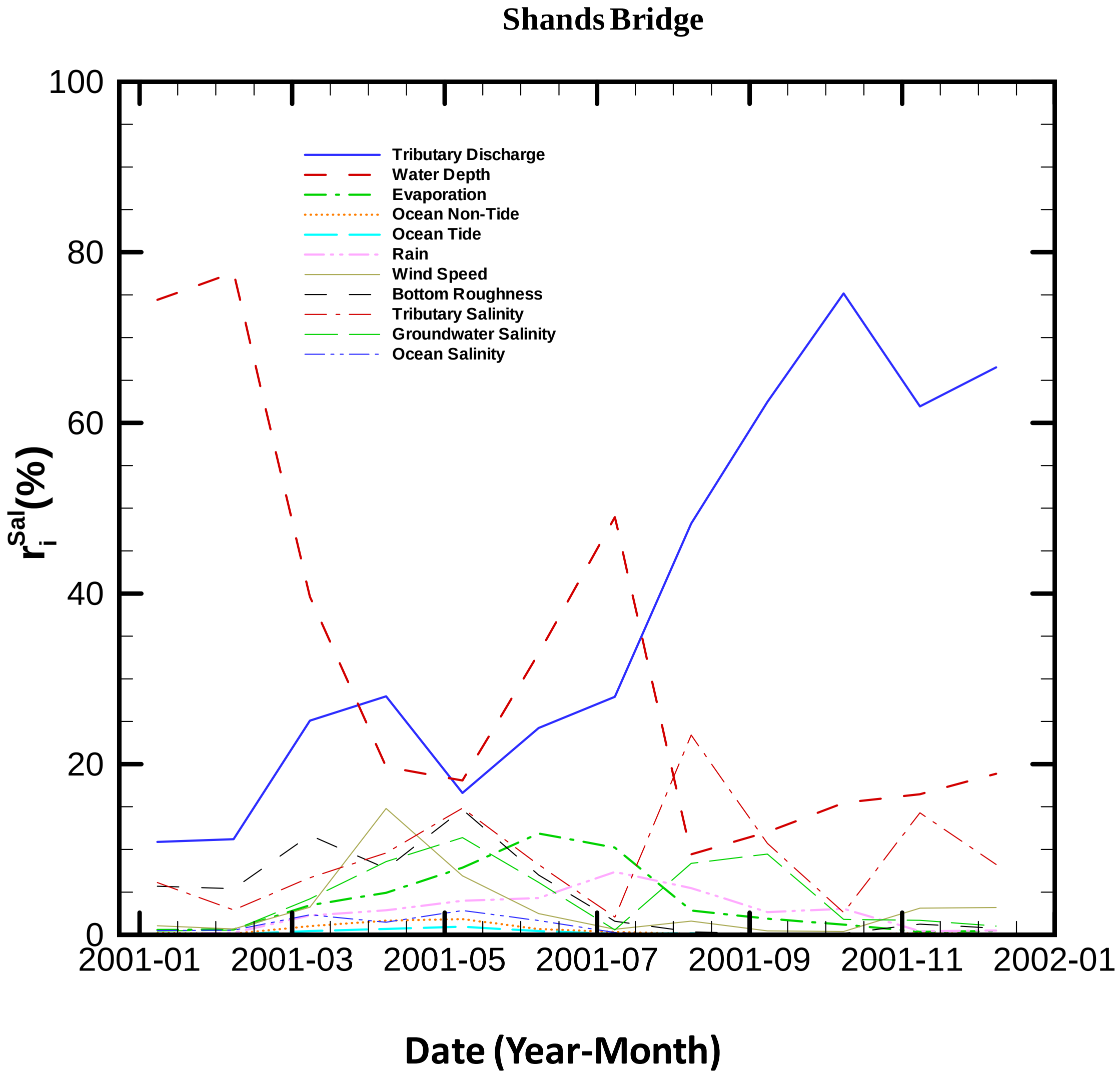

Figure 3–76. Percent contribution of input variables to the total uncertainty of predicted salinity change (r^{Sal}) at Shands Bridge.

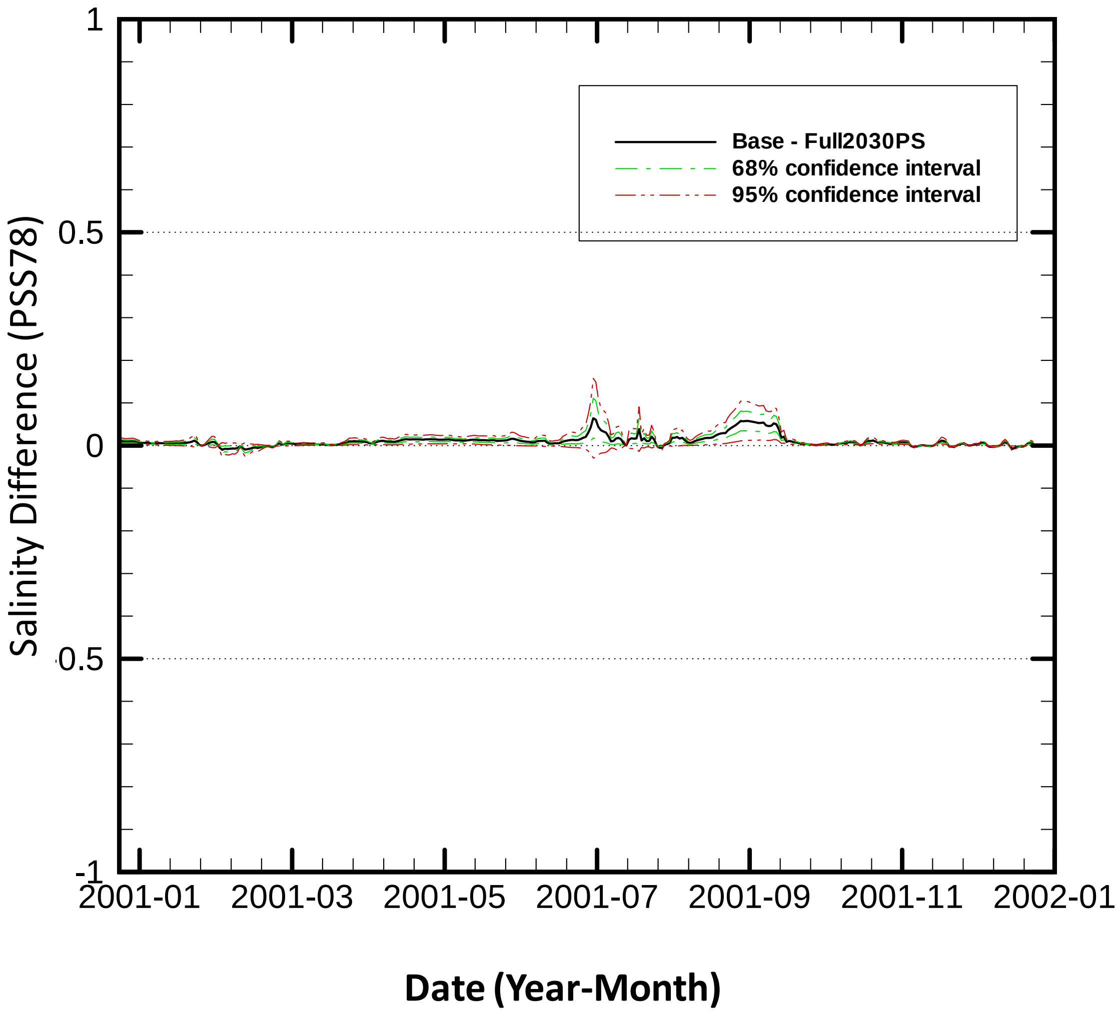

Figure 3–77. Simulated difference in hourly salinity between the Base1995NN and Full2030PS scenarios at Racy Point, with confidence intervals for the year 2001.

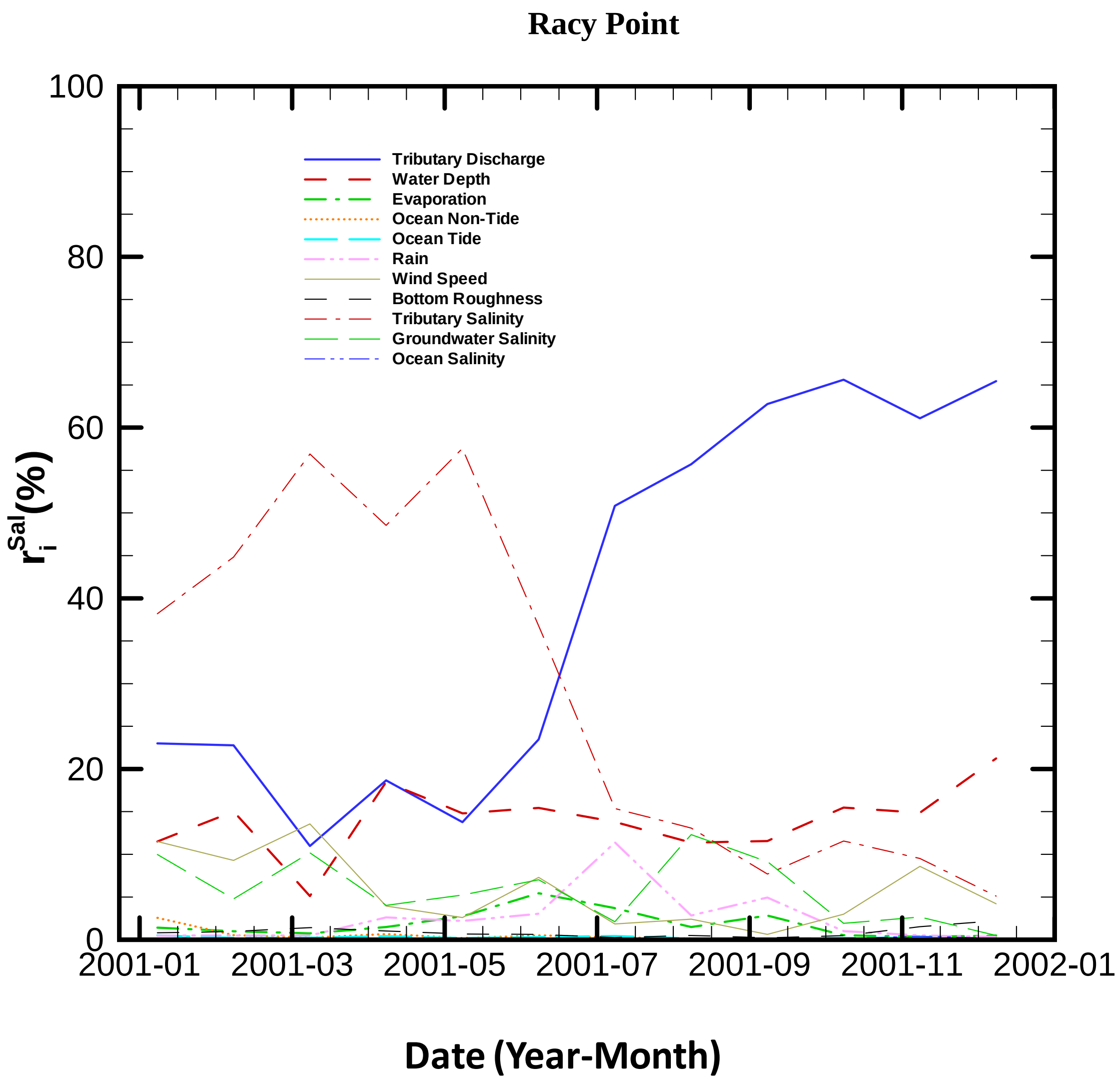

Figure 3–78. Percent contribution of input variables to the total uncertainty of predicted salinity change (r^{Sal}) at Racy Point.

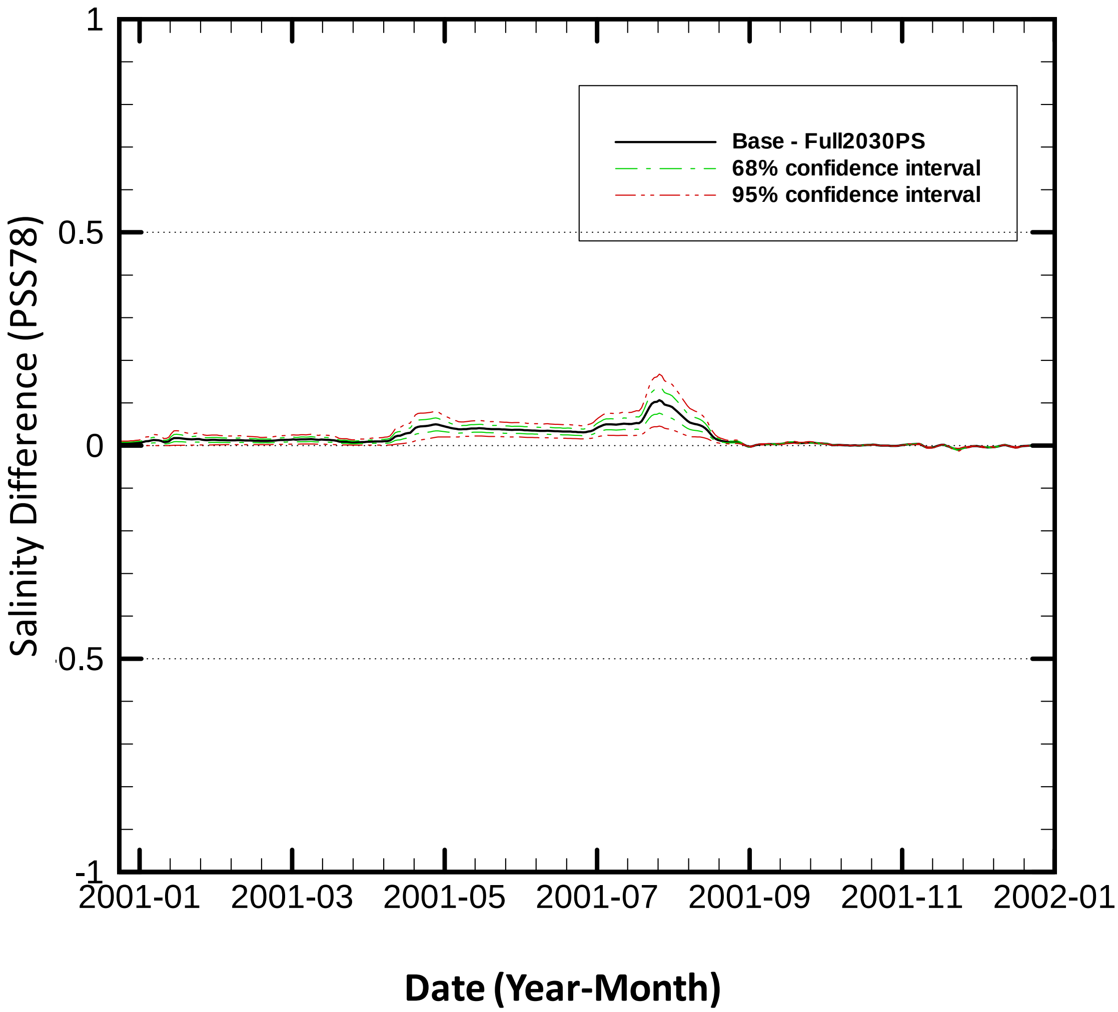

Figure 3–79. Simulated difference in hourly salinity between the Base1995NN and Full2030PS scenarios at Lake George, with confidence intervals for the year 2001.

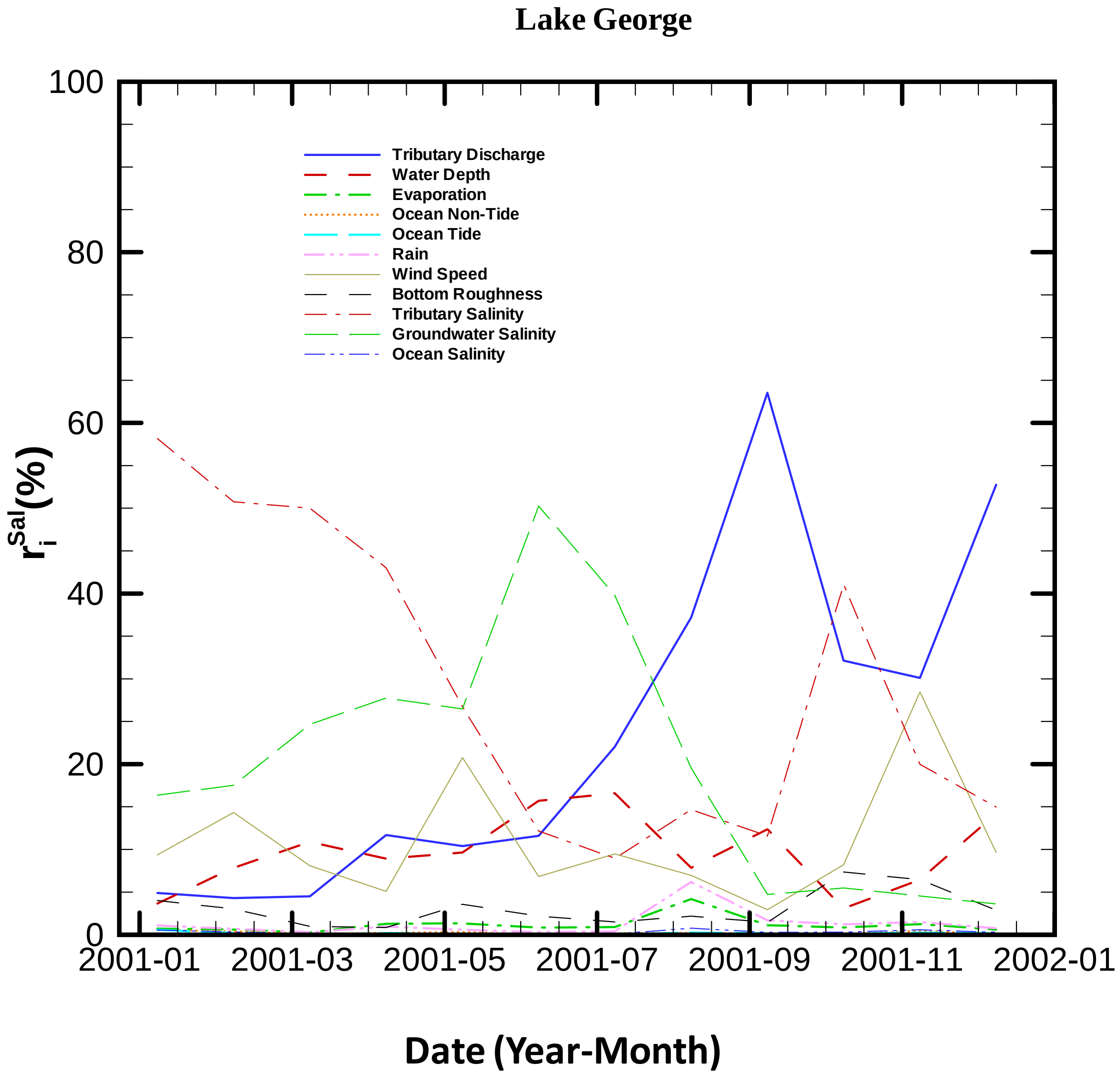

Figure 3–80. Percent contribution of input variables to the total uncertainty of predicted salinity change (r^{Sal}) at Lake George.

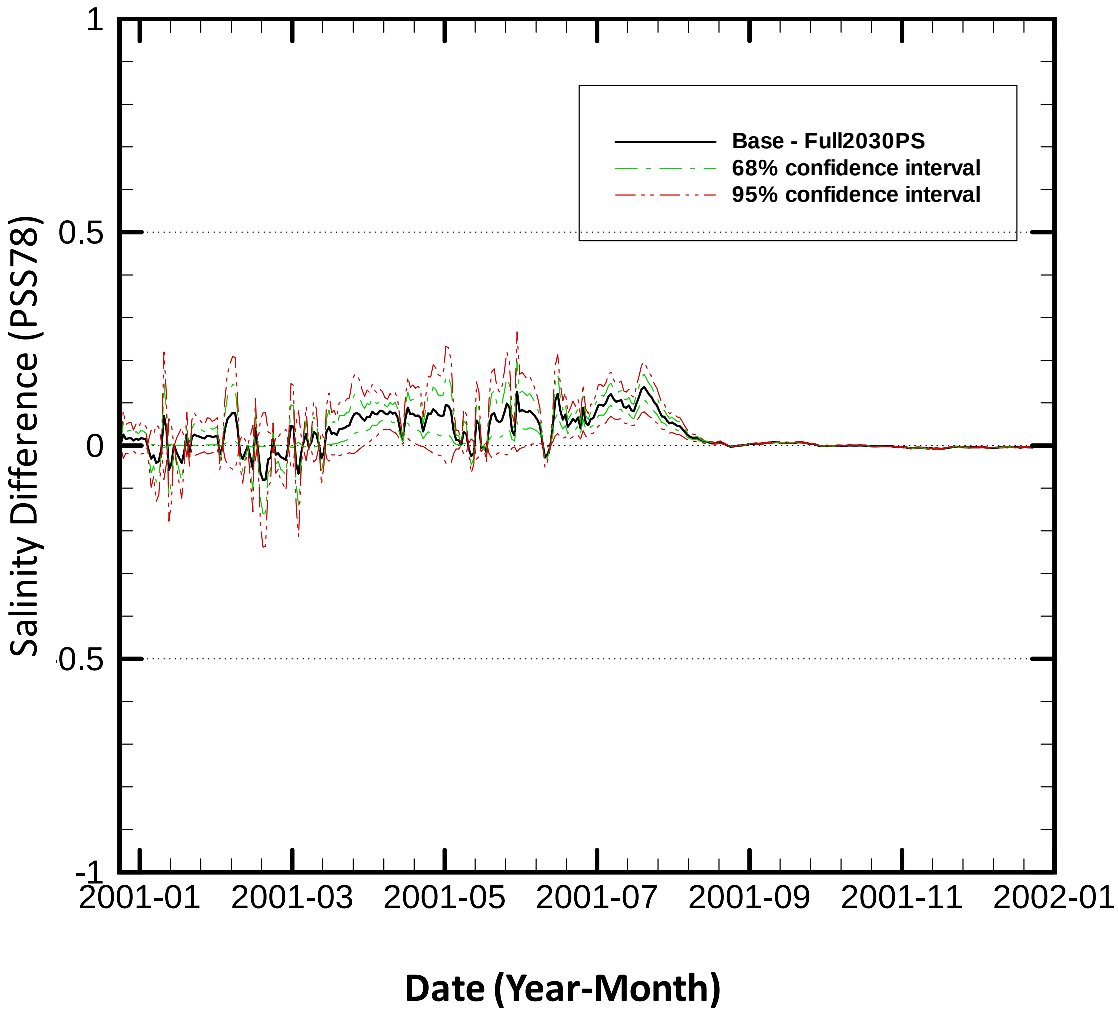

Figure 3–81. Simulated difference in hourly salinity between the Base1995NN and Full2030PS scenarios at DeLand with confidence intervals for the year 2001.

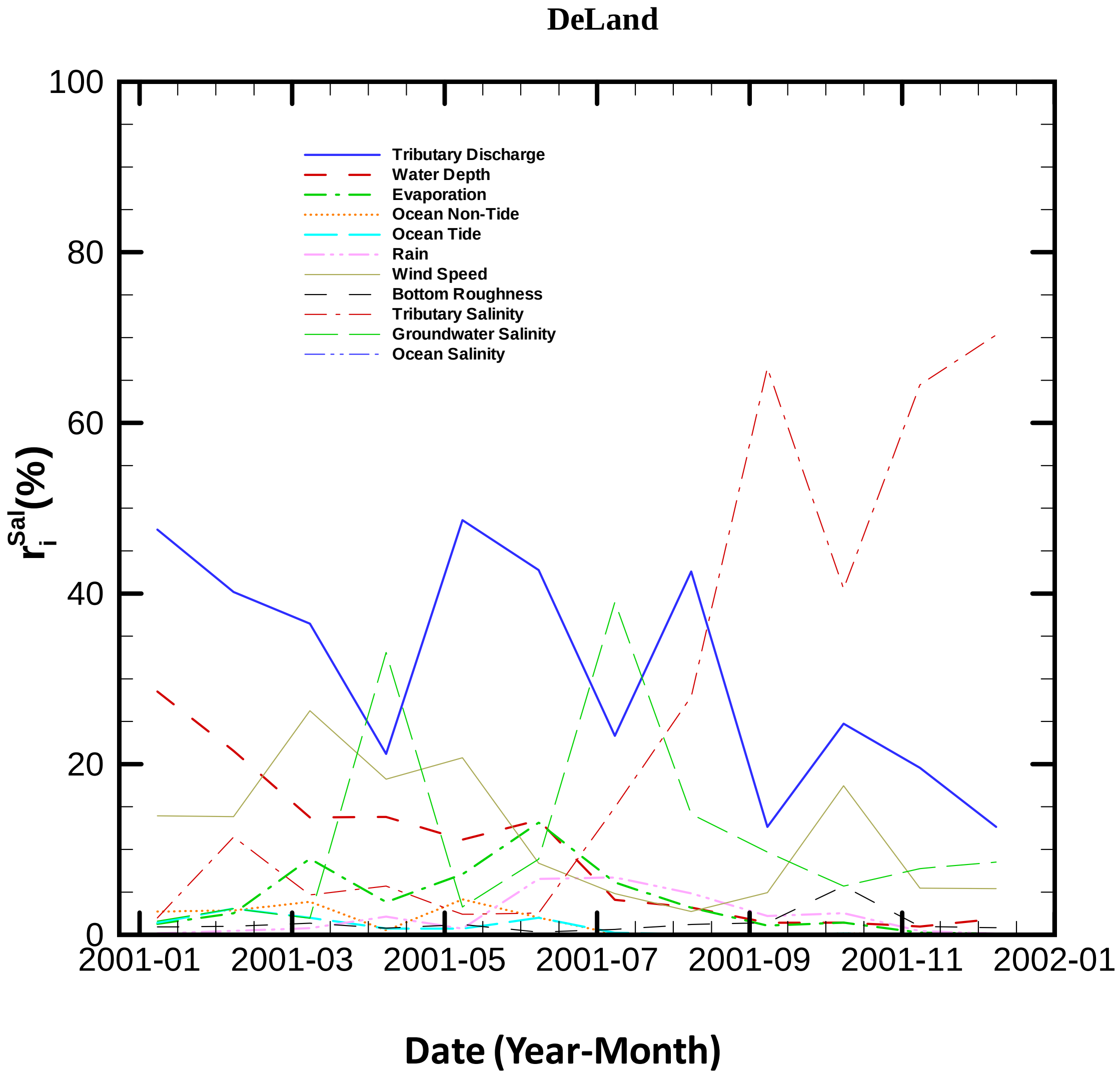

Figure 3–82. Percent contribution of input variables to the total uncertainty of predicted salinity change (r^{Sal}) at DeLand.

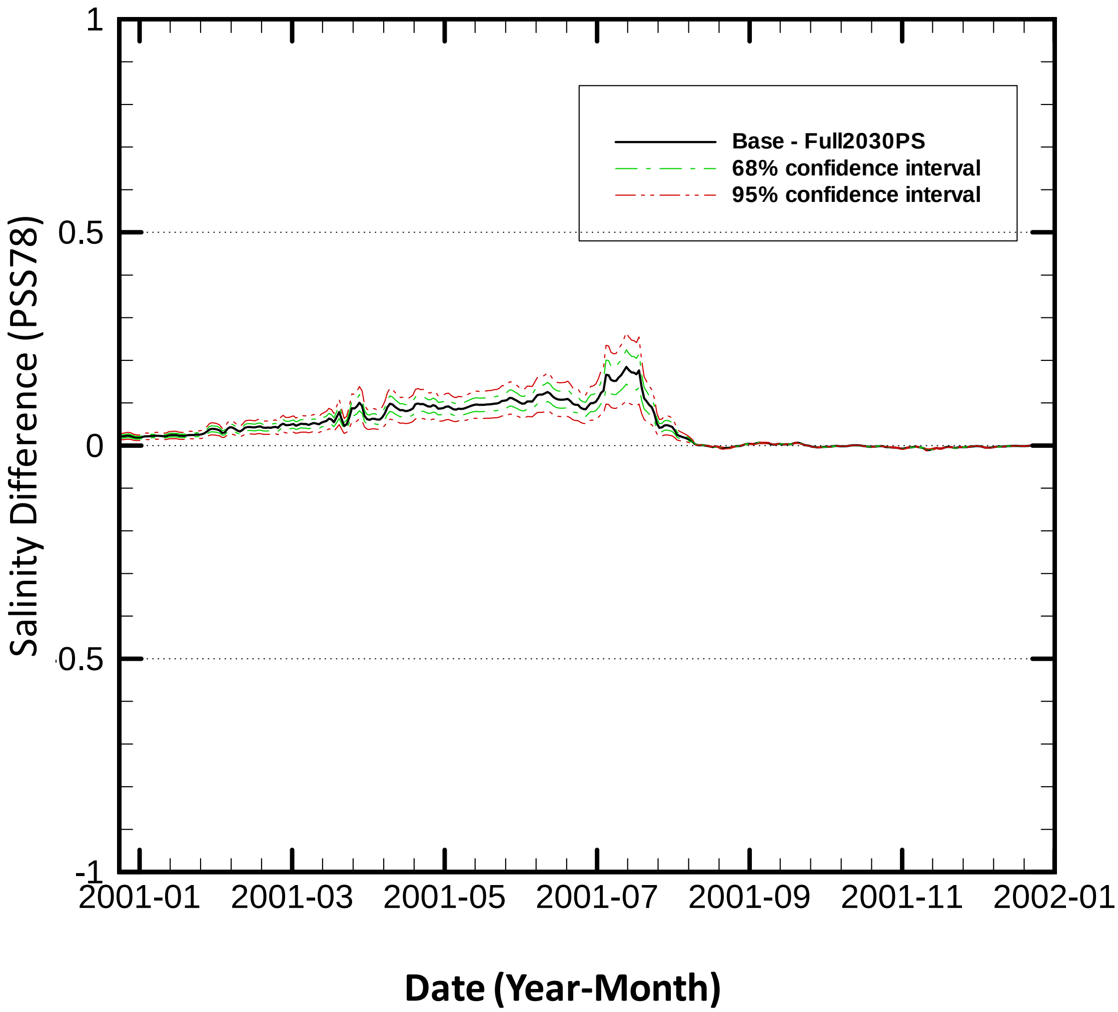

Figure 3–83. Simulated difference in hourly salinity between the Base1995NN and Full2030PS scenarios at Lake Monroe, with confidence intervals for the year 2001.

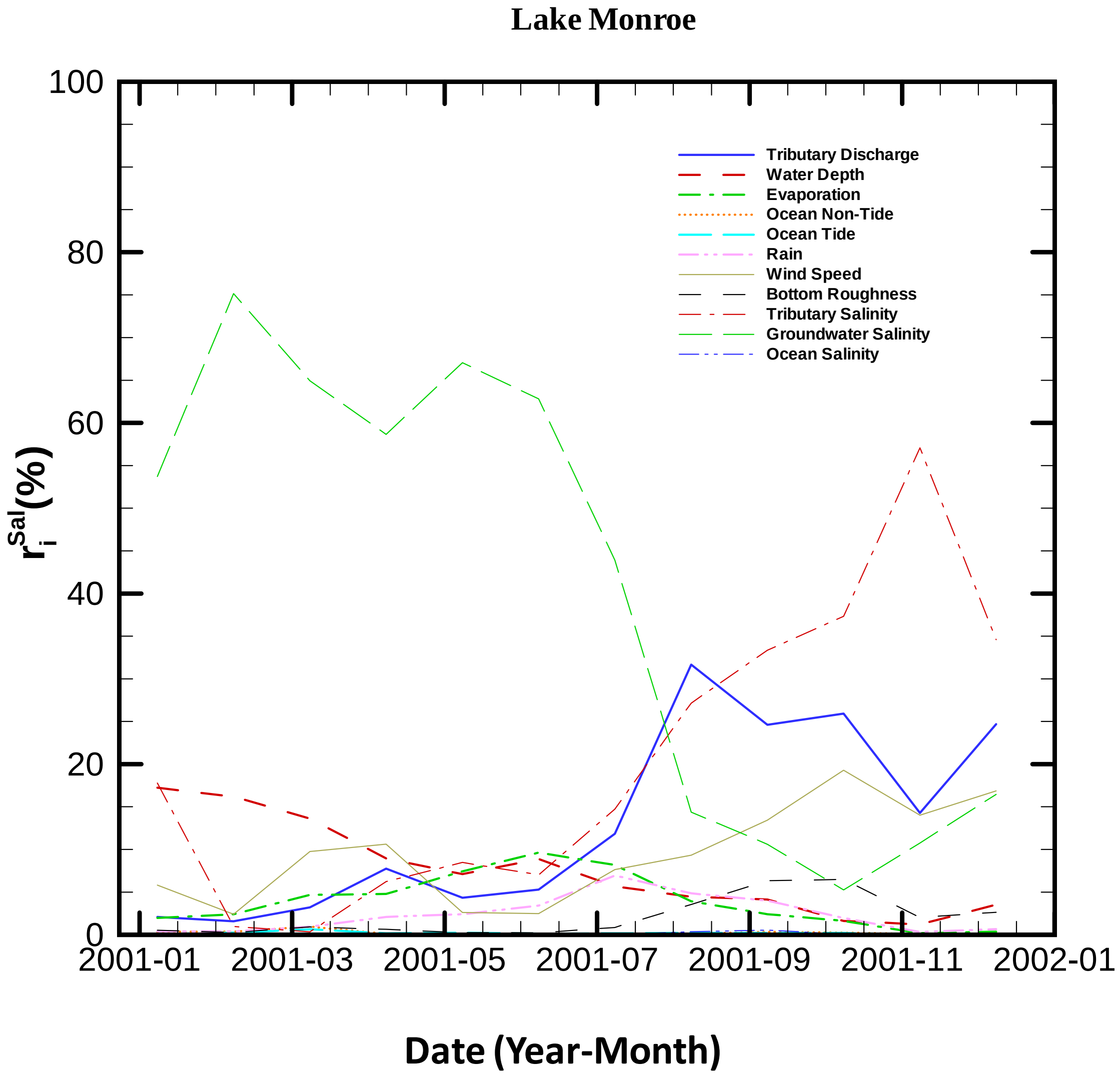

Figure 3–84. Percent contribution of input variables to the total uncertainty of predicted salinity change (r^{Sal}) at Lake Monroe.

3.3.4 Summary of Model Uncertainty

The FOEA analysis provides three principle results for evaluating model uncertainty: sensitivity analyses (*DSC*s), error bars on predicted model output, and the percent contribution to uncertainty assigned to each model input variable. The results of the sensitivity analyses are most useful for model calibration in that these analyses demonstrate clearly how the model responds to equal percent adjustments to the input variables. The error bar analysis demonstrates times and locations of greatest model uncertainty in output variables. Finally, the analysis of the percent contribution of input variables to uncertainty provides a useful means of assessing whether improved knowledge of the input variables could improve the model predictions.

In general, the input variables identified as most sensitive also contribute the most to the output uncertainty. For example, tidal water level is most sensitive to depth (Figure 3–2), and depth also contributes the most to the uncertainty in tidal water level predictions (Figure 3–22).

An exception to this rule occurs for estuarine salinity, which is most sensitive to depth and the specification of ocean salinity. However, ocean salinity does not contribute greatly to the uncertainty of salinity prediction in the estuarine reach because its estimated variance is small. Although depth remains an important contributor to uncertainty, tributary discharge becomes an important contributor to uncertainty for the prediction of estuarine salinity.

The error bar analysis identified three conditions of notable output uncertainty. The first condition is for predicted water level in the middle St. Johns River during period of high discharge. Uncertainty for this condition is dominated by uncertainty in tributary discharge. The second condition is for predicted current speed in the middle St. Johns River channel (not lakes), where uncertainty is again dominated by uncertainty in tributary discharge. Finally, the third condition is for predicted salinity in the estuarine river. Uncertainty of salinity in this reach is dominated by uncertainty in both depth and tributary discharge. For all these conditions, the greatest improvement to model prediction is gained by minimizing uncertainties in tributary discharges entering the modeled system.

3.4 Summary and Conclusions

Uncertainty is evaluated for WSIS using three types of evidence: weight of supporting evidence (SE), strength of predictive models (PM), and degree of understanding of mechanisms (UM). These criteria are assessed and combined to yield five qualitative uncertainty categories—very low, low, medium, high, and very high (see Table 3–1). Because the EFDC hydrodynamic model is a highly mechanistic model based on physical laws of motion, UM is considered strong for the hydrodynamic modeling. PM is primarily evaluated by comparison of predicted model output with observed data using confirmation and calibration statistics. SE is evaluated by professional judgment considering the integrity and quality of observed data, but also the adequacy of available data for evaluating model predictions.

In general, predicted model output from the EFDC hydrodynamic model has very low or low uncertainty. Exceptions include (a) water level in Lake Harney under flood conditions, (b) daily fluctuations of discharge through the mouth of Lake Jesup, (c) salinity at the leading edge of ocean salinity intrusions, and (d) salinity in Lake Woodruff. Model uncertainties are summarized in Section 3.2 above for each WSIS river reach for water level (Table 3–6), discharge (Table 3–7), salinity (Table 3–8), and water age (Table 3–9).

Predicted change of output variables between scenarios has lower uncertainty than prediction of absolute values for a single scenario. Predicted changes have very low uncertainty for all output variables with the single exception of Lake Woodruff salinity.

4 ANALYSIS OF THE EFFECT OF REJECT WATER FROM REVERSE OSMOSIS PLANTS

4.1 INTRODUCTION

Water withdrawal from the two middle St. Johns River locations of Yankee Lake and near SR 46 at Lake Jesup (Figure 4–1) could require the use of reverse osmosis to remove chloride and other salts, because chloride levels in the middle St. Johns River exceed the secondary drinking water standard of 250 mg L^{-1}(Sawyer, McCarthy and Parkin 1994) approximately 50% of the time. Although exceeding the chloride standard does not pose a risk to human health, the aesthetic quality of the water is compromised. Treatment of water by reverse osmosis would generate a waste stream, called reject water, of higher chloride concentration than the ambient level of the river. From a hydrodynamic perspective, this process has the effect of reducing flushing of the receiving water body without reducing salt flux to the water body. This process could increase concentrations of chloride and other salts in the river, particularly during periods of low river flow.

This section provides a screening level analysis of the far field effects of reject water on salinity in the middle St. Johns River. Salinity is used as a surrogate for all salts entering the river with the reject water. As a screening level analysis, assumptions regarding the control and management of reject water are conservative, and no attempt is made to optimize the process or mitigate for locations where, or times when, salinity levels appreciably exceed ambient conditions.

Applied Technology and Management, under a contract with SJRWMD, added subroutines to the EFDC hydrodynamic model to simulate the withdrawal of water at ambient river salinity and the return of reject water a higher salinity concentration (Applied Technology and Management 2010). Applied Technology and Management applied this model to examine the effects of reject water released near withdrawal locations at Yankee Lake and near SR 46 at Lake Jesup (CH2M HILL 2008). This section expands the Applied Technology and Management study to include examination of wider spatial and temporal distribution of effects than those provided by the original study.

This analysis of the mixing of reject water with river water over a large area is termed far field to distinguish it from near field analyses commonly used in the design of reject water outfalls. A near field analysis examines the initial mixing of reject water as it exits a pipe, diffuser, or other conveyance. According to Florida Administrative Code (FAC), the reject water must be mixed with ambient river water to reach the water quality criterion within a horizontal distance of two times the natural water depth (FAC 62-4.244). CH2MHILL previously conducted a near field mixing zone analysis of reject water at the proposed water withdrawal locations (CH2M HILL 2008). Because depths near the two proposed withdrawal locations vary from 1.8 to 11 m, the required near field mixing zone length is 3.7 to 22 m. This length is much smaller than the typical EFDC hydrodynamic model cell length of 75 m in this area. The EFDC hydrodynamic model, then, cannot be used to simulate the near field mixing of the reject water.

Although a near field analysis examines the characteristics of the mixing of reject water with ambient river water at much smaller spatial scales than is possible with the EFDC hydrodynamic model, a near field model does not continue to track the fate of the reject water outside the initial near field mixing zone. In addition, a near field mixing zone study assumes a constant current (CH2M HILL 2008) across the study area, and does not consider the dynamic variability of currents.

The EFDC hydrodynamic model is considered a far field model for examining the mixing of reject water, because it assumes the reject water is well mixed where it enters the first model cell. Although the EFDC hydrodynamic model is incapable of examining the near field characteristics of the initial mixing of the reject water, the model can examine, over a wide area of the river, the accumulation of salts carried with the reject water. The EFDC hydrodynamic model is an effective far field model due to its ability to account for mass conservation and dynamic transport and mixing of salinity. The far field analysis used here examines the mixing and movement of reject water over a range of flow conditions—including storm events, drought conditions, and reverse flows—over a 10-yr period, and tracks the fate of the reject water over a 45-km river reach centered near the outlet of Lake Monroe.

Not surprisingly, results show that the greatest increases in salinity occur at the discharge locations for reject water. The upstream discharge location near SR 46 at Lake Jesup exhibits greater increases in salinity than the downstream location at Yankee Lake, even though both locations have the same withdrawal rate of 50 mgd.

At both locations, the largest increases in salinity occur during low flow conditions with greater than 4-yr recurrence periods. Salinity differences, then, are small for most days. Under even moderate flow conditions, salts released in reject water are readily flushed from the system.

Salinity effects are small in Lake Monroe. Daily averaged salinity differences in Lake Monroe are less than 0.2 PSS78 for 90% of days, and never exceeded 0.3 PSS78 under any flow conditions.

4.2 Methods and Scenario Descriptions

The Applied Technology and Management 2010 study investigated withdrawal rates of 50 mgd, 25 mgd, 12.5 mgd, 6 mgd, and 3 mgd from each withdrawal location (Applied Technology and Management 2010). This section examines only the Full Withdrawal scenario (Full1995NN) that includes 50-mgd withdrawals each from two middle St. Johns River locations, Yankee Lake and near SR 46 at Lake Jesup (Figure 4–1). A withdrawal of 55 mgd from the upper St. Johns River is included in this scenario as a flow reduction entering Lake Harney, but this withdrawal is not evaluated for reject water. The Full1995NN scenario is compared against the base scenario, Base1995NN. Throughout this section, the Full1995NN scenario is referred to as the scenario case and the Base1995NN scenario as the base case. The scenarios are fully described in section 2 and summarized in Table 4–1.

Table 4–1. Scenarios used in the analysis of reject water from reverse osmosis plants.

Scenario Name	Description
Base1995NN	1995 land use conditions, no withdrawal, no upper St. Johns River projects, no sea level rise increase
Full1995NN	1995 land use conditions, full (155-mgd) withdrawal, no upper St. Johns River projects, no sea level rise increase

The simulation of return of reject water to the river requires that water be removed from one model cell (intake) and returned to another model cell (discharge) at a higher salinity. The locations of intake and discharge are shown below for both near SR 46 at Lake Jesup (Figure 4–2) and Yankee Lake (Figure 4–3). Identical to the Applied Technology and Management study, the scenario case (Full1995NN) assumes an 85% recovery volume and a 0.99 salinity rejection fraction.

Both cases are run for the model simulation period of 1996 through 2005 with 1995 as the spin-up year. Where Julian dates are used for model output, Julian day 1.0 equates to 1 January 1995. Simulated salinity is output at hourly intervals. Salinity values are then vertically averaged within each model cell, and temporally averaged by 1-, 7-, and 30-day averaging periods.

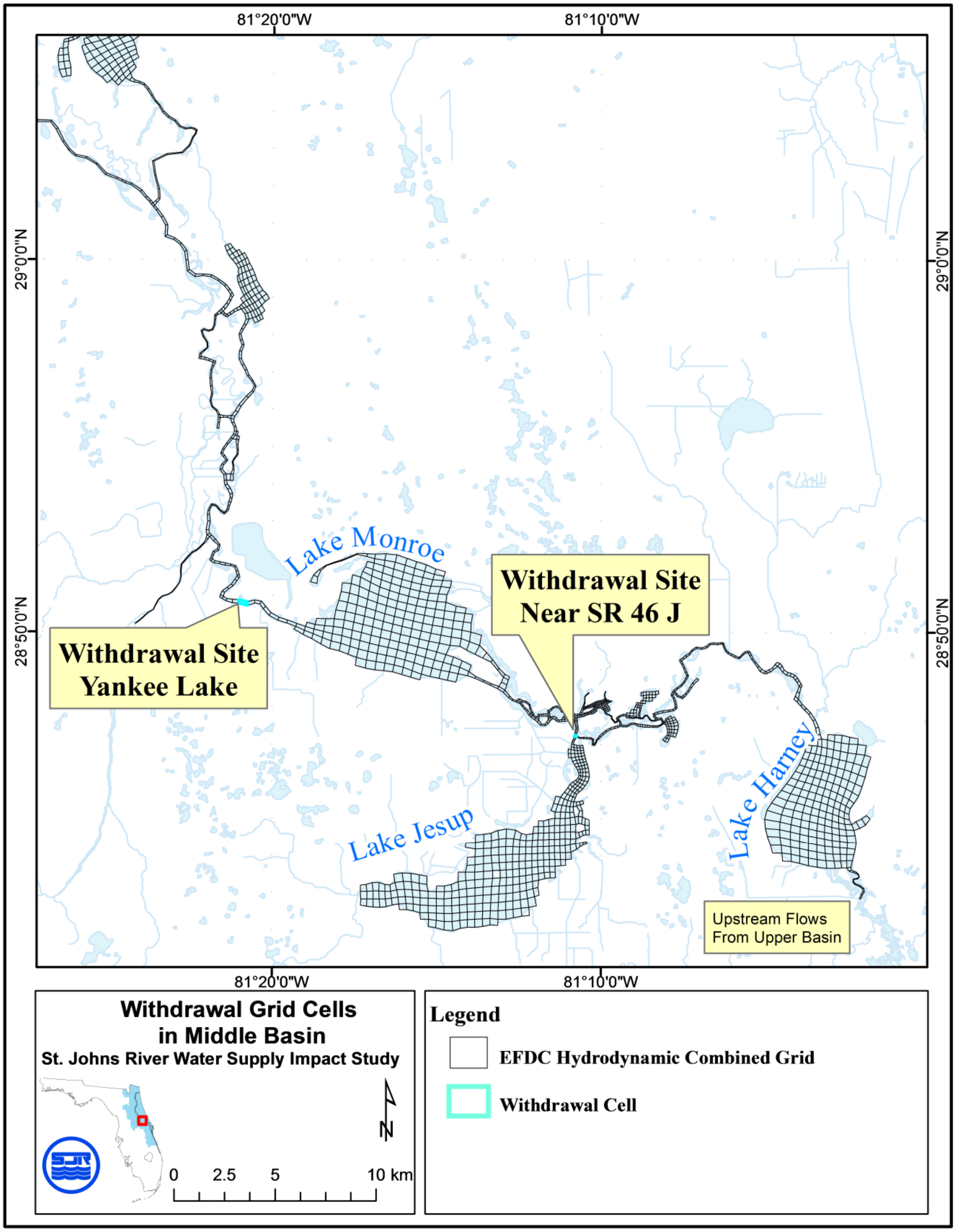

Figure 4–1. Locations of water withdrawal sites in the middle St. Johns River.

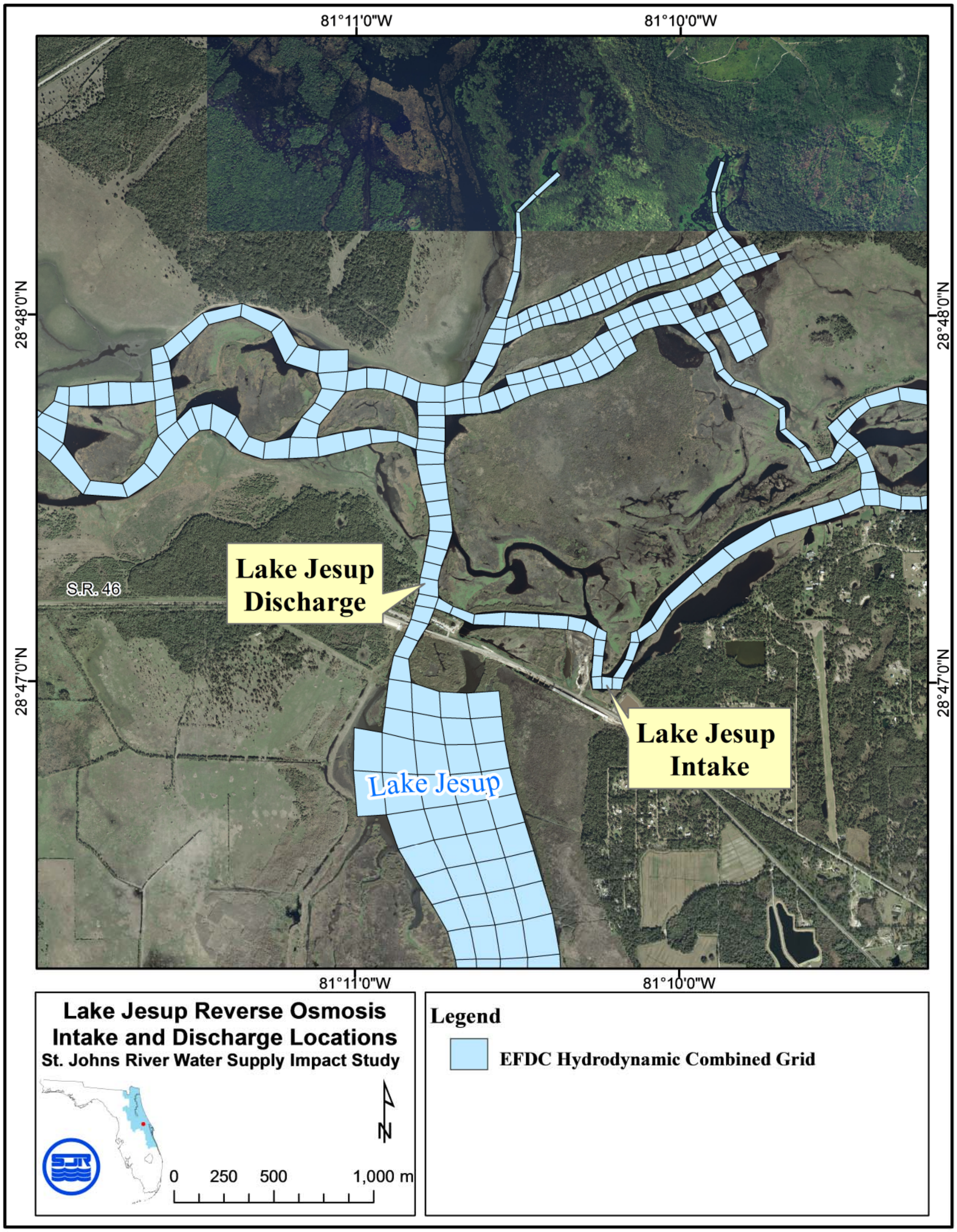

Figure 4–2. Locations of intake and discharge for simulation of the return of reject water to the St. Johns River at SR 46 at Lake Jesup.

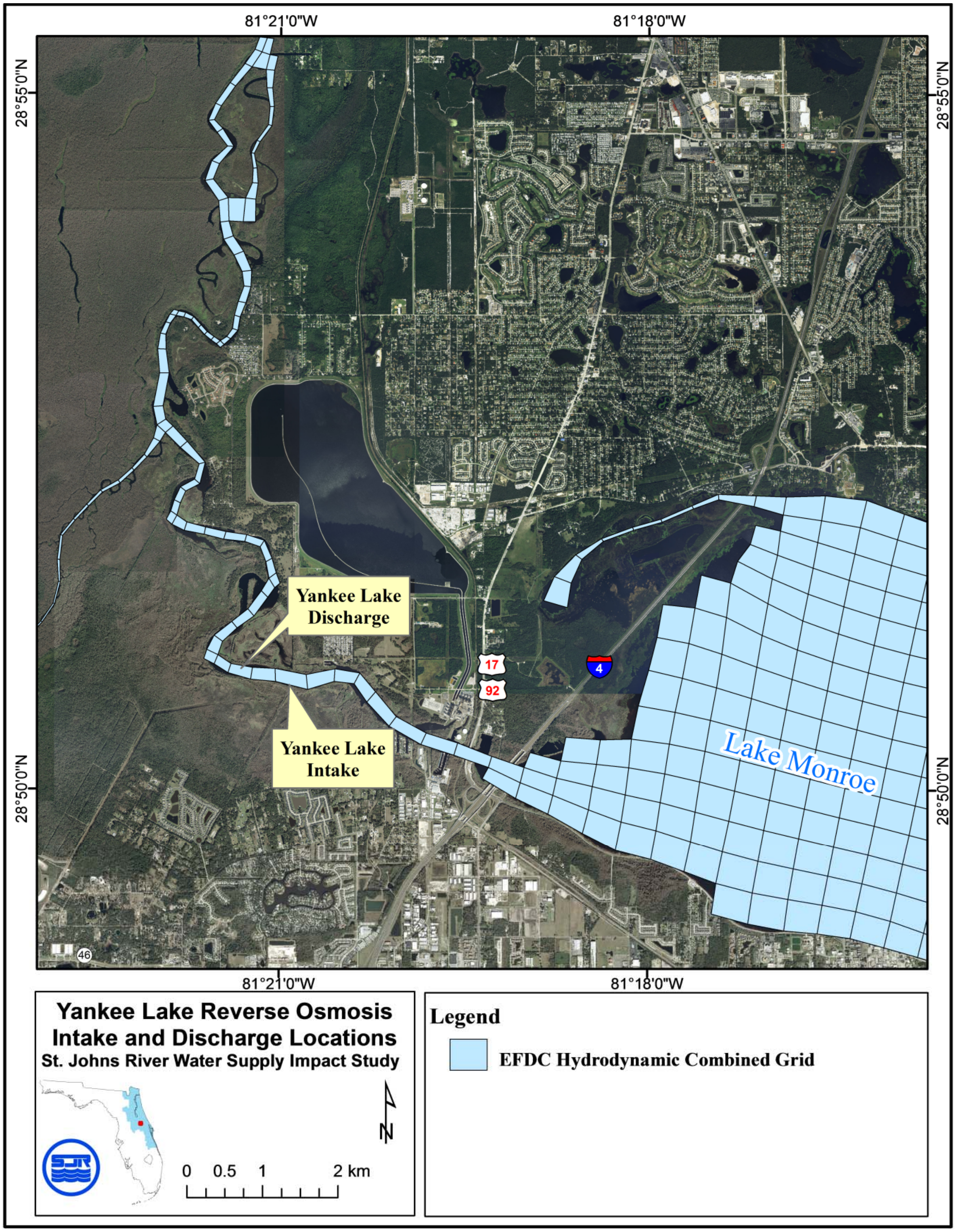

Figure 4–3. Locations of intake and discharge for simulation of return of reject water to the St. Johns River at Yankee Lake. EFDC = Environmental Fluid Dynamics Code.

4.3 RESULTS

4.3.1 SALINITY AT DISCHARGE LOCATIONS

This section shows salinity results as 10-year time series from 1996 to 2005 at the individual discharge locations. The individual time series for the base case (Base1995NN) and the scenario case (Full1995NN), as well as the salinity differences between the two cases are shown. Figure 4–4 identifies low flow and high flow by seasonally averaged (4-month) discharge at Astor for the 1996 to 2005 simulation period. The largest salinity differences occur during an extended drought period between Julian days 2,000 and 2,300.

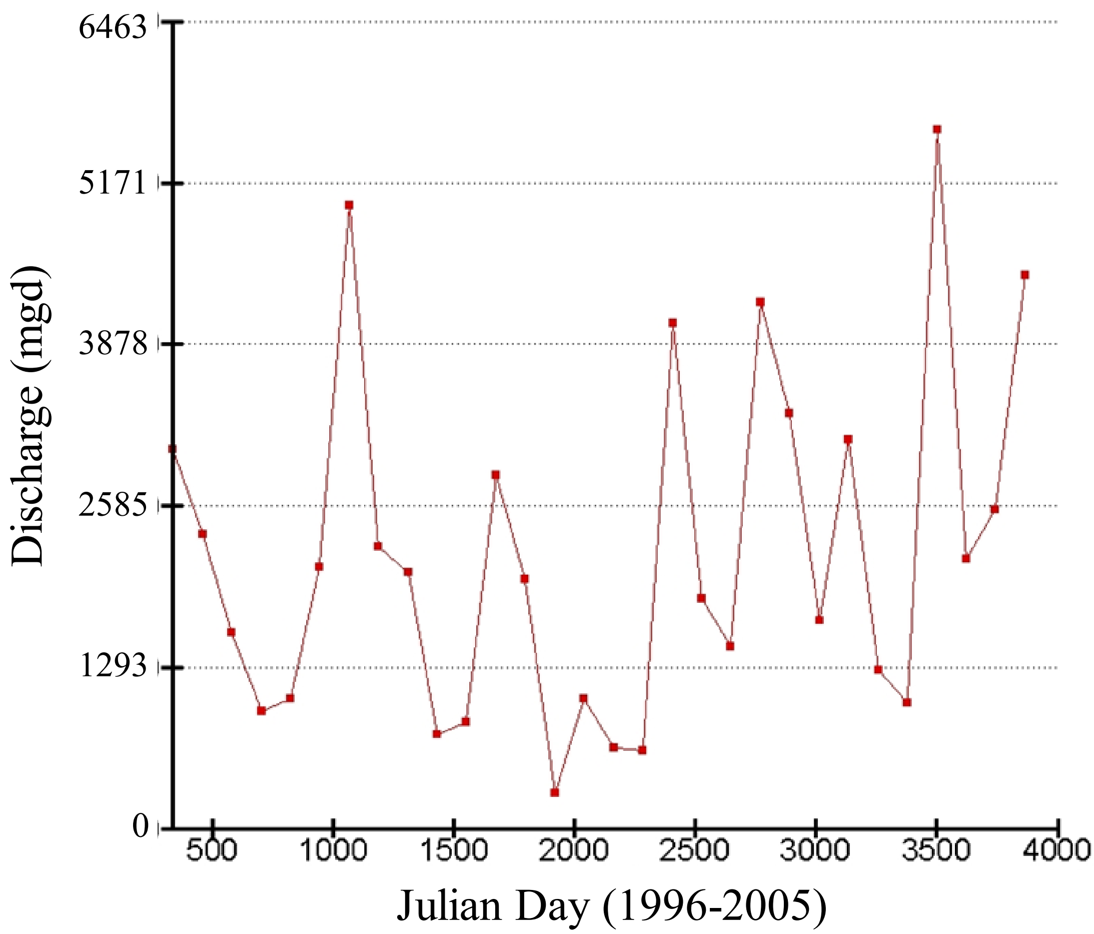

Figure 4–4. Seasonally averaged discharge at Astor, 1996 through 2005.

SR 46 at Lake Jesup Discharge Location

Time series of salinity comparing the base case (Base1995NN) and scenario case (Full1995NN) are shown below for 1-day (Figure 4–5), 7-day (Figure 4–7), and 30-day (Figure 4–9) averaging periods near SR 46 at Lake Jesup. Time series of salinity differences are shown in Figure 4–6, Figure 4–8, and Figure 4–10, for the 1-, 7-, and 30-day averaging periods, respectively.

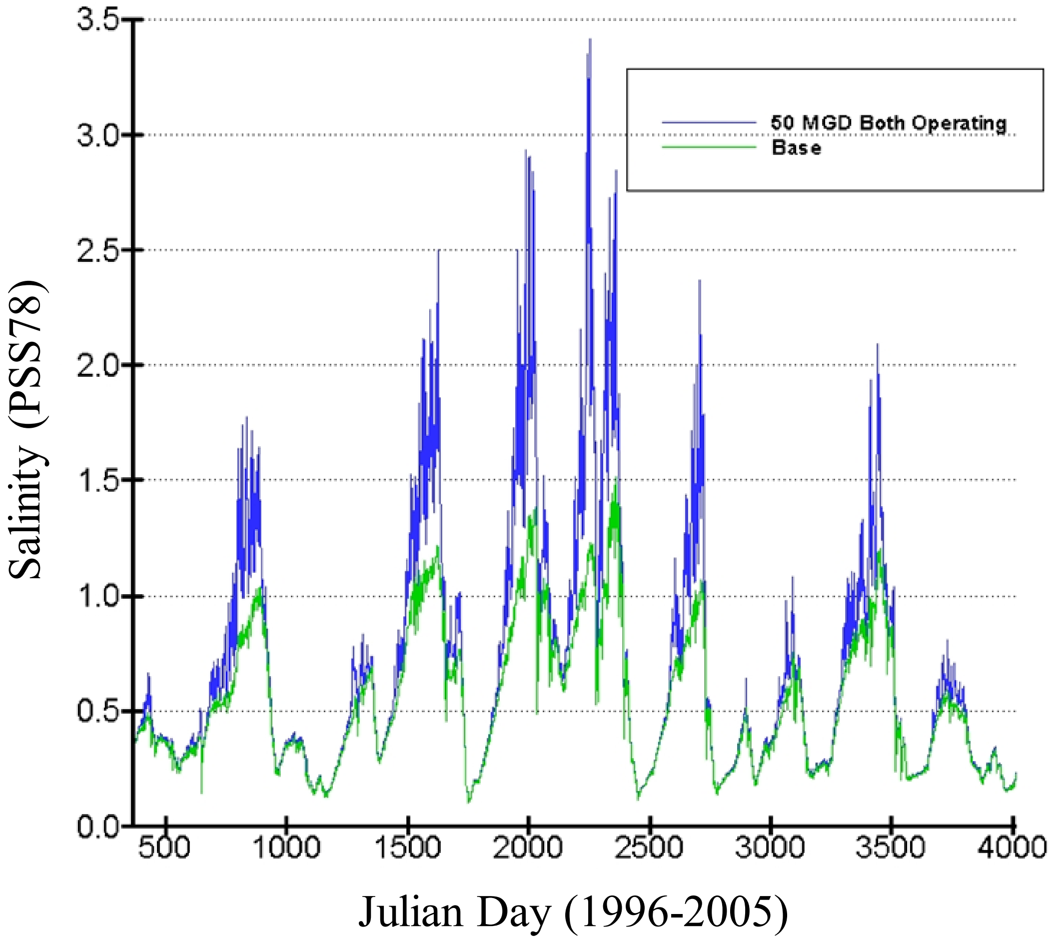

Figure 4–5. Daily (1-day) and vertically averaged salinity at discharge location of reject water near SR 46 at Lake Jesup, 1996 to 2005, for the base case (green, Base1995NN) and scenario case (blue, Full1995NN).

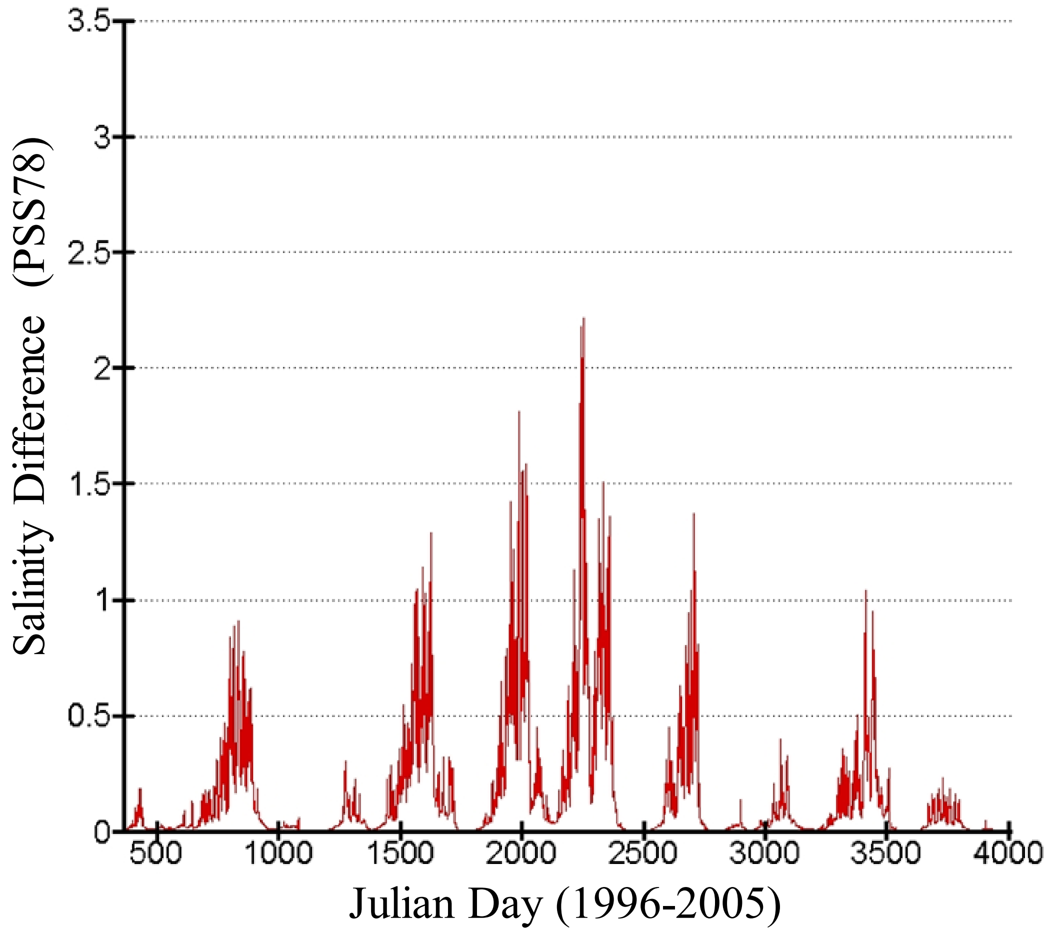

Figure 4–6. Difference of daily (1-day) averaged salinity between scenario case (Full1995NN) and base case (Base1995NN) at discharge location of reject water near SR 46 at Lake Jesup, 1996 to 2005.

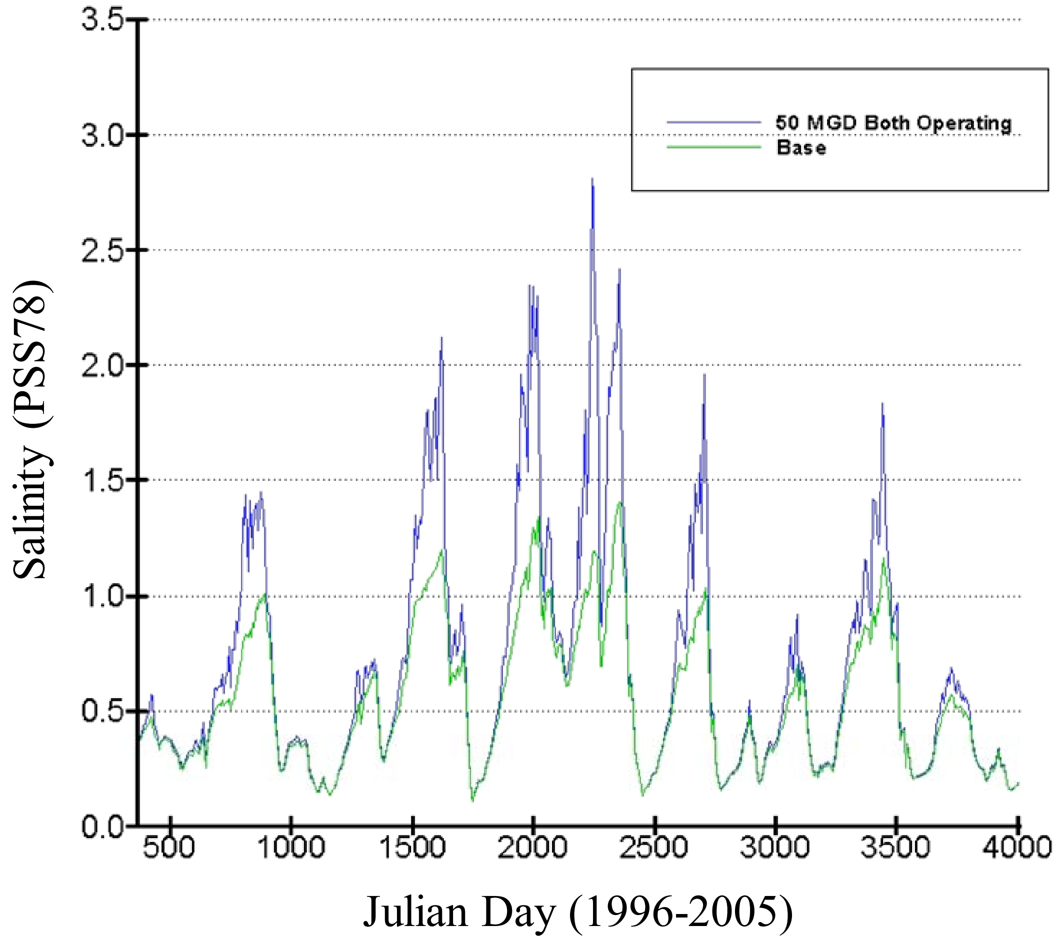

Figure 4–7. Vertically averaged and 7-day averaged salinity at location of discharge of reject water near SR 46 at Lake Jesup, 1996 to 2005, for the base case (green, Base1995NN) and scenario case (blue, Full1995NN).

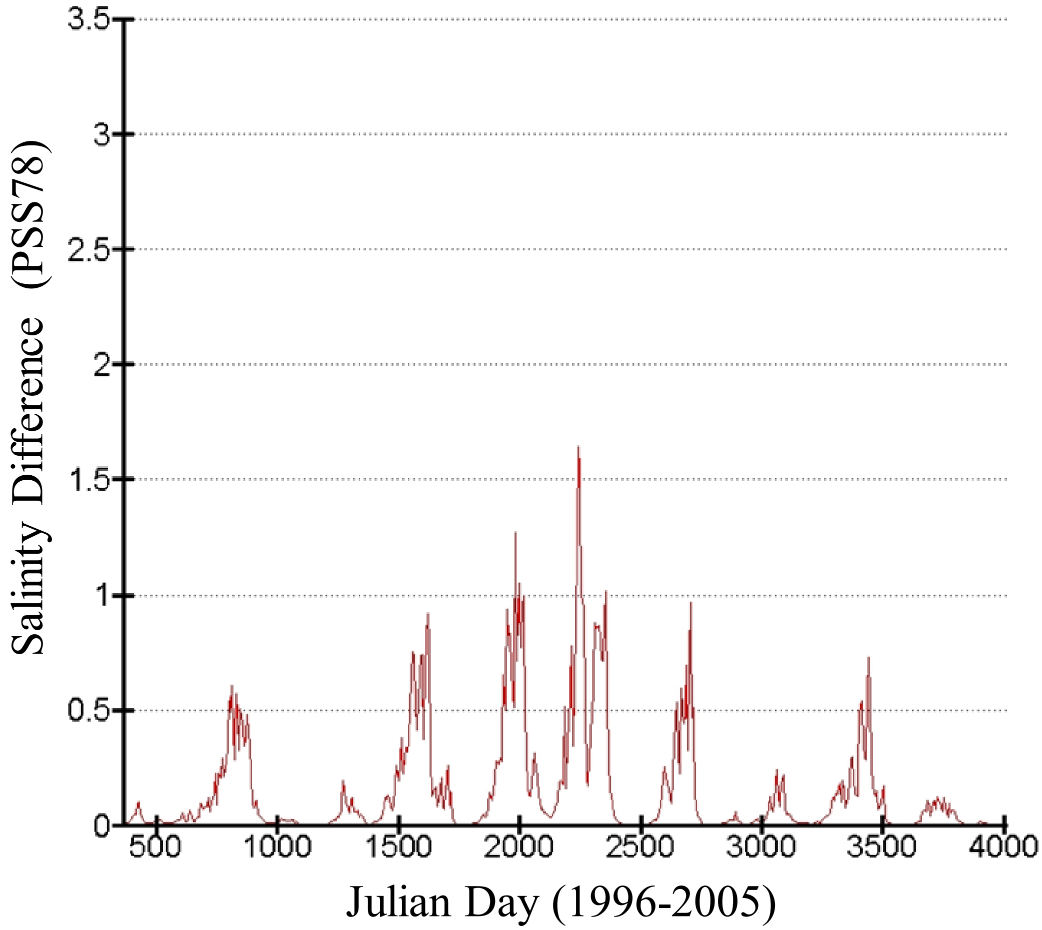

Figure 4–8. Difference of 7-day averaged salinity between scenario case (Full1995NN) and base case (Base1995NN) at location of discharge of reject water near SR 46 at Lake Jesup, 1996 to 2005.

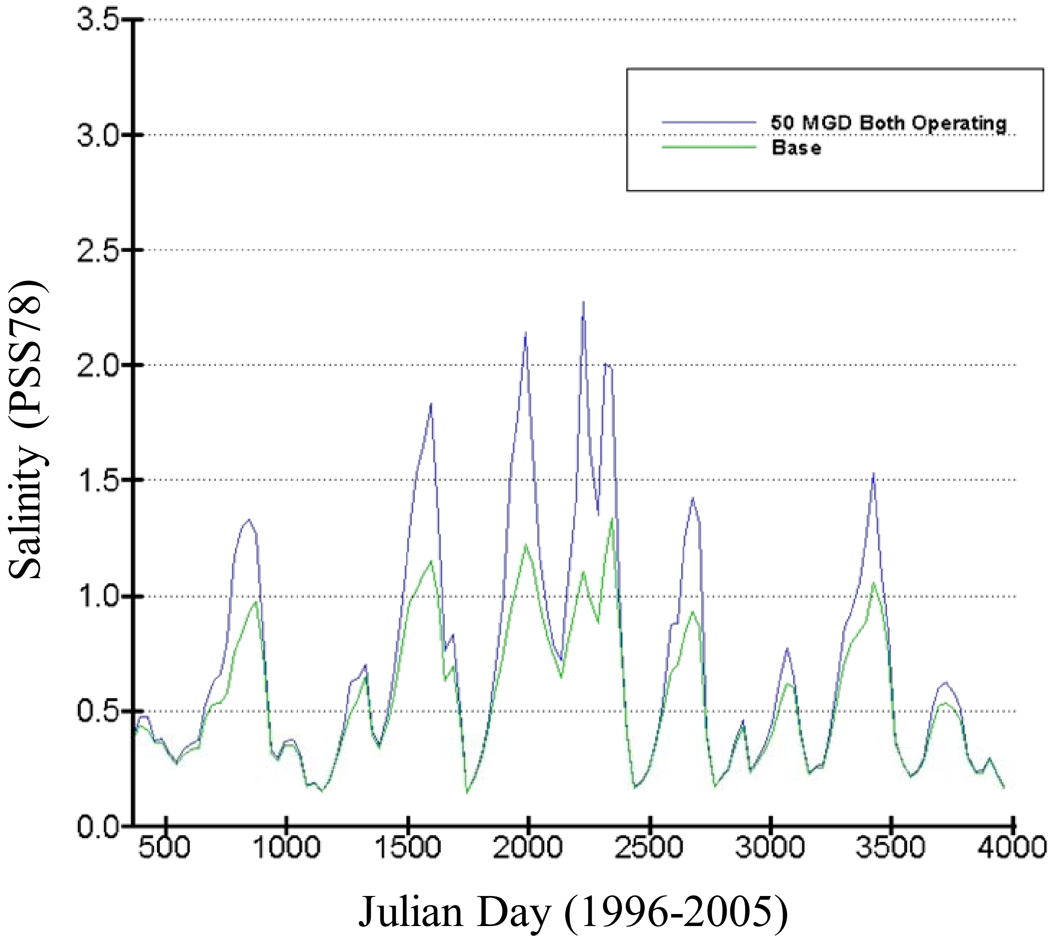

Figure 4–9. Vertically averaged and 30-day averaged salinity at location of discharge of reject water near SR 46 at Lake Jesup, 1996 to 2005, for the base case (green, Base1995NN) and scenario case (blue, Full1995NN).

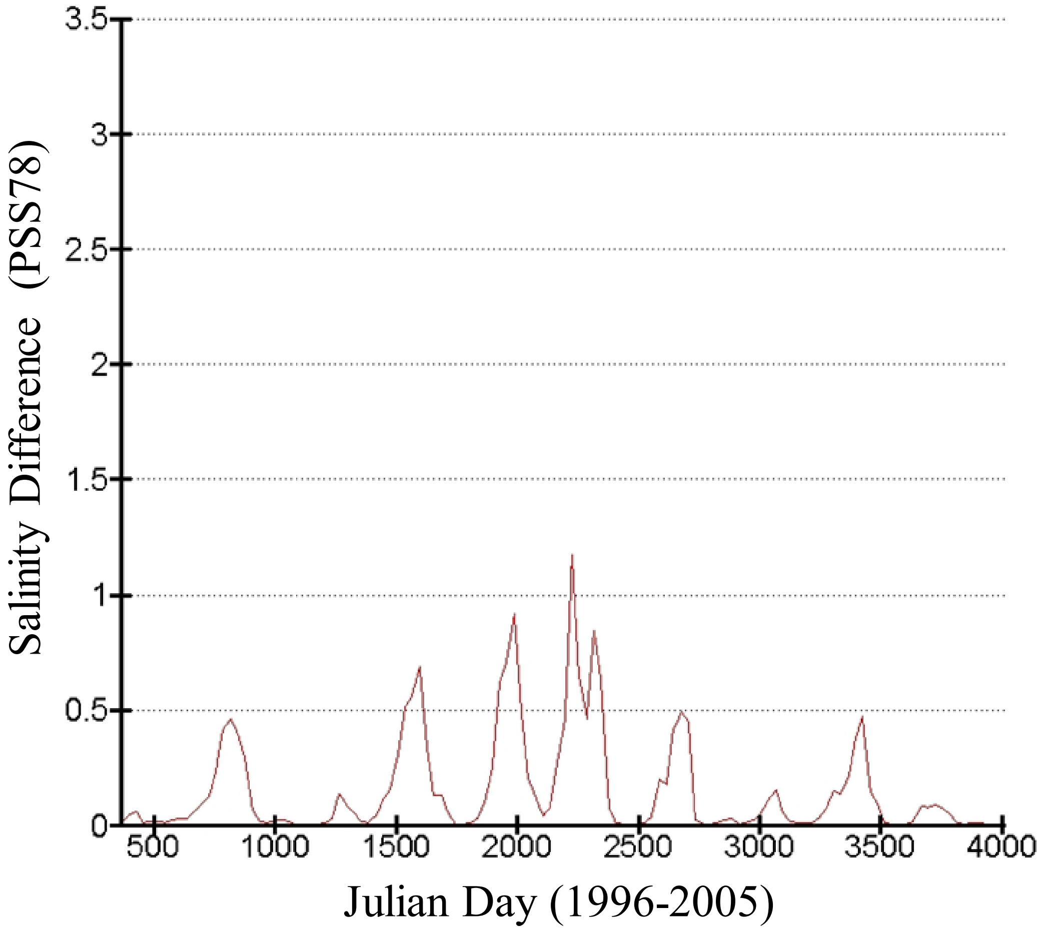

Figure 4–10. Difference of 30-day averaged salinity between scenario case (Full1995NN) and base case (Base1995NN) at location of discharge of reject water near SR 46 at Lake Jesup, 1996 to 2005.

Salinity differences between the scenario case (Full1995NN) and base case (Base1995NN) are largest during periods of low flow and smallest during periods of high flow. The maximum 1-day difference of salinity was 2.2 PSS78, the maximum 7-day difference was 1.6 PSS78, and the maximum 30-day difference was 1.2 PSS78.

Yankee Lake Discharge Location

Similar time series plots of salinity and salinity differences for the Yankee Lake location are shown below. Salinity is compared for 1-day (Figure 4–11), 7-day (Figure 4–13), and 30-day (Figure 4–15) averaging periods, and the associated difference plots are shown in Figure 4–12, Figure 4–14, and Figure 4–16.

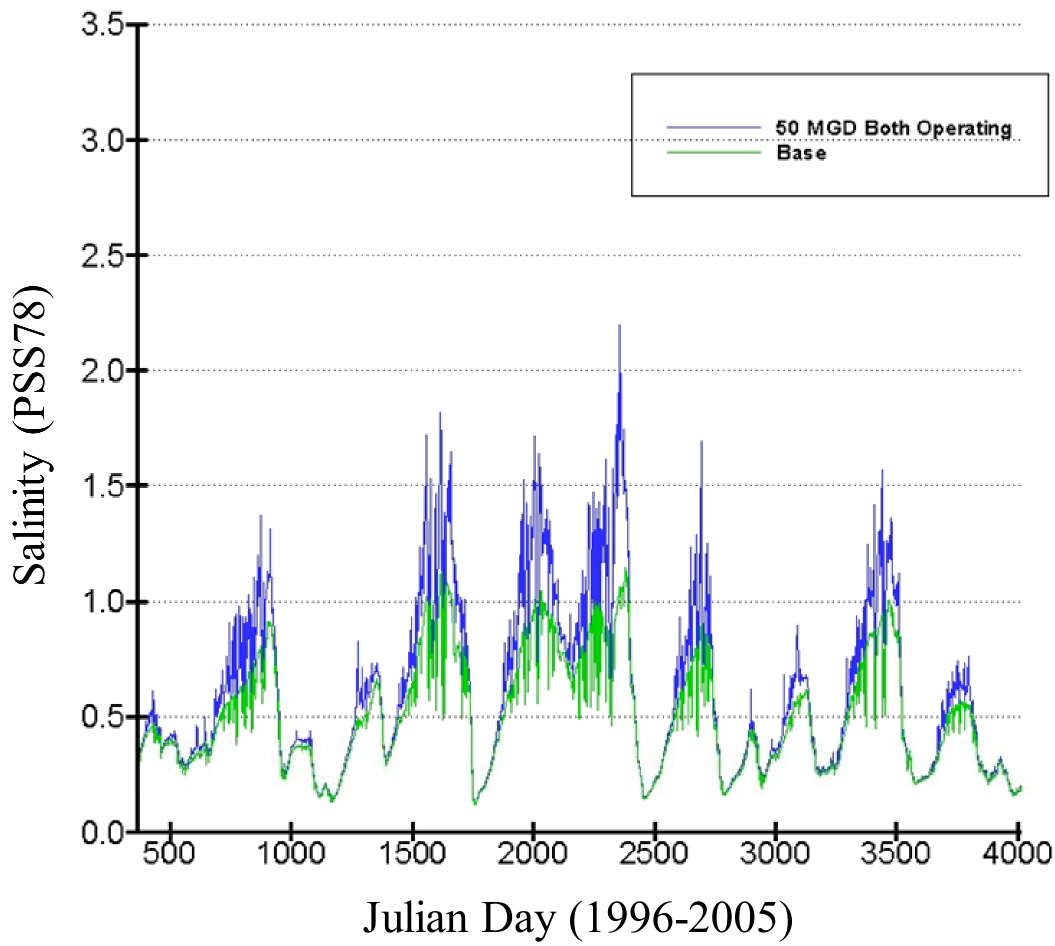

Figure 4–11. Daily and vertically averaged salinity at the Yankee Lake location, 1996 to 2005, for the base case (green, Base1995NN) and scenario case (blue, Full1995NN).

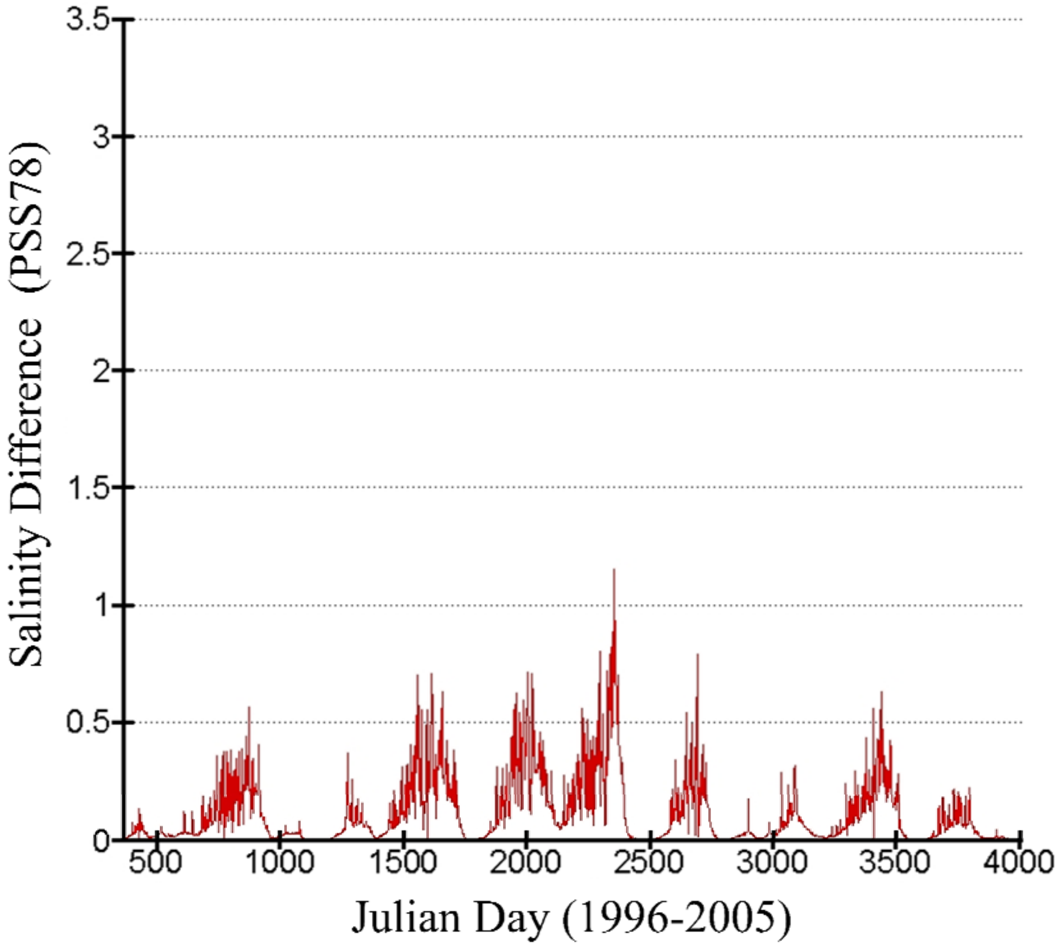

Figure 4–12. Difference of daily averaged salinity between the scenario case (Full1995NN) and base case (Base1995NN) at the Yankee Lake location, 1996 to 2005.

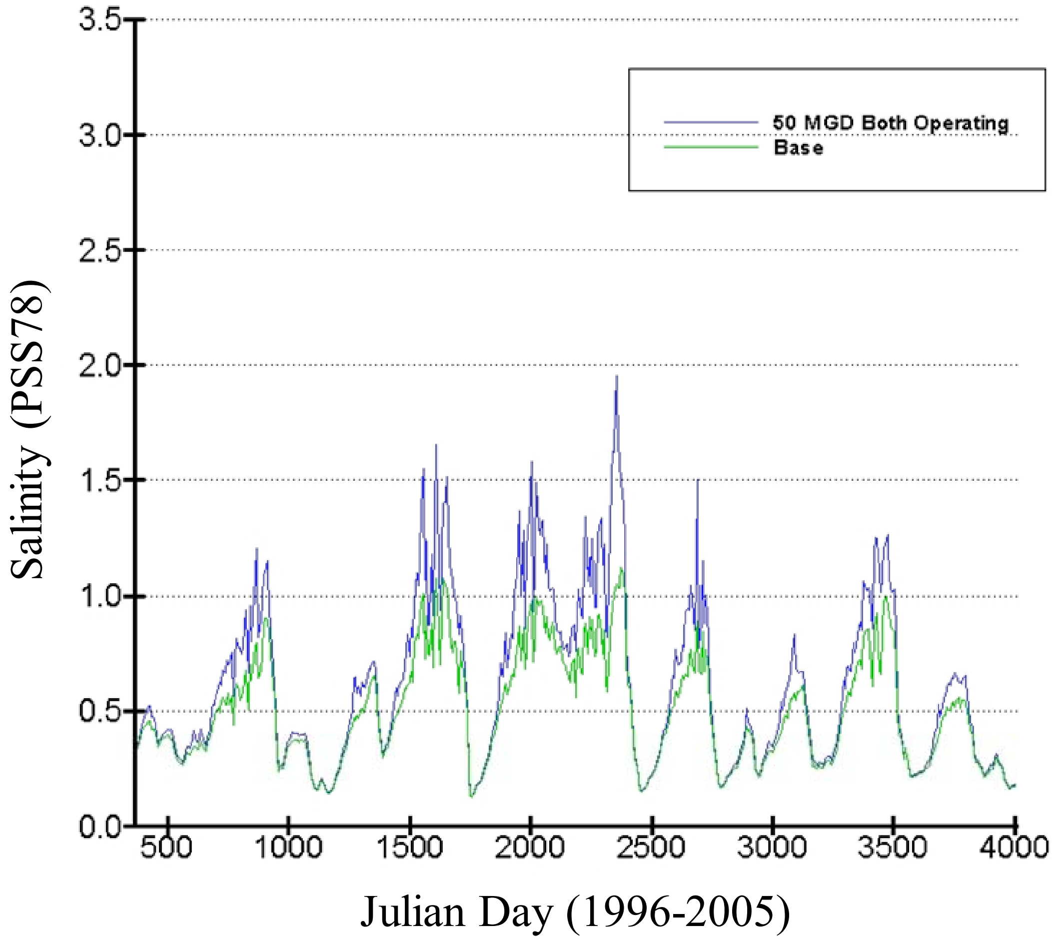

Figure 4–13. Vertically averaged and 7-day averaged salinity at the Yankee Lake location, 1996 to 2005, for the base case (green, Base1995NN) and scenario case (blue, Full1995NN).

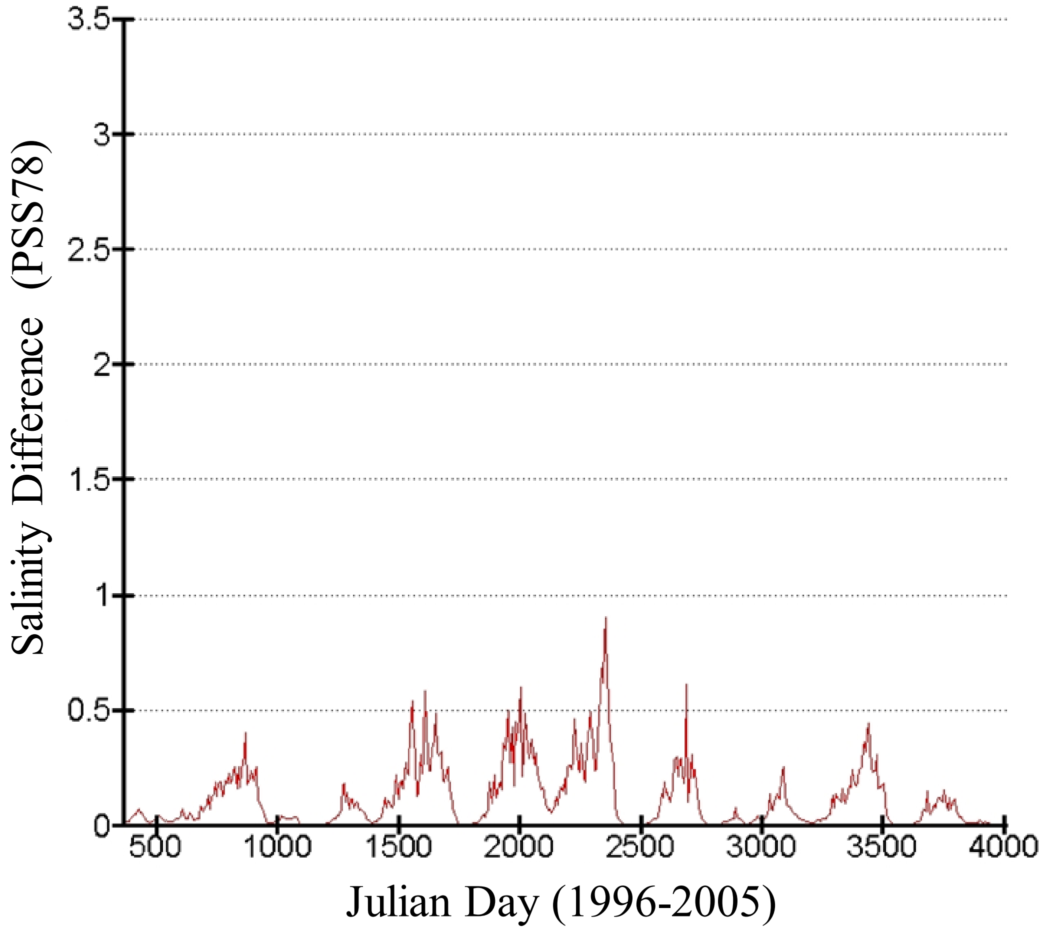

Figure 4–14. Difference of 7-day averaged salinity between the scenario case (Full1995NN) and base case (Base1995NN) at the Yankee Lake location, 1996 to 2005.

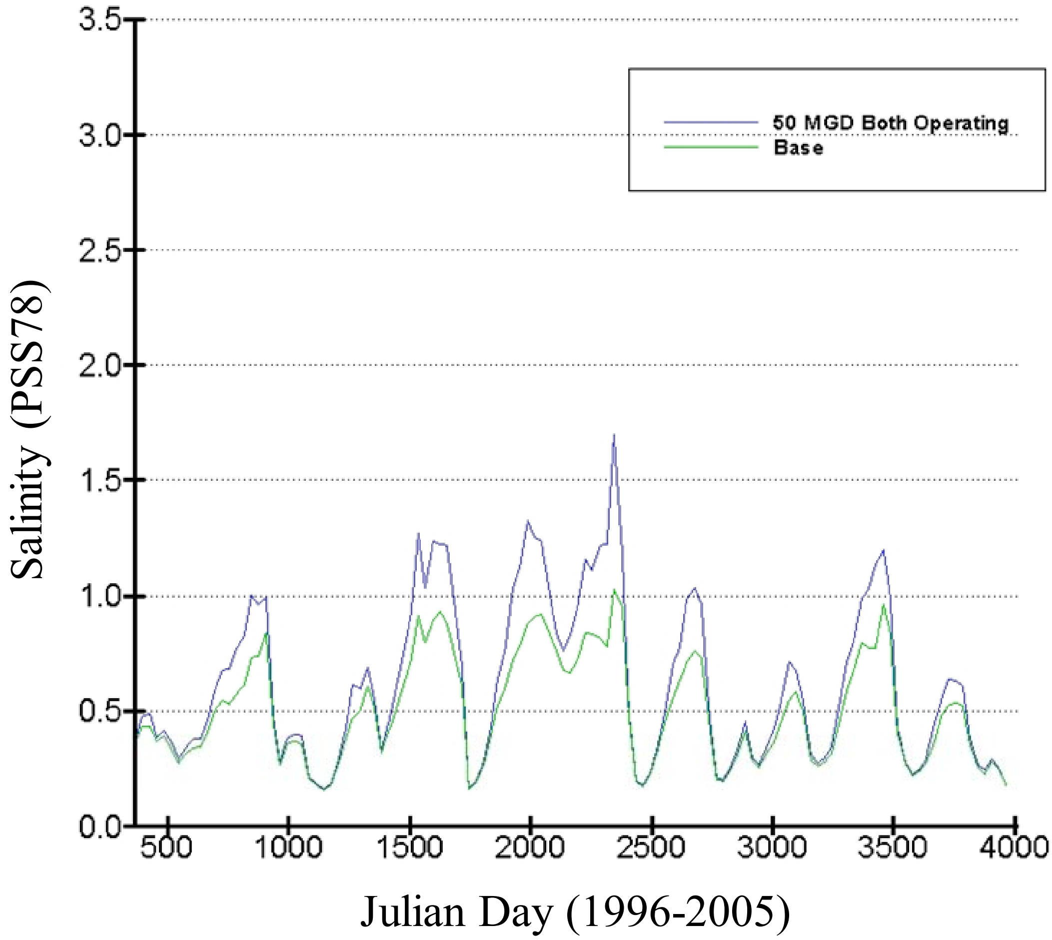

Figure 4–15. Vertically averaged and 30-day averaged salinity at the Yankee Lake location, 1996 to 2005, for the base case (green, Base1995NN) and scenario case (blue, Full1995NN).

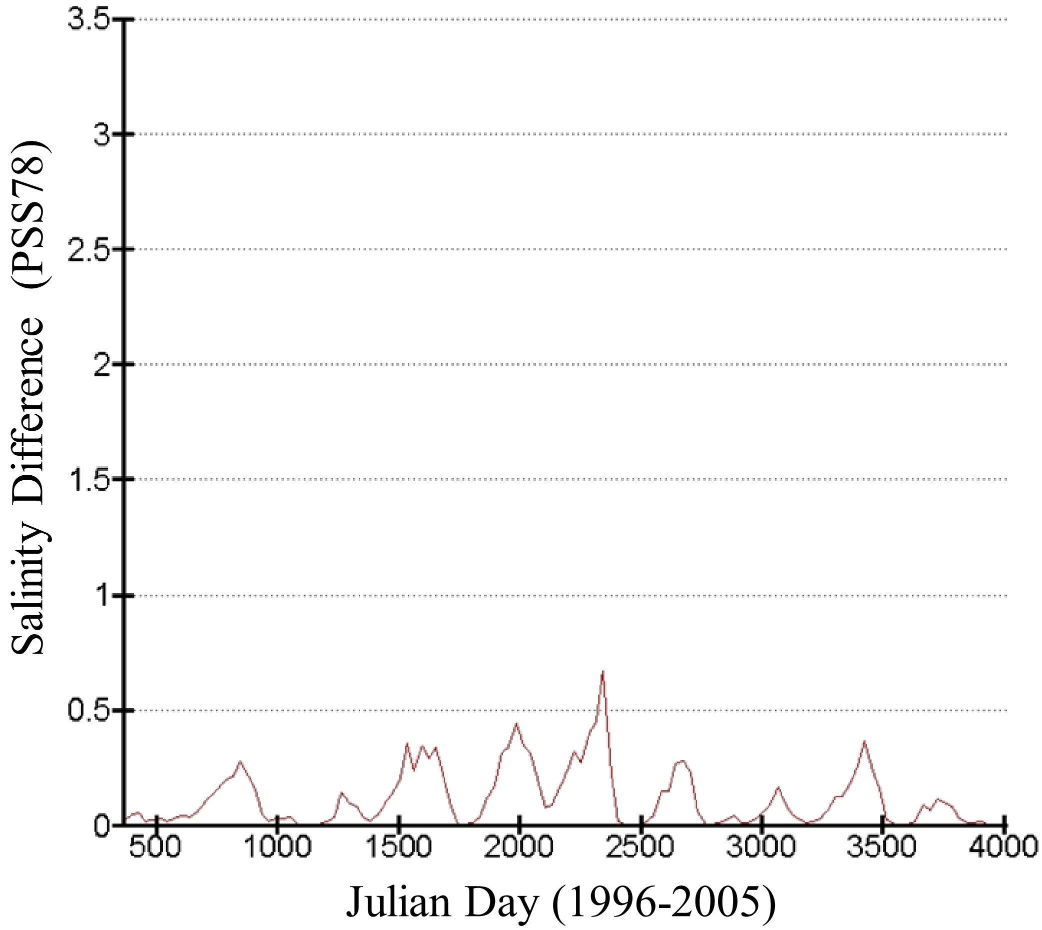

Figure 4–16. Difference of 30-day averaged salinity between the scenario case (Full1995NN) and base case (Base1995NN) at the Yankee Lake location, 1996 to 2005.

Maximum salinity during low flow periods are, in general, lower at Yankee Lake than at SR 46 at Lake Jesup. Although Yankee Lake is downstream of SR 46 at Lake Jesup and receives the effects of reject water from both withdrawal locations, it occupies an area of higher flushing. Maximum differences in salinity between the scenario (Full1995NN) and base (Base1995NN) cases are also less at Yankee Lake than near SR 46 at Lake Jesup. Maximum salinity differences at Yankee Lake are 1.2, 0.9, and 0.7 PSS78 for the 1-, 7-, and 30-day averaging periods, respectively.

Recurrence Intervals of Low Flow Events in Model Simulation Period

Because periods of highest salinity and greatest salinity differences occur during periods of low flow in the river, it is instructive to estimate the severity of low flow conditions for the 10-yr model simulation period relative to long-term flow statistics. Because long-term discharge (1958 to the present) is available at DeLand, this station is used as an index of river discharge for the middle St. Johns River in general. The common low flow statistic 7Q10 (7-day averaged discharge with a 10-yr recurrence interval) is -775 mgd (-34 m^3s^{-1}) at DeLand (Kroening 2004). The minimum 7-day simulated discharge at DeLand for the 10-yr model simulation period is almost identical to this value at -845 mgd (-37 m^3s^{-1}), and occurred on Julian day 2,699 (22 May 2002).

The largest simulated salinity events occurred between Julian days 1,800 (5 December 1999) and 2,400 (27 July 2001) (Figure 4–5) and are associated with low flow events of longer duration than 7 days. For 120-day averaged discharge, the record low flow event observed at DeLand (1958 to 2008) was 84 mgd (3.7 m^3s^{-1}) and occurred on Julian day 2,023 (15 July 2000). This event has a recurrence of about 50 years. Three other years in the model simulation period had 120-day low flow events with recurrence intervals greater than 4 years. These events, in order of severity, occurred on Julian day 1,573 (22 April 1999), Julian day 2,264 (13 March 2001), and Julian day 2,661 (14 April 2002), and had discharge levels of 343 mgd (15.0 m^3s^{-1}), 455 mgd (19.9 m^3s^{-1}), and 551 mgd (24.1 m^3s^{-1}), respectively.

4.3.2 Salinity Along a Longitudinal Transect

The spatial extent of salinity differences between the scenario case (Full1995NN) and base (Base1995NN) case is examined in this section by comparing the distribution of salinity over a longitudinal transect that contains the two withdrawal locations (Figure 4–17). The transect endpoints (A and B) are located downstream and upstream of the withdrawal sites, respectively, and define a 45-km long transect. Differences in salinity along transect AB for 1-, 7-, and 30-day averaging periods are presented below.

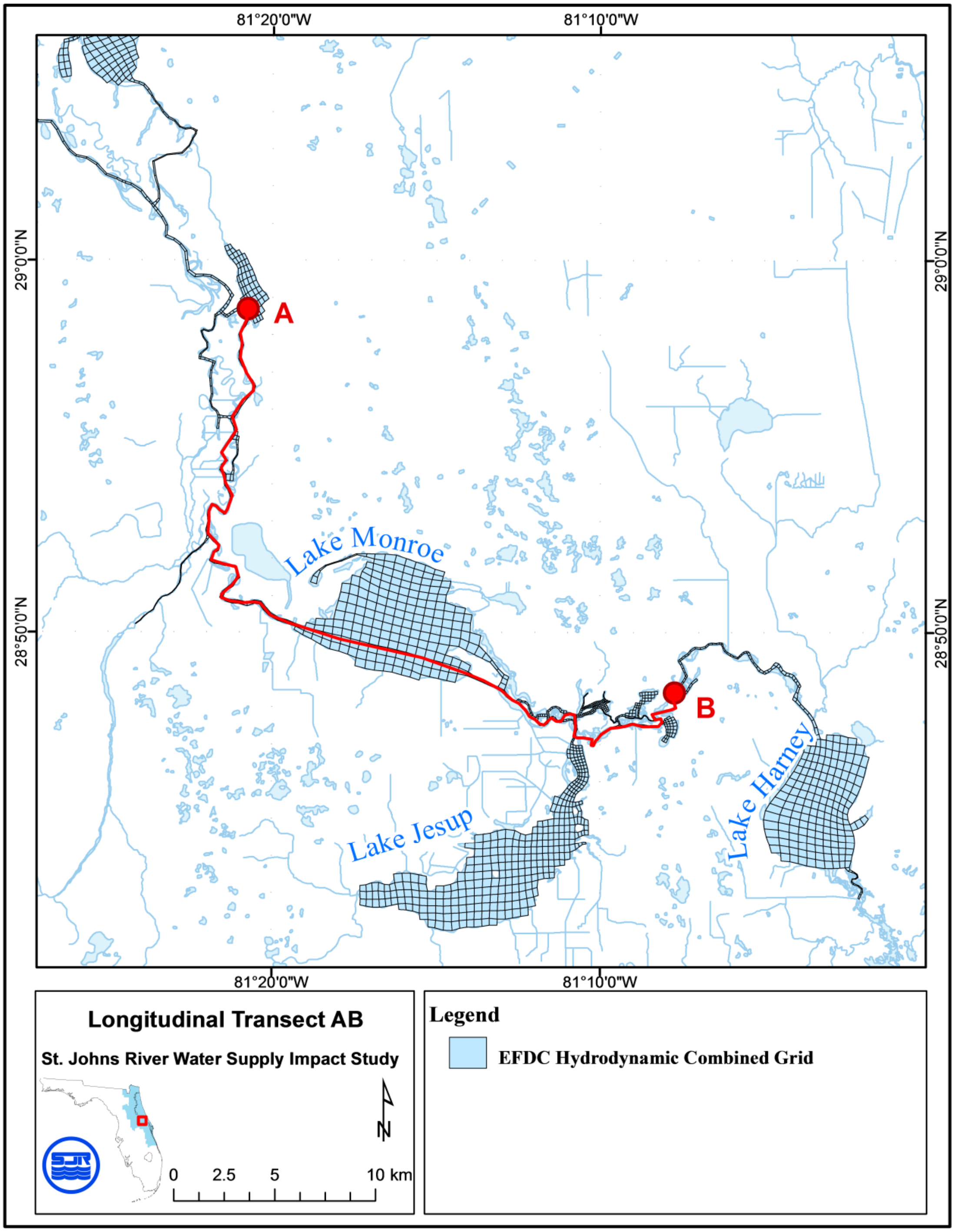

Figure 4–17. Location of longitudinal transect AB.

Daily Averaged Salinity

The distribution of daily averaged salinity for the base case (Base1995NN) over the 10-yr simulation period along the transect AB is described by the 10th, 50th, 90th, and 99th percentile levels (Figure 4–18). Moving downstream from B to A, the 90th and 99th percentile salinities dip near Lake Jesup (x = 38,000 m), decline slowly toward Lake Monroe (x = 25,000 m), flatten inside Lake Monroe (x = 18,000 m), and then drop abruptly at the confluence with the Wekiva River (x = 13,000 m). The greatest range of salinity occurs upstream of Lake Jesup.

Daily averaged salinities increase along the transect for the scenario case (Full1995NN), but particularly for the extreme high level represented by the 90th and 99th percentiles (Figure 4–19). As expected, relative maxima of salinity (Figure 4–19) and the largest differences between the scenario (Full1995NN) and base case (Base1995NN) (Figure 4–20) occur at the labeled discharge locations for reject water.

For the majority of days, salinity differences are small across the transect. Salinity differences are less than 0.2 PSS78 for 75% of days, and less than 0.1 PSS78 for 50% of days.

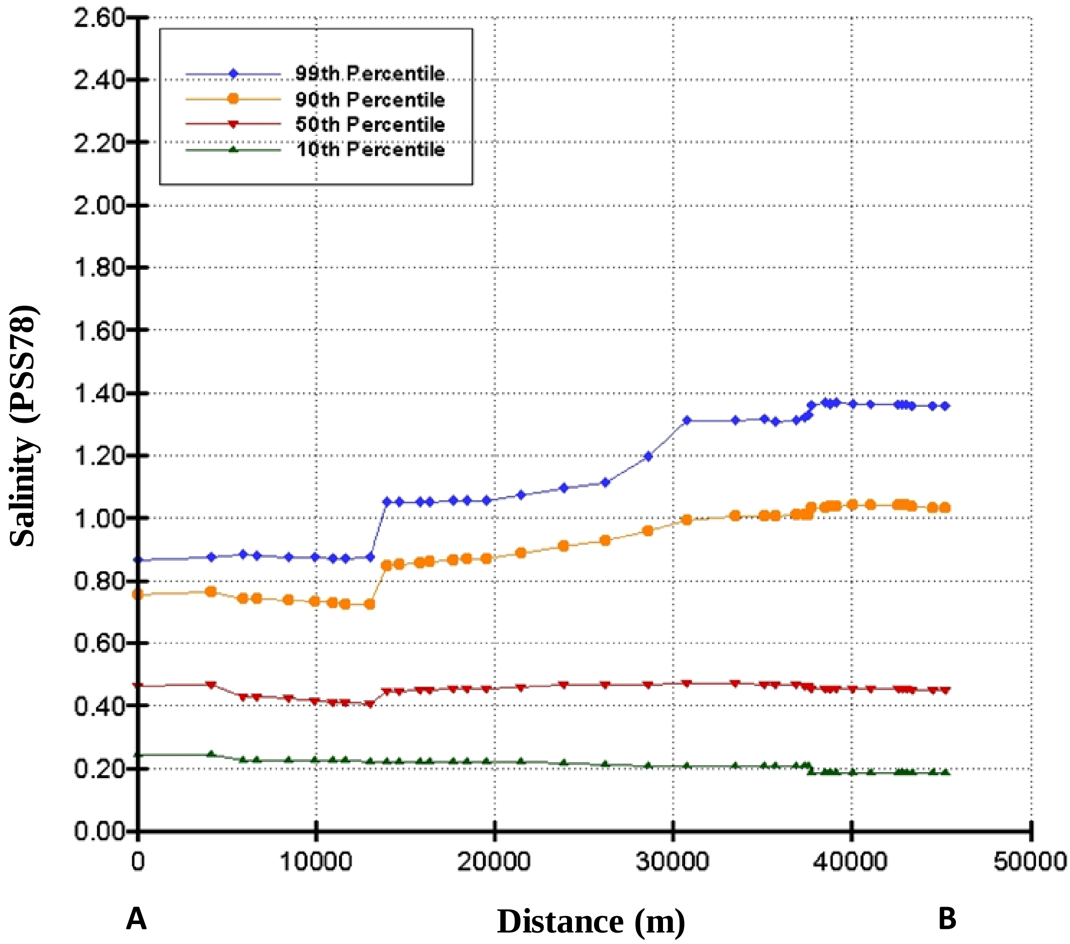

Figure 4–18. Daily averaged salinity distribution along transect AB for the base case (Base1995NN).

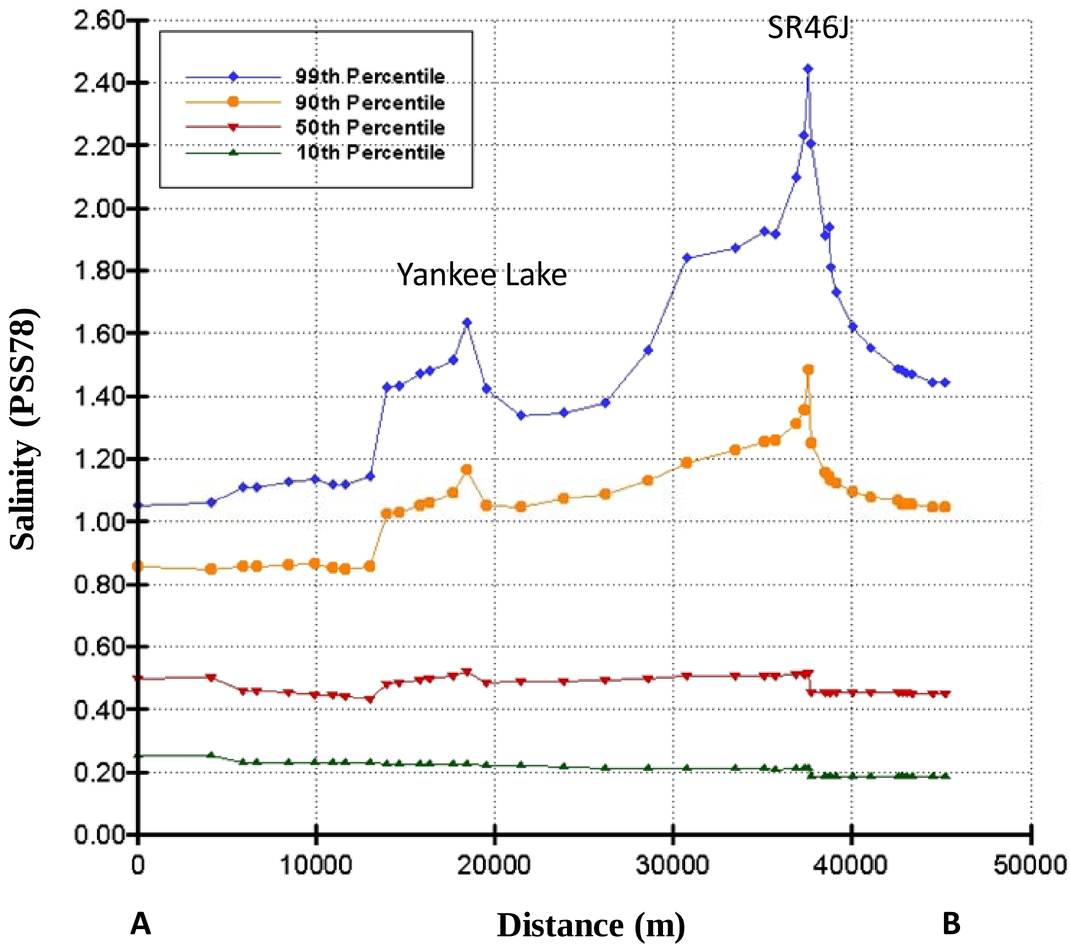

Figure 4–19. Daily averaged salinity distribution along transect AB for the scenario case (Full1995NN).

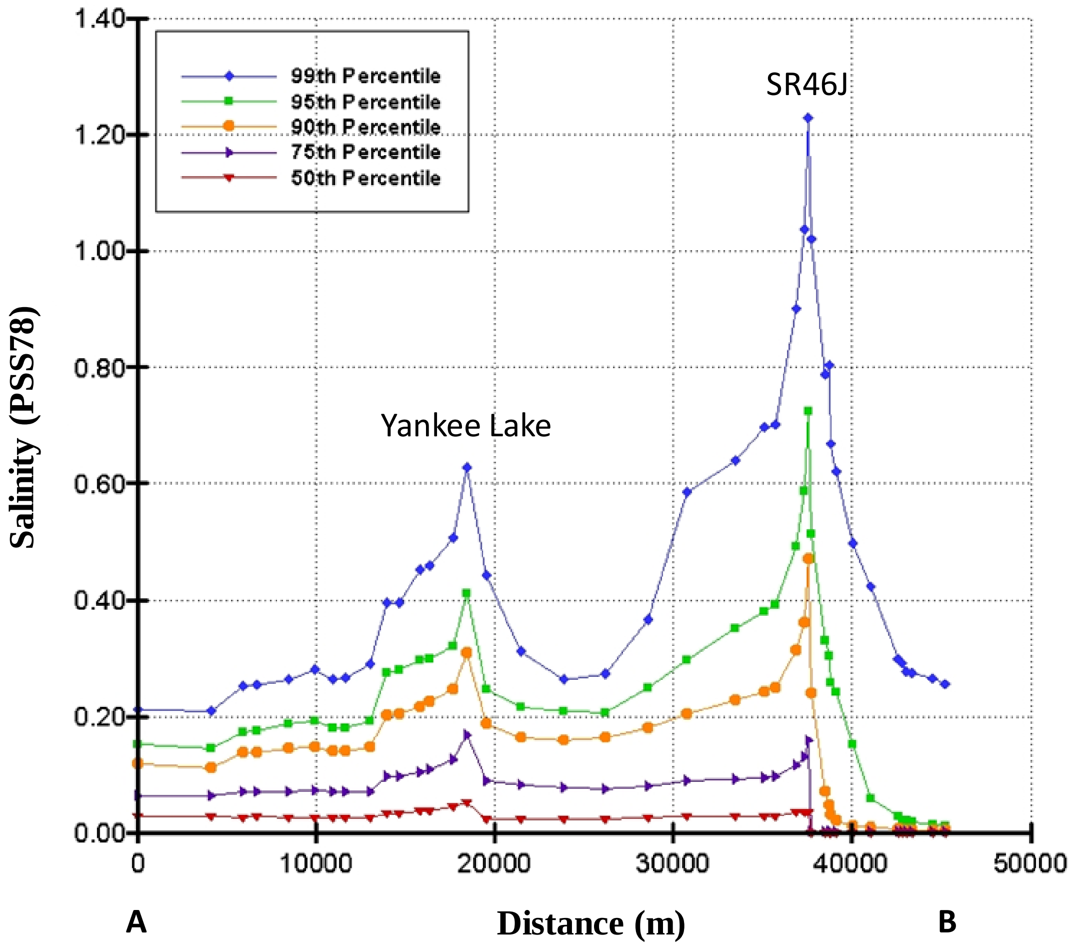

Figure 4–20. Distribution of daily average salinity differences (scenario case (Full1995NN) minus base case (Base1995NN)) along transect AB.

4.3.3 7-Day Averaged Salinity

Salinity magnitude and spatial patterns for 7-day averaged salinity are nearly identical to daily averaged salinity for the base case (Base1995NN) (Figure 4–21). Similar to daily averaged values, 7-day averaged salinities increase near the discharge locations (Figure 4–22). The highest 7-day averaged salinity, 2.3 PSS78, occurs near SR 46 at Lake Jesup (Figure 4–23); and the greatest 7-day averaged salinity difference, 1.0 PSS78, also occurs near SR 46 at Lake Jesup. Salinity differences are less than 0.2 PSS78 for 75% of days.

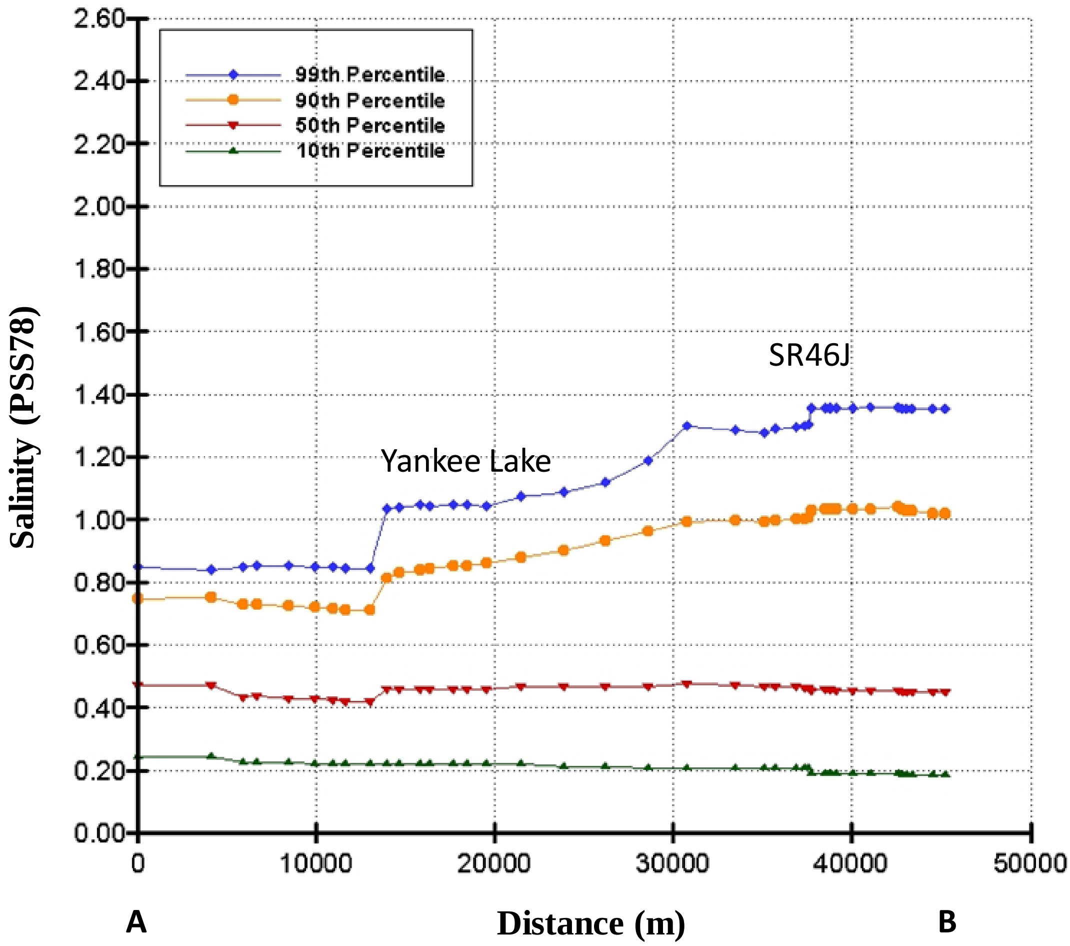

Figure 4–21. 7-day averaged salinity distribution along transect AB for the base case (Base1995NN).

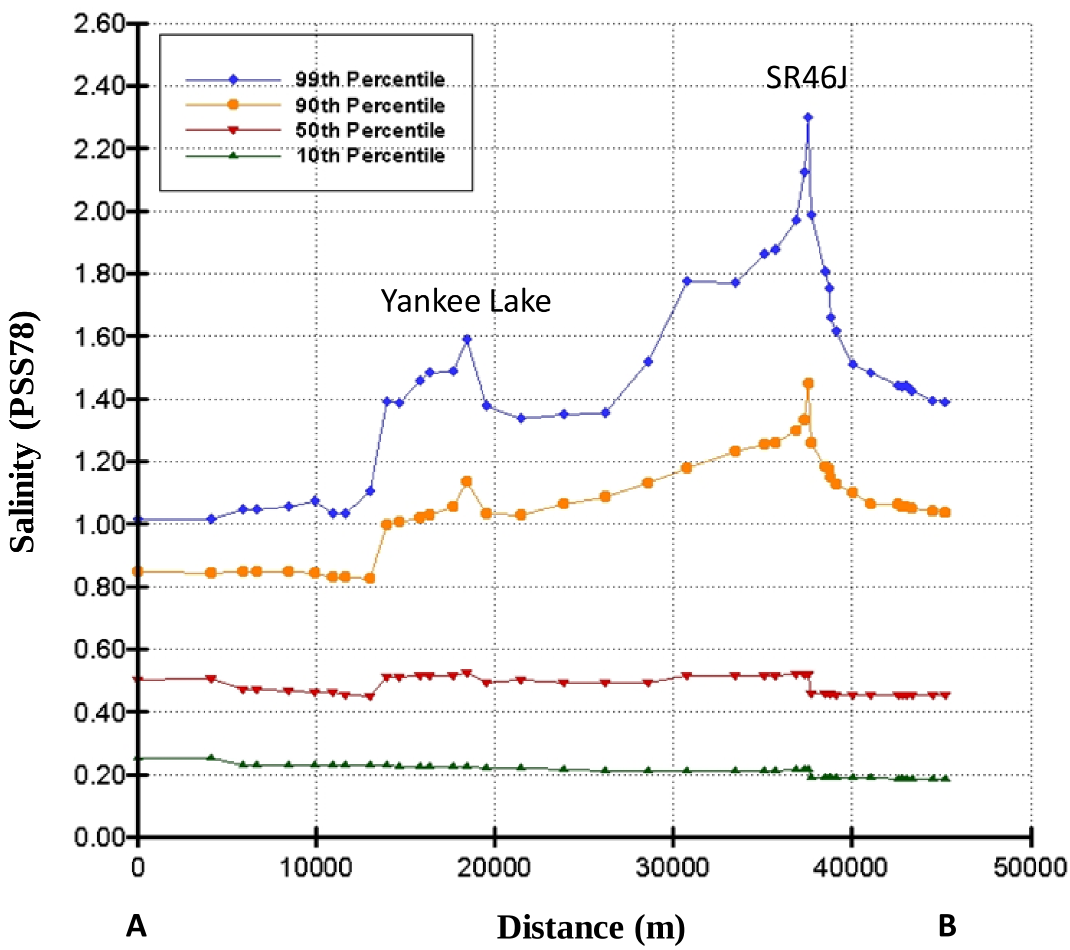

Figure 4–22. 7-day averaged salinity distribution along transect AB for the scenario case (Full1995NN). SR46J = SR 46 at Lake Jesup.

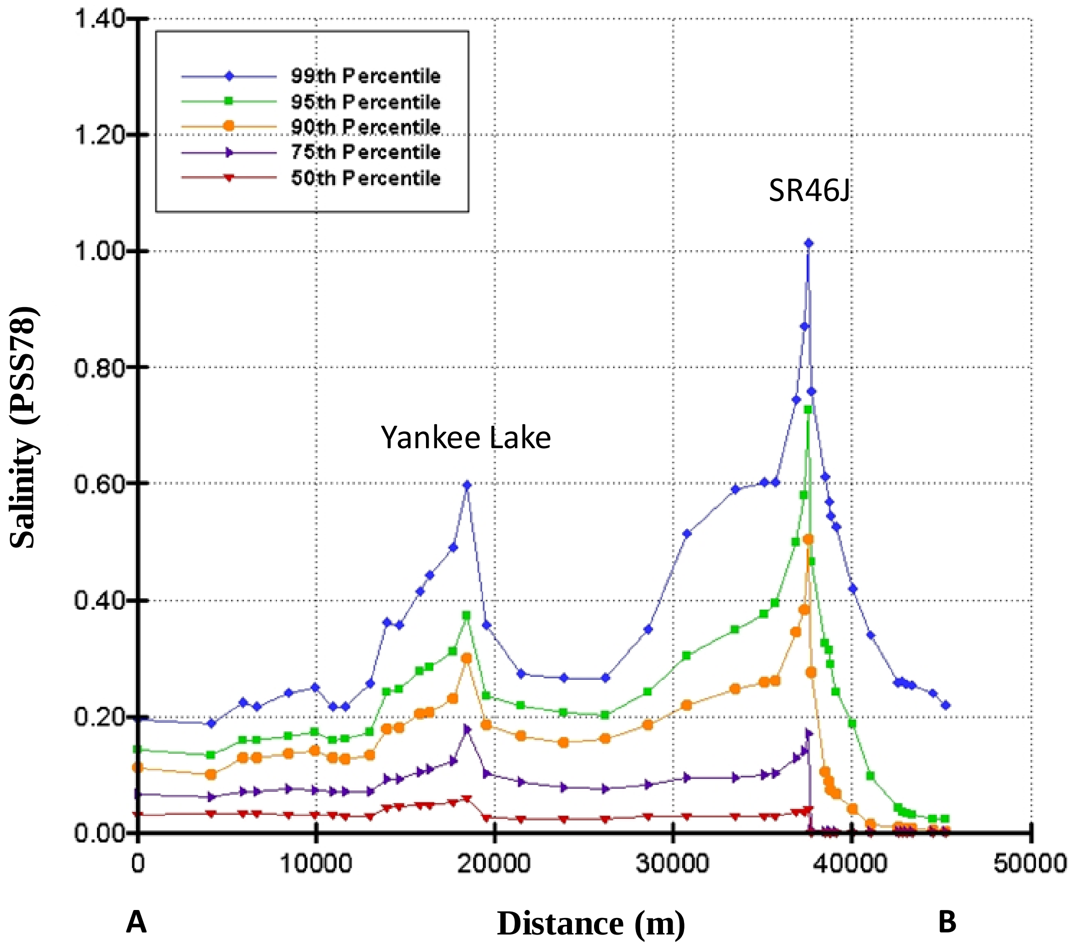

Figure 4–23. Distribution of 7-day average salinity differences between scenario case (Full1995NN) and base case (Base1995NN) along transect AB. SR46J = SR 46 at Lake Jesup.

4.3.4 30-Day Averaged Salinity

The greatest range of 30-day averaged salinity for the base case (Base1995NN) occurs upstream of SR 46 at Lake Jesup (Figure 4–24). The 10th percentile low salinity is 0.20, and the 99th percentile is 1.29. 30-day averaged salinities for the scenario case (Full1995NN) are greatest near the discharge locations (Figure 4–25). A high for 30-day averaged salinity of 2.1 PSS78 occurs near SR 46 at Lake Jesup. The greatest salinity difference of 0.92 also occurs at this location (Figure 4–26).

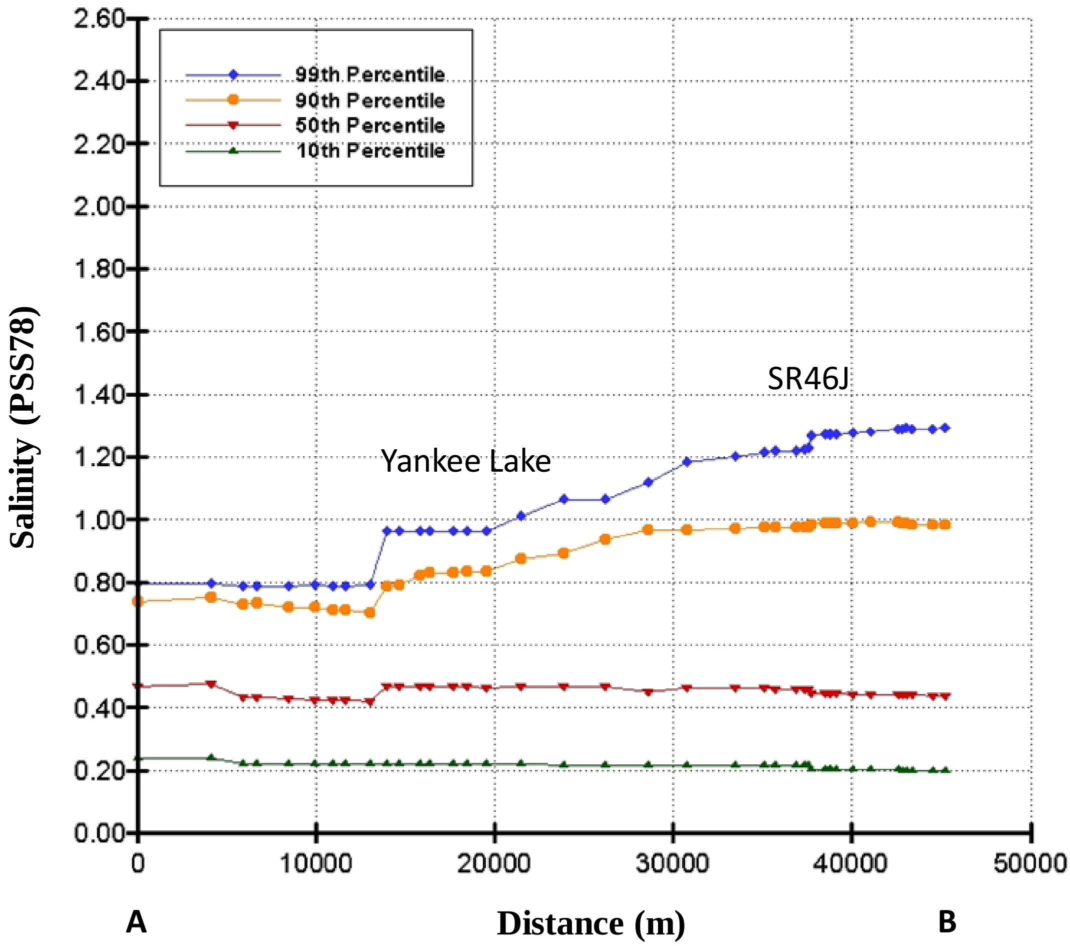

Figure 4–24. 30-day averaged salinity distribution along transect AB for the base case (Base1995NN). SR46J = SR 46 at Lake Jesup.

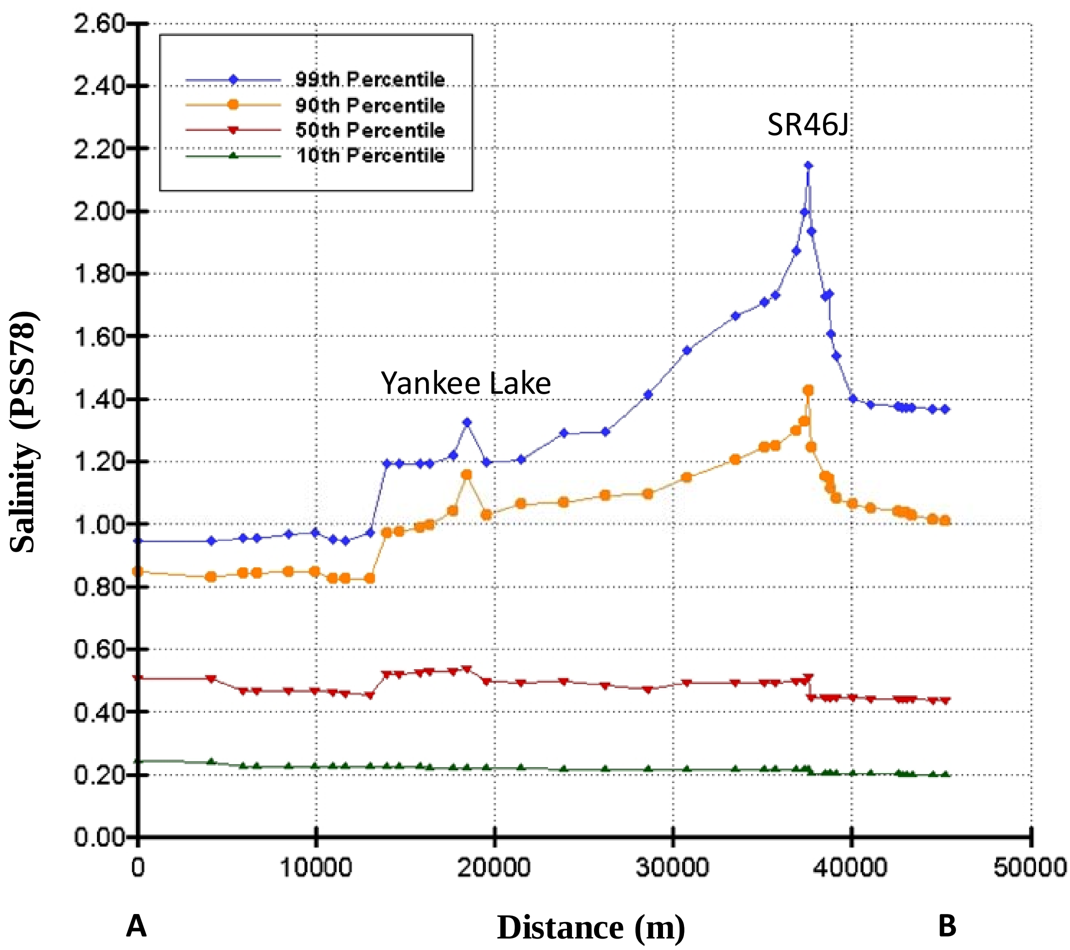

Figure 4–25. 30-day averaged salinity distribution along transect AB for the scenario case (Full1995NN). SR46J = SR 46 at Lake Jesup.

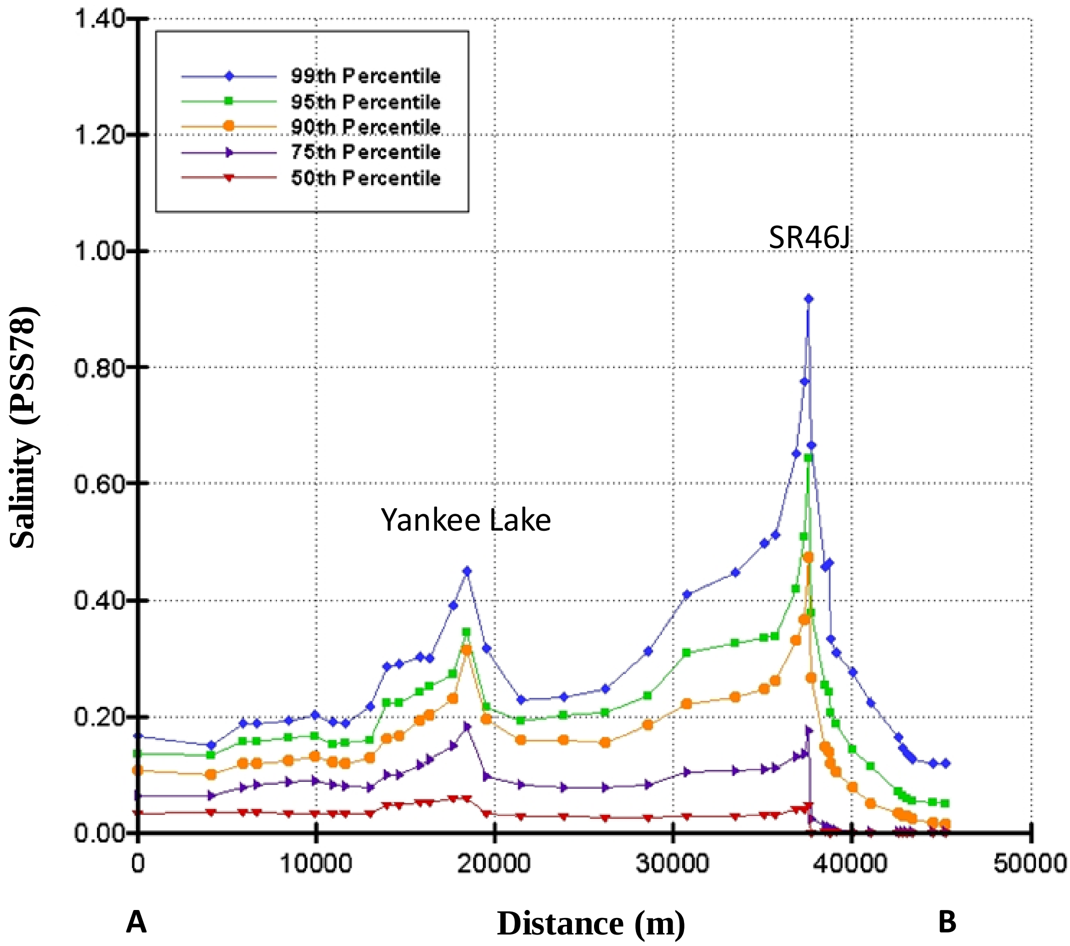

Figure 4–26. Distribution of 30-day average salinity differences between scenario case (Full1995NN) and base case (Base1995NN) along transect AB. SR46J = SR 46 at Lake Jesup.

Summary of Salinity Differences at Discharge Locations

A summary of the distribution of simulated salinity differences at the discharge locations are provided in Table 4–2 for 1- , 7-, and 30-day averaged salinity. Salinity differences at these two locations represent relative maxima along transect AB.

Table 4–2. Simulated salinity differences between scenario case (Full1995NN) and base case (Base1995NN) for 1- , 7-, and 30-day averages at Yankee Lake and near SR 46 at Lake Jesup (SR46J) for 50th through 99th percentiles.

Percentile	1-Day Averaged		7-Day Averaged		30-Day Averaged	
	Yankee Lake	SR46J	Yankee Lake	SR46J	Yankee Lake	SR46J
99th	0.63	1.23	0.60	1.01	0.45	0.92
95th	0.41	0.72	0.37	0.73	0.35	0.64
90th	0.31	0.47	0.30	0.50	0.31	0.47
75th	0.17	0.16	0.18	0.17	0.18	0.18
50th	0.05	0.04	0.06	0.04	0.06	0.05

4.4 Summary and Conclusions

The greatest salinity impacts due to reject water occur closest to the discharge locations. Salinity impacts are greater near SR 46 at Lake Jesup than at Yankee Lake because of lower flushing at the former location. The largest daily averaged salinity difference between the base (Base1995NN) and scenario (Full1995NN) cases is 1.23 PSS78, and occurs near SR 46 at Lake Jesup.

The highest salinities, as well as the greatest differences in salinity between the two cases, occur during periods of low flow and low flushing. The greatest differences in salinity occur only for infrequent events with return periods greater than 4 years. The largest salinity difference reported in this study occurs during conditions simulating a 50-yr drought.

Salinity differences are small for most days. For example, salinity differences between the base (Base1995NN) and scenario case (Full1995NN) are less than 0.2 PSS78 for 75% of days. Under even moderate flow conditions, salts released in reject water are readily flushed from the system.

Lake Monroe is positioned between the two discharge locations, but salinity in the lake is relatively unaffected by the discharge of reject water. Daily averaged salinity differences in Lake Monroe are less than 0.2 PSS78 for 90% of days, and never exceed 0.3 PSS78.

5 Conclusions and Discussion

5.1 Water Level

Water levels in the lower and middle St. Johns River will increase primarily due to sea level rise and secondarily due to increased runoff from urbanization. Increased water levels caused by these two factors dominate reductions in water level due to proposed water withdrawals of 155 mgd upstream of DeLand and 107 mgd from the Ocklawaha River. At the proposed water withdrawal amounts, reduction of water levels in the lower and middle St. Johns River is inconsequential. Water levels throughout this reach are certain to rise through the year 2030 and beyond, with or without proposed surface water withdrawals.

Water level variability over the lower 300 km of the St. Johns River is dominated by ocean water level, not discharge, when discharge is below the median value. Under these conditions, changes in discharge have little effect on water level. Ocean water level effects extend far up the river because of the river's low hydraulic slope. The river's bottom slope is inconsequential to river flow because bottom elevation is everywhere below mean sea level to Lake Harney. Even if there were no freshwater flow into the St. Johns River at all, the mainstem river and connected lakes of the lower and middle St. Johns River would remain submerged.

The importance of ocean water level effects on water levels in the St. Johns River also means that the effects of sea level rise extend over the lower 300 km of the river, from the river mouth to Lake Harney. At present rates of sea level rise, water levels in the St. Johns River will increase approximately 14 cm between 1995 and 2030. For a high rate of sea level rise that incorporates uncertainty due to global climate change, water levels increase approximately 28 cm during the same period. The rate of sea level rise in the middle St. Johns River is lower than in the lower portion of the river because the full amount of sea level rise is not realized in the middle basin under high flow conditions. But under high flow conditions, increased runoff due to urbanization of watersheds also increases water levels in the middle St. Johns River. As a result, water levels will rise throughout the lower and middle St. Johns River over all flow conditions by the year 2030.

Among future conditions examined in this chapter, only sea level rise affects water levels. An additional water withdrawal of 107 mgd from the Ocklawaha River has essentially no effect on water levels in the St. Johns River, because the Ocklawaha River enters downstream of Lake George. Channel deepening and reuse of wastewater also have inconsequential effects on river water levels.

From the perspective of water supply, the middle and lower St. Johns River have essentially infinite storage capacity because the river surface is nearly at sea level and cannot be drawn down lower than sea level. Withdrawing water from a closed reservoir in excess of resupply would eventually deplete the reservoir, whereas deficit withdrawal of water from the lower or middle St. Johns River cannot deplete the river. Deficit withdrawal instead pulls water into the lower St. Johns River from the ocean and increases salinity in the estuarine reach. In addition, water withdrawals from the St. Johns River decrease flushing. Decreased flushing could increase salinity in areas of the river upstream of the estuarine reach where salinity is dominated by groundwater inflow. Decreased flushing is also associated with degradation of water quality. These effects of withdrawals are discussed below.

5.2 Salinity

5.2.1 Salinity in the St. Johns River

Changes to salinity in areas upstream of the estuarine reach are small for both forecast and future conditions. Salinity in Lake George and the middle St. Johns River typically varied less than 0.05 PSS78 for both forecast and future scenarios. The oligohaline character of the middle St. Johns River is biologically important, but we found no evidence that it would appreciably change due to water withdrawal or any of the other factors considered for WSIS. The only possible change to salinity in the middle St. Johns River related to water withdrawal is the return of reject water from reverse osmosis, if that technology is required for water treatment.

Salinity in the estuarine reach of the river is increased by water withdrawals, sea level rise, and channel deepening and decreased by urbanization of watersheds and structural changes to the USJRB. The estuarine reach of the river extends over the lower 80 km of river from the river mouth to Shands Bridge. The upper portions of the estuarine reach, between Buckman Bridge and Shands Bridge, are typically fresh to oligohaline, with salinity below 1 PSS78, but experience infrequent ocean incursions of higher salinity during droughts. Increased salinity in this upper reach is a concern because this reach contains salt-intolerant submersed aquatic vegetation, which provides important structural habitat for biota (see Chapter 9. Submersed Aquatic Vegetation).

Urbanization of watersheds and a 155-mgd water withdrawal have the greatest effects on estuarine salinity for 2030 forecast conditions. Because these two factors work in opposition, the resulting salinity change is negligible between projected 2030 conditions, including withdrawal, and 1995 hindcast conditions. Mean salinity at Acosta Bridge increases only 0.04 PSS78; and 10-yr high salinity events at Shands Bridge increase only 0.35 PSS78 for 1- to 30-day periods.

Salinity alterations in the estuarine reach due to a 155-mgd withdrawal are small even without considering urbanization of watersheds. The isolated effect of a 155-mgd withdrawal increased mean salinity 0.1 to 0.3 PSS78 between Shands and Acosta bridges. This level of increase is very small relative to the range of salinity conditions occurring in this reach of the river, where salinity varies from 0.3 to more than 20 PSS78. Because differences in mean values might obscure more important changes to high salinity events, we also examined changes to 2-, 5-, and 10-yr high salinity events over a range of durations. Salinity changes were remarkably similar for high salinity events over a wide range of frequency and duration. Salinity levels increase 0.4 to 0.65 PSS78 for high salinity events with frequencies ranging from 2 to 10 years, and durations ranging from 1 day to 1 year. A 155-mgd withdrawal produced no anomalous, large shifts in salinity.

The combined effect of all future factors increases mean salinity 3 PSS78 at Acosta Bridge, and 0.1 to 1.0 PSS78 between Shands and Buckman bridges. All factors used for future conditions (channel deepening, a 262-mgd water withdrawal, increased sea level rise, and wastewater reuse) increase salinity in the estuarine reach compared with projected 2030 conditions. The channel deepening scenario (CHND2030PS) contributes the largest single effect on salinity, and results in an increase of mean salinity of 1.7 PSS78 at Acosta Bridge. The effect of channel deepening on salinity, however, declines toward Shands Bridge more rapidly than for effects caused by other future factors.

The combination of future factors (FALL2030PH) simulates the unlikely, simultaneous occurrence of uncertain events. Even for this extreme scenario, the salinity regime of the river is not appreciably altered. This result indicates that the present salinity regime of the river will remain fairly stable into the future. Sea level rise will slowly increase salinity in the estuarine reach, however, and the future rate of sea level rise will largely determine the rate at which the broad expanse of the lower St. Johns River upstream of Acosta Bridge transitions from an oligohaline to mesohaline estuarine system.

The removal of wastewater discharge for reuse had only a minor effect on salinity, particularly in relation to channel deepening, sea level rise, and water withdrawal. Wastewater reuse improves water quality of the river by reducing nutrient loads. It also protects regional water resources by conserving water, which reduces demand on other water supply sources. In our opinion, the benefits of wastewater reuse far outweigh any possible deleterious hydrodynamic effects. Wastewater reuse should be encouraged throughout the St. Johns River Basin.

5.2.2 Effects of Reject Water from Reverse Osmosis

Water withdrawal from the middle St. Johns River for public water supply could require treatment to remove excessive chloride and other salts. Reverse osmosis is a common treatment methodology that generates a waste stream of concentrated salts. The discharge of this waste stream back to the river as reject water could increase salinity near the discharge locations. A far field analysis of the effects of reject water on salinity in the middle St. Johns River shows that discharge of reject water from a 50-mgd water withdrawal into the narrow river channel between Lakes Monroe and Jesup could increase salinity from a background level of 1.5 to 3 PSS78 during drought periods. Discharge of reject water at a location below Lake Monroe (Yankee Lake) has less effect on salinity. These results indicate that the far field effects of reject water on salinity should be incorporated into the design and permitting of reverse osmosis plants in the middle St. Johns River.

5.3 Water Age

Water age differences for both forecast and future conditions are small (~5 days) relative to the large natural variation (20 to 200 days) of water age for the river. The greatest change to water age due to a 155-mgd withdrawal occurs in Lake George. Water age differences are greatest when absolute water age is high, and water age differences caused by a 155-mgd withdrawal only rarely exceed 10% of ambient water age. The 10-yr high water age event in Lake George increases in length by 10 to 14 days for durations of 1 day to 1 year. Events that are more moderate show less of an absolute increase in water age; the 2-yr high water age for the same range of durations increases about 6 days. The percent increase of water age remains at 4% to 5% over all frequencies and durations of high events.

For 2030 conditions, the increase in water age due to a withdrawal is offset by a decrease in water age due to increased runoff from urbanization. Mean water age in Lake George under projected 2030 conditions, with a 155-mgd water withdrawal, increases only 2.7 days compared with 1995 hindcast conditions.

For future conditions, water age in Lake George is relatively unaffected by channel deepening, so water age changes under future conditions are not as large as for salinity. Also, an additional 107-mgd withdrawal from the Ocklawaha River has an insignificant effect on water age in Lake George.

Water age changes over both forecast and future conditions, then, are unlikely to contribute appreciably to water quality alterations in the St. Johns River. Compared with the expected increase of stormwater flows caused by urbanization of watersheds, which could increase delivery of nutrients, toxics, and pathogens to the river, the water quality impacts of increased water age are trivial. The deleterious effects of pollution resulting from increased stormwater runoff is a far greater threat to water quality than the small predicted changes to water age.

5.4 RECOMMENDATIONS

- The removal from the river of wastewater discharge for reuse has an extremely small effect on water level, salinity, and water age. Wastewater reuse should be encouraged as a means of water conservation and for its benefit to water quality of the river. The benefits of wastewater reuse far outweighs any possible deleterious impacts to hydrodynamic variables.
- Urbanization of watersheds will increase surface runoff to the St. Johns River and increase loadings of nutrient, sediment, toxics, and bacteria. The use of the river for water supply requires careful consideration of the river's future water quality both for protecting natural functions of the system and, also, to protect the quality of the supply source.
- Water quality analyses should include the likelihood of increasing salinity and salinity stratification in the estuarine reach of the river. Future increases in salinity and salinity stratification are likely due to sea level rise, water withdrawals, and channel deepening. Understanding how changing patterns of salinity affect water quality issues such as phytoplankton production, toxin-producing algae, and low dissolved oxygen would enhance our ability to manage the river system into the future.
- The design and permitting of reverse osmosis plants that discharge reject water to the river should include a far-field analysis of salinity.
- All other factors being equal, water withdrawal facilities should be placed as far downstream as possible to minimize hydrodynamic alterations.

5.5 FUTURE WORK

The WSIS hydrodynamic study provides a thorough analysis of the effects of water withdrawal, both in isolation and in conjunction with expected and uncertain future conditions, on water level, salinity, and water age throughout the lower and middle St. Johns River. The need for additional water supply assumes an increase in population within the basin, which will also cause increased urbanization of watersheds and consequently increased stormwater runoff to the river. Although this study considers the hydrodynamic effects of increased stormwater runoff, the effects on river water quality due to increased loads of nutrients, sediment, toxics, and bacteria are not addressed. A clear understanding of the effects of population growth on water quality is needed for comprehensive management of St. Johns River resources.

Our recommendations for future work focus on development of a suite of interconnected groundwater, hydrologic, hydrodynamic, and water quality models for quantifying sources of pollutants to the river, simulating transport and mixing within the river, and simulating water quality transformations (e.g., the incorporation of inorganic phosphorus into algae).

Groundwater models exist for the area but do not include dissolved transport. Groundwater transport models, which include dissolved transport, would be helpful to assess the sources and magnitude of pollutants entering the river through groundwater flows.

The HSPF hydrologic model developed for WSIS to simulate surface water runoff to the river should be expanded to include simulation of watershed loading of pollutants.

The EFDC hydrodynamic model developed for WSIS can simulate mixing and transport within the river. Uncertainty analysis demonstrated the sensitivity of the EFDC hydrodynamic model to depth. Additional future work should include updating bathymetry in the middle St. Johns River, Lake George, and Crescent Lake.

A water quality model that incorporates input from the groundwater, hydrologic, and hydrodynamic models is needed to estimate the fate of pollutants entering the river.

In summary, the following items are recommended for future work:

- Development of a groundwater transport model to quantify sources of nutrients entering the river from both the surficial and confined aquifers
- Addition of nutrient and sediment load estimates in the HSPF hydrologic model to predict change in loadings to river caused by urbanization of watersheds
- Update the bathymetry of the middle St. Johns River
- Development of a mechanistic water quality model of the lower and middle St. Johns River to evaluate the effects of future loading on in-stream water quality

Finally, the EFDC hydrodynamic model used for WSIS treated the lower St. Johns River, Lake George, and middle St. Johns River as a single, interconnected hydrodynamic system. The hydrodynamic effects of water withdrawals in the middle St. Johns River were tracked downstream more than 300 km to the river mouth. The regional extent of WSIS sets a precedent for management of the St. Johns River that should continue in future studies. A comprehensive suite of models aimed at examining future water quality changes should, as much as possible, consider the entire river as a single, interconnected system.

REFERENCES

Applied Technology and Management. *Hydrodynamic Modeling of Withdrawals from the Middle St. Johns River for the Water Supply Impact Assessment. Contract #26519.* Palatka, FL: Prepared for the St. Johns River Water Management District, 2010.

Beck, M. B. "Water quality modeling: A review of the analysis of uncertainty." *Water Res. Res.*, 1987: Vol. 23(8): 1393-1442.

Blumberg, A. F., and N. Georgas. "Quantifying uncertainty in estuarine and coastal ocean circulation modeling." *J. Hydr. Eng.*, 2008: Vol. 134(4): 403-415.

Brown, L., and T. Barnwell. *The enhanced stream water quality models QUAL2E and QUAL2E-UNCAS: Document and user manual.* Athens, GA: Rep. No. EPA 600/3-87/007, 1987.

CH2M HILL. *Feasibility Evaluations for St. Johns River Membrane Water Plant Demineralization Concentrate Management. Special Publication SJ2009-SP10.* Palatka, FL: Report prepared for St. Johns River Water Management District, 2008.

Dornstauder, A. *Water Resource Policies and Authorities Incorporating Sea-Level Change Considerations in Civil Works Programs.* Washington, D.C.: USACE, 2009.

Environmental Consulting & Technology, Inc. *Water Resources and Human-Use Values Assessment: Lake Monroe, Volusia, and Seminiole Counties, FL.* Palatka, FL: SJRWMD, Spec. Pub. SJ2007-SP15, 2008.

Hagen, S. C., and D. M. Parrish. "Mesh Requirements for Tidal Modeling in the Western North Atlantic." *J. Computational Fluid Dynamics*, 2004: Vol. 18(7): 585-595.

Hall, G. *Ocklawaha River Water Allocation Study.* Palatka, FL: SJRWMD, Tech. Pub. SJ2005-1, 2005.

Intergovernmental Panel on Climate Change. "Guidance notes for lead authors of the IPCC fourth assessment report on addressing uncertainties." July 2005. http://ipcc-wg1.ucar.edu/wg1/Report/AR4_UncertaintyGuidanceNote.pdf (accessed 2010).

Kroening, S. E. "Streamflow and Water-Quality Characteristics at Selected Sites of the St. Johns River in Central Florida, 1933-2002: U.S. Geological Survey Scientific Investigations Report 2004-5177." 2004, 102.

Lewis, E. L., and R. G. Perkin. "Salinity: Its definition and calculation." *J. Geophysical Res.*, 1978: Vol. 83 (C1): 466-478.

Martin, J. L., and S. C. McCutcheon. *Hydrodynamics and Transport Modeling for Water Quality Modeling.* Boca Raton, FL: CRC Press, Inc., 1999.

Matott, J. L., L. Shawn, J. E. Babendreir, and S. T. Purucker. "Evaluating uncertainty in integrated environmental models: A review of concepts and tools." *Water Res. Res.*, 2009: Vol. 45, W06421, pp. 1-14.

Rahmstorf, S. "A sem-empirical approach to projecting future sea-level rise." *Science*, 2007: Vol 315: 368-370.

Robison, C. P. *Middle St. Johns River Minimum Flows and Levels Hydrologic Methods Report.* Palatka, FL: Tech. Pub. SJ2004-2, SJRWMD, 2004.

Sawyer, C. N., P. L. McCarthy, and G. F. Parkin. *Chemistry for Environmental Engineering.* New York: McGraw-Hill, Inc., 1994.

St. Johns River Water Management District. *District Water Supply Plan, 2005, Technical Publication SJ2006-2.* Palatka, Florida: St. Johns River Water Management District, 2006.

U.S. Army Corps of Engineers. *Incorporating Sea-Level Change Considerations in Civil Works Programs Engineering Circular 1165-211.* Washington, DC: Department of the Army, 2009.

Viessman, W., J. Knapp, G. Lewis, and T. Harbaugh. *Introduction to Hydrology*. New York: Harper & Row, Publishers, Inc., 1977.

Zhang, H. X., and S. L. Yu. "Applying the first-order error analysis in determining the margin of safety for total maximum daily load computations." *J. Env. Eng.*, 2004: Vol. 130(6): 664-673.